

Co-Optimization of Fuels & Engines

# Top 13 Blendstocks Derived from Biomass for Mixing-Controlled Compression-Ignition (Diesel) Engines

Bioblendstocks with Potential for Decreased Emissions and  
Improved Operability



## About the Co-Optimization of Fuels & Engines Project

This is one of a series of reports produced by the Co-Optimization of Fuels & Engines (Co-Optima) project, which is a U.S. Department of Energy (DOE)-sponsored multi-agency project that was initiated to accelerate the introduction of affordable, scalable, and sustainable biofuels and high-efficiency, low-emission vehicle engines. The simultaneous fuels and vehicles research and development is designed to deliver maximum energy savings, emissions reduction, and on-road performance.

Co-Optima brings together two DOE Office of Energy Efficiency and Renewable Energy (EERE) research offices, nine national laboratories, and numerous industry and academic partners to make improvements to the types of fuels and engines found in most vehicles currently on the road and to develop revolutionary engine technologies for longer-term, higher-impact solutions. This first-of-its-kind project will provide industry with the scientific underpinnings required to move new biofuels and advanced engine systems to market faster while identifying and addressing barriers to commercialization.

In addition to the EERE Vehicle Technologies and Bioenergy Technologies Offices, the Co-Optima project team included representatives from the National Renewable Energy Laboratory and Argonne, Idaho, Lawrence Berkeley, Lawrence Livermore, Los Alamos, Oak Ridge, Pacific Northwest, and Sandia National Laboratories. More detail on the project, as well as the full series of reports, can be found at [www.energy.gov/fuel-engine-co-optimization](http://www.energy.gov/fuel-engine-co-optimization).

## Availability

This report is available electronically at no cost from <http://www.osti.gov/bridge>.

## Citation

Please cite this report as follows:

Gaspar, D. J. 2021. Top 13 Blendstocks Derived from Biomass for Mixing-Controlled Compression-Ignition (Diesel) Engines: Bioblendstocks with Potential for Lower Emissions and Increased Operability. PNNL-31421. Pacific Northwest National Laboratory, Richland, WA.

## Note

This report was prepared as an account of work sponsored by an agency of the U.S. government. Neither the U.S. government nor any agency thereof, nor any of their employees, makes any warranty, express or implied, or assumes any legal liability or responsibility for the accuracy, completeness, or usefulness of any information, apparatus, product, or process disclosed, or represents that its use would not infringe privately owned rights. Reference herein to any specific commercial product, process, or service by trade name, trademark, manufacturer, or otherwise does not necessarily constitute or imply its endorsement, recommendation, or favoring by the U.S. government or any agency thereof. The views and opinions of authors expressed herein do not necessarily state or reflect those of the U.S. government or any agency thereof.

## Report Contributors and Roles

### Lead Author

Daniel J. Gaspar, Pacific Northwest National Laboratory

### Contributing Authors

#### **Formation and Impacts of Soot on Engine Operation and Engine Testing**

- Charles J. Mueller, Sandia National Laboratories
- Robert L. McCormick, National Renewable Energy Laboratory
- Jonathan Martin, National Renewable Energy Laboratory
- Sibendu Som, Argonne National Laboratory
- Gina M. Magnotti, Argonne National Laboratory
- Jonathan Burton, National Renewable Energy Laboratory

#### **Bioblendstock Discovery, Production, and Screening**

- Derek R. Vardon, National Renewable Energy Laboratory
- Vanessa L. Dagle, Pacific Northwest National Laboratory
- Teresa L. Alleman, National Renewable Energy Laboratory
- Nabila A. Huq, National Renewable Energy Laboratory
- Daniel A. Ruddy, National Renewable Energy Laboratory
- Martha A. Arellano-Trevino, National Renewable Energy Laboratory
- Alex Landera, Sandia National Laboratories
- Anthe George, Sandia National Laboratories
- Gina M. Fioroni, National Renewable Energy Laboratory
- Eric R. Sundstrom, Lawrence Berkeley National Laboratory
- Ethan Oksen, Lawrence Berkeley National Laboratory
- Michael R. Thorson, Pacific Northwest National Laboratory
- Richard T. Hallen, Pacific Northwest National Laboratory
- Andrew J. Schmidt, Pacific Northwest National Laboratory
- Eugene Polikarpov, Pacific Northwest National Laboratory
- Eric Monroe, Sandia National Laboratories
- Joey S. Carlson, Sandia National Laboratories
- Ryan W. Davis, Sandia National Laboratories
- Andrew D. Sutton, Los Alamos National Laboratory
- Cameron M. Moore, Los Alamos National Laboratory

- Lelia Cosimbescu, Pacific Northwest National Laboratory
- Karthikeyan K. Ramasamy, Pacific Northwest National Laboratory
- Michael D. Kass, Oak Ridge National Laboratory

**Analysis**

- Troy R. Hawkins, Argonne National Laboratory
- Avantika Singh, National Renewable Energy Laboratory
- Andrew Bartling, National Renewable Energy Laboratory
- Pahola Thathiana Benavides, Argonne National Laboratory
- Steve Phillips, Pacific Northwest National Laboratory
- Hao Cai, Argonne National Laboratory
- Yuan Jiang, Pacific Northwest National Laboratory
- Longwen Ou, Argonne National Laboratory
- Michael Talmadge, National Renewable Energy Laboratory
- Nicholas Carlson, National Renewable Energy Laboratory
- George G. Zaines, Argonne National Laboratory
- Matthew Wiatrowski, National Renewable Energy Laboratory
- Yunhua Zhu, Pacific Northwest National Laboratory
- Lesley J. Snowden-Swan, Pacific Northwest National Laboratory

The authors wish to thank the many additional contributors at the national laboratories, in industry and at academic institutions who performed research and analysis reported herein.

## Acknowledgments

This research was conducted as part of the Co-Optimization of Fuels & Engines (Co-Optima) project sponsored by the U.S. Department of Energy (DOE) Office of Energy Efficiency and Renewable Energy (EERE), Bioenergy Technologies and Vehicle Technologies Offices. Co-Optima is a collaborative project of multiple national laboratories initiated to simultaneously accelerate the introduction of affordable, scalable, and sustainable biofuels and high-efficiency, low-emission vehicle engines.

The following EERE officials and managers played important roles in establishing the project concept, advancing implementation, and providing ongoing guidance:

Michael Berube, Deputy Assistant Secretary for Transportation

*Bioenergy Technologies Office*

Valerie Reed, Acting Director

Alicia Lindauer, Technology Manager

James Spaeth, Program Manager

Trevor Smith, Technology Manager

*Vehicle Technologies Office*

David Howell, Acting Director

Gurpreet Singh, Program Manager

Kevin Stork, Technology Manager

Mike Weismiller, Technology Manager

The national laboratory project management team consisted of:

Dan Gaspar, (Technical Monitor), Pacific Northwest National Laboratory

Anthe George, Sandia National Laboratories

Robert McCormick, National Renewable Energy Laboratory

Robert Wagner, Oak Ridge National Laboratory

## Table of Contents

Abbreviations and Acronyms .....	x
Executive Summary .....	xii
<b>1 Introduction.....</b>	<b>1</b>
1.1 Purpose .....	1
1.2 Background .....	1
1.3 Research Methodology and Approach .....	2
1.4 Overview of Content .....	3
<b>2 Fuel Properties, Candidate Identification, and Blendstock Screening .....</b>	<b>4</b>
2.1 Target Fuel Properties .....	4
2.1.1 Impacts of Soot on Engine Operation.....	5
2.1.2 Soot Formation in Diesel Combustion.....	6
2.2 Tiered Screening Process to Evaluate Target Values of Critical Fuel Properties .....	8
2.2.1 Prediction Tools .....	9
2.2.2 Compatibility Assessment Approach.....	11
2.3 Candidates .....	11
2.4 Screening Results .....	13
2.4.1 Merit Table.....	13
2.4.2 Infrastructure Compatibility Results.....	16
2.5 Potential Adoption Impacts and Barriers .....	17
2.5.1 Analysis of Bioblendstock Economic, Environmental, and Scalability Metrics ...	17
2.5.2 Refinery Integration .....	20
2.6 Engine-Related Investigations and Impacts .....	22
2.6.1 Conventional Diesel Engine Experiments .....	22
2.6.2 Ducted Fuel Injection.....	23
2.7 Technical Summary.....	25
<b>3 Top 13 MCCI Biofuel Candidates.....</b>	<b>29</b>
3.1 Top Eight Candidates with Minimal Fuel Property, TEA, or LCA Barriers .....	29
3.1.1 Renewable Diesel Fuel .....	31
3.1.2 Fischer-Tropsch Diesel Fuel.....	33
3.1.3 HTL Fuel Blendstocks Derived from Sewage Sludge, Algae, and Algae/Wood Blends .....	36
3.1.4 Farnesane .....	41
3.1.5 Isoalkanes Derived from Volatile Fatty Acids.....	43
3.1.6 Ethanol-to-Distillate – Isoalkane Blendstock .....	49
3.1.7 Biodiesel (Fatty Acid Methyl Esters) .....	51

3.1.8 Fatty Acid Fusel Esters .....	55
3.2 Top Five Candidates with Fuel Property, TEA, and/or LCA Barriers .....	59
3.2.1 Short-Chain Esters from Oilseed Crops.....	59
3.2.2 Polyoxymethylene Ethers and Derivatives .....	62
3.2.3 4-Butoxyheptane.....	66
3.2.4 Alkoxyalkanoates Derived from Lactate Esters .....	69
3.2.5 Fatty Alkyl Ethers.....	74
3.3 Candidates with substantial life cycle, techno-economic and/or fuel property barriers to adoption determined to be unsuitable for use .....	79
3.3.1 Oligocyclopropanes .....	80
3.3.2 1,1'-Bicyclohexane and 1,1'-Bicyclopentane.....	82
3.3.3 Substituted Cycloalkanes Derived from Myrcene .....	85
3.3.4 <i>n</i> -Undecane .....	87
3.3.5 Long-Chain Linear and Branched Alcohols .....	89
3.3.6 Hexyl Hexanoate.....	93
3.3.7 Dioxolanes .....	94
3.3.8 Oxetanes.....	99
3.3.9 Dipentyl Ether.....	101
<b>4 Conclusions.....</b>	<b>103</b>
<b>5 References.....</b>	<b>104</b>
<b>Appendix A – Analysis Metrics .....</b>	<b>127</b>

## Figures

Figure 1.	Life cycle GHG emissions for a selection of the candidates evaluated in this report. ....	18
Figure 2.	Bioblendstock screening results for technology readiness, economic viability, and environmental impact metrics. ....	19
Figure 3.	MFSP for bioblendstocks derived from TEA results. ....	20
Figure 4.	Potential economic value of MCCI bioblendstocks from primary refinery impact analysis. ....	21
Figure 5.	Exhaust gas dilution sweep from 25%–43% to investigate NO <sub>x</sub> -soot tradeoff for nine fuels at 600 rpm and 3.3 bar gross mean effective pressure (or engine load). ....	23
Figure 6.	Soot/NO <sub>x</sub> tradeoff plot for DFI vs. CDC. ....	24
Figure 7.	Experimental results comparing hot, in-cylinder soot (SINL) for DFI and CDC with three fuels. ....	24
Figure 8.	Top 13 performing blendstocks with the potential to reduce criteria and GHG emissions. ....	30
Figure 9.	Process flow diagram for RD production. ....	32
Figure 10.	RD life cycle GHG emissions and MFSP. ....	32
Figure 11.	Process flow diagram for FT diesel production. ....	34
Figure 12.	FT diesel life cycle GHG emissions and MFSP. ....	34
Figure 13.	Gas chromatograms showing hydrocarbon distributions of HTL oils derived from four feedstocks. ....	37
Figure 14.	Process flow diagram for HTL oil production. ....	38
Figure 15.	Diesel from wet waste-derived HTL bio-oil life cycle GHG emissions and MFSP. ....	39
Figure 16.	Diesel from algae-derived HTL bio-oil life cycle GHG emissions and MFSP. ....	40
Figure 17.	Process flow diagram for farnesane production. ....	42
Figure 18.	Farnesane life cycle GHG emissions and MFSP. ....	43
Figure 19.	Process flow diagram for production of isoalkanes from VFAs. ....	46
Figure 20.	Isoalkanes from VFAs life cycle GHG emissions and MFSP. ....	48
Figure 21.	Process flow diagram for production of an isoalkane blendstock from ethanol. ....	50
Figure 22.	Process flow diagram for production of FAME (biodiesel) from FOG and methanol. ....	53
Figure 23.	Market-average life cycle GHG emissions and MFSP for FAME made from FOG and methanol, showing the variation in market cost. ....	53
Figure 24.	Comparison of FAME vs. FAFE properties for DCN, net volumetric heat of combustion, and CP. ....	57
Figure 25.	Market-average life cycle GHG emissions and MFSP for FAFEs made from FOG and methanol, showing the variation in market cost. ....	58
Figure 26.	Life cycle GHG emissions and MFSP for short chain esters from cuphea oil, using production values for canola oil as a proxy. ....	61
Figure 27.	Life cycle GHG emissions and MFSP for short chain esters from cuphea oil, using estimated production values for cuphea oil. ....	62
Figure 28.	Process flow diagram for production of 4-butoxyheptane from woody biomass. ....	64

Figure 29. Life cycle GHG emissions and MFSP for POMEs. ....	65
Figure 30. Process flow diagram for production of 4-butoxyheptane from corn stover. ....	68
Figure 31. Life cycle GHG emissions and MFSP for 4-butoxyheptane. ....	69
Figure 32. Chemical coupling of lactate esters with fusel alcohols to generate an AOA. ....	70
Figure 33. Structures of AOA ether-esters evaluated for use as MCCI blendstocks. ....	71
Figure 34. Process flow diagram for production of alkoxyalkanoates derived from lactate esters, based on current lactic acid production process. ....	72
Figure 35. Process flow diagram for production of alkoxyalkanoates derived from lactate esters, based on target production process. ....	73
Figure 36. Life cycle GHG emissions and MFSP for alkoxyalkanoates derived from lactate esters. ....	74
Figure 37. The chemical structure of FAEs is similar to fatty acid methyl esters. ....	75
Figure 38. Full property measurements of FAE derivatives and a FAME for comparison. ....	76
Figure 39. Life cycle GHG emissions and MFSP for FAEs produced from soybean oil. ....	78
Figure 40. Life cycle GHG emissions and MFSP for FAEs produced from yellow grease. ....	78
Figure 41. Life cycle GHG emissions and MFSP for FAEs produced from a 60/40 mixture of soybean oil and yellow grease. ....	79
Figure 42. Predicted fuel properties for five oligocyclopropanes. ....	81
Figure 43. Cyclopropanated oligomers produced by aerobic fermentation of sugars showing varying degrees of cyclopropanation. ....	81
Figure 44. Myrcene homo- and hetero-coupled Diels-Alder products. ....	86
Figure 45. Structures of dioxolanes 1–9 referenced in this section. ....	95
Figure 46. Dioxolane peroxide formation and terminal oxidation product. ....	98
Figure 47. Synthetic variants of oxetanes evaluated in this work. ....	100

## Tables

Table 1.	Tier 1 Fuel Property Criteria.....	9
Table 2.	Tier 2 Fuel Property Criteria.....	9
Table 3.	Functional groups potentially appropriate for use as MCCI bioblendstocks. ....	12
Table 4.	Merit table showing MCCI bioblendstocks and their fuel property values. ....	14
Table 5.	Compatibility rating summary for bioblendstocks and common infrastructure elastomers determined via exposure studies. ....	16
Table 6.	Fuel property values for pure 5-ethyl-4-propylnonane and as a 20% blend with fossil diesel. ....	45
Table 7.	Selected measured properties of certification diesel, ETD diesel, and a 15% blend of ETD with the certification diesel for engine testing. ....	50
Table 8.	Properties are summarized for esters of palmitic acid derived from a variety of short chained alcohols. ....	56
Table 9.	Fuel properties measured for two POME mixtures. ....	63
Table 10.	Fuel property values for 4BH as a neat bioblendstock and as a 20% blend with fossil diesel. ....	67
Table 11.	MCCI properties. ....	71
Table 12.	Select fuel properties. ....	84
Table 13.	Comparative fuel properties of Diels-Alder myrcene products.....	85
Table 14.	Fuel property values for <i>n</i> -undecane as a neat bioblendstock and as a 20% blend with fossil diesel. ....	88
Table 15.	Predicted fuel properties of branched, long-chain alcohols.....	90
Table 16.	Mixed alcohol kinematic viscosities measured using the ASTM D445 method and DCN measured using ASTM D6890.....	91
Table 17.	Measured densities and kinematic viscosities for a variety of single alcohols measured at 40°C.....	91
Table 18.	Fuel properties of select dioxolanes. ....	96
Table 19.	Fuel properties of oxetanes shown in Figure 47.....	100

## Abbreviations and Acronyms

BB	dibutyl
BSI	boosted spark ignition
CDC	conventional diesel combustion
CHO	cyclohexanone
CN	cetane number
Co-Optima	Co-Optimization of Fuels & Engines
CPO	cyclopentanone
DBM	dibutoxymethane
DEF	diesel exhaust fluid
DFI	ducted fuel injection
DPF	diesel particulate filters
DNPE	dipentyl-ether
DOE	U.S. Department of Energy
EERE	Office of Energy Efficiency and Renewable Energy
EGR	exhaust-gas recirculation
EPA	Environmental Protection Agency
ETD	ethanol to distillate
FAE	fatty alkyl ethers
FAFE	fatty acid fusel esters
FAME	fatty acid methyl esters
FOG	fats, oils, and greases
FT	Fischer-Tropsch
GDE	gallon of diesel equivalent
GGE	gasoline gallon equivalent
GHG	greenhouse gas
HEFA	hydroprocessed esters and fatty acids
HNBR	hydrogenated nitrile rubber
HTL	hydrothermal liquefaction
LCA	life cycle analysis
LHV	lower heating value
MCCI	mixing-controlled compression ignition
MFSP	minimum fuel selling price
NaOH	sodium hydroxide
NBR	nitrile rubbers

NO <sub>x</sub>	nitrogen oxides
NSC	normalized soot concentration
PAH	polyaromatic hydrocarbons
POME	polyoxymethylene ethers
PNNL	Pacific Northwest National Laboratory
RD	renewable diesel
SCR	selective catalytic reduction
SINL	spatially integrated natural luminosity
TEA	techno-economic analysis
ULSD	ultra-low sulfur diesel
VFA	volatile fatty acid
YSI	yield sooting index

## Scientific Nomenclature

°C	degrees Centigrade
$\Delta H^f$	heat of fusion
$\Delta C_p^{sl}$	heat capacity change upon fusion
μm	micrometers
cSt	centistokes (1 mm <sup>2</sup> /s; measure of kinematic velocity)
gCO <sub>2</sub> e/MJ	grams carbon dioxide equivalent per megajoule
g/L	grams per liter
MJ/kg	megajoules per kilogram (measure of specific energy)
MJ/L	megajoules per liter (measure of energy density)
mm <sup>2</sup> /s	millimeters squared per second (measure of kinematic viscosity)
$P^{Fp}$	flash point
pS/m	pico-siemens per meter
R	gas constant
T	system temperature in degrees Kelvin
MP	melting point temperature
X	molar fraction
γ	activity coefficient

## Executive Summary

### Purpose

Reducing the impacts of medium- and heavy-duty (MD/HD) ground transportation can be enabled by fuel-engine combinations that use lower compression ignition liquid fuels and reduce criteria pollutant emissions. Fuels and blendstocks combined with advanced engine technologies could reduce the cost of ownership and the emission of pollutants, including soot, nitrogen oxides (NO<sub>x</sub>) and greenhouse gases (GHGs), from MD/HD vehicles. This report describes the evaluation and screening of MD/HD mixing-controlled compression ignition (MCCI) biofuel candidates for further development and commercialization. The report is aimed at 1) biofuel researchers looking to better understand options to reduce criteria pollutant and GHG emissions while maintaining efficiency and meeting requirements for engine operability and 2) engine researchers who want to evaluate biofuels that meet diesel fuel properties for their impact on conventional and advanced diesel combustion strategies.

- The Co-Optima tiered screening process was used to efficiently screen thousands of blendstocks using a merit table approach.
- Eight blendstocks—six hydrocarbons and two esters—were identified with the potential to reduce emissions with minimal barriers to adoption.
- One additional ester and four ether blendstocks were determined to have significant potential to reduce emissions with additional research and development required to overcome at least one significant barrier to adoption and use.
- Each of these 13 blendstocks has the potential to be produced at a competitive cost and reduce GHG emissions by at least 60%.
- Co-Optima researchers identified barriers to adoption and key research gaps to be addressed in future research.

The candidates were identified using a two-tier screening process based on fuel properties, followed by analysis to assess cost, technology readiness, and life cycle impacts. The most promising blendstocks fell into three categories: 1) market or near-market biofuels with minimal barriers to market introduction, 2) candidates offering improved properties but with at least one significant barrier to market introduction, 3) biofuels that initially looked promising but were determined to be unsuited for commercial adoption for fuel property or operability reasons.

The Co-Optimization of Fuels & Engines (Co-Optima) team includes experts of nine national laboratories: Argonne National Laboratory, Idaho National Laboratory, Lawrence Berkeley National Laboratory, Lawrence Livermore National Laboratory, Los Alamos National Laboratory, the National Renewable Energy Laboratory, Oak Ridge National Laboratory, Pacific Northwest National Laboratory, and Sandia National Laboratories. The team's expertise includes biofuel development, fuel property testing and characterization, combustion fundamentals, modeling and simulation from atomic scale to engine scale, and analysis including techno-economic analysis and life cycle analysis.

## Approach

Co-Optima researchers used the tiered screening process previously developed to screen potential blendstocks for light-duty transportation. The screening process uses a combination of computational approaches, small volume testing, and generation of larger volumes of promising candidates with no showstopper barriers (e.g., operability, combustion performance, safety, toxicity, etc.) for more detailed screening. Thousands of blendstocks were evaluated with candidates derived from the full range of production pathways (i.e., the fuel properties of which can be found in the Fuel Property Database).<sup>1</sup> While most of the blendstocks were single compounds, several complex mixtures derived thermochemically also were evaluated.

Maximizing operability and minimizing engine-out emissions requires fuels with lower sooting potential, acceptable cetane number (CN), lower pour point, lower cloud point (or freezing point for single molecules), and acceptable energy density. Acceptable fuels must meet all other diesel fuel specifications as outlined in ASTM Standard D975 and have the potential to be made at scale at a cost acceptable to the market with a reduction of at least 60% in GHG emissions relative to petroleum diesel for the neat blendstock (the GHG emissions of the finished fuel is dependent on the blend level of the blendstock). For fermentation-derived blendstocks, lignin valorization to co-products (with at least twice the value of the power and heat derived by burning the lignin) is required to achieve cost targets. Additional blendstock properties including lower sulfur content, lower aromatic content and higher CN may provide some additional value by allowing refiners to blend base fuels which do not currently meet diesel specifications.

## Findings and Top Blendstocks

The eight blendstocks that met the fuel property requirements and have minimal barriers to adoption include six hydrocarbons and two esters. These blendstocks are identified below:

- Hydrocarbons: 1) farnesane; 2) a diesel-boiling-range hydrocarbon blendstock produced via the Fischer-Tropsch process; 3) hydrothermal liquefaction bio-oils derived from sewage sludge, algae, and algae/wood blends; 4) an isoalkane mixture catalytically derived from ethanol, 5) an isoalkane mixture produced by catalytic conversion of volatile fatty acids (VFA) produced from food waste, and 6) hydroprocessed esters and fatty acids (also called renewable diesel).
- Esters: 1) fatty acid methyl esters/biodiesel and 2) fatty acid fusel esters.

One additional ester and five ethers were identified with significant potential to reduce emissions but with at least one significant barrier to adoption and use identified. These blendstocks include short-carbon-chain esters produced from oilseed crops, 4-butoxyheptane, polyoxymethylene ethers and end-exchanged derivatives, a family of alkoxyalkanoates derived from fusel alcohols and lactate esters, and fatty alkyl ethers.

The top 13 blendstocks are shown in Figure ES-1.

---

<sup>1</sup> Fuel Property Database: <https://fuelsdb.nrel.gov/fmi/webd/FuelEngineCoOptimization>. Accessed October 15, 2020.

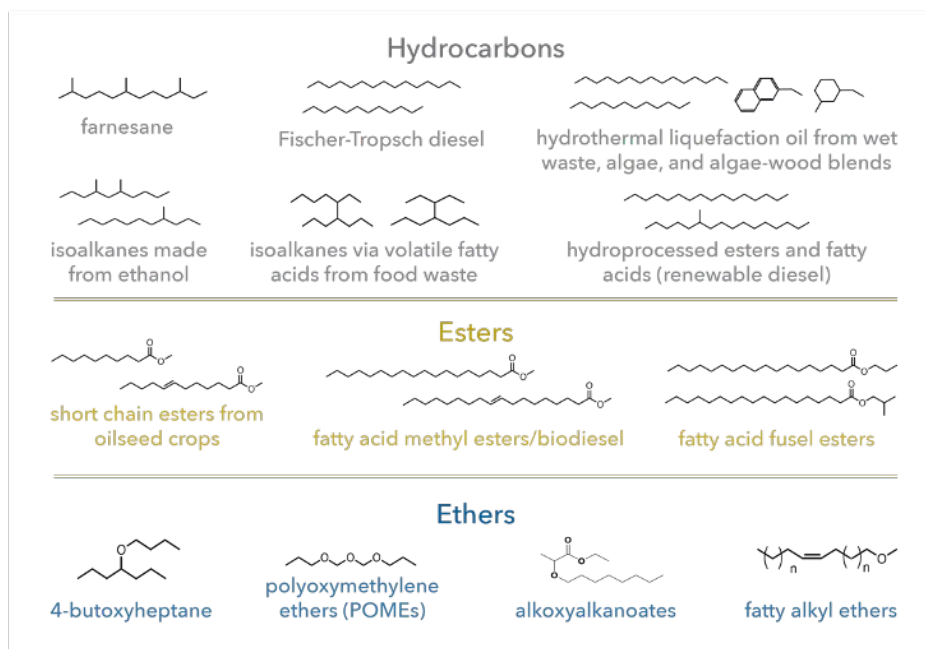


Figure ES1. Top 13 performing blendstocks with the potential to reduce criteria and GHG emissions. The 13 blendstocks comprise 6 hydrocarbons, 3 esters, and 4 ethers.

Many additional candidate blendstocks were evaluated but determined barriers significant enough that the Co-Optima team eliminated them from further consideration. The barriers vary by blendstock. They include high life cycle GHG emissions, low energy density (lower heating value), poor oxidative stability, high projected cost with no alternative production routes identified, incompatibility with infrastructure components, and high water solubility.

Analysis and preliminary experimental results indicate the blendstocks identified have the potential, consistent with industry targets, to increase indicated brake thermal efficiency by up to 1%, reduce particulate matter emissions by 50% to 99% and  $\text{NO}_x$  emissions by 50% to 99%, and are likely compatible with the fuel infrastructure and legacy fleet, while reducing GHG emissions by 62 to 89%.

### Barriers and Challenges

There are challenges for introducing the most promising blendstocks identified by Co-Optima into the market. Foremost, only three (i.e., biodiesel, Fischer-Tropsch diesel, and renewable diesel) are currently allowed in market fuels, although if the hydrocarbon and ester blendstocks meet the diesel and biodiesel specification, respectively, they would likely be able to enter the market relatively quickly. Any new blendstocks would have to go through the normal fuel registration process. Prior to the fuel registration process, fuel system and infrastructure compatibility, impacts on the emissions control system, and health and safety would have to be established. Of course, all blendstocks must meet challenging cost targets to be viable in the marketplace, and the production costs of all early-stage biofuels are higher than petroleum-derived diesel fuel. Deriving additional value through lower sulfur content and higher CN may help provide a market driver. The early stage of research for many of these fuels presents additional technical uncertainty and market risk. Furthermore, the modeled potential GHG reductions must be achieved in practice. Finally, reduced emissions and environmental impacts must be confirmed in multicylinder engine tests.

# 1 Introduction

## 1.1 Purpose

The Co-Optimization of Fuels & Engines (Co-Optima) initiative focuses on developing new high-performance fuels that can boost engine efficiency and reduce emissions when combined with advanced combustion approaches. For medium-duty (MD)/heavy-duty (HD) vehicles, harmful emissions (criteria and greenhouse gas [GHG] emissions) were reduced. Current diesel engines are very efficient (Heggart 2019), with complex emissions control systems engineered to reduce emissions of criteria pollutants, which include nitrogen oxides (NO<sub>x</sub>), particulate matter (PM) including soot and other forms, and unburned hydrocarbons. There is an opportunity to exploit fuel properties and composition to reduce soot and NO<sub>x</sub> emissions and improve operability, particularly by using biomass- and waste-derived fuels that may offer unique properties and lower carbon intensity.

To identify improved fuels, Co-Optima adopted the Central Fuel Hypothesis, which states that by identifying target values for critical fuel properties that maximize efficiency and emissions performance for a given engine architecture, then fuels with those properties (regardless of chemical composition) will provide comparable performance. This approach provides a basis for generalizing knowledge of engine behavior to evaluate potential fuels and their properties. For diesel engines, the efficiency of engine operation is less sensitive to specific fuel combustion characteristics, although changing fuel properties does offer other potential performance advantages as described below. Therefore, this effort focuses on improving operability and reducing emissions (criteria pollutants—specifically PM and NO<sub>x</sub>—and GHGs). These goals are consistent with an industry viewpoint that the most important metrics are total cost of ownership, fuel economy, engine brake thermal efficiency, emissions reductions in PM, NO<sub>x</sub>, hydrocarbons and carbon monoxide, and compatibility with the current infrastructure and the legacy fleet (Deur 2018).

This report identifies the top diesel boiling-range, biomass-derived blendstock candidates for blending with a petroleum-based diesel fuel identified by the Co-Optima initiative. The top candidates are defined as those with 1) the highest potential to improve operability and decrease engine-out emissions while reducing GHG emissions and 2) no large barriers to adoption. Additional identified candidates have analysis gaps, data gaps, or barriers to adoption that additional research and development may address.

## 1.2 Background

Previously, the Co-Optima initiative published the first systematic assessment of the suitability of a broad range of biomass-derived molecules and mixtures across many chemical families for use as boosted, or turbocharged, spark ignition (BSI) blendstocks (Gaspar 2019). Compared to BSI engines, mixing-controlled compression ignition (MCCI) engines already are quite efficient. Furthermore, MCCI engine efficiency is relatively insensitive to changes in fuel properties. However, improvements in emissions and operability can be enabled by changes in fuel properties and composition. Specifically, cold start and overall emissions (PM, NO<sub>x</sub>, and GHGs) and operability, particularly in cold weather, may be improved.

This report describes Co-Optima research aimed at identifying critical fuel properties that can decrease harmful emissions from diesel engines to increase the sustainability of MD and HD transportation vehicles. Past efforts to develop alternative liquid fuels derived from biomass have focused on factors affecting cost including titer, rate and yield, or conversion efficiency and selectivity for biochemical and thermochemical approaches, respectively. The decades of work on biofuels has led to the development and use of ethanol, biomethane, and bio-derived diesel fuels, including fatty acid methyl esters (biodiesel, also known as FAME) and renewable diesel (RD) (and more specifically, RD produced by hydroprocessing esters and fatty acids [HEFA]).

As with the previous Co-Optima effort that focused on BSI fuel-engine co-optimization, these results draw on extensive databases that document key fuel properties and structure-property relationships for many hydrocarbon and oxygenated molecules. This understanding covers unbranched hydrocarbons (n-paraffins), branched hydrocarbons (iso-paraffins), cyclic hydrocarbons (naphthenes), aromatic hydrocarbons, esters, ethers, alcohols, ketones, aldehydes, and carboxylic acids. The behavior of mixtures of classes of hydrocarbons are fairly well understood as is the mixing behavior of some esters. Other oxygenates are less well understood. This report describes Co-Optima's efforts to identify blendstocks that can improve operability and emissions performance (reducing both GHG and criteria emissions such as PM and NO<sub>x</sub>). Co-Optima identified target values of critical fuel properties, blendstocks that exhibit these properties and the potential economic and environmental impacts of their adoption.

The Co-Optima team includes experts in biomass conversion; fuel chemistry, fuel testing, combustion, and engines; and in the development and application of techno-economic analysis (TEA) and life cycle analysis (LCA) models. The team also includes experts with extensive experience in the development of alternative fuels, their co-optimization with engines, and analysis of their economic and environmental impacts.

### 1.3 Research Methodology and Approach

To advance our understanding of the properties of single molecules and mixtures, Co-Optima cast a wide net to identify a range of oxygenates and hydrocarbons suitable for use in an MCCI engine. From the beginning, Co-Optima researchers have posed the following questions:

- What fuel do engines really want?
- What fuel options work best?
- What will work in the real world?

Impacts on soot reduction and other important properties that affect performance (e.g., lower heating value, cold weather performance, water solubility, etc.) were evaluated using Co-Optima's tiered screening approach. The output was visualized using a merit table, and the most promising mixtures and molecules were identified. Co-Optima adapted the tiered screening process developed for BSI blendstocks (McCormick 2017, Gaspar 2018). After fuel property suitability was established through the screening process, TEA, and LCA of promising MCCI candidates were conducted. The approach uses a merit table to visualize how well the candidate blendstocks meet fuel property targets. Fuel properties were measured, both neat and blended with a base Environmental Protection Agency (EPA) certification diesel fuel, using commercial

testing services and capabilities at the participating national laboratories. Various modeling methods were used to estimate fuel properties prior to selecting candidates for testing.

## 1.4 Overview of Content

The rest of the report is organized as follows: Section 2 details the fuel property targets aimed at reducing emissions and improving operability (Section 2.1), the fuel property-based screening process (Section 2.2), the candidate blendstock chemistries (Section 2.3), and the results of the screening process applied to the candidates (Section 2.4). Section 2.5 describes the assessment of potential impacts of and barriers to market adoption. Section 2.6 summarizes the results of engine testing of blends of candidate blendstocks with petroleum diesel, and while the technical summary in Section 2.7 wraps up the description of our approach.

For top-performing blendstocks, summaries of the fuel chemistry and properties, production from biomass, TEA and LCA results, and challenges, barriers and research and development (R&D) needs are organized into three groups in Section 3. These groups describe our assessment of the candidates as follows:

1. Those meeting fuel property requirements and TEA and LCA targets with minimal barriers to adoption (Section 3.1)
2. Those with promising fuel properties but one or more significant barriers to adoption (Section 3.2).
3. A set of promising blendstocks whose barriers to adoption were determined to be great enough to warrant exclusion (Section 3.3).

## 2 Fuel Properties, Candidate Identification, and Blendstock Screening

This section describes Co-Optima's motivation for reducing emissions and improving operability, the resulting fuel properties, their target values, and the screening process deployed. The impacts of soot formation in diesel engines are described, along with a summary of soot formation processes. The tiered screening process and the target values of the critical fuel properties are described, along with the use of structure-property relationships developed in Co-Optima and elsewhere to estimate fuel properties prior to synthesis and fuel property testing. Compatibility assessments are described, as well. This section then summarizes the TEAs, LCAs, and refinery impact analyses that were performed to ascertain which blendstocks have the best market and environmental impact potential. Finally, this section describes the results of engine testing, using both conventional diesel combustion (CDC) and ducted fuel injection (DFI), aimed at understanding the potential impacts of using advanced biofuel blends developed by Co-Optima.

### 2.1 Target Fuel Properties

Co-Optima has determined that the biggest opportunities for fuel-engine co-optimization are through improvements in increased cetane number (CN), cold-weather operability (CRC 2016) (cloud point/freezing point and pour point), and in-cylinder soot emission reductions, while increasing, or at least minimizing reduction, in fuel energy content (lower heating value [LHV]). Reducing in-cylinder soot generation and emission may be accomplished through modest increases in CN (Kurtz and Polonowski 2017), particularly during cold-start, reductions in fuel soot-forming propensity (Co-Optima has used yield sooting index [YSI]) (McEnally and Pfefferle 2011] as the measurement method to compare the sooting tendencies of fuels), and development of modified combustion approaches (e.g., DFI). The formation of soot and NO<sub>x</sub> is covered in detail in Section 2.1.1.

Cetane number is a measure of the reactivity or ignitability of the fuel. Cetane number is measured in a single cylinder, continuously variable compression ratio Cooperative Fuel Research (CFR) engine. More commonly, a derived cetane number (DCN) is determined by measuring ignition delay using a constant volume vessel such as an ignition quality tester, fuel ignition tester or advanced fuel ignition delay analyzer, the output of which can be empirically related to the CN scale. The minimum CN required for a market fuel depends on location, ranging from 40 (the lowest in the United States) to 53 (in California). Co-Optima targeted a minimum of 40, with higher values expected to add value in some markets and under some conditions.

Cold-weather operability improvements are aimed at eliminating barriers to use in colder climates (Lanjekar and Deshmukh 2016, CRC 2016). These improvements entail reducing the cloud point, pour point, and freezing point to below the ASTM D975 fuel specification. The use of FAME biodiesel currently is limited due to potential for crystallization of saturated components out of the fuel at lower temperatures, depending on the feedstock characteristics, as detailed in Section 3.1.1. Co-Optima researchers sought blendstocks whose use would not be limited geographically or seasonally.

Finally, energy density is critically important to owners and operators. Energy density is the amount of energy stored in the fuel as a function of volume (or mass, for specific energy). The energy density is reduced by decreases in liquid density and by the number of oxygen atoms (which reduces the number of hydrogens and therefore the number of exothermic carbon-oxygen and hydrogen-oxygen bonds formed during combustion). Another way to increase energy density is to include strained rings such as cyclopropane, cyclobutane or strained fused rings (as in exo-tetrahydrodicyclopentadiene, the primary constituent of JP-10) that release significant energy when the bonds are broken. Increasing energy density beyond the energy density of petroleum diesel is difficult. The energy density of petroleum diesel fuel is approximately 42 MJ/kg (Bacha 2007, Alternative Fuels Data Center 2021), although the specific energy of petroleum diesel can vary and values as high as 45 MJ/kg can be found. The highest predicted energy density of any of the blendstocks pursued by Co-Optima was 47 MJ/kg (for one of the larger oligocyclopropane molecules). In any event, minimizing reductions in energy content for oxygenates or hydrocarbons helps to maintain lower operating expenses, which is the most important metric for commercial transportation.<sup>2</sup>

The motivation behind minimizing engine-out soot emissions arises from the coupling of soot emissions to owning and operating expenses through efficiency, NO<sub>x</sub> emissions, emissions controls, and engine durability. In most diesel applications, fuel is the primary operating expense. Therefore, higher efficiency means that the same amount of work can be done with less fuel and cost. Nevertheless, reducing NO<sub>x</sub> emissions also is important because they are expensive to mitigate, and engine durability affects maintenance costs and system uptime. Lower engine-out soot emissions can enable lower owning and operating expenses as described below.

### 2.1.1 Impacts of Soot on Engine Operation

*Efficiency* – Many modern diesel engines are equipped with diesel particulate filters (DPF) to attenuate tailpipe soot emissions to within legislated limits. Soot emissions can be problematic especially under transient operating conditions. Excessive soot emissions can lead to an increased pressure drop across the DPF due to excessive soot loading, which is one cause of lower engine efficiency (Sing 2009). When this happens, a forced DPF regeneration is required to oxidize the soot that has accumulated in the DPF and to reduce its pressure drop back to an acceptable level. A forced regeneration is accomplished by burning fuel with the primary objective of producing heat rather than shaft work. This raises the DPF temperature to a point where soot oxidation can occur, which cleans the DPF to some extent, but burning fuel for heat rather than work is a second cause of lower engine efficiency. Third, the mere presence of a DPF introduces a back pressure that can negatively impact efficiency, a problem that grows as non-regenerable ash builds up in the filter over time (Sappok 2009, Sappok and Wong 2010).

*NO<sub>x</sub> emissions* – In addition to fuel costs, another major operating cost is diesel exhaust fluid (DEF), which is used to curtail tailpipe NO<sub>x</sub> emissions via selective catalytic reduction (SCR) (Ou 2019). To minimize DEF costs, engine manufacturers seek to minimize engine-out NO<sub>x</sub> emissions, but this is challenging because high-efficiency operation usually results in engine-out

---

<sup>2</sup> Co-Optima has used gasoline gallon equivalent (GGE, sometimes written gge) to normalize the cost or GHG emissions of a blendstock. Using GGE instead of diesel gallon equivalent (DGE or dge) or gallon of diesel equivalent (GDE or gde) permits a direct comparison on an energy basis with other analyses for gasoline blendstocks. The average energy density of gasoline is about 0.904 times the average energy density of diesel.

NO<sub>x</sub> emissions that far exceed legislated limits. On the positive side, for such steady-state, high-efficiency operation, soot emissions usually can be brought into compliance with a DPF that regenerates continuously (i.e., forced regenerations are not required). This is the current state-of-the-art for on-road vehicles, but SCR systems have high up-front costs, induce an additional back-pressure penalty, and DEF consumption rates with this approach can be high (Ou 2919). One alternative to SCR for NO<sub>x</sub> control is charge-gas dilution via exhaust-gas recirculation (EGR). This approach is highly effective at reducing engine-out NO<sub>x</sub> which can reduce the SCR and corresponding DEF requirements. A major challenge is that increased dilution through EGR increases soot emissions. This is commonly called the “soot-NO<sub>x</sub> tradeoff.”

*Durability* – Under many CDC operating conditions, a large amount of soot is produced within the combustion chamber. Most of this soot is subsequently oxidized before the exhaust valves open, leading to manageable engine-out soot emissions. Nevertheless, some fraction of the soot produced within the combustion chamber deposits on the cylinder liner, piston rings, and other in-cylinder surfaces due to thermophoresis. These soot particles are abrasive, and they accumulate in the engine lubricating oil, where they contribute to accelerated wear and the potential premature failure of all lubricated components.

*Advantages of low-soot combustion* – A low-soot fuel and combustion system can help in all three areas discussed above: efficiency, NO<sub>x</sub> emissions, and durability. It can improve efficiency by lowering the rate of DPF soot loading and minimizing the number of forced regenerations. Eliminating the DPF is unlikely, as it is sized for the ash content of the exhaust. The low-soot fuel and combustion system can enable greater use of EGR for NO<sub>x</sub> control. This would lower initial SCR system costs as well as operating expenses by decreasing DEF consumption (the rate of which is proportional to engine-out NO<sub>x</sub> emissions) (Ou 2919). EGR also is effective at lowering NO<sub>x</sub> emissions at cold-start and light-load conditions where an SCR catalyst is ineffective because light-off temperature cannot be maintained. Finally, a low-soot fuel and combustion system could enhance engine durability and uptime while lowering maintenance costs by minimizing the deposition rate of soot in the lubricating oil.

Co-Optima has taken a two-pronged approach to exploit potential fuel-engine cooperative effects: use of renewable, low-sooting fuels in CDC and in new combustion approaches such as DFI. The fuels aspect of the effort is described in detail in the rest of this report.

### 2.1.2 Soot Formation in Diesel Combustion

In MCCI combustion, the fuel is injected into hot compressed air and almost immediately (i.e., <1 millisecond) ignites because of the fuel’s high reactivity (ensured by the requirement of a minimum CN). Combustion rates in this ignited fuel spray are limited by rates of fuel mixing with the air. Soot forms in fuel-rich, oxygen-poor regions of the spray; therefore, soot formation is affected by spray parameters such as injection pressure and the physical properties of the fuel; that is, better fuel-air mixing results in lower soot formation. Most of the soot formed is later consumed by diffusion combustion as it mixes with the remaining excess air at high temperatures (soot burnout). Engine operation strategies that increase peak cylinder temperature or oxygen concentration, such as advanced injection timing or boost, increase the amount of soot burnout and reduce engine-out soot emissions. On the other hand, strategies that reduce temperature or

oxygen, such as retarding injection timing or exhaust gas recirculation, increase engine-out soot emissions. Apart from spray physics and engine operation conditions, the formation of soot particles involves both chemical reactions and physical processes: 1) formation of aromatic and polyaromatic hydrocarbons (PAH), 2) nucleation of primary soot particles, 3) growth of the primary particles, and 4) particle agglomeration (Frenklach 2002, Richter and Howard 2000, Raj 2014).

*Chemical soot formation tendency of the fuel* – The molecular structure of the fuel controls the rate of formation of the first aromatic ring and subsequent PAH so different fuels can produce different amounts of soot. A review outlines many of the pathways proposed for the formation of the first aromatic ring for different types of hydrocarbon molecules (Richter and Howard 2000); however, the mechanism of aromatic ring formation is not well understood for most oxygenates. The hydrogen abstraction-acetylene addition mechanism is the major pathway for PAH ring growth (Frenklach 2002, Frenklach 1985). This is a two-step reaction sequence with aromatic radical formation by hydrogen abstraction followed by acetylene addition. Ring-ring condensation reactions also can occur as PAH concentrations increase (Unterreiner 2004).

Because of the key role of molecular structure in soot formation, several methods have been developed to assess the chemical soot formation tendency of individual molecules and complex fuels. The smoke point (ASTM Standard D1322-19) was introduced in the 1930s and is a measure of the maximum height of a diffusion flame that can be achieved without producing soot. Smoke point measurements exhibit apparatus-dependent flame heights, which led to the introduction of the Threshold Sooting Index (Calcote and Manos 1983) to compare data from different laboratories. The Oxygen Extended Sooting Index was developed to scale smoke point measurements while considering the reduced stoichiometric air required for oxygenate combustion (Barrientos 2013). This research demonstrated that fuel organic oxygen content is not sufficient to predict the sooting tendency of a molecule and that subtle variations in molecular structure can have large effects.

The YSI applies optical methods to measure soot volume fraction in a flame and has been used to quantify the soot formation tendency of hundreds of compounds (McEnally and Pfefferle 2007, Das 2017, McEnally 2017, McEnally 2018). Studies of the YSI of oxygenates were the first to indicate that some oxygenate functionality may increase sooting tendency (McEnally 2011) relative to similar hydrocarbon molecules. YSI is used by many groups, including Co-Optima researchers, as a fuel-ranking metric for the chemical tendency to form soot.

*Factors that affect mixing and fuel evaporation in MCCI combustion* – Fuel molecular structure is the source of fuel physical properties; hence, it indirectly affects the degree of mixing occurring in the fuel spray. Fuel physical properties such as density, viscosity, surface tension, heat capacity, heat of vaporization, and volatility are known to affect spray development and atomization-spray properties such as liquid penetration length, lift-off length, spray cone-angle, mean droplet diameter, and turbulent intensity (Kim 2016, Som 2010).

Many of these dependencies of fuel physical properties on spray development can be linked to their impact on flow development inside a fuel injector (Torreli 2017, Magnotti and Som 2019, Som 2010). Using computational fluid dynamics simulations, researchers have explored the impact of fuel properties on internal flow development, either through controlled parametric

variations in selected fuel properties or through comparisons of selected fuels, such as conventional diesel fuel with biodiesel (Som 2010) or gasoline-like (Torelli 2017) fuels. These studies have shown that differences in fuel mass delivery can be largely attributed to differences in liquid density, with minor effects due to differences in liquid viscosity. Cavitation has been the focus of much of the analysis due to experimental observations that link changes in spray behavior (e.g., enhanced atomization, wider spray spreading angle, etc.) with the occurrence of cavitation. In general, liquid viscosity and vapor pressure have been noted to influence the propensity of cavitation in which decreases in viscosity and increases in the saturation pressure are found to promote cavitation formation.

*Engine Operating Parameters Effect on Soot Formation and Burnout* – The most important engine operating parameter affecting fuel-air mixing rates (and thus soot formation) is the injection pressure. The higher the injection pressure, the higher the flow rate of fuel into the cylinder, and the higher the rate of fuel-air mixing that can occur during the brief period before combustion begins. This period of ‘ignition delay’ of <1 ms is not long enough for all the fuel to be injected in most high-load conditions, and thus the initial autoignition will light a rich premixed flame on the still-incoming fuel/air jet. Compared to the autoignition, this flame will reach hotter temperatures and burn at higher local fuel/air ratios, both of which will increase soot formation. Thus, it is desirable to inject as much of the fuel as possible during the ignition delay, although too much can lead to high pressure rise rates, which increase engine noise (i.e., diesel knock) and can damage the engine.

The engine’s in-cylinder conditions in terms of bulk temperature, pressure, gas motion, and oxygen concentration can influence soot formation rates. However, because soot formation in CDC is largely inevitable, these conditions are optimized more to maximize soot burnout than minimize soot formation. These conditions are largely dictated by the engine design, speed/load condition, and fuel, but there are a few operating parameters that can make these conditions more beneficial to soot burnout. One such parameter is the start of injection timing, with earlier (“advanced”) injections increasing the temperature and pressure during soot burnout, and later (“retarded”) injections doing the opposite.

## 2.2 Tiered Screening Process to Evaluate Target Values of Critical Fuel Properties

Co-Optima used a tiered screening process to evaluate candidate bioblendstock fuel properties. The two tiers were split into fuel properties measured for a neat blendstock (Tier 1) and those measured as a blended fuel (Tier 2). As described in the previous section, fuel properties selected for valuation in Tier 1 have the potential to improve performance (CN, YSI, melting point (MP), and freezing point/cloud point) or must be maintained to prevent degraded performance (LHV, flash point, water solubility). Tier 2 fuel properties focused on determining whether a given blendstock could meet the requirements as described in the diesel fuel standard (ASTM D975) when blended into a diesel base fuel. These requirements are listed in Table 1 and Table 2.

Table 1. Tier 1 Fuel Property Criteria.

Fuel Property	Greatly Exceeds	Exceeds Criteria	Meets Criteria
Lower heating value (MJ/kg)*	>40	31 to 40	25 to 30
CN	>50	46 to 50	40 to 45
Flash point (°C)	>70	61 to 70	52 to 60
MP (°C)	<-50	-50 to -26	-25 to 0
Water solubility (g/L)	<0.05	0.05 to 0.99	1 to 20
YSI	<50	50 to 149	150 to 200

Table 2. Tier 2 Fuel Property Criteria.

Fuel Property	Meets Criteria
Distillation T90 (°C)	<338
Flash point (°C)	≥52
Cloud point (°C)	<0
Kinematic viscosity (cSt @ 40°C)	1.9 to 4.1
Lubricity (μm)	≤520
Conductivity (pS/m)	≥25
Oxidation stability (min)	>60
Blending cetane	≥40

## 2.2.1 Prediction Tools

The MCCI properties considered in this study may be measured with an associated ASTM protocol that leads to an accurate measured value. However, these do not readily lend themselves to high-throughput, low-cost evaluations. Computational models offer a route to accurate, and quick predictions of these physical properties, without the need to synthesize promising, but unproven, MCCI fuel candidates. Several computational techniques have been developed and deployed in Co-Optima to screen MCCI blendstock candidates either as pure components or blends, or both.

*Energy density/specific energy* – Ab initio quantum mechanics calculations yield accurate energetics of molecules. When coupled with an appropriate equation of state, accurate predicted energy densities and specific energies can be obtained. The CBS-QB3 method has been used as the quantum mechanics method of choice and has been successfully implemented for molecules containing up to ~60 atoms.

*Cetane number* – A number of CN prediction tools have been developed within Co-Optima. One such tool developed by Co-Optima researchers (Whitemore 2016), is based on the eXtreme Gradient-Boosted decision tree model, which yields absolute errors of roughly 10.7 CN units. The limited amount of data above a CN of 80 limits the accuracy of this tool, leading to underpredicted values for CNs that are >80. However, molecules with a CN <80 are predicted with greater accuracy. Another prediction tool developed by Co-Optima researchers<sup>3</sup> using a different machine-learning approach features a Maximum Average Error of ~8 cetane units. While the approaches outlined above predict neat molecules, other work by Co-Optima

<sup>3</sup> P St. John, YJ Kim, JY Cho, and S Kim. Unpublished work.

researchers (Heredia-Langner 2020) has used statistical models of  $^{13}\text{C}$  nuclear magnetic resonance spectra to predict CN for complex mixtures. This method uses a set of regressions based on 27 different regions within the spectra. These regressions help to correlate each structural sub-group to the CN. Using these correlations, this model is able to predict CN, usually to within the accepted reproducibility of DCN measurements. One advantage of this method is that it requires only 200  $\mu\text{L}$  of sample.

*Melting point* – Accurate methods for predicting the MP of pure components remains a challenge. Several group contribution methods have been developed over the past decades, but none give consistently accurate predictions (Marrero and Gani 2001, Joback and Reid 1987, Yalkowsky and Alantary 2018). However, an accurate solid-liquid equilibrium equation for the MP of complex, multi-component systems has been previously derived. This equation (Eq. 1) requires the MP,  $T_m$ , heat of fusion,  $\Delta H^{sl}$ , and heat capacity change upon fusion,  $\Delta C_p^{sl}$  for each component in the system (Poling 2001). In addition, R is the gas constant, T is the system temperature in degrees Kelvin,  $\chi$  is the molar fraction, and  $\gamma^l$  is the activity coefficient. In practice, the heat capacity term can be neglected with minimal loss of accuracy. Analyzing over 400 binary mixture data points from the literature, the solid-liquid equilibrium equation is accurate with an average absolute deviation of 2.8°C.

$$x_k \gamma_k^l = \exp \left\{ \left( \frac{\Delta H_k^{sl}}{RT_{mk}} \right) \frac{T - T_{mk}}{T} + \frac{\Delta C_{pk}^{sl}}{R} \left[ \ln \left( \frac{T}{T_{mk}} \right) - \frac{T - T_{mk}}{T} \right] + \frac{l}{1} \right\} \quad (\text{Eq. 1})$$

*Flash point* – The flash point of single molecules can be estimated from the boiling point (Carroll 2011) and the chemical structure. Accurate relationships for the flashpoint of complex, multicomponent systems also are available. The most accurate, and widely used relationship is Liaw's law, which is shown in Equation 2 (Liaw et al. 2002). Liaw's law depends on the vapor pressure of each pure component at its flashpoint,  $P_{Flash\ point}$ , as well as the vapor pressure of the entire system,  $P_s$ . With the proper choice of an equation of state, these vapor pressure terms can be determined. Liaw's law has been successfully applied to systems of MCCI importance, such as FAME and their analogues.

$$\sum_i \frac{\chi_i P_i}{P_{Flash\ point}} = 1 \quad (\text{Eq. 2})$$

*YSI* – YSI quantifies the tendency of a molecule to form soot when added to a methane-air flame and has been used by Co-Optima researchers to rank fuels in terms of chemical sooting tendency. A group contribution model based on data for over 400 pure compounds can accurately predict YSI. The model decomposes each compound into single-carbon atom fragments and using regression against the 400 plus compound database assigns a sooting tendency contribution to each fragment. An online tool for predicting YSI from a molecule's SMILES string is available (St. John 2017).

*Viscosity* – One of the most accurate approaches to predicting the viscosities of MCCI fuels is the SUPERTRAPP method (Ely and Hanley 1981, Huber and Hanley 1996), where the measurements of the fluid of interest are correlated to a known fluid measured at the same thermodynamic state. The SUPERTRAPP method is based on the idea of extended corresponding states, which notes that two fluids will behave similarly if they are measured

at the same reduced thermodynamic point ( $T_r$ ,  $P_r$ ,  $\rho_r$ ). It relies on a reference fluid for which accurate thermophysical data is available. The relevant equation governing the SUPERTRAPP method can be written as follows:

$$\eta_{mix}(\rho, T, X) = \Delta\eta^{Enskog} \eta_0(\rho_0, T_0) F_\eta \quad (\text{Eq. 3})$$

where the subscript mix refers to the fluid of interest, and the subscript 0 refers to the reference fluid, which in this case is propane. Accuracies for pure components are generally within 15%, when compared to experimentally measured values.

## 2.2.2 Compatibility Assessment Approach

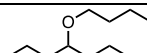
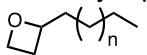
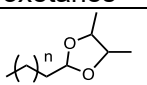
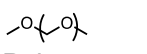
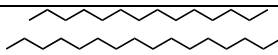
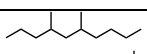
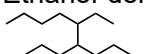
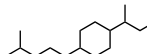
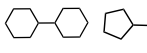
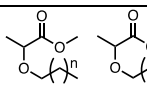
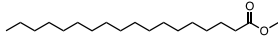
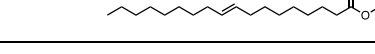
Assessing the compatibility of fuels and materials was accomplished through controlled exposure studies. Fuel compatibility efforts focused on polymeric materials because hydrocarbons and diesel boiling range oxygenates are not known to directly cause corrosion of metals because they are not highly acidic and do not contain water (Kass 2018). However, corrosion can happen if the fuel molecular structure degrades to a more acidic structure or via microbial action (Kass 2018, Christensen and McCormick 2014, Zukleta 2012). The impacts to infrastructure polymers are less clear and exposure tests must be performed. A solubility analysis (such as the common Hansen solubility parameters approach) (Hansen 2007) also is useful for predicting compatibility based on mutual solubility.

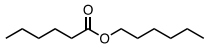
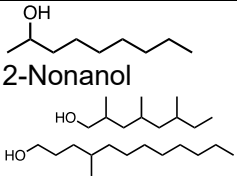
Exposure studies and solubility analyses were performed on elastomer materials common to fuel storage and delivery systems (Kass 2011, Kass et al, 2020). Blendstocks evaluated include a relatively broad spectrum of promising molecules that encompassed a full range of chemistries of interest. They included 1-octanol, 1-nonanol, butylcyclohexane, methyl decanoate, hexyl hexanoate, di-isobutylene, a methyl- and dimethyl furan mixture, tri(propylene glycol) methylether, ketones, a dioxolane mixture, 4-butoxyheptane, biodiesel, and RD. A total of 17 elastomer materials were evaluated for volume swell and hardness change. This list includes materials such as fluoroelastomers, nitrile rubbers (NBR), hydrogenated NBR (HNBR) and NBR blends with polyvinyl chloride, but also legacy materials such as epichlorohydrin. The blendstocks were miscible with diesel and evaluated as blends (up to 30 wt%).

## 2.3 Candidates

Co-Optima examined a full range of chemistries that can be derived from biomass and used as blendstocks or fuels for MCCI combustion. Building on the large body of work for hydrocarbons and reasonably extensive body of work for some materials (e.g., FAMEs, other long-chain esters, ethers, alcohols), Co-Optima researchers have identified some new chemistries in these and other molecular classes. By analyzing diesel fuel requirements, previous work in Co-Optima and elsewhere, and information from the literature, Co-Optima researchers determined the chemistries shown in Table 3 are most suitable for use as MCCI blendstocks. Although initially included in Co-Optima research, ketones were determined in the course of this research to be incompatible with elastomers found in the fuel distribution and storage system; therefore, they were eliminated from further consideration (see Section 2.4.2) and are not included in this table. Other chemistries, such as aromatic hydrocarbons, aldehydes, carboxylic acids, were ultimately determined to be unsuitable for use as diesel blendstocks.

Table 3. Functional groups potentially appropriate for use as MCCI bioblendstocks.

Functional Group	Suitability	Potential Advantages/Shortcomings	Examples
<b>Ethers</b>			
<i>mono-ethers</i> <b>R-O-R'</b>	Very good	Pros: Very high autoignitability. CN depends upon branching.  Cons: Stability; peroxide forming; materials compatibility.	 4-butoxyheptane  oxetanes
<i>polyethers</i> <b>R-(O-R')<sub>n</sub>-R''</b> where n=2-10	Very good	Pros: Very high autoignition propensity. Potential for reduced emissions. CN depends upon branching.  Cons: Possible hydrolysis under mild aqueous acid conditions. Cost. Some ethers are toxic.	 Dioxolanes  Polyoxymethylene ethers
<b>Alkanes (saturated aliphatic hydrocarbons)</b>			
<i>n-alkanes</i> <b>CH<sub>3</sub>-(CH<sub>2</sub>)<sub>n</sub>-CH<sub>3</sub></b> where n=6-18	Excellent	Pros: Outstanding diesel with high CN increasing with chain length (e.g., hexadecane CN =100).  Cons: High freezing point.	 Wet waste-derived HTL oils
<i>iso-alkanes</i> <b>R-CH-R'R''</b>	Excellent	Pros: Branching can improve cold flow properties.  Cons: Highly branched species exhibit lower CN	 Ethanol-derived isoalkanes  5-Ethyl-4-propylnonane and related
<i>cyclic alkanes/naphthenes</i> <b>C<sub>n</sub>H<sub>2n</sub> (saturated); C<sub>n</sub>H<sub>2n-2</sub> (unsaturated)</b>	Fair	Pros: Substituted naphthenes may exhibit good cetane (1-methyl-3-dodecylcyclohexane ~70)  Cons: Low cetane for unsubstituted naphthenes (decalin ~36). Increased sooting tendency.	 Myrcene-derivatives  Di-cyclohexanes and di-cyclopentanes  Oligocyclopropanes
<b>Esters</b>			
<i>methyl and other esters of fatty acids</i>	Excellent	Pros: Good cetane for higher carbon number compounds. Improved lubricity. Saturated and mono-unsaturated desirable. Currently used as biodiesel, up to 20%. CN depends upon branching.	 Alkoxyalkanoates (AOAs)  

		Cons: Potential cold flow problems. Poly-unsaturated have lower CN and oxidation stability issues. Water solubility/hygroscopicity can limit infrastructure compatibility.	Fatty acid methyl esters (biodiesel)  Hexyl hexanoate
<b>Alcohols</b>			
<i>mono-functional alcohols</i> <b>R-OH</b>	Good	Pros: Acceptable CN for n-alcohols with ~C8 and higher; longer chains behave more like alkanes. CN depends upon branching and chain length.  Cons: Water solubility/hygroscopicity may be high. CN is marginal especially for C8–C10 (38–42); infrastructure compatibility comparable to esters. MP may pose issues with n-alcohols (iso-alcohols have lower MP). Viscosity is high.	 2-Nonanol  Mixed branched primary alcohols

## 2.4 Screening Results

### 2.4.1 Merit Table

As a quantitative merit function like the one used for BSI blendstocks could not be developed for MCCI bioblendstocks, a merit table (Table 4) was constructed to enable a visual evaluation of the performance of the fuels that passed the Tier 1 screening. For many of the blendstocks evaluated, select properties were predicted prior to any fuel property measurements. This enabled researchers to focus on the most promising chemistries. The color-coded merit table allows ready visualization of trends for given classes of molecules. Orange denotes that a candidate meets criteria, blue that it exceeds requirements, and green that it greatly exceeds the required values. For select bioblendstocks, N/A indicates fuel property data was not collected because of sample or volume constraints. Tables 1 and 2 show the fuel property criteria used for screening.

All of the molecules in the merit table show promise based on Tier 1 criteria. Of the entire suite of molecules evaluated to date, 20 exceed or greatly exceed the Tier 1 criteria in all categories where the data is available. About half of these molecules (or classes of molecules) were discovered in the current evaluation, thus demonstrating the importance of an iterative process in conducting fuel screening in which information gained is used to inform subsequent molecule selection and testing. In this list were chemical functionalities that included 10 hydrocarbons, 5 esters, 6 ethers, and 2 alcohols.

Table 4. Merit table showing MCCI bioblendstocks and their fuel property values. Refer to Table 1 for target values. Blendstocks in table meet the Tier 1 screening criteria. HEFA = hydroprocessed esters and fatty acids; HTL = hydrothermal liquefaction; FAME = fatty acid methyl esters; POME = polyoxymethylene ether; LHV = lower heating value; CN = cetane number; YSI = yield sooting index.

MCCI Bio-Blendstocks		LHV	CN	Cloud/ Melting Point	Flash Point	Water Sol	YSI	Greatly exceeds or exceeds criterion	#
Section 3.1	Renewable diesel/HEFA (mixture)	44.1	>70	-5 to -34	>61	<0.1	-	Meets criterion	#
	Fischer-Tropsch diesel (mixture)	44	>70	-5 to -30	>61	<0.1	-	Does not meet criterion	#
	HTL oil from wet waste, algae, wood/algae (mixture)	42 to 44	40 to 48	-10 to 20	>55	<0.1	-	Not measured or predicted	-
	Farnesane	43.3	58.6	-73	110	<0.1	110		
	Isoalkanes from volatile fatty acids (mixture)	44	48 to 73	-53 to -30	62 to 74	<0.1	-		
	EtOH-to-isoalkanes (mixture)	43.8	55 to 68	-60	>54	<0.1	-		
	Biodiesel/FAME (mixture)	37.5	>47	-5 to 15	>93	<0.1	-		
Fatty acid fusel esters (mixture)	40 to 41	50 to 60	<-10	>130	<0.1	104 to 127*			
Section 3.2	Short chain esters, oil seed crops (mixture)	34	52	-18	111	<0.1	50*		
	POMEs (series)	19 to 30	73 to 75	<0	62 to 63	0.5 to 2.98	2 to 37		
	4-Butoxyheptane	39	80	<-80	64	<0.1	58		
	Alkoxyalkanoates (series)	25 to 37	26 to 83	<-10	65 to 117	<0.1*	22 to 144		
	Fatty alkyl ethers (series)	41 to 42	74 to 104	-5 to -16	>150	<0.1	163 to 198		
Section 3.3	Oligocyclopropanes (series)	43 to 47*	28 to 58*	-	-	<0.1*	-		
	Bicyclohexanes/ bicyclopentanes	34 to 42	42 to 48	-60 to -100	53 to 92	<0.1	110		
	Derivatives of myrcene (series)	42 to 43	43 to 58	<-40	88 to 150	-	131 to 187		
	n-Undecane	44.2	71	<-26	65	<0.1	65		
	Long chain linear & branched alcohols	>40	22 to >50	-19 to -41*	>96	-	36 to 69*		
	Hexyl hexanoate	34.8	40	-55	99	<0.1*	61*		
	Dioxolanes (series)	28 to 34	33 to 91	<-100	32 to 70	-	36 to 69		
	Oxetanes (series)	37 to 39*	55 to 63*	<-100	-	<0.1*	52 to 90*		
Dipentyl ether	39	111	-69	57	<0.1	44			
Representative structures selected for mixtures and series of molecules		* Predicted - Not measured Color based on limiting value for ranges							

Lower heating value, or energy density is important to commercial users because higher energy density increases vehicle range between refueling events. The merit table shows that the hydrocarbon bioblendstocks all had gravimetric energy densities in the range of 31–40 MJ/kg, with 5-ethyl-propylnonane being notable as it greatly exceeds the >40 MJ/kg criterion at 44 MJ/kg (comparable to petroleum-derived diesel fuel). Promisingly, a number of oxygenated bioblendstocks that span ester, ether, and alcohol chemical functionalities also exceed the energy density criterion due to their long aliphatic side chains. Short-chain esters derived from oilseed crops and the smaller POMEs were the only bioblendstocks that just met the LHV criterion (25–30 MJ/kg) with a heating value of 29.6 and 19–30 MJ/kg, respectively.

Higher CNs may decrease cold start emissions (Kurtz and Polonowski 2017), with ethers generally greatly exceeding criteria (CN >50). All ethers except for the smaller of the multifunctional AOA ether-esters had CNs above 60, with dipentylether and 4-butoxyheptane both >70. All the hydrocarbon bioblendstocks displayed CNs that greatly exceed criteria, except for 5-ethyl-propylnonane (CN = 48). Of the esters, soy biodiesel and short-chain esters derived from oilseed crops also greatly exceed the CN criterion due to their long aliphatic chains, while hexyl hexanoate only met the CN criterion with a CN of 40 due to its ester functionality in the middle of the molecule that interrupts the methylene chain. Finally, 2-nonanol also met criteria (CN = 40) due to the alcohol functional group that generally reduces CN for a given chain length relative to a hydrocarbon with an equivalent carbon number and conformer structure.

Melting points correlated well with bioblendstock molecular structure, as highly branched molecules were identified that greatly exceed criteria (MP  $\leq$  -50°C) and have potential for improving cold flow properties in the blend. Highly branched hydrocarbons included farnesane (MP = -73°C) and 5-ethyl-4-propylnonane (MP < -80°C). Ethers displayed weaker intramolecular forces, with the linear molecules butylal (MP = -58°C) and dipentyl ether (MP = -69°C) greatly exceeding criteria, as well as several of the branched dioxolanes. Among the esters, the long aliphatic side chains of biodiesel and short-chain esters derived from oilseed crops raised the MP to only meet criteria (MP = 0 to -25°C), while hexyl hexanoate greatly exceeds the criterion (MP = -55°C) due to its shorter side chain and ester functionality in the center of the molecule. It should be noted predictions of MP are one of least reliable predictions and measurements are necessary to confirm performance.

Safe fuel handling and storage require a flash point >52°C (as required by ASTM D975) and low water solubility. These two properties were evaluated for all bioblendstocks in the merit table. Flash point is readily estimated for a given molecular structure with current prediction tools based on boiling point; see Section 2.1.2 for more information on flash point prediction. This allowed for rapidly screening and eliminating high volatility molecules, with all of the bioblendstocks except the smallest dioloxanes exceeding the 52°C target. The water solubility of oxygenated compounds was evaluated to determine whether issues might arise during handling and storage. This ensured the oxygenate bioblendstocks contained sufficiently long aliphatic side chains to meet the <20 g/L criterion, with all bioblendstocks displaying water solubility of <1 g/L.

Finally, YSI was used to evaluate the intrinsic sooting potential of bioblendstocks based on their molecular structure relative to fossil diesel that can have a YSI >200. The merit table shows that ethers all exceed or greatly exceed the YSI criterion (YSI <50). Because the

hydrocarbon bioblendstocks all have low or no aromatic content, they exceed the YSI criterion (YSI 50–149). Hydrocarbon blendstocks with saturated rings (myrcene derivatives, di-cyclohexanes, oligocyclopropanes with YSI values ranging from 122 to 198) have a higher YSI than isoalkanes (farnesane and 5-ethyl-4propylnonane with YSI values of 110). These YSI values were still less than the value of typical fossil fuel-derived diesel (~240).

## 2.4.2 Infrastructure Compatibility Results

The results of the exposure studies described in Section 2.2 are shown in Table 5. These results of this assessment are based on measured volume swell of common elastomers exposed to diesel miscible blendstocks.

Table 5. Compatibility rating summary for bioblendstocks and common infrastructure elastomers determined via exposure studies.

MCCI Blendstock	Fluoro-carbon	Fluoro-silicone	Poly-urethane	ECO	OZO	HNBR	NBR
RD							
Biodiesel							
Butylcyclohexane							
Mixed dioxolanes							
4-Butoxyheptane							
n-Undecane							
Methyl decanoate							
Hexyl hexanoate							
1-Octanol							
1-Nonanol							
2-Nonanone							
2-Pentanone							
TPMGE							

ECO = epichlorohydrin; HNBR = hydrogenated nitrile butadiene rubber; NBR = nitrile butadiene rubber; OZO = polyvinyl chloride/nitrile butadiene rubber blends; TPGME = tri(propylene glycol) methyl ether, a polyether derived from methane; Methyl decanoate is a component of short-chain esters derived from oilseed crops; Butyl cyclohexane is a component of HTL oil derived from a wood/algae mixed feedstock.

Suitable  
Borderline  
Unsuitable

In general, many of the blendstocks showed acceptable suitability. Exceptions noted in this study include both ketones and tri(propylene glycol) methyl ether. The alkanes and 4-butoxyheptane exhibited the best overall compatibility behavior. These results are in good agreement with solubility analyses, which show that polarity greatly influences compatibility. Based on these results and other data, the ketones were determined by unsuitable for use as diesel blendstocks. Polyethers require further study.

## 2.5 Potential Adoption Impacts and Barriers

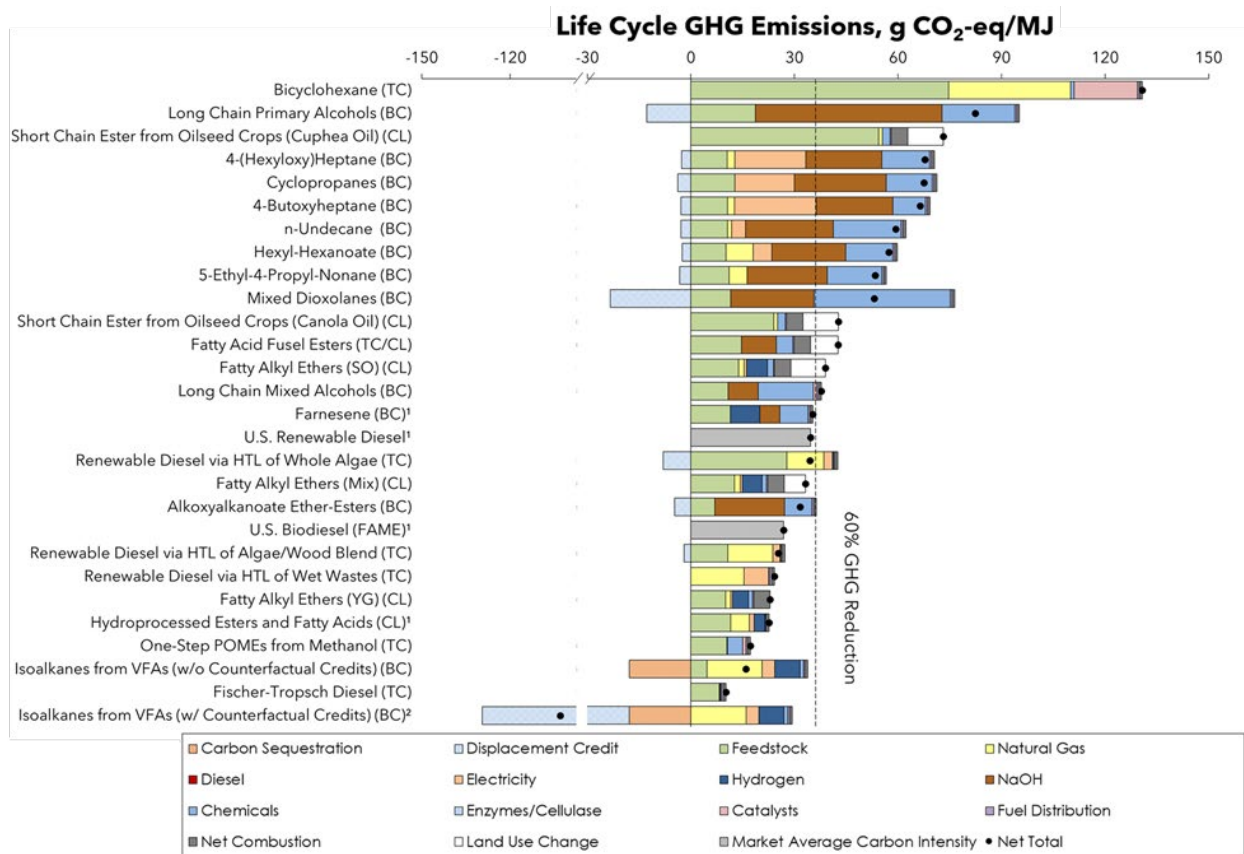
### 2.5.1 Analysis of Bioblendstock Economic, Environmental, and Scalability Metrics

The Co-Optima analysis team provided TEAs and LCAs for more than 15 Co-Optima MCCI bioblendstocks, with more underway. TEA was conducted by using the outputs of a rigorous process model developed using process simulation software (Aspen Plus, ChemCAD) in a cost model developed in Microsoft Excel. LCA was conducted using The Greenhouse Gases, Regulated Emissions, and Energy use in Technologies (GREET) model to estimate life cycle GHG emissions, fossil energy use, and water consumption (Wang 2020). LCA results determined for each blendstock are shown in Figure 1. Note the indirect land-use change impacts in white for three blendstocks which use cultivated oilseed crops (short-chain esters from oilseed crops, fatty acid fusel esters and fatty acid alkyl ethers). These blendstocks were not eliminated from consideration, given the potential availability of alternative fatty acid components.

These analyses were used to rank each bioblendstock on favorability across 19 metrics relevant for understanding technology readiness, economic viability, and environmental impact. Figure 2 summarizes the results of the analysis for bioblendstocks identified in this report.

The production pathway and summary of economic and environmental results may be found in the respective bioblendstock descriptions in Section 3. Figure 3 shows the relative minimum fuel selling prices (MFSP) normalized on an energy basis for the candidate blendstocks based on the TEA. A description of how favorability was categorized for each metric is given in Appendix A.

Several key observations may be derived from this analysis. First, biochemically produced MCCI blendstocks have unfavorable LCA metrics due to the CO<sub>2</sub> emitted during fermentation and the GHG emissions associated with the sodium hydroxide (NaOH) used during feedstock deconstruction. Note also that life cycle GHG emissions include contributions from life cycle fossil fuel consumption; two blendstocks had life cycle fossil fuel consumption that fell into the “neutral” range, but total GHG emissions were determined to be “unfavorable”. Second, feedstock and conversion costs dominate the cost of nearly all the candidate blendstocks. This particularly includes purified sugars and algae. Research to reduce the cost of these feedstocks and conversion processes could address these shortcomings. Finally, while the blendstock production pathways mostly omitted co-product production, in some cases production of a co-product is inevitable. The co-products included were glycerine (FAME/biodiesel), polyurethane (algae), and sodium sulfate (all others).



<sup>1</sup> GHG emissions of these pathways are from either an earlier study or average of market fuels.

<sup>2</sup> The negative GHG emissions from the "Isoalkanes from Volatile Fatty Acids" pathway are because of the credits from avoided emissions from landfill of the food waste feedstock.

Figure 1. Life cycle GHG emissions for a selection of the candidates evaluated in this report. The colors represent the contribution from feedstock and process inputs. For comparison, GHG emissions from petroleum diesel are approximately 91 gCO<sub>2</sub>e/MJ. The negative contributions depicted by the purple bars reflect credits associated with the displacement of conventional production practices for the co-products of bioblendstock production. The black circles denote the net GHG emissions. The gray bars for U.S. Renewable Diesel and U.S. Biodiesel represent average values derived from the California Air Resources Board certified pathway carbon intensities. The vertical dotted line represents the 60% GHG emission reduction level required of advanced biofuels in the United States. SO refers to soybean oil, YG is yellow grease and Mix is a 60:40 mix of soybean oil and yellow grease.

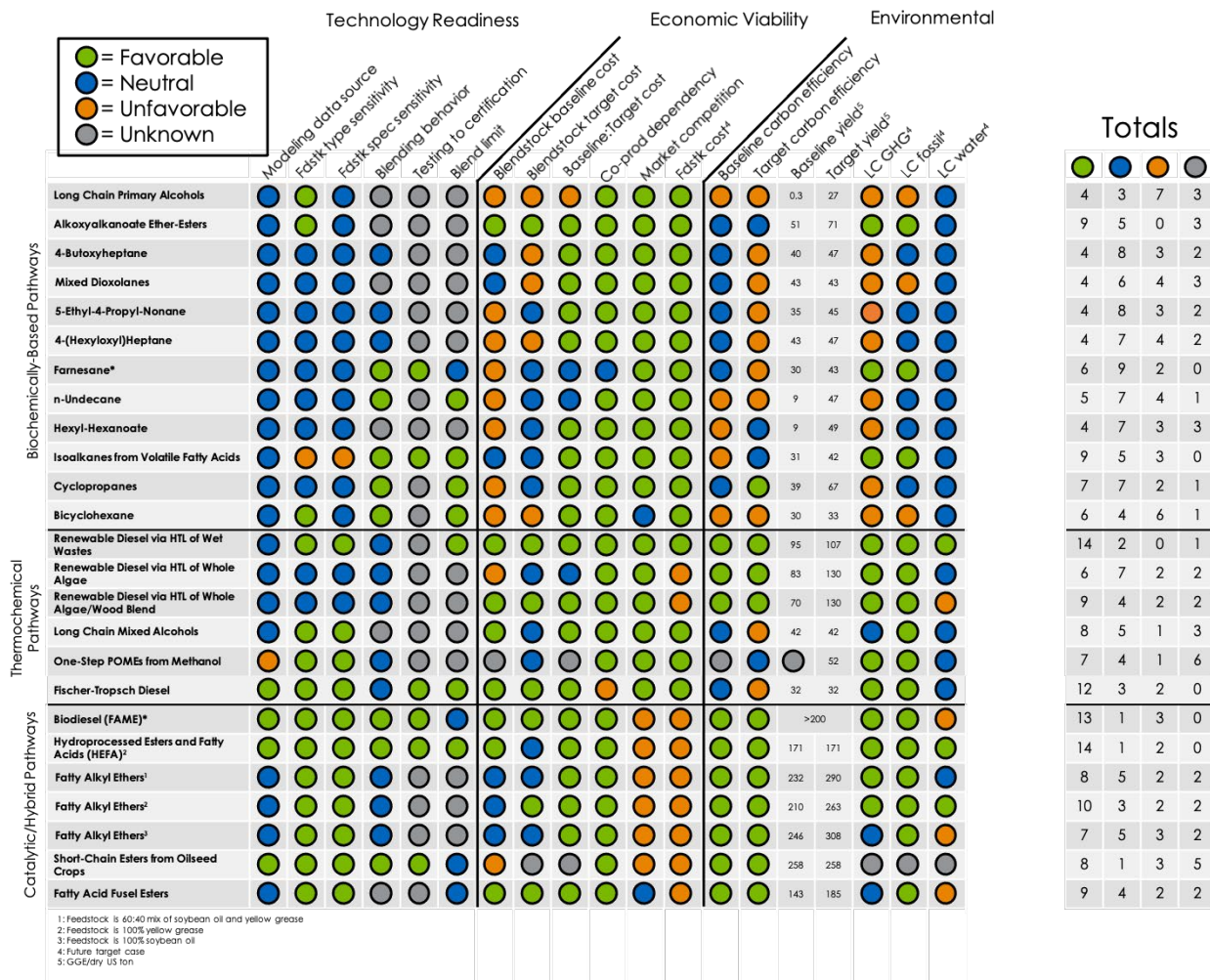


Figure 2. Bioblendstock screening results for technology readiness, economic viability, and environmental impact metrics. Routes produced biochemically do not include the valorization of lignin to co-products. Definitions for favorability of each metric may be found in the appendix. GGE = gasoline gallon equivalent, HTL = hydrothermal liquefaction, LC = life cycle, POME = polyoxymethylene ether, HEFA = hydroprocessed esters and fatty acids. FAME = fatty acid methyl esters. \*Production cost, carbon efficiency, and yield data for these pathways were estimated based on market research and/or prior TEAs and may have economic and process assumptions that differ from other bioblendstock pathways evaluated in this report.

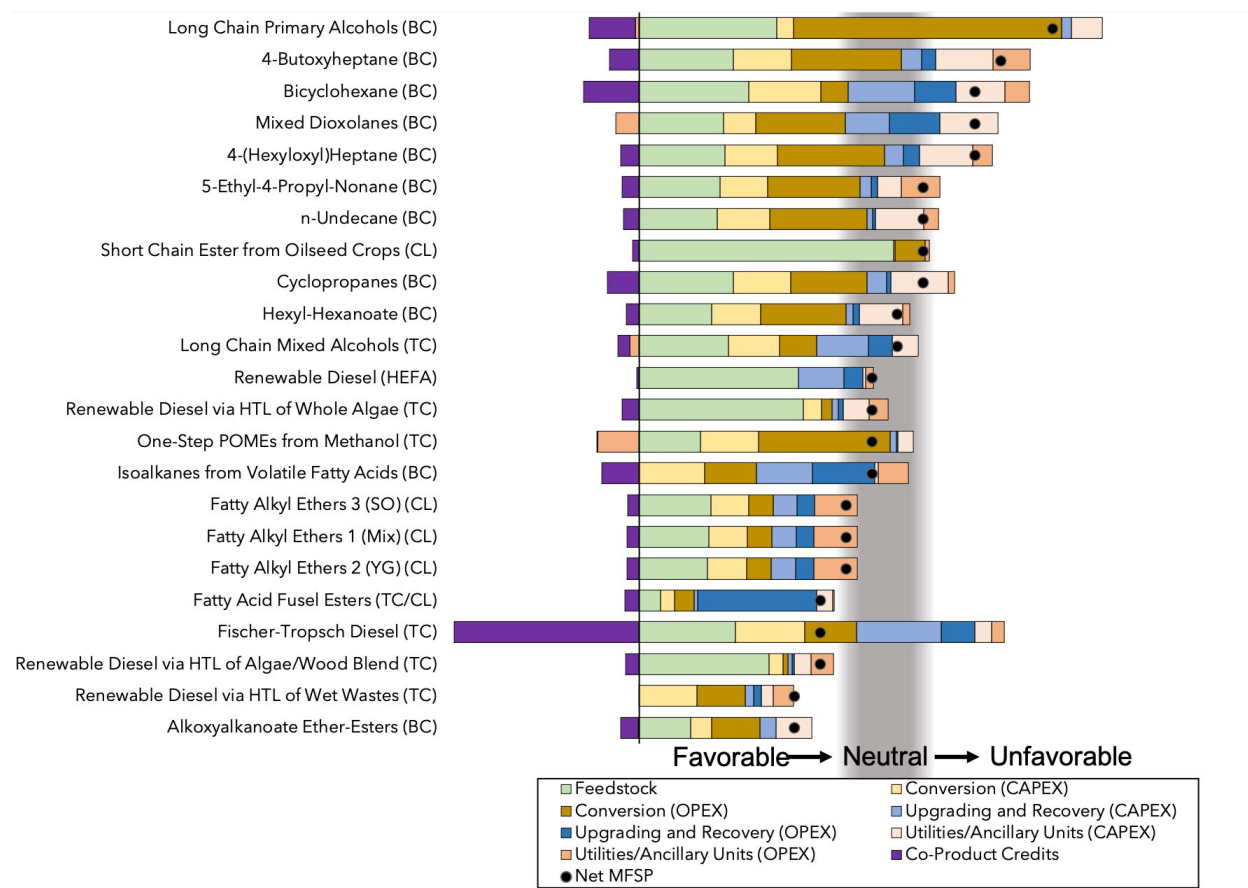


Figure 3. MFSP for bioblendstocks derived from TEA results. CAPEX = capital expense, OPEX = operating expense, HTL = hydrothermal liquefaction, POME = polyoxymethylene ether, SO = soybean oil, YG = yellow grease, and mix is a 60:40 mix of soybean oil and yellow grease.

### 2.5.2 Refinery Integration

Integrating bioblendstocks with superior fuel properties will be an important strategic consideration for petroleum refineries to adapt to increasingly stringent fuel quality specifications and rapidly changing market demands. This refinery impact analysis is intended to identify fuel properties that would generate market pull for bioblendstocks from refiners. Particularly, full refinery linear programming models were built in Aspen PIMS, based on 1) representative refinery configurations from the U.S. Energy Information Administration, 2) properties of bioblendstocks, 3) ASTM fuel specifications, 4) pricing data from Oil Price Information Service by IHS Markit, and 5) future fuel market projections from the Energy Information Administration and ADOPT models.

As shown in Figure 4, eight MCCI bioblendstocks were evaluated at 10, 20 and 30 vol% blend levels and two case scenarios. In the base case scenario (marked by solid bars), only the ultra-low sulfur diesel (ULSD) fuel is prevalent in the market, while in the alternative scenario (marked by stripe bars), both ULSD and the high-cetane California diesel fuel constitute the diesel market. The California Air Resources Board has set stricter standards for diesel fuel

(found in CCR Section 2282(h)), resulting in higher CN (>53 vs. >40 for conventional diesel fuel), lower aromatic (<21% vs. <35%) and nitrogen (<500 ppm vs. not specified) content, and a specified specific gravity (<0.84 vs. 0.876). In this work, the potential economic value of MCCI bioblendstocks was represented by the calculated break-even value to petroleum refineries as feedstocks.

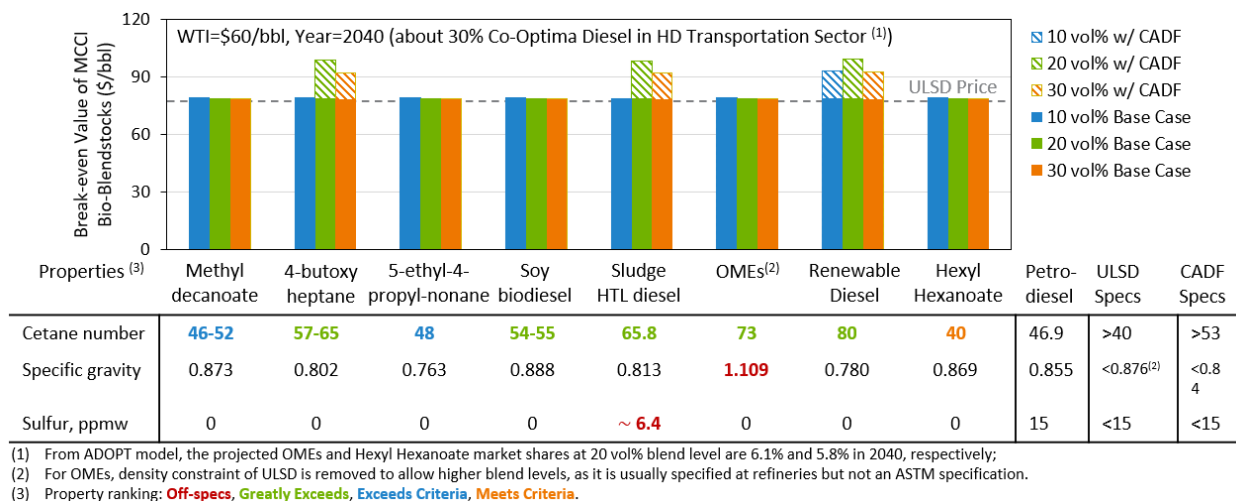


Figure 4. Potential economic value of MCCI bioblendstocks from primary refinery impact analysis. 10%, 20% and 30% w/CADF refers to blending into petroleum diesel according to both ULSD and CADF specifications, while 10%, 20% and 30% Base Case refers to blending into petroleum according to the ULSD specification.

Figure 4 indicates that the MCCI bioblendstocks may offer higher economic value at lower blending levels to meet ULSD specifications. The bioblendstock properties that impose constraints on finished diesel specifications are the most important properties that may impact the potential economic value of bioblendstocks. For the base case scenario, sulfur content (regulated nationally by the EPA) has the most significant impact because it is expensive for refiners to remove sulfur via hydroprocessing, while CN has little impact. Because the CN of petroleum-based diesel typically is in the range of 42–45 (Kurtz and Polonowski 2017), adding a high-cetane bioblendstock will not add much economic value in a market that does not demand high-cetane diesel. On the other hand, as shown by the striped bars, high-cetane MCCI bioblendstocks will create extra value in a market demanding high-cetane diesel (i.e., California diesel fuel), the likes of which could expand in the future. Alternatively, a reconfigured refinery with low CN streams could blend in suboptimal blendstocks to meet the CN specification.

The environmental benefits of MCCI bioblendstocks are the subject of ongoing analysis and are derived by coupling Aspen PIMS simulations with LCAs. The developed PIMS-LCA model uses an input-output framework to track refinery intermediate flows, emissions, and final product slate. The integrated PIMS-LCA supports multiple environmental metrics, allocation schemes, and a broad understanding of the contribution of process material and energy consumption to refinery-wide environmental impacts.

## 2.6 Engine-Related Investigations and Impacts

Concurrent with blendstock modeling, testing, and analyses, Co-Optima researchers have conducted engine testing to evaluate the performance of conventional and advanced diesel combustion using both conventional diesel and diesel base fuel blended with blendstocks that can be derived from biomass and/or waste. The primary goals of these engine tests are to understand the impact of the blendstocks on efficiency and emissions, particularly soot and  $\text{NO}_x$ . The following sections briefly describe two sets of engine experiments that contributed to the Co-Optima evaluation of candidate blendstocks and the chemical characteristics that improve performance.

### 2.6.1 Conventional Diesel Engine Experiments

Co-Optima researchers evaluated a series of blendstocks in a diesel engine to determine the fuels' impact on  $\text{NO}_x$  and soot emissions. The single-cylinder engine, sized for medium duty trucks, is based on the 6.7 L Ford Power Stroke<sup>®</sup> diesel engine. Three engine operating conditions were chosen to examine the fuels: 1) one near idle, 2) one at mid-speed and mid-load, and 3) one at higher-speed and mid-load. Start of fuel injection and EGR sweeps were performed for each fuel blend at each of the three operating conditions. Engine speed, load, intake temperature and pressure, and exhaust pressure were all kept constant. The mass of fuel injected in the main injection event was varied to maintain load; this was required because the LHV of the fuel varied with the bioblendstock.

Eight bioblendstocks were mixed with EPA emissions certification diesel at 30 vol% and examined over the three operating conditions. Figure 5 shows the soot and  $\text{NO}_x$  emissions measured for a series of EGR sweeps from 25% to 43% for the bioblendstocks tested at one of the operating points. All the blendstocks reduced both  $\text{NO}_x$  and soot relative to the conventional diesel fuel, with oxygenate blendstocks showing the largest effect. The brake-specific fuel consumption (BSFC) for all fuels except two was within the margin of error of that measured for petroleum diesel. The POME fuel lowered BSFC (increased efficiency) by about 1% compared to petroleum diesel and the hexyl hexanoate raised BSFC (lowered efficiency) by about 2%.

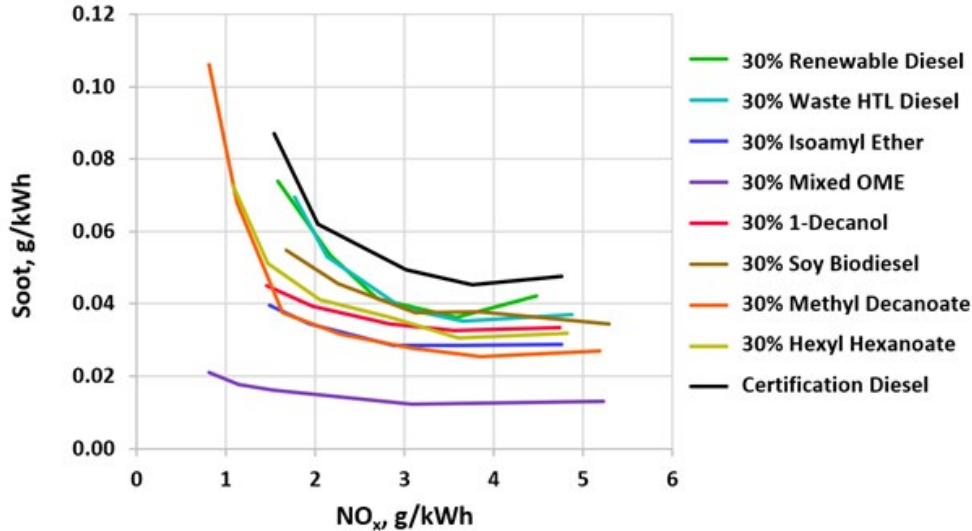


Figure 5. Exhaust gas dilution sweep from 25%–43% to investigate NO<sub>x</sub>-soot tradeoff for nine fuels at 600 rpm and 3.3 bar gross mean effective pressure (or engine load). Single-cylinder research engine version of a 2017 Ford 6.7L Scorpion diesel engine with stock components.

It is important to note that these results were obtained with no changes to engine calibration; the more EGR-tolerant fuels can use more EGR and advance the start of ignition to get to lower BSFC at the same or lower levels of NO<sub>x</sub>/soot. Finally, importantly, these results apply to low engine speed and load conditions, where lower exhaust temperatures may make emission control catalysts less effective.

## 2.6.2 Ducted Fuel Injection

Co-Optima researchers have also been developing a new fuel/charge-gas mixing approach, DFI. DFI is a new and simple mechanical technology to enhance the preparation of fuel/charge-gas mixtures within the combustion chambers of MCCI engines, with the goal of attenuating or preventing soot formation. DFI involves injecting fuel along the axis of a small cylindrical duct within the combustion chamber to achieve more-complete local premixing at or near the end of the duct where ignition occurs.

DFI is a new technology in a relatively early stage of development. Nevertheless, it has been shown to curtail soot formation dramatically in combustion-vessel (Mueller 2017, Gehmlich 2018, Fitzgerald 2018, Svensson and Martin 2019) and single-cylinder optical-engine (Nilsen 2019, Tanno 2019, Nilsen 2020) experiments. Low soot levels have been achieved with commercial diesel fuel even when relatively high levels of charge-gas dilution are employed (Nilsen 2019, Nilsen 2020, Ashley 2017), as shown in Figure 6. This characteristic enables simultaneous, cost-effective, dramatic attenuation of both soot (via DFI) and NO<sub>x</sub> (via dilution), thereby breaking the long-standing “soot/NO<sub>x</sub> tradeoff” for MCCI engines without requiring the introduction of a new fuel.

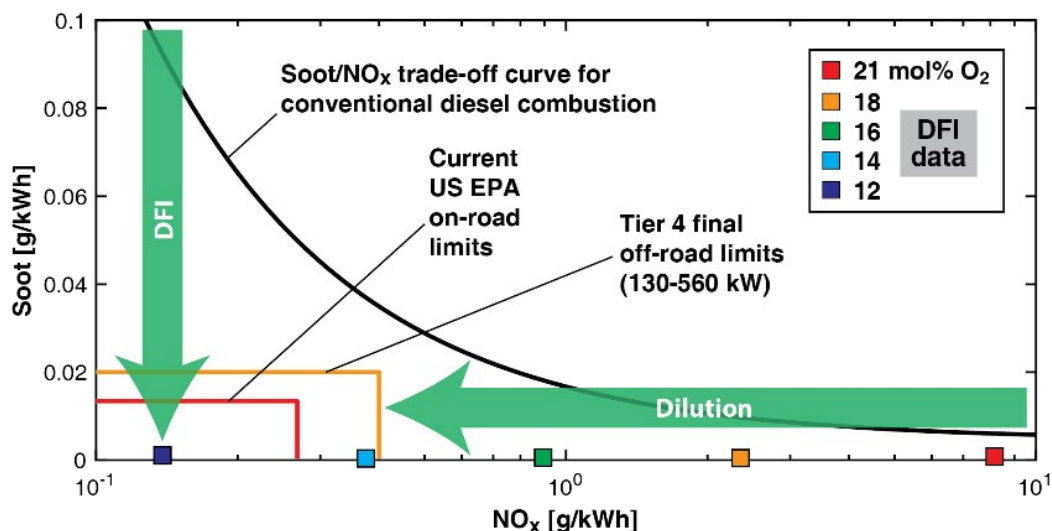


Figure 6. Soot/ $\text{NO}_x$  tradeoff plot for DFI vs. CDC.

Although DFI does not require the use of a new fuel, Co-Optima researchers have further discovered that DFI has a synergistic effect with oxygenated renewable fuels, such that even larger soot-reduction benefits can be achieved when the two are used together (Mueller 2020). Figure 7 shows spatially integrated natural luminosity (SINL) measurements as a function of engine crank angle for three different fuels under both CDC and DFI operating conditions.

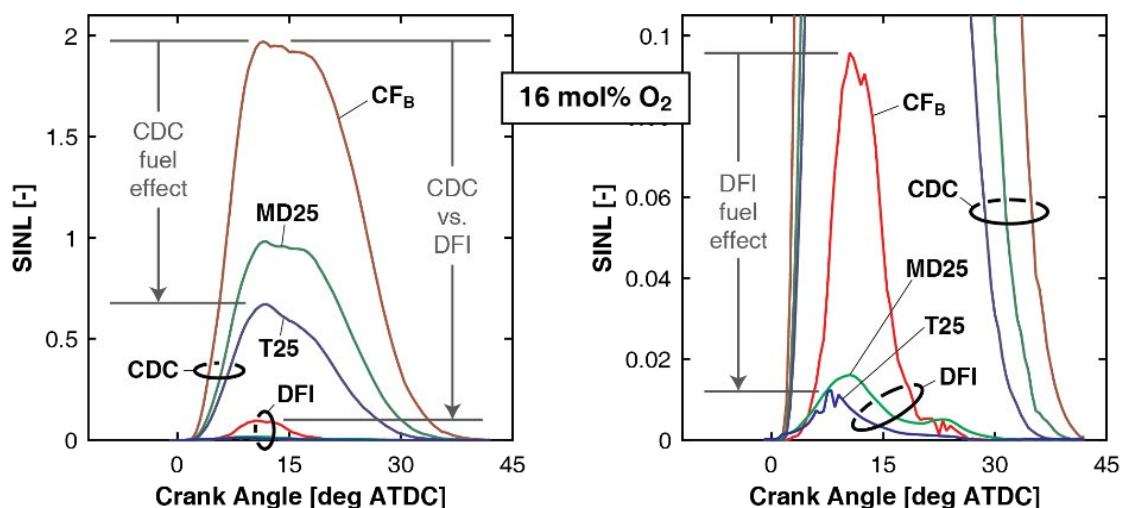


Figure 7. Experimental results comparing hot, in-cylinder soot (SINL) for DFI and CDC with three fuels. The data in the two plots are identical, but the vertical scale on the right plot has been magnified to show the DFI results. These data are for a 16% intake-oxygen mole fraction, representing an intake dilution level that would likely be used to control  $\text{NO}_x$  formation.

SINL is an indicator of the amount of hot, in-cylinder soot present within the combustion chamber under these test conditions. The three fuels tested were a baseline, non-oxygenated No. 2 emissions certification diesel (denoted  $\text{CF}_B$ ) and two blends containing potential renewable

oxygenates. The first oxygenated blend contained 25 vol% of methyl decanoate in CF<sub>B</sub> (denoted MD25), and the second contained 25 vol% of tri-propylene glycol mono-methyl ether in CF<sub>B</sub> (denoted T25).

As shown in Figure 7, DFI with either oxygenated blend lowered SINL by approximately two orders of magnitude relative to CDC with 100% diesel fuel. Switching from CDC to DFI with diesel accounted for one order of magnitude (see left side of Figure 7) and switching from diesel to an oxygenated blend under DFI conditions accounted for the second order of magnitude (see right side of Figure 7). Oxygenate blending produced a larger relative SINL reduction under DFI conditions (right side) than under CDC conditions (left side), and changing from CDC to DFI lowered SINL more than oxygenate blending under CDC conditions (left side). The results were essentially the same regardless of the intake-mixture dilution level. These findings indicate that DFI and oxygenate blending are a powerful combination for making even diluted autoigniting mixtures lean enough to inhibit soot formation.

The ability of DFI and oxygenated renewable fuels to slash soot formation under conditions that also lower NO<sub>x</sub> formation suggests a promising path toward the next generation of high-efficiency, cost-effective, high-performance MCCI engines and fuels. While the compatibility of DFI with current diesel fuel means it does not depend on a new fuel for implementation, increasing the oxygenated biofuel content would increase sustainability and facilitate further attenuation of soot and NO<sub>x</sub> emissions. The amount of oxygenated blendstock needed and the best oxygenate chemistry and fuel properties for enabling DFI to meet current and future NO<sub>x</sub> and PM regulations are still to be determined.

Ongoing Co-Optima research includes strengthening the fundamental understanding of fuel oxygen content, ignition quality, molecular structure, and base-diesel-fuel composition effects on DFI, testing DFI over a wider range of engine operating conditions, and working with industry partners to move the most-advantageous fuel and DFI configurations toward production applications.

## 2.7 Technical Summary

Co-Optima researchers identified several key takeaways for fuel-engine co-optimization in the course of this systematic study of bioblendstocks suitable for use in diesel and advanced MCCI engines. Among these insights are a deeper understanding of fuel chemical structure impacts on soot formation and opportunities for emissions reductions, new chemical structure-fuel property relationships, themes derived from evaluation of the techno-economics of a wide range of chemistries and conversion approaches, and newly identified opportunities for refinery value derived from bioblendstock properties. Some of these insights are related to barriers to adoption identified for bioblendstock molecules or mixtures; in some cases, these barriers are also R&D opportunities.

After careful study, Co-Optima researchers concluded that there was little to no potential for efficiency improvement from changes in the fuel, except as a second-order effect (see Section 1.2.1). As a result, the focus by Co-Optima researchers on understanding and mitigating emissions led to several important learnings. First, Co-Optima researchers have shown that aromatic-free blendstocks (hydrocarbons and oxygenates) can reduce soot formation in

conventional and advanced MCCI engines. Generally, for the hydrocarbons, increasing saturation (reducing aromaticity and double bonds) decreases soot-forming potential, as does decreasing branching (to a point). By changing engine operating conditions (especially increasing EGR), these reductions can also reduce NO<sub>x</sub> formation. Oxygenated fuels reduce soot and NO<sub>x</sub> production further, correlating with oxygen content (possibly up to a plateau at the 30 vol% blend level examined). Among the oxygenates, the degree of soot-forming potential reduction is correlated with O:C ratio as well as molecular weight (lower soot for smaller molecules). POMEs reduce soot production because every carbon atom is already bound to an oxygen atom, inhibiting carbon-carbon bond formation. Finally, combining oxygenated fuels with DFI can reduce production of soot by 99% or more, while increasing EGR can simultaneously reduce NO<sub>x</sub> emissions by 99%.

Structure-property relationships were developed for other critical fuel properties, as well. As described in the prediction tools, energy density is a straightforward function of the composition and structure of a molecule and its density. Maintaining or increasing low temperature operability is straightforward chemically for those hydrocarbons and esters mixtures that do not meet diesel fuel specifications— increase branching, possibly include some mono-unsaturated components. Technologies (conventional plant breeding, genetic engineering, chemical processing) that can shorten fatty acid chain length, introduce light branching (such as one methyl group), and/or reduce saturated fatty-acid content by

### Key Technical Learnings

- Emissions reductions in NO<sub>x</sub>, soot and GHGs may be enabled by new combustion approaches, as well as by new fuels in both new engines and the legacy fleet.
- DFI and oxygenated blendstocks act synergistically to reduce soot formation while allowing NO<sub>x</sub> reduction from EGR, with important details still to be determined.
- Hydrocarbons, esters and ethers all have potential as performance-advantaged MCCI blendstocks.
- Aromatic-free bioblendstocks all reduce soot, with oxygenates reducing soot more than hydrocarbons, and linear and branched species reducing soot more than cyclic species.
- As expected, acceptable CN can be achieved by inclusion of either a reactive bond like a strained ring or ether, or by including molecules with long (C6+), saturated straight hydrocarbon moieties, longer if a reactivity-reducing moiety such as an alcohol is present.
- Improvements in low temperature operability can be achieved by a wide range of chemistries.
- Increasing the energy density of bioblendstocks beyond that of conventional diesel is very challenging, especially for oxygenates. All strained ring compounds appear to fail one or more technical or economic target.
- Ethers remain interesting due to their very high CN and very low soot-forming potential, especially POMEs, but substantial barriers to adoption such as compatibility and oxidative stability remain.
- Feedstock and conversion operating costs dominate the cost of nearly all blendstocks studied.
- GHG emissions contributions from fermentation and NaOH used in feedstock deconstruction must be reduced for fermentation-produced bioblendstocks to meet a 60% GHG reduction target.

having higher mono-unsaturated fatty-acid content are a useful target for future research in this area.

The connection between chemical structure and CN is well understood. Specifically, increased chain length (especially C6+) and reactive bonds (such as ethers and/or strained rings) increase CN. Moieties that inhibit autoignition such as alcohols, ketones or alkenes decrease CN.

Additional barriers were identified by Co-Optima researchers for some blendstocks. Alcohols and some esters have high kinematic viscosity. For the alcohols, this high kinematic viscosity persists for branched and straight-chain alcohols and for mixtures. Thus, alcohols may be suitable for use at lower blend levels, but not as neat fuels without blending into a low viscosity base fuel.

Some ethers have exhibited low oxidation stability, which can be mitigated with an antioxidant additive. Additional testing is underway for some. Furthermore, at least one of the dioxolanes has provided some evidence that they may form crystalline peroxides with heat and concentration. Additional research is underway to determine if peroxides are formed by dioxolanes, and if so, which dioxolanes form peroxides and under what conditions.

Compatibility for some esters and ethers is marginal with some polymers, and the one polyether studied generated significant swell in several polymers. The extent to which ethers are or are not compatible with fuel system materials must be established. Additional research is warranted.

The integrated analyses conducted by Co-Optima analysts put candidate blendstocks on a common footing. For all candidate blendstocks, the potential for production at scale and at a MFSP that is competitive in the market is inherently dependent on the consistent availability (at large volumes) and cost of waste and/or biomass feedstocks. As Figure 7 indicates, feedstock cost is a large fraction of overall cost. The potential for low-cost production of low GHG MCCI blendstocks also requires low-cost production processes. For many of the blendstock processes analyzed, operating production costs were one of the largest contributors to the modeled cost. Decreasing the number of steps or amount used of a reactant such as hydrogen or NaOH can decrease these costs.

One driver for Co-Optima's research on MCCI blendstocks is to identify options to reduce the GHG footprint of MD/HD ground transportation. LCA analyses indicate direct production of MCCI blendstocks by fermentation leads to higher GHG emissions than other approaches. The primary contributors are the GHGs associated with the production of NaOH used in feedstock deconstruction to produce sugars for fermentation, and the emission of some fraction of the carbon in sugar as CO<sub>2</sub>. Research to address these two sources could decrease the GHG emissions of fermentation-produced blendstocks and intermediates.

Finally, analysis of the potential impact to refineries of an increase in the use of biomass—and waste-derived MCCI blendstocks revealed several potential benefits—particularly in providing CN and very low to zero sulfur. The use of lower cost base fuels that do not meet diesel specifications and are blended with low sulfur and/or high CN blendstocks could reduce refinery costs. In markets where higher CN is required (California and some world markets), the higher CN provided by the lower-carbon intensity blendstock could provide additional value.

Ultimately, the results of this Co-Optima research and analysis show these blendstocks have the potential to meet technical targets set forth by industry for reducing emissions, increasing efficiency, and ensuring compatibility (Gaspar 2018). The insights generated by Co-Optima MCCI research point to underlying relationships that can inform future fuel and blendstock development efforts, as well as R&D opportunities to overcome barriers identified in these efforts.

### 3 Top 13 MCCI Biofuel Candidates

This section lists the candidate blendstocks with the best combination of merit table entries. Section 3.1 describes the eight candidates with minimal fuel property, techno-economic, or life cycle barriers. Several of the candidates are already market fuels blended up to 20% in petroleum diesel. This group includes HEFA RD, Fischer-Tropsch (FT) diesel, HTL bio-oils derived from sewage sludge, algae or algae/wood mixed feedstocks, farnesane, isoalkanes derived from upgrading of VFAs derived from food waste (with 5-ethyl-4-propylnonane as one example component), isoalkanes derived from catalytic upgrading of ethanol, biodiesel (FAME), and fatty acid fusel esters.

Section 3.2 contains five additional candidates that show significant promise but for which a significant barrier to deployment was identified. This group includes short chain esters from oilseed crops (candidate oilseed crops are not cultivated for fuel purposes and feedstock costs remain very high); polyoxymethylene ethers including end-exchanged derivatives (LHV, water solubility, and infrastructure compatibility); 4-butoxyheptane (does not meet 60% GHG emissions reduction target due to significant emissions associated with the sodium hydroxide used during pretreatment and conditioning of the feedstock); AOAs derived from lactate (some fuel property data gaps, potential oxidative stability and infrastructure compatibility barriers); and fatty alkyl ethers (FAE)) (flash point, oxidative stability, and competition for feedstock with FAME biodiesel). Figure 8 shows the 13 blendstocks described in Sections 3.1 and 3.2.

Finally, Section 3.3 contains nine candidates that were considered and tested but ultimately determined to be unsuitable for use as MCCI blendstocks. Hundreds of candidates were screened out at the beginning of Co-Optima research on this topic, and many other candidates were abandoned along the way. Enough testing or analysis was done for these candidates to warrant inclusion in this report. These bioblendstocks are oligocyclopropanes (cost, GHG emissions); myrcene derivatives (cost, GHG emissions); bicyclohexanes/bicyclopentanes (cost, GHG emissions); n-undecane (cost, GHG emissions); long-chain linear and branched alcohols (viscosity, CN, GHG emissions); hexyl hexanoate (cost, GHG emissions); dioxolanes (LHV, oxidative stability and peroxide formation, water solubility, GHG emissions); oxetanes (no viable route from biomass); and dipentyl ether (oxidative stability and peroxide formation).

The level of detail in the blendstock descriptions varies. Some of the blendstocks are at an early stage in development, leading to significant knowledge gaps. Market fuels, on the other hand, have extensive data behind their production and use, generating very specific barriers to further adoption and use.

#### 3.1 Top Eight Candidates with Minimal Fuel Property, TEA, or LCA Barriers

The eight blendstocks that met all fuel property targets and presented minimal barriers to adoption are described in this section and shown in Figure 8, along with the five additional candidates which met fuel property targets but presented significant barriers to adoption.

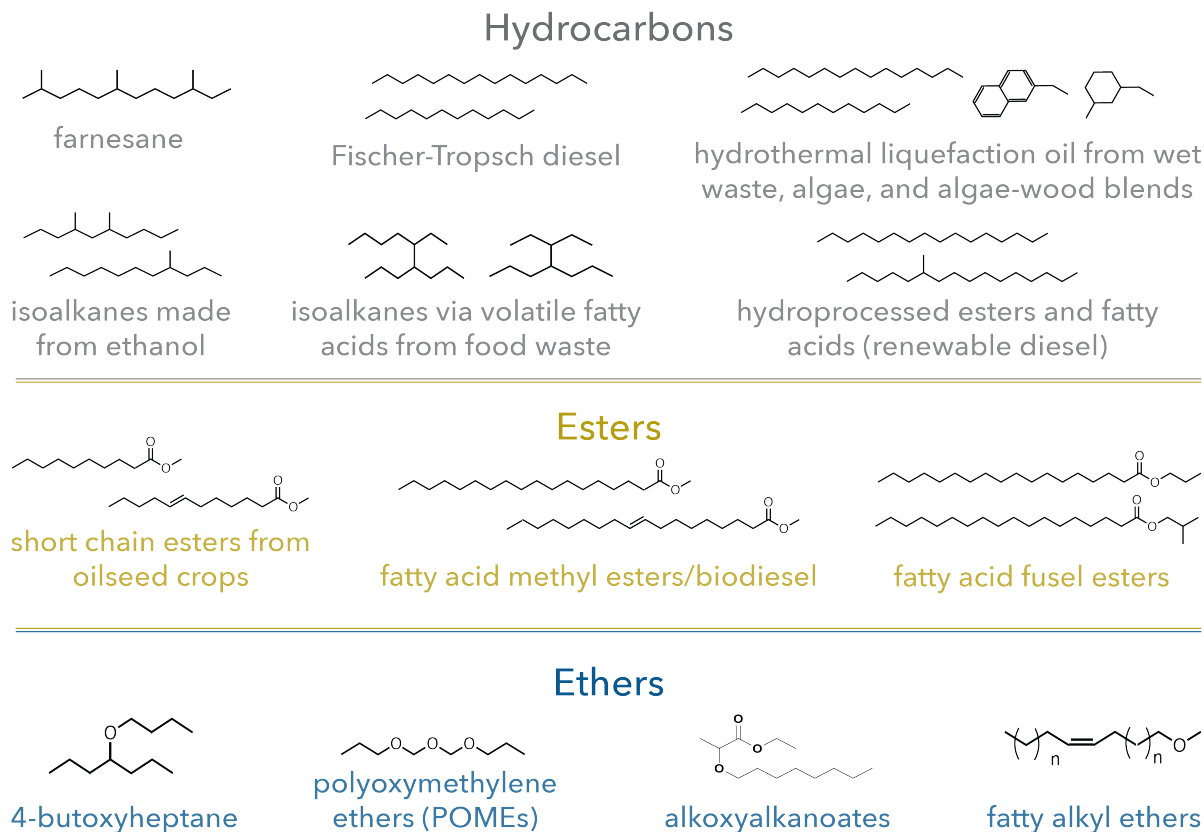


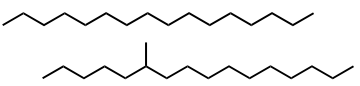
Figure 8. Top 13 performing blendstocks with the potential to reduce criteria and GHG emissions. The 13 blendstocks comprise 6 hydrocarbons, 3 esters and 4 ethers. The hydrocarbons, fatty acid methyl esters and fatty acid fusel esters present minimal barriers to adoption.

### 3.1.1 Renewable Diesel Fuel

Renewable diesel, as known as HEFA or green diesel, is a market fuel composed of diesel boiling range hydrocarbons made from renewable feedstocks. As a complex mixture whose composition depends on the feedstock(s) and processing conditions, specific fuel property values depend on specific feedstock, production, and processing used. Cost and low temperature operability remain barriers to wider adoption and use.

#### 3.1.1.1 Property Summary

RD readily meets the ASTM D975 properties for diesel fuel when additives are used for lubricity and conductivity (McCormick and Alleman 2016) and can be used and blended like conventional diesel fuel. RD contains no aromatics (<1%) (Neste 2020) and has a boiling range similar to conventional diesel fuel (Smagala 2013). The CN of RD typically is >70.

Renewable Diesel Fuel	
	
Formula	~C <sub>8</sub> -C <sub>22</sub> alkanes and isoalkanes
CN	>70
T <sub>b</sub> (°C)	<330
Flash point (°C)	>61
Cloud point (°C)	-5 to -34
Water solubility (mg/L)	<0.1
YSI	—
Energy density (MJ/L)	34.4
Specific energy (MJ/kg)	44.1
Viscosity (mm <sup>2</sup> /s@40°C)	2-4
Density (kg/m <sup>3</sup> @15°C)	770-790

#### 3.1.1.2 Production from Biomass

The feedstock for commercial production of RD is fats, oils, and greases (FOG), which may be sourced from oil crops (e.g., soybean, corn, canola or other oilseed crops) or wastes such as tallow. To produce RD from these feedstocks, hydrogenation reactions are used to saturate double bonds and remove oxygen, followed by isomerization to lower cloud point and T90. The initial deoxygenated product cloud point can be above 20°C (Smagala 2013) so isomerization is necessary even for warm climate operation. Figure 9 provides high-level process diagram for the production of RD.

#### 3.1.1.3 TEA/LCA

An average of the California Air Resources Board certified pathway carbon emissions was used to generate an average GHG emissions reduction. This is the value shown in Figure 1 in Section 2.5.1. Note that the average meets the cellulosic biofuel criterion of at least 60% GHG emission reduction compared to petroleum diesel fuel, in the range of 68–80% or more. Feedstock and energy consumption are the key drivers of the total GHG emissions. Currently produced at commercial scale, a previous TEA indicated an MFSP between \$3–5/GGE for HEFA biodiesel depending on the starting feedstock (waste vs. clean oil), production scale, and co-product sales (such as propane). The life cycle GHG emissions and MFSP are shown in Figure 10.

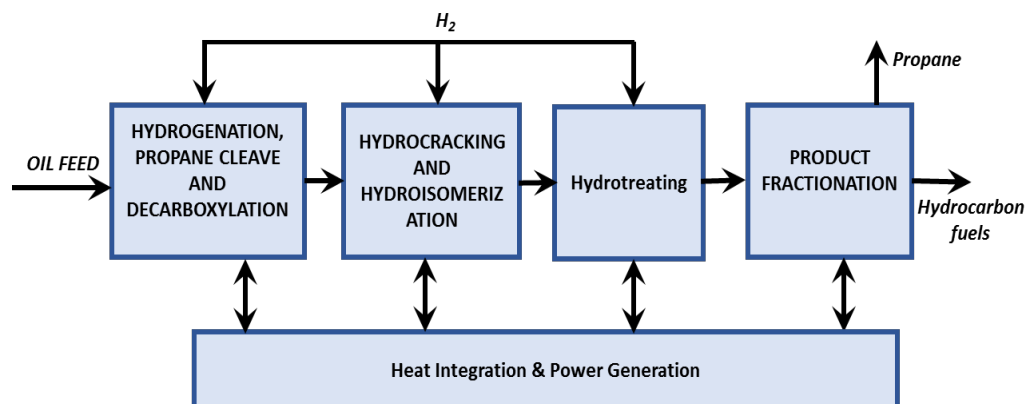


Figure 9. Process flow diagram for RD production.

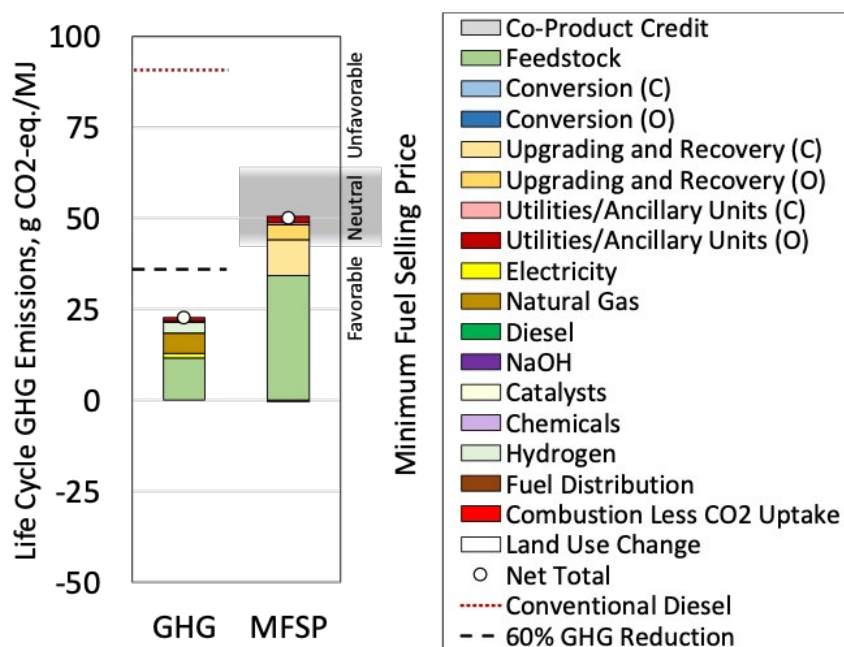


Figure 10. RD life cycle GHG emissions and MFSP.

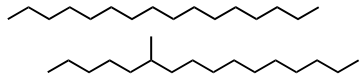
### 3.1.1.4 Challenges, Barriers, and R&D needs

Although RD technology is fully mature, challenges still exist to reduce cost and ensure sufficient feedstock is available for continued market growth. RD competes with biodiesel for the same feedstocks. Consistent availability of increasing feedstock volumes may remain a barrier, even as new production capacity comes online (Bomgardner 2020) (several oil refiners have announced plans to convert older refineries to the production of RD). The HEFA process also is used to produce renewable aviation fuel, which may limit the potential for HEFA RD to expand in the ground transportation market (Tao 2017). Pretreatment of lower quality feedstocks also remains a challenge. The catalysts used to produce RD are highly sensitive to contaminants in the feedstocks and pretreatment may be needed to ensure long-term successful RD production. Development of more robust catalysts could also address this challenge.

Production economics and cold weather operability remain challenges for RD. On average, production costs for RD are higher than for converting the same feedstock to biodiesel (Müller-Langer 2014, Dangol 2017). Additionally, the isomerization or hydroisomerization step required to lower cloud point also results in cracking to light gases and lower molecular weight products that do not boil in the diesel range, thus reducing diesel (or jet) fuel yield (Starck 2016). The naphtha byproduct produced has very low octane number and hence very low value. Achieving lower cloud point for winter operation requires more severe isomerization conditions leading to an even higher yield loss. While commercial scale process yields are proprietary, laboratory-scale deoxygenation yielded 74% diesel boiling range products starting from algae in a recent study (Kruger 2017). Subsequent isomerization to produce a  $-12^{\circ}\text{C}$  cloud point product (minimally acceptable wintertime diesel fuel) reduced overall yield of diesel product to 50–60%. While commercial scale process yields may be better, this factor significantly increases the cost of RD production for wintertime use.

### 3.1.2 Fischer-Tropsch Diesel Fuel

Fischer-Tropsch diesel is a market fuel composed of diesel boiling range hydrocarbons made via the gas-phase conversion of synthesis gas, a mixture of hydrogen and carbon monoxide, into hydrocarbons, the FT process. The synthesis gas has historically most commonly been produced from natural gas reforming or coal gasification. However, efforts to gasify wood waste (Natarajan 2014), municipal solid waste (aimed primarily at jet fuel; Shahabuddin 2020) and other renewable resources have increased in recent years. First developed in the 1920s, the FT process catalytically polymerizes the synthesis gas into a mixture of hydrocarbon molecules whose reaction products are primarily *n*-alkanes described by an Anderson-Schulz-Flory distribution. Like renewable diesel, the high fraction of *n*-alkanes leads to high cloud and pour points. As a result, the FT diesel production process usually incorporates a hydroisomerization step. The high capital cost of gasification processes remains a primary hurdle to widespread adoption; gasification benefits from economies of scale, which drives toward increased size for a profitable gasification FT plant. However, feedstock logistics for biomass and waste resources are harder to scale to the size of a commercial gasification-FT plant. Approaches to address this challenge have been proposed (Wright 2008). Furthermore, processibility of biomass and waste products have challenged many projects initially proposed to use solid biomass (van der Drift 2006); commercial adoption of FT diesel using waste and biomass feedstocks remains quite limited (Shahabuddin 2020). Novel approaches to feedstock preparation and processing, improvements to the catalyst for higher single-pass conversion rate, higher hydrothermal stability, and lower deactivation rates could improve plant performance. Cost remains the primary barrier to wider adoption and use, while low temperature operability could pose a challenge for very high blend levels of FT diesel in a base fuel without suitable mitigation or more aggressive hydroisomerization.

Fischer-Tropsch Diesel Fuel	
	
Formula	$\sim\text{C}_{10}\text{-C}_{22}$ alkanes and isoalkanes
CN	>70
$T_b$ ( $^{\circ}\text{C}$ )	<330
Flash point ( $^{\circ}\text{C}$ )	>61
Cloud point ( $^{\circ}\text{C}$ )	10 to -34
Water solubility (mg/L)	<0.1
YSI	–
Energy density (MJ/L)	34
Specific energy (MJ/kg)	44
Viscosity ( $\text{mm}^2/\text{s}@40^{\circ}\text{C}$ )	2–4
Density ( $\text{kg}/\text{m}^3 @15^{\circ}\text{C}$ )	770–790

### 3.1.2.1 Property Summary

The FT process can produce very high-quality diesel fuel, with very low sulfur and aromatic content. The fuel can be used and blended like conventional diesel fuel. The resulting fuel has very high CN (typically >70) and density, distillation properties, viscosity and energy density comparable to petroleum diesel. The primary fuel property limitations are very poor lubricity and high cloud/pour point (Bacha 2007, Lappas 2011).

### 3.1.2.2 Production from Biomass

Figure 11 shows a high-level process flow diagram to produce diesel from biomass via the FT process, and Figure 12 shows the FT diesel life cycle GHG emissions and MFSP.

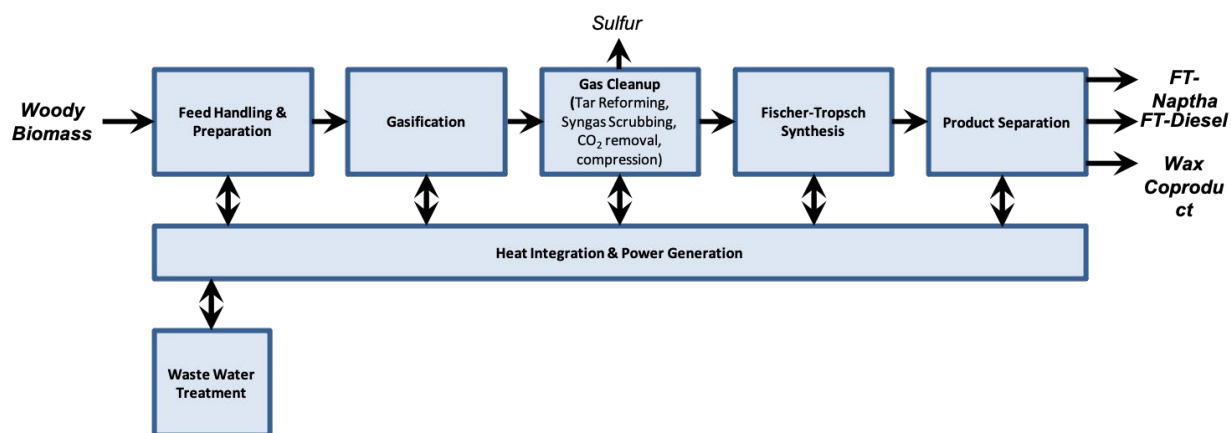


Figure 11. Process flow diagram for FT diesel production.

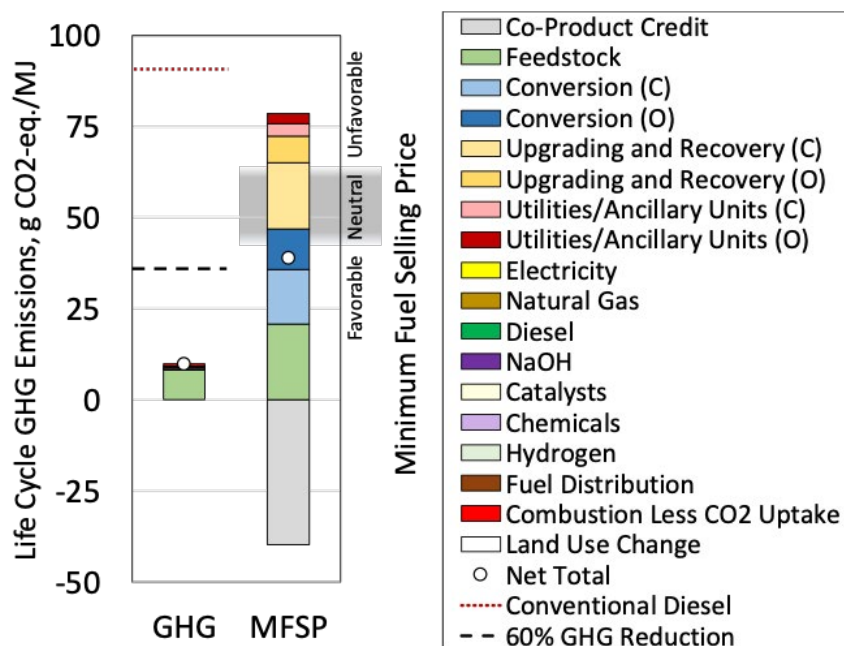


Figure 12. FT diesel life cycle GHG emissions and MFSP.

The process starts with the gasification of biomass to syngas; for a review of biomass and waste gasifier technologies currently in use, including strengths, weaknesses and appropriate use scales see Shahabuddin (2020). The resulting syngas undergoes a series of cleanup steps, including removal of CO<sub>2</sub>, sulfur compounds, nitrogen compounds, alkali metals, chlorine and other contaminants; adjustment of the CO-to-hydrogen ratio (likely via the water-gas shift reaction [van der Drift 2006]); and reforming of tars. The adjusted syngas undergoes catalytic conversion to hydrocarbons using an FT catalyst (usually Fe or Co on a suitable substrate). The choice of operating conditions and catalyst determine the product distribution, including carbon chain-length distribution, olefin content and aromatic content. As the FT reactions are highly exothermic, reactor design is important to ensure necessary control of the reaction temperature. Approaches include fixed-bed, fluidized-bed and microchannel fixed bed reactors. The final step in the FT diesel production process is product separation, typically achieved via distillation and often with some hydrocracking and isomerization as noted above.

### 3.1.2.3 TEA/LCA

Techno-economic analysis for FT diesel from biomass leveraged existing modeling efforts by Tan et al. where forestry residues are gasified to syngas which subsequently undergoes FT synthesis yielding four primary products: gasoline, jet, and marine diesel fuel as well as a wax co-product (Tan 2019). Under Co-Optima, downstream separation was modified slightly to achieve fuels properties criteria for MCCI engines, while the lighter cut and wax fraction were assumed sold as co-products. MFSP for the diesel fraction was favorable and among the lower cost cluster of Co-Optima fuels at approximately \$3.5/GGE. Considerable heavy wax is formed in the synthesis stage approximately 10% of input biomass carbon vs. approximately 17% and 10% for the diesel and naphtha fractions, respectively. Including additional hydrocracking of wax co-product would potentially increase fuel yield at the expense of additional capital and operating costs. FT diesel exceeds the advanced biofuel criterion with the potential to reduce about 89% of GHG emissions as compared to petroleum diesel. Fossil fuel consumption is also favorable with a 90% reduction compared to petroleum diesel. Note that this analysis did not include a hydroisomerization step, necessary to ensure low temperature performance, that would decrease carbon yield and increase cost and life cycle GHG emissions slightly.

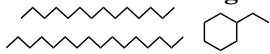
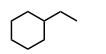
### 3.1.2.4 Challenges, Barriers, and R&D needs

Although FT technology is one of the most mature processes for conversion of biomass to fuel, commercial production of FT fuels remains limited. The primary reason is the large scale and high capital cost of gasification processes, combined with the difficulty of economically producing, collecting and converting biomass on the same scale. These challenges have limited production of second-generation biofuels produced using the FT process. Approaches to incorporate distributed processing via, e.g., distributed pyrolysis, have some potential to enable the central FT plant scale required, while permitting use of biomass as the feedstock (Wright 2008).

Beyond production economics, cold weather operability remains a challenge for FT diesel. Furthermore, the isomerization or hydroisomerization step required to lower cloud point also results in cracking to light gases and lower molecular weight products that do not boil in the diesel range, thus reducing diesel (or jet) fuel yield, as described in the RD description.

### 3.1.3 HTL Fuel Blendstocks Derived from Sewage Sludge, Algae, and Algae/Wood Blends

HTL is a process that uses hot, pressurized water in the condensed phase to convert biomass or wet waste into a thermally stable oil product, also known as “biocrude,” that then can be thermocatalytically upgraded to a hydrocarbon fuel blendstock. HTL is a conceptually simple process with a 44 wt% biocrude yield, which can be applied to a wide range of wet waste feedstocks at similar processing conditions. These include algae (Elliott 2013), wood (Jindal and Jha 2016), manure (Yin 2010), wet wastes such as sewage sludge (Zu 2018, Marrone 2017, Marrone 2018), and blends (Gao 2015, Chen 2014) of these feedstocks with each other and with FOG. The primary barriers to adoption include cost and scale, including optimizing upgrading approaches to cost-effectively remove S and N, as well as low-temperature operability.

<b>HTL Blendstock from Sewage Sludge</b>		<b>HTL Blendstock from Algae</b>	
Formula	n-alkane rich hydrocarbon mixture 	n-alkane rich hydrocarbon mixture 	
CN	55-68	55-68	
T <sub>b</sub> (°C)	N/A	N/A	
Flash point (°C)	>55	61.5	
Cloud Point (°C)	-10 to 20	-60.1	
Water solubility (mg/L)	<0.1	-0.1	
YSI	–	–	
Energy density (MJ/L)	34.5-35.5	34.6	
Specific energy (MJ/kg)	43-44	43.8	
Kinematic viscosity	2.7	2.5	
mm <sup>2</sup> /s@40°C)			
Density (g/mL@40°C)	0.800-0.808	0.791	
<b>HTL Blendstock from 50/50 Algae/Wood Blend</b>		<b>HTL Blendstock from Wood</b>	
Formula	n-, iso- and cycloalkanes with some aromatics 	n-, iso- and cycloalkanes, some aromatics 	
CN	40	29.7	
T <sub>b</sub> (°C)	–	–	
Flash point (°C)	>55	55.5	
Cloud Point (°C)	-60.1	-25	
Water solubility (mg/L)	<0.1	<0.1	
YSI	–	–	
Energy density (MJ/L)	35.6	36.9	
Specific energy (MJ/kg)	42.3	42.0	
Kinematic visc. (@ 40°C)	2.5	2.3	
Density (g/ml @ 40°C)	0.843	0.879	

### 3.1.3.1 Property Summary

The HTL process uses hot, pressurized water in the condensed phase to convert wet feedstocks such as algae with or without wood into a thermally stable oil product, also known as “biocrude,” which can then be thermocatalytically upgraded to hydrocarbon fuel blendstocks. The biocrude can be upgraded with high yields (around 70%) into a diesel-rich fuel blendstock. The fraction of each type of hydrocarbon found in a HTL bio-oil is highly dependent on both the feedstock composition and the specific processing conditions.

The chemical composition of the diesel fraction derived from algae primarily consists of *n*-alkanes, rich in carbon lengths between 14 and 18. The most common isomers have a carbon in the 2-position, such as 2-methyl-heptadecane or 2-methyl-hexadecane. HTL bio-oils generated from algae and/or mixed algae-wood feedstocks consist of primarily *n*-alkanes (from the algae) and a combination of iso-alkanes, cycloalkanes, and aromatics (from the wood), with the fraction of aromatics dependent on the hydrotreating process. The fuel properties of these bio-oils depend on the feedstock(s) and processing, including distillation. The higher fraction of *n*-alkanes in the algae-derived blendstocks leads to a higher CN compared to the wood-derived and wood/algae-derived blendstocks with their higher aromatic content. Figure 13 shows the gas chromatograph-mass spectrometry traces of upgraded HTL biocrudes from sewage sludge, a combination of sewage sludge and FOG, algae and swine manure.

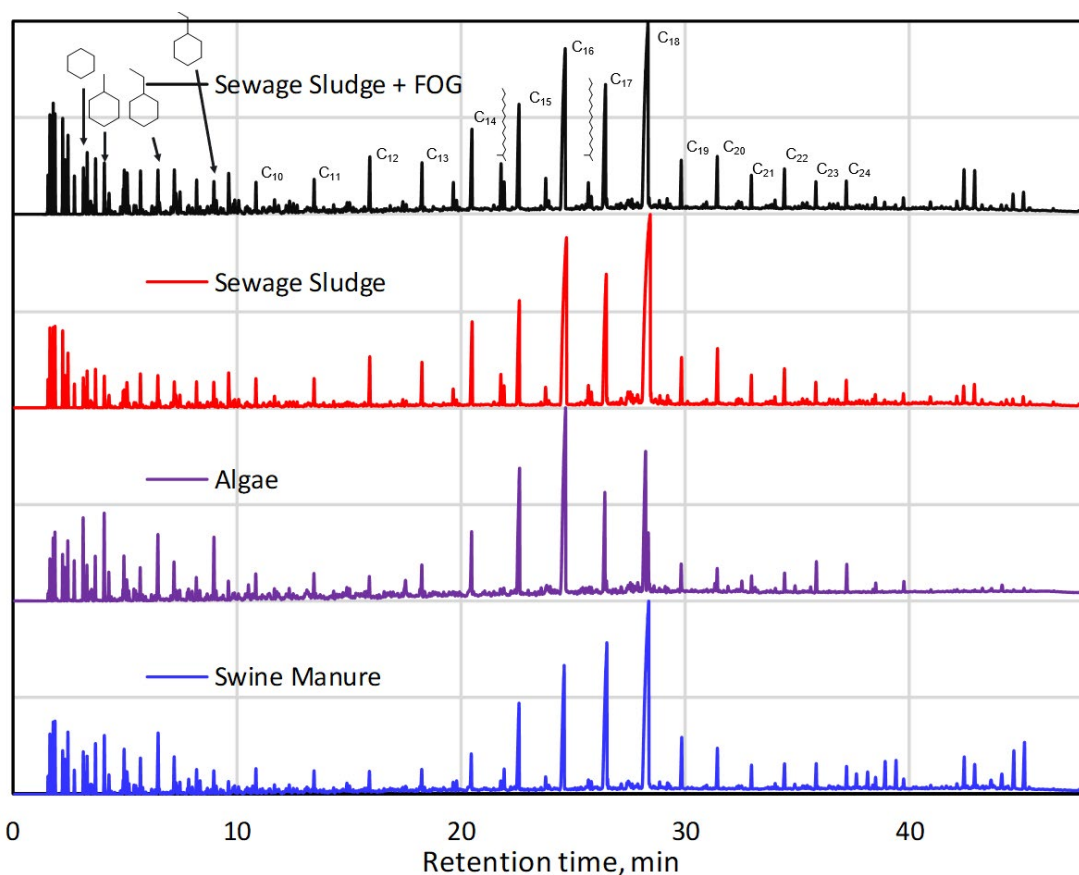


Figure 13. Gas chromatograms showing hydrocarbon distributions of HTL oils derived from four feedstocks. Peak identifications were made using mass spectrometry.

From the gas chromatograms, one can see that the major products are the n-alkanes in each sample (as denoted by the carbon number from C10 to C24) with molecules with even carbon numbers more abundant than molecules with odd carbon numbers. Furthermore, the cycloalkane content (denoted by arrows pointing from cyclohexane and substituted cyclohexane molecules) varies by feedstock. Finally, the relative amount of 2-methylalkanes (located between the n-alkane peaks with a drawing of the molecule placed above) also varies; for these samples the order of abundance is algae < swine manure < sewage sludge < sewage sludge plus FOG. The relative abundance of iso-alkanes is highly dependent on the feedstock and processing conditions. For instance, the composition of wet waste changes seasonally and geographically, leading to varying lipid, protein and carbohydrate content, which impacts the product chemical composition.

A typical HTL diesel-range fuel or blendstock has a density of 0.808 g/ml, C, H, and O (wt%) of 86.8%, 14.4%, and 0.6%, respectively, sulfur concentration of 4.8ppm, and a DCN of 69.3. In 2020, Pacific Northwest National Laboratory (PNNL) completed a 44-hour run using sewage sludge from the Great Lakes Water Authority (Detroit) in MHTLS matching and exceeding bench-scale runs in terms of biocrude oil quality (H:C ratio = 1.65, density = 0.95, moisture = 3.5%), yield (41 wt%), and processability. The campaign produced a fuel with a flash point of 55°C, pour point of 6°C, and a cloud point of 5.1°C. The simulated distillation of the undistilled fuel is described below

### 3.1.3.2 Production from Biomass

Figure 14 shows a generic process flow diagram for the production of diesel from waste and biomass feedstocks via HTL.

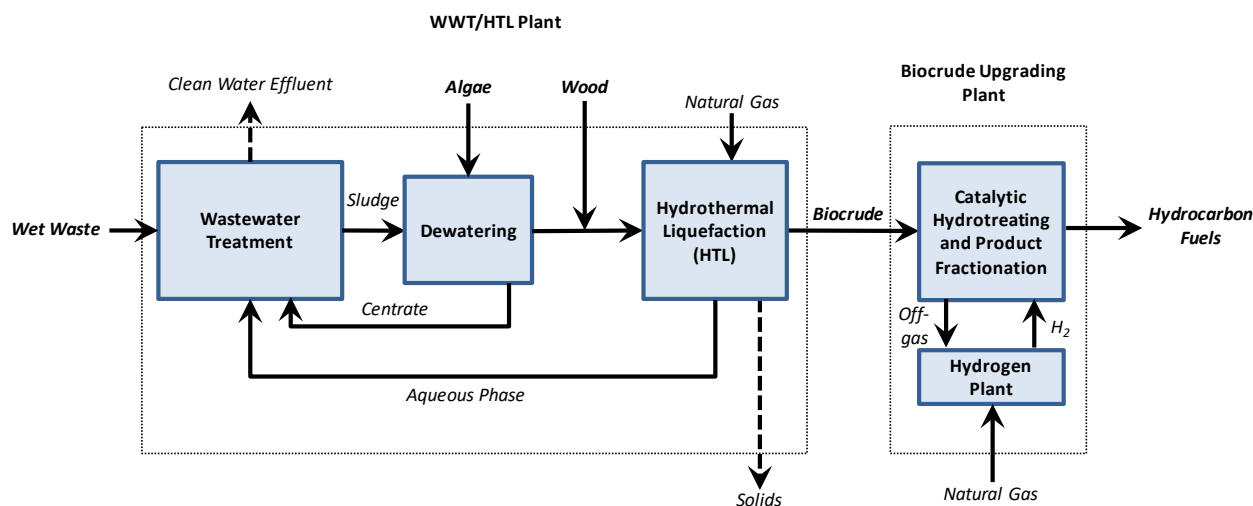


Figure 14. Process flow diagram for HTL oil production.

HTL of sewage sludge to produce a HTL biocrude followed by hydrotreating the HTL biocrude to produce a fuel blendstock has been scaled up to continuous flow reactors to produce over 3 gallons of a diesel range fuel. Many reports of process conditions and modifications to optimize product production rates and yields can be found in the references provided in this report (Elliott

2013, Guo 2015, Jarvis 2018, Gai 2015, Chen 2014, Jindal and Jha 2016, Yin 2010, Xu 2018, Marrone 2017, Marrone 2018). The process for converting wood or algae to biocrude via HTL uses processed wood residues (pellets or powder) and/or wet algae feedstock but is otherwise identical to that used for wet wastes.

### 3.1.3.3 TEA/LCA

A recent resource analysis estimates that 77 million dry tons per year of wet wastes are generated annually, 65% of which are underutilized for any beneficial purpose (DOE 2017). Approximately 14 million dry tons of the total resource is wastewater residuals (sludge and biosolids) generated at the nation's wastewater treatment plants (Seiple 2017). Based on data generated for HTL of wet waste at PNNL, a TEA determined a FY 2020 MFSP for fuel derived from HTL of \$4.31/GGE with a projected FY2022 MFSP of \$2.77/GGE (Figure 15). These costs are for a HTL plant scale of 110 dry ton/day sludge feed and an upgrading plant scale of 38 million gallons/year biocrude feed (Snowdon-Swan 2017). All costs are in 2016 dollars.

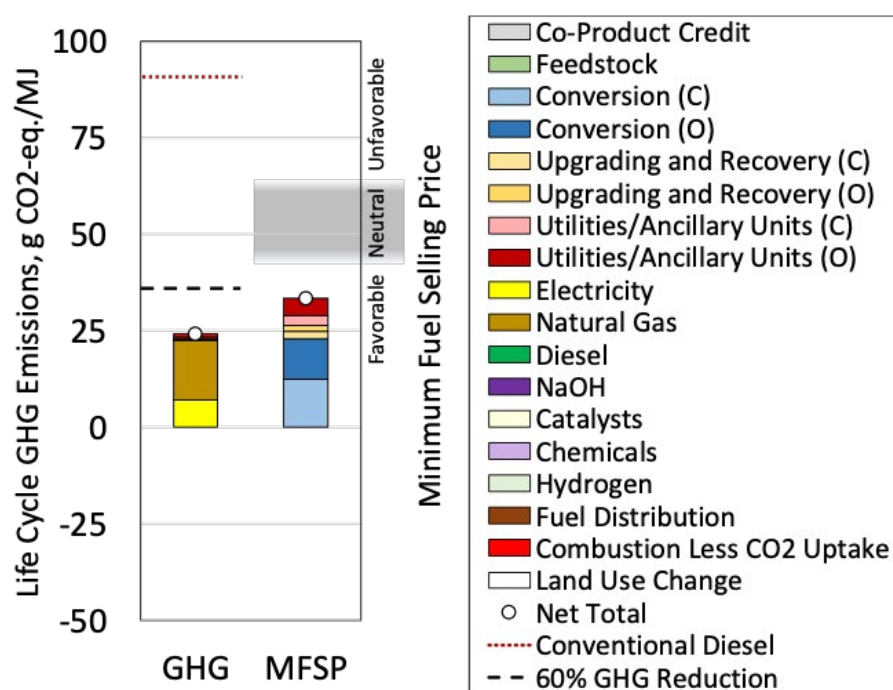


Figure 15. Diesel from wet waste-derived HTL bio-oil life cycle GHG emissions and MFSP.

MFSP for whole algae and algae/wood blends are higher, with the MFSP of the most recent published whole algae case from 2016 at approximately \$13/GGE (2016). A more recent case from 2020, currently under review, yields an MFSP <\$8/GGE (Figure 16). The whole algae target case projects an MFSP of \$4.44/GGE. Algae/wood blends are projected to be significantly cheaper, such that both feedstocks fall into the neutral (whole algae) or favorable (algae/wood blends) classification.

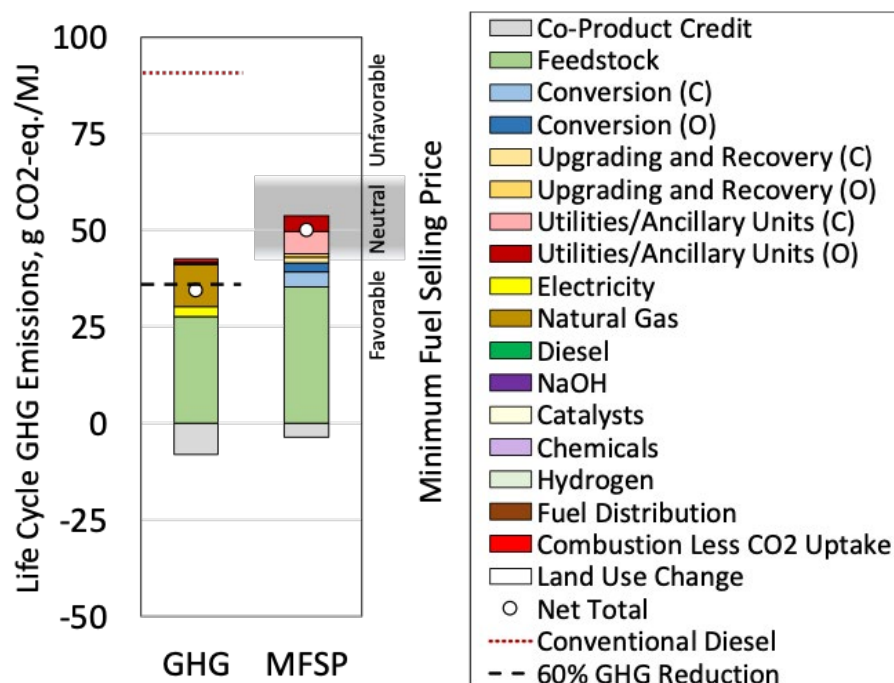


Figure 16. Diesel from algae-derived HTL bio-oil life cycle GHG emissions and MFSP.

Renewable diesel produced via HTL of wet wastes has the potential to reduce life cycle GHG emissions by 73%. The major contributor to the GHG emission of RD from wet wastes is the energy used in biocrude production, followed by bio-oil upgrading to RD where natural gas is consumed for hydrogen production, and finally electricity and catalysts (Cai 2020). Diesel blendstocks generated by HTL of algae and mixed algae-wood feedstocks can reduce GHG emission by 62–72%. The HTL conversion step is the primary contribution to GHG emissions, followed by CO<sub>2</sub> capture and transport to the algae pond, and algae dewatering (Cai 2020).

### 3.1.3.4 Challenges, Barriers, and R&D Needs

*Production and Separation.* While production has been scaled to the gallon scale, full-scale commercial production has not been demonstrated. Ongoing research and development needs include achieving long hydrotreating catalyst lifetimes and developing inexpensive and sufficient treatment of the HTL aqueous stream to enable recycling to the headworks of a wastewater treatment plant or direct discharge.

*Upgrading.* The extent of biocrude hydrotreating strongly influences fuel properties such as S, sooting propensity, and nitrogen content (an increase in which leads to increased NO<sub>x</sub> emissions). Research to define hydrotreating conditions to meet the ultralow sulfur diesel specification and reduce nitrogen content to ensure low engine NO<sub>x</sub> emissions needs to be conducted.

*Fuel Properties.* Given the large fraction of the product that is composed of n-alkanes, the cloud point and pour point can exceed target values. Decreasing the top end of the distillation cut point can bring these properties into line with the specification but reduces the yield substantially. Adding an isomerization step to increase branching and decrease cloud and pour point is straightforward, although adding a unit operation also adds cost. Research to identify low-cost methods to improve pour and cloud point for some HTL bio-oils could eliminate the need for this step. The high aromatic content in lignin leads to a significant fraction of aromatics in the bio-oil. The aromatics have poor CN and increased sooting propensity. Deep hydrotreating to saturate the double bonds in the aromatics decreases the sooting propensity and increases CN to some degree but adds significant cost and GHG emissions (through the increased use of hydrogen). New approaches to convert the aromatics to higher-CN, lower-sooting components could help overcome this limitation.

The main barrier to commercialization of HTL of algae and algae blends is the cost of the algae feedstock. Wood residues typically do not provide target values of critical fuel properties, although the combination of algae and wood together can do so. The TEA (Jones 2014) conducted on algae-derived bio-oils indicated these blendstocks could not meet the \$5.50/GGE upper limit established by Co-Optima for favorable assessment if co-products are excluded. More recent analyses have projected costs as low as \$4.45 by 2030 (DOE 2020), indicating this blendstock can meet the Co-Optima cost criterion. Outside of feedstock cost, capital cost is the main barrier to entry, with heat exchangers representing a significant fraction of the capital cost. Unlike HTL of wet wastes, the aqueous stream from the algae HTL process can be recycled to the algae process, both recovering the nutrients and addressing the aqueous stream liability.

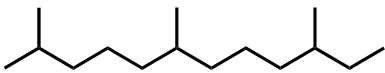
The researchers gratefully acknowledge the collaboration with the Great Lakes Water Authority who provided the sewage sludge and partnered in HTL development.

### 3.1.4 Farnesane

Farnesane is a branched C15 hydrocarbon suitable for use as a drop-in diesel replacement. Typically produced via fermentation of sugars, the primary barrier to market adoption and use of farnesane is cost and scale of production.

#### 3.1.4.1 Property Summary

Farnesane has a DCN of 58.6 and an LHV of 43.3 MJ/kg. In MCCI engine testing, neat farnesane demonstrated significant reductions in total hydrocarbon and particulate emissions compared to petroleum diesel (Soriano 2018), although it does require additives to meet D975 requirements for conductivity and lubricity.

<b>Farnesane (2,6,10-trimethyldodecane)</b>	
	
Formula	C <sub>15</sub> H <sub>32</sub>
CN	58.6
T <sub>b</sub> (°C)	198
Flash point (°C)	110
MP (°C)	-73
Water solubility (mg/L)	<0.1
YSI	110
Energy density (MJ/L)	33.5
Specific energy (MJ/kg)	43.3
Kinematic viscosity (mm <sup>2</sup> /s@40°C)	14
Density (kg/m <sup>3</sup> @15°C)	0.773

### 3.1.4.2 Production from Biomass

Farnesane is a branched sesquiterpene used in fuel, cosmetic, lubricant, and flavor and fragrance applications. Farnesane has been used commercially as a jet fuel additive (approved for blending into jet fuel at up to 10 volume percent in ASTM D7566) and has demonstrated promising diesel fuel properties (Soriano 2018, George 2015). Amyris, Inc., has scaled biochemical production of farnesane to forty million liters per year in production capacity, achieving titers as high as 130 g/L via the mevalonate pathway in engineered *Saccharomyces cerevisiae* (Meadows 2016). Farnesane can be produced from lignocellulosic sugars produced through a combination of feedstock pretreatment, enzymatic hydrolysis, and biological upgrading via aerobic fermentation to farnesene. After downstream processing to remove cells, separate the aqueous and organic phases, and remove hydrophobic contaminants, farnesene is reduced to farnesane by a hydrogenation reaction (Gray 2014).

### 3.1.4.3 TEA/LCA

Overall process design and economic projections for farnesane production from lignocellulosic biomass have previously been reported by (Davis 2013) and are shown in Figures 17 and 18, respectively.

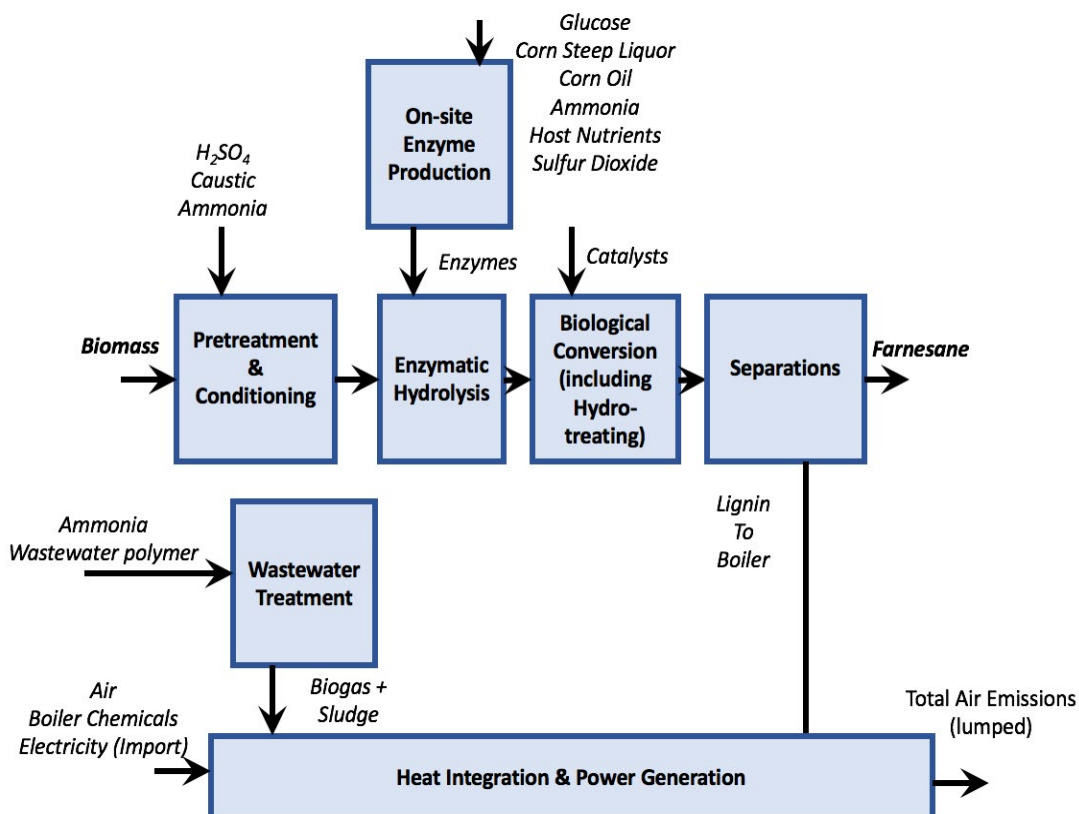


Figure 17. Process flow diagram for farnesane production.

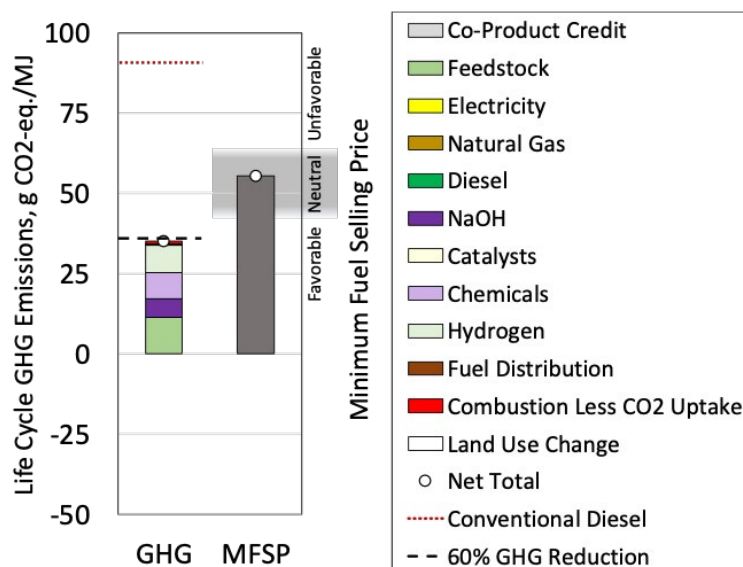


Figure 18. Farnesane life cycle GHG emissions and MFSP.

Based on this 2013 study, projections of MFSP for farnesane depend on metabolic pathway and range between \$5–\$6/GGE. Davis and colleagues also estimate MFSP using a theoretical anaerobic pathway at \$4.4/GGE due to lower costs associated with anaerobic fermentation and an overall higher metabolic mass yield. Life cycle GHG emissions of farnesane can achieve approximately a 61% reduction in GHG emissions compared to petroleum diesel. The major contributor to the GHG emissions is upstream emissions due to feedstock production.

#### 3.1.4.4 Challenges, Barriers, and R&D Needs

Farnesane is one of the most mature advanced biofuels, with commercial production demonstrated in 200,000-L scale fermenters at titers and yields approaching maximum theoretical values (Meadows 2016). Widespread deployment of farnesane as a biofuel is primarily dependent on reductions in the cost of cellulosic sugars. While overall production cost could be lowered significantly via anaerobic production (Davis 2013), anaerobic production of sesquiterpenes via the mevalonate pathway has not yet been reduced to practice.

#### 3.1.5 Isoalkanes Derived from Volatile Fatty Acids

Isoalkanes derived from VFAs are a promising class of diesel blendstocks. 5-ethyl-4-propylnonane is a C<sub>14</sub> isoalkane that can be derived from the catalytic upgrading of butyric acid, representing a broader class of hydrocarbons that can be derived from acid fermentation products (Hui 2019, Fioroni 2019a, b). This includes mono-carboxylic acids produced with engineered microorganisms (e.g., butyric acid), as well as mixed C<sub>3</sub>–C<sub>8</sub> carboxylic acids, also referred to as VFAs, produced from mixed microbial consortia. While the GHG emissions for 5-ethyl-4-propylnonane produced via fermentation of lignocellulosic biomass and subsequent upgrading do not achieve the 60% reduction sought by Co-Optima, an isoalkane mixture produced from VFAs derived from food waste does meet the GHG emissions reduction target, and in fact provides negative carbon emissions by avoiding landfilling the food waste.

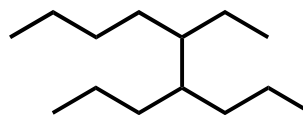
### 3.1.5.1 Property Summary

Isoalkanes such as 5-ethyl-4-propylnonane demonstrate high cetane, low freezing point and reduced sooting tendency (Table 6). The high degree of structural branching within this C14 and related compounds results in an MP below  $-80^{\circ}\text{C}$ , falling well below the  $0^{\circ}\text{C}$  target. The boiling point of  $230^{\circ}\text{C}$  is also well below the Tier 1 cutoff limit of  $338^{\circ}\text{C}$ , while the flash point of  $74^{\circ}\text{C}$  was suitably high to ensure low flammability.

The high degree of branching resulted in a relatively low density of  $0.78\text{ g/mL}$  and kinematic viscosity at  $40^{\circ}\text{C}$  of  $1.49$ . The CN of 48 was slightly above that of typical petroleum diesel, with a comparable energy density of  $44\text{ MJ/kg}$ . The fully saturated hydrocarbon structure resulted in a YSI of 98 that was less than half the value of fossil diesel due to the lack of aromatics.

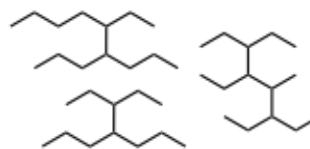
Sufficient quantities of 5-ethyl-4-propylnonane were produced for Tier 2 fuel property testing as a 20 vol% blend in clay-treated petroleum diesel (Emam 2018). The clay treatment removes additives that modify the diesel fuel properties so that the impact of the bioblendstock can be determined. The blend showed a marked decrease in normalized sooting concentration (NSC) of 11% and slightly decreased cloud point of  $-12^{\circ}\text{C}$ . The low viscosity observed with the neat bioblendstock fell within the acceptable range when blended at 20 vol%, with a value of  $2.08\text{ cSt}$  at  $40^{\circ}\text{C}$ . The lubricity and conductivity of the blend both did not meet the specification, likely due to the lack of additives, while the oxidation stability of the blend slightly improved.

#### Isoalkanes derived from volatile fatty acids



Formula	$\text{C}_{14}\text{H}_{30}$
CN	48
$T_b$ ( $^{\circ}\text{C}$ )	230
Flash point ( $^{\circ}\text{C}$ )	74
MP ( $^{\circ}\text{C}$ )	$-80$
Water solubility (mg/L)	$<0.1$
YSI	98
Energy density (MJ/L)	34.3
Specific energy (MJ/kg)	44.0
Kinematic viscosity ( $\text{mm}^2/\text{s}@40^{\circ}\text{C}$ )	1.49
Density ( $\text{g/mL}@40^{\circ}\text{C}$ )	0.78

#### Isoalkanes Derived from Volatile Fatty Acids



Formula	isoalkane-rich hydrocarbons
CN	73
$T_b / T_{90}$ ( $^{\circ}\text{C}$ )	268
Flash point ( $^{\circ}\text{C}$ )	62
Cloud Point ( $^{\circ}\text{C}$ )	$-53$
Water solubility (mg/L)	$<0.1$
YSI/NSC	$-/0.49$
Energy density (MJ/L)	34.6
Specific energy (MJ/kg)	44.4
Density ( $\text{g/mL}@40^{\circ}\text{C}$ )	–

Table 6. Fuel property values for pure 5-ethyl-4-propylnonane and as a 20% blend with fossil diesel (Huo 2019, Fioroni 2019). – = not measured; \*tests with 80% pure 5-ethyl-4-propylnonane.

5-Ethyl-4-propylnonane properties	Neat (94%) blendstock	Clay-treated petroleum diesel	20% Blend of 5-ethyl-4-propylnonane in clay-treated petroleum diesel
MP (°C)	<-80	–	–
Cloud point (°C)	<-80	-9.7	-12
Boiling point/T90 (°C)	230	335	327
Flash point (°C)	74	61	54
Density (g/mL)	0.78	0.86	0.85
Kinematic viscosity at 40°C (cSt)	1.49	2.66	2.08
LHV (MJ/kg)	44	42.9	43
Cetane number	48	47	46
YSI/NSC	98/0.37	NA/1	NA/0.89
Water solubility (mg/L)	< 0.1	–	–
Carbon residue (wt%)	–	0.09	–
Lubricity (mm)	–	0.520	0.538*
Conductivity (pS/m)	–	1	1*
Oxidation stability (min)	–	69.6	76.6*

In addition, a mixed isoalkane-rich bioblendstock was produced from VFAs derived from the anaerobic fermentation of food waste. Relative to 5-ethyl-4-propylnonane, the neat bioblendstock demonstrates a higher CN of 73, which may be due to a lower degree of branching that results when using carboxylic acids with shorter chain length. The isoalkane mixture displayed a low freezing point of -53°C, and a NSC half of fossil diesel fuel at 0.49 (see Table 6). Energy density (34.6 MJ/L) and specific energy (44.4 MJ/kg) were comparable to 4-ethyl-5-propylnonane and petroleum diesel. The T90 boiling point of the mixture was 268°C, below the Tier 1 cutoff limit of 338°C. The flash point of 62°C was also suitably high. Work is in progress to evaluate the Tier 2 fuel properties of the mixed isoalkanes blended with clay-treated petroleum diesel.

### 3.1.5.2 Production from Biomass

5-Ethyl-4-propylnonane can be produced from corn stover via deconstruction of biomass to sugars, fermentation of sugars to a butyric acid intermediate, and a catalytic upgrading and separation step to 5-ethyl-4-propylnonane. Research into this bioblendstock and conversion pathway is currently being actively pursued with both baseline and future target cases and economic assessments described in detail in existing reports (Davis 2018, Davis 2020). Figure 19 shows a generic process flow diagram for this process. In brief, under the future target case, corn stover is processed in a continuous alkaline extraction/deacetylation step followed by mechanical refining for increased enzymatic access to the biomass fibers.

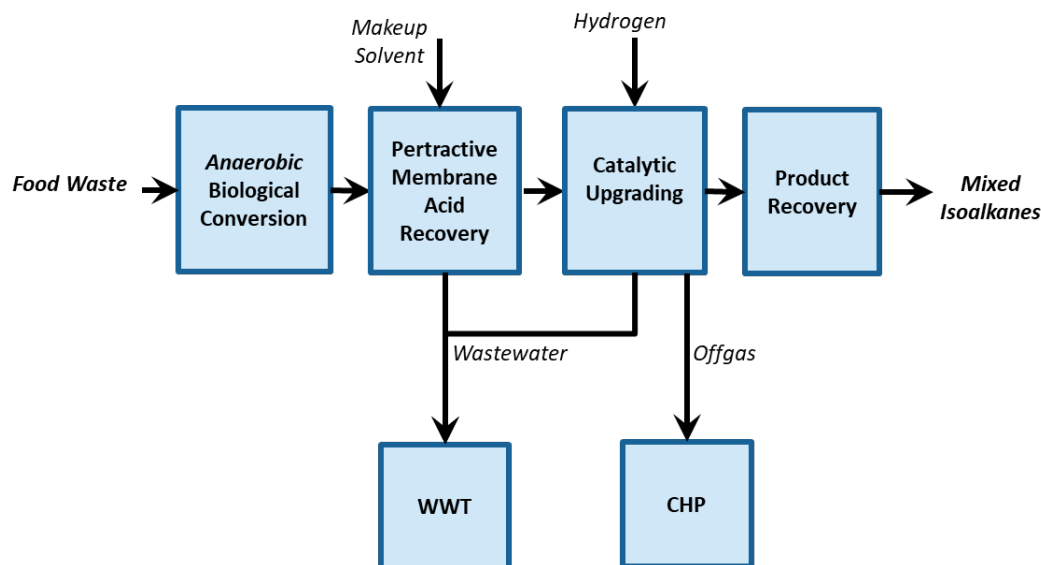


Figure 19. Process flow diagram for production of isoalkanes from VFAs.

This pretreated material is sent through a continuous enzymatic hydrolysis process where sugars are removed as they are produced via a microfiltration membrane. Clarified and concentrated sugars are routed to the fermentation area of the process, using *Clostridium tyrobutyricum* to produce butyric acid via fed-batch fermentation, with butyric acid being continuously removed through a pump-around loop incorporating a pertractive membrane system with a solvent. Acids are separated from the solvent phase through distillation and then catalytically upgraded through a ketonization step to produce 4-heptanone, which is later upgraded across a condensation step to an oxygenated C14 molecule. Downstream hydrotreating removes oxygen from the molecule, leaving the product 5-ethyl-4-propylnonane. The target case process evaluated within Co-Optima varies from the existing published report cited above in that lignin will no longer be valorized to co-product, but rather routed to boilers for process heat and energy, which provides a consistent basis across evaluated MCCI bioblendstocks albeit reducing economic and sustainability credits as may be generated from a parallel lignin-to-co-product train.

Isoalkanes can also be produced from VFAs with carbon chain lengths ranging from C3-C8. Similar to the process described above for 5-ethyl-4-propylnonane, anaerobic digestion can be performed with a mixed microbial consortium that arrests methanogenesis (Atasoy 2018, Granda 2009). This fermentation process has been demonstrated with a variety of wet waste feedstocks, including food waste, sewage sludge, algae, manure, and lignocellulosic biomass (Atasoy 2018, Granda 2009, Venkateswar et al. 2020). Separation technologies are being developed to recover VFAs from fermentation broth for downstream processing, including extraction, distillation, electrodialysis, and membranes processing (Fasahati 2014, Saboe 2018, Venkateswar et al. 2020). Once recovered in their neat form, VFAs can be upgraded to isoalkanes catalytically using the same sequence of unit operations for 5-ethyl-4-propylnonane—ketonization, condensation, and hydrodeoxygenation.

Isoalkanes can also be produced from VFAs with carbon chain lengths ranging from C3-C8. Like the process described above for 5-ethyl-4-propylnonane, anaerobic digestion can be performed with a mixed microbial consortium that arrests methanogenesis (Atasoy 2018, Granda 2009). This fermentation process has been demonstrated with a variety of wet waste feedstocks, including food waste, sewage sludge, algae, manure, and lignocellulosic biomass (Atasoy 2018, Granda 2009, Venkateswar et al. 2020). Separation technologies are being developed to recover VFAs from fermentation broth for downstream processing, including extraction, distillation, electrodialysis, and membranes processing (Fasahati 2014, Saboe 2018, Venkateswar et al. 2020). Once recovered in their neat form, VFAs can be upgraded to isoalkanes catalytically using the same sequence of unit operations for 5-ethyl-4-propylnonane—ketonization, condensation, and hydrodeoxygenation (Davis 2018).

The techno-economic model for production of isoalkanes from VFAs assumes the use of food waste as a feedstock at a scale of 250 wet U.S. tons per day (Bhatt 2020). Food waste, assumed to be available at zero cost, is fed directly to arrested anaerobic digestion with no pretreatment. Here, it is converted to VFAs in the C2-C6 range by a mixed microbial consortium. The VFAs are recovered from the aqueous phase via solvent extraction across a pertractive membrane and are subsequently isolated from the solvent by distillation (Saboe 2018). Following this, the VFAs undergo a sequence of catalytic upgrading operations (ketonization, condensation, and hydrodeoxygenation) for upgrading to diesel- and naphtha-range fuels, consistent with the pathway for 5-ethyl-4-propylnonane (Davis 2018). Naphtha-range fuels are assumed to be sold as a co-product. TEA for production of isoalkanes from food waste-derived VFAs found an MFSP of \$4.3/GGE for the diesel-range fuels. Total fuel production was approximately 1.0 MM GGE/year, corresponding to a total fuel yield of 53 GGE/dry ton. Approximately 80% of fuel production attributed to diesel-range fuels. This relatively low production cost can be largely attributed to a lack of costs associated with the food waste feedstock and pretreatment.

This bioblendstock reports favorable GHG emissions, particularly when considering the credit for the displacement of conventional waste management practices for the food waste feedstock. A second version of the result is shown without the displacement credit to bound the result. The first value reflects the system-wide change caused by replacing conventional waste management with the fuel production pathway today, while the second represents a situation where the feedstock is already well managed prior to implementation of the conversion process. These approaches give different LCA results. The LCA results show that this bioblendstock can achieve negative GHG emissions (-103 gCO<sub>2e</sub>/MJ) considering avoided methane emissions and 16 gCO<sub>2e</sub>/MJ with the second approach. These can be compared to petroleum diesel with life cycle GHG emissions of 91 gCO<sub>2e</sub>/MJ. In the first approach, it is considered food waste will be diverted from landfill, therefore the emissions credits resulted from the avoided emissions from landfilling food waste play an important role in reducing total emissions. In both cases, carbon sequestration credits are applied due to landfilling of the solid waste stream produced as a byproduct of this fuel production process. The solid waste stream contains 46% of the feedstock carbon. Since the solid waste is from an arrested anaerobic digestion process, it is assumed that it has similar carbon stability to conventional anaerobic digestate. Therefore, 20% of carbon in the solid waste is eventually sequestered. In addition, A small amount of CH<sub>4</sub> (0.05 g CH<sub>4</sub>/kg C landfilled) is emitted during accounted for in both approaches (Han 2011, Wang 2020). The rest of the carbon within the solid waste is emitted as CO<sub>2</sub>.

### 3.1.5.3 TEA/LCA

The MFSP of 5-ethyl-4-propylnonane using current baseline experimental parameters of conversions, yields, and recoveries was among the highest cost pathways evaluated within this report at over \$8/GGE in 2016 dollars. Future research progress under target case assumptions offers the potential of reducing MFSP to near \$5.5/GGE, which is among the middle-third of MFSP for evaluated MCCI bioblendstocks. Challenges for this and all biochemical pathways will be in overcoming biomass recalcitrance across feedstock compositional and physical variabilities and improving biomass deconstruction to sugars and sugar upgrading to reach research targets. As currently modeled, life cycle GHG emissions and fossil energy use of 5-ethyl-4-propylnonane do not meet the 60% emission and energy reduction criterion compared to conventional diesel. One of the reasons is the significant amount of NaOH used in the pretreatment step. While these numbers do not include the impacts of lignin-based co-products, Co-Optima researchers demonstrated in their target case evaluation of 5-ethyl-4-propylnonane that routing lignin and other residual streams through a parallel deconstruction, fermentation, and upgrading step could ultimately produce adipic acid to be sold as a co-product. With such additional co-product revenues, they highlighted a path to reduce MFSP below \$2.5/GGE for this pathway (Davis 2018). This approach could work for other biochemical pathways aimed at production of MCCI bioblendstocks if research targets can be met.

The TEA and LCA for production from food waste (or other waste source) are in progress. We expect that, depending on the waste disposal practice for the feedstock used to produce VFAs, significant cost and greenhouse gas reductions would be realized due to low waste feedstock costs and avoided methane emissions (Lee 2018, Gálvez-Martos 2021). The results of these analyses are shown in Figure 20.

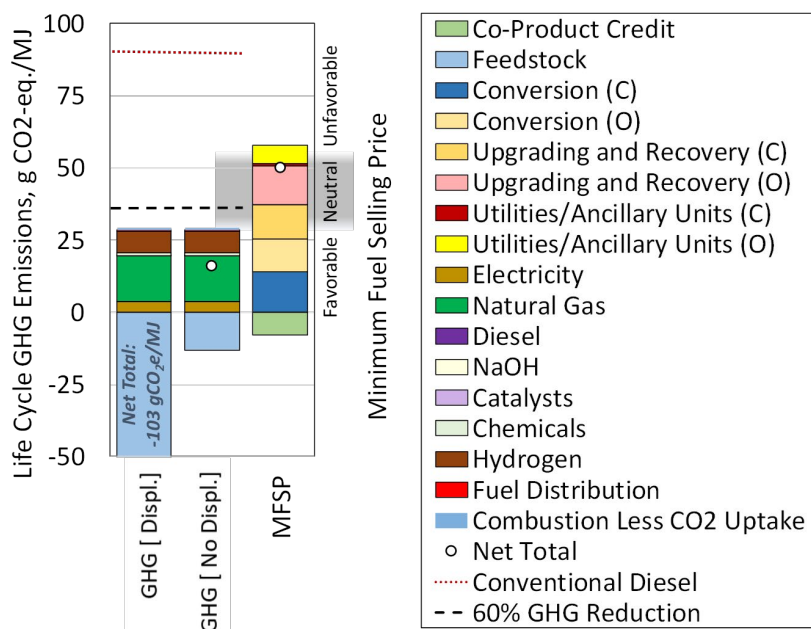


Figure 20. Isoalkanes from VFAs life cycle GHG emissions and MFSP. Displ. refers to the credits for the displacement of conventional waste management practices.

### 3.1.5.4 Challenge, Barriers, and R&D Needs

The production cost and technology readiness level remain the key challenges for the scalable production. Currently, conversion efforts have been limited to bench-scale experiments at the 100-mL scale. While this has been shown with model and fermentation-derived butyric acid, additional work is needed to transition the process chemistry to continuous reactors for liter-scale validation of recycle loops and final fuel properties that can be impacted by side products and biogenic impurities. While production costs and GHG emissions associated with deconstructing lignocellulosic sugars may be addressed with the use of wet waste feedstocks (Cavalcante 2017), further R&D is needed to evaluate the fuel properties of bioblendstocks derived from varying waste compositions (e.g., manure, wastewater sludge, etc.). Waste composition can alter the volatile fatty acid carbon chain length distribution, degree of hydroxylation, and extent of branching (Cavalcante 2017), which may influence the overall conversion process performance and final fuel properties.

### 3.1.6 Ethanol-to-Distillate – Isoalkane Blendstock

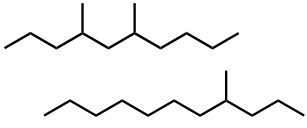
Catalytic oligomerization of ethylene derived from dehydration of ethanol can produce a mixture of hydrocarbons of varied carbon chain lengths that can be separated by distillation to form high quality jet and diesel fuels. This ethanol-to-distillate (ETD) process has been reduced to practice by PNNL in partnership with LanzaTech to produce jet and diesel fuels (Lilga 2017a, 2017b, 2018a, 2018b; Brooks 2016). The primary challenges to adoption and use are to increase scale of production and reduce productions costs.

#### 3.1.6.1 Property Summary

The alkane/isoalkane mixture produced from ethanol consists of C<sub>8</sub>+ isomers that is dominated by even-number carbon chains. The chemical compositions of the jet and diesel cuts are controlled by the distillation ranges.

The isoalkane mixture has demonstrated cloud point and pour points below -60°C and CN >54. Isoalkanes in the distillate fuel range have very low water solubility.

Testing of the heavy distillate range blendstock was conducted in 2016 by Colorado State University, including as a 15% blend in a certification diesel. The test diesel blend met or exceeded all ASTM D975 diesel fuel property specifications. One finding was that the heat release from the ETD fuel occurred slightly earlier than the standard diesel and some reduction in brake-specific total hydrocarbon emissions was

Ethanol-to-Distillate Isoalkanes	
	
Formula	~C <sub>8</sub> -C <sub>24</sub> isoalkanes
CN	55-68
T <sub>b</sub> (°C)	–
Flash point (°C)	>54
Cloud Point (°C)	-60.1
Pour Point (°C)	-66.0
Water solubility (mg/L)	<0.1
YSI	N/A
Energy density (MJ/L)	35.0
Specific energy (MJ/kg)	43.8
Kinematic viscosity (mm <sup>2</sup> /s@40°C)	2.0-4.8
Density (g/mL@40°C)	0.786

also noted. Table 7 lists some of the measured fuel properties of the ETD diesel fuel, its 15% blend in certification diesel and a neat certification diesel fuel for comparison.

Table 7. Selected measured properties of certification diesel, ETD diesel, and a 15% blend of ETD with the certification diesel for engine testing.

Fuel	Volume of renewable fuel (%)	Density (g/mL)	C (wt %)	H (wt %)	O (wt %)	LHV (MJ/kg)	DCN
Certification diesel	0	0.848	87.1	12.9	0.0	42.8	45.5
ETD	100	0.791	85.0	15.0	0.0	43.8	66.7
ETD blend	15	0.840	86.8	13.2	0.0	42.9	46.2

### 3.1.6.2 Production from Biomass

The ETD production process starts with gasification of biomass followed by syngas fermentation to produce ethanol. Next, ethanol is dehydrated to form ethylene, which is then oligomerized to C4–C6 olefins followed by further oligomerization to longer chain olefins. The olefins then hydrogenated to produce the alkane/isoalkane mixture that is fractionated by distillation to obtain jet and diesel fuel blendstocks. However, in principle, ethanol from any source could be used as the feedstock. The process is shown in Figure 21.

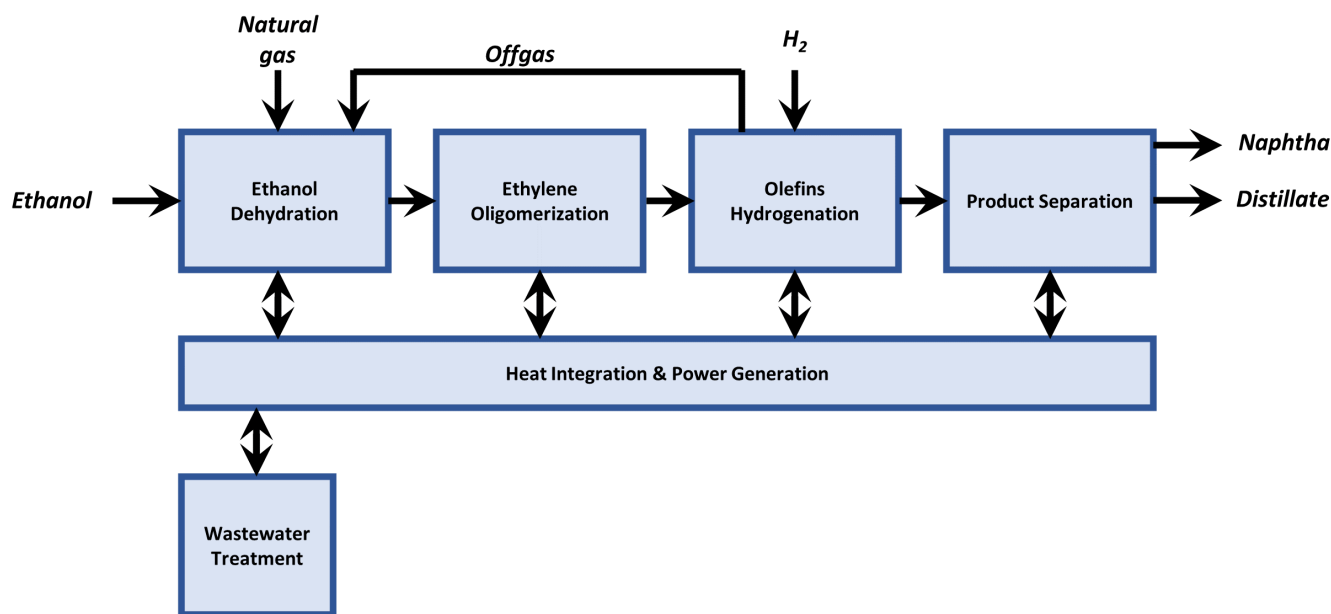


Figure 21. Process flow diagram for production of an isoalkane blendstock from ethanol.

### 3.1.6.3 TEA/LCA

Several feedstocks for the ETD process have been evaluated include corn stover, woody biomass, and cellulosic residues. Techno-economic and life cycle analyses were conducted for biomass-generated syngas utilizing LanzaTech's gas fermentation technology and PNNL's ETD process. The TEA determined an MFSP of \$3.00 including co-product credits for a 2,3-

butanediol co-product, while the LCA indicated that a reduction of more than 90% in GHG emissions could be achieved for this route from biomass to fuel blendstock and chemicals (Harmon 2017). Furthermore, many LCAs have been performed for ethanol-to-jet production approaches starting from sugar and lignocellulosic feedstocks. Depending on co-product and other assumptions, these analyses have generated a wide range of GHG emissions, from -27 to 80 gCO<sub>2e</sub>/MJ (Han 2017). The most direct comparison for an ETD MFSP with other Co-Optima analyses is for a biomass-derived gasification approach, starting from ethanol at \$2/gal to produce the MCCI blendstock and a gasoline co-product (sold at \$1.5/gal). If hydrogen is derived from the ethanol feedstock, the MFSP is \$5.10/gge, whereas if the hydrogen is produced externally, the MFSP is \$4.29/gge. LanzaTech efforts to utilize waste gas streams negate the need for a biomass gasifier for syngas production, which greatly improves the economic and environmental benefits of the gas fermentation plus gas to liquids technology.

#### 3.1.6.4 Challenges, Barriers, and R&D Needs

The primary challenges are to increase scale of production and reduce productions costs, as the product meets all fuel property requirements. One approach to increasing scale is to increase the number of production sites and feedstocks. For example, further development of the technology is currently focused on utilization of off-gas waste streams, such as those found steel mills and refineries. This includes LanzaTech's Freedom Pines site, which is currently conducting a demonstration project for DOE-Bioenergy Technology Office with plans for commercial plants in the world market.

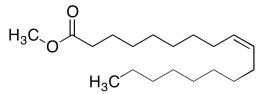
#### 3.1.7 Biodiesel (Fatty Acid Methyl Esters)

Biodiesel is composed of fatty acid methyl esters, typically with 16 or 18 carbons, often mono-unsaturated. Biodiesel is used in the market, usually at low blending levels (5% or lower), with barriers to higher blend levels and wider adoption including low temperature operability, trace metal contaminants, and oxidative stability.

### 3.1.7.1 Property Summary

Biodiesel is produced from the transesterification of triglycerides, or esterification of fatty acids, with an alcohol. The transesterification reaction produces fatty acid alkyl esters and the co-product glycerin. Methanol is the most common alcohol used in this reaction, leading to the production of fatty acid methyl esters or FAME.

Specific properties of biodiesel, such as cloud point and CN, depend on the feedstock used. Minimum property requirements for biodiesel as a transportation fuel are set in ASTM International Specification D6751: *Standard Specification for Biodiesel Blend Stock (B100) for Middle Distillate Fuels*. Properties of biodiesel and biodiesel blends will vary with the blend level, diesel fuel quality, and biodiesel properties.

<b>Biodiesel</b>	
	
Chemical Formula	C16 and C18 FAME
CN	>47
T <sub>b</sub> (°C)	360
Flash point (°C)	>93
Cloud point (°C)	-5 to 15
Water solubility (mg/L)	<0.1
YSI	–
Energy density (MJ/L)	33.0
Specific energy (MJ/kg)	37.5
Kinematic viscosity (mm <sup>2</sup> /s@40°C)	1.9 to 6.0
Density (@15°C)	0.88

Biodiesel is commonly blended with conventional diesel fuel at 5% or lower, and sometimes up to 20%, by volume (vol%) prior to use in vehicles. Common notation is “Bxx,” where xx is the vol% biodiesel in a blend. For example, B20 is a 20 vol% blend of biodiesel in 80 vol% conventional diesel fuel. Blends up to B5 are considered D975 compliant diesel fuel and can be sold without disclosure of biodiesel content. For blends between B6 and B20, ASTM Specification D7467: *Standard Specification for Diesel Fuel Oil, Biodiesel Blend (B6–B20)* covers the fuel quality to ensure fit-for-purpose blends. These blends must also be identified to consumers through specific pump labeling. Figures 22 and 23 show the results of these analyses.

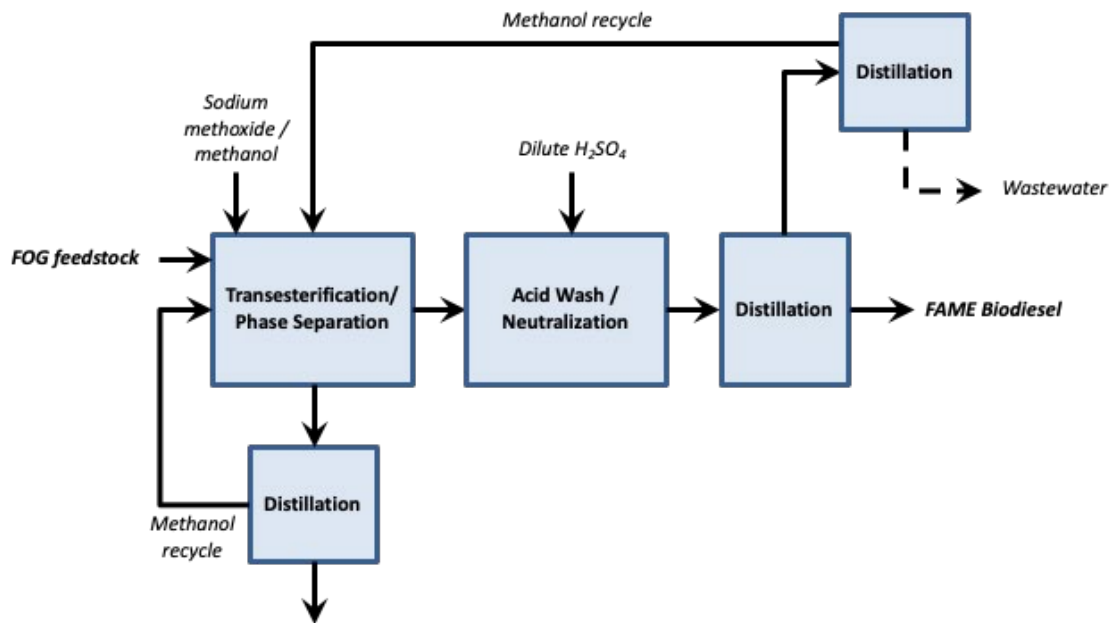


Figure 22. Process flow diagram for production of FAME (biodiesel) from FOG and methanol.

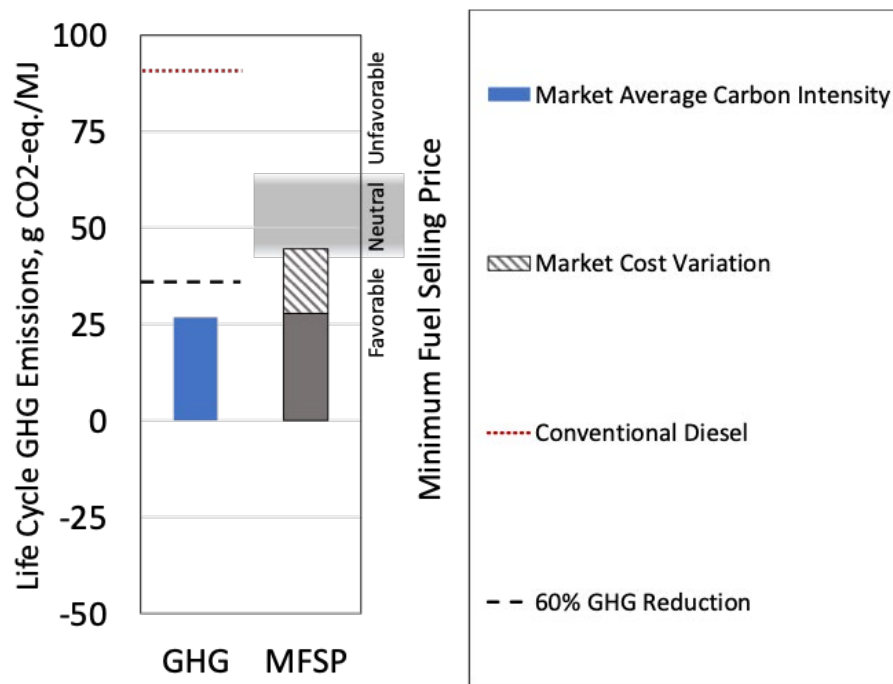


Figure 23. Market-average life cycle GHG emissions and MFSP for FAME made from FOG and methanol, showing the variation in market cost.

### 3.1.7.2 Production from Biomass

Biodiesel is produced commercially from FOGs including soybean oil, canola, and various animal fats like lard, tallow, and poultry fats. U.S. biodiesel producers used 12 different lipid feedstocks in 2018, the largest of which were soybean oil (54% of the total), corn oil (15%), used cooking oil (12%), canola oil (9%), white grease (4%), and tallow (3%) (Fuels Institute 2020).

### 3.1.7.3 TEA/LCA

The production and use of biodiesel reduce GHG emissions compared to petroleum-derived diesel fuel. This pathway can meet the cellulosic biofuel criterion of at least 60% GHG emission reduction, with the certified LCFS pathways generating GHG emissions reductions in the range 39 to 90%. Feedstock and energy consumption are the key drivers of the total GHG emissions.

Biodiesel market prices vary and track approximately with the cost of petroleum derived fuels. While production costs will depend on process scale and feedstock used, U.S. five-year market prices have fluctuated approximately between \$2.43/GGE to \$3.88/GGE.

### 3.1.7.4 Challenges, Barriers, and R&D Needs

The years of industry experience in producing and using biodiesel as a commercial blendstock have helped identify several opportunities for improvement. One of the largest challenges facing biodiesel is the need for additional feedstocks to support market expansion. Several potential new feedstocks are being investigated, but few are fully commercial. Assuming adequate feedstock is available, biodiesel markets could expand significantly by blending at levels well below 20%. However, barriers exist for blending at levels of 20% and higher. Among these barriers, low-temperature operability is the most prominent for biodiesel produced from the feedstocks in use today. Residual metals in biodiesel may prove incompatible with future ultra-low NO<sub>x</sub> emission control systems and may need to be removed. Stability towards oxidation in the liquid phase in storage or onboard the vehicle may also become a more significant issue as blend levels increase.

Cold-weather (or low-temperature) operability can limit the use of biodiesel in some regions. The cloud point of biodiesel varies with feedstock. At the molecular level, the cloud point of FAME is affected by chain length and the degree of saturation. Molecules with saturated fatty acid chains will have higher cloud point than mono- or poly-unsaturated chains. Cloud point is also lower for shorter chains. The most common biodiesel feedstocks are C16 and C18 dominant. Depending on the fraction of C16 and C18 FAME and the degree of saturation, the cloud point of biodiesel varies from -5°C to over 15°C. A wintertime diesel fuel will generally have a cloud point below -12°C, and sometimes much lower.

Today cloud point challenges are managed by blenders in the market in several ways. Commonly, blenders reduce blend content, for example from B20 to B10, to mitigate cloud point issues. Blenders may also reduce the cloud point of the petroleum diesel used for blending by blending in No. 1 grade diesel, which will lower the cloud point of the biodiesel blend. Low temperature operability additives, which reduce the temperature where filter clogging will occur by a few degrees, may also be used. Despite these strategies, maintaining high blend levels or moving to higher blend levels in colder climates will become a significant barrier to

biodiesel use as markets expand. Research on crop modification (conventional plant breeding, genetic engineering) to reducing saturated fatty acid content or chain length, or on methods to chemically modify the fatty acid chain structure, or other approaches to reducing cloud point is needed.

Residual metals in biodiesel come from the transesterification catalysts (either Na or K methoxide) and from process water used to extract impurities from the crude product (Ca). The alkali metals (Na and K) have been shown to poison some NO<sub>x</sub> reduction catalysts in diesel emission control systems (Williams 2014, Brookshear 2017) and all the metals result in ash that accumulates in diesel particle filters potentially leading to reduced filter life (Lance 2016). As diesel emission standards are tightened in the future, removal of these metals to much lower levels may be required. While technologies exist for metals removal, their application would increase production cost. Research to develop a heterogeneous catalyst for transesterification could eliminate the alkali metal contamination. This is a challenging problem because the liquid phase transesterification reactions occur in a multiphase system.

The poly-unsaturated fatty acid chains present in biodiesel present bis-allylic carbon atoms with a weak C-H bond that can break, leading to a stabilized radical that can react with oxygen. This initiates a peroxidation chain reaction very similar to low-temperature combustion but occurring at very low oxygen concentration and over days to weeks as compared to milliseconds. These reactions can lead to the formation of acids and gums that can negatively impact engine operation and durability. Antioxidant additives are used very successfully today to control oxidation of biodiesel and biodiesel blends in storage (Christensen 2014, Christensen 2018). However, expanding biodiesel blending above 20% may present additional challenges requiring a better understanding of how antioxidant mixtures function, or modification of the biodiesel to reduce or remove the di- or tri-unsaturated fatty acid chains.

### 3.1.8 Fatty Acid Fusel Esters

Fatty acid fusel esters (FAFEs) are long-chained ester compounds that resemble FAMEs, using a mixture of C2–C5 (fusel) alcohols instead of methanol to esterify the fatty acid precursors. Barriers to adoption and use include high viscosity and the need to demonstrate scalable, low-cost production meeting GHG emissions reduction targets.

### 3.1.8.1 Property Summary

The fuel properties of FAFEs are modified by the substitution of the fusel alcohol mixture for methanol. These changes include increased DCN and LHV, improved cold flow, and increased kinematic viscosity. These properties are summarized for esters of palmitic acid derived from a variety of short chained alcohols in Table 8. FAFEs also were synthesized using mixtures of fusel alcohol products generated from co-culture fermentations as described by Liu (2017, 2020) and Wu (2016), which are often comprised primarily of isobutanol and isopentanol isomers. These FAFE mixtures show an increase in DCN of +5, a 2% increase in net heat of combustion, and a cloud point 4°C lower than a FAME sample produced from the same lipid source.

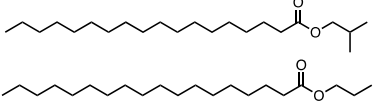
<b>Fatty Acid Fusel Esters</b>	
	
Formula	$C(R_2)C_2H_4O$
DCN	50-60
$T_b$ (°C)	197-282
Flash point (°C)	>130*
MP (°C)	<-10
Water solubility (mg/L)	<0.1*
YSI	104-127*
Energy density (MJ/L)	>30
Specific energy (MJ/kg)	40-41
Kinematic viscosity $mm^2/s@40^\circ C$	2.9-3.7
Density (g/mL@40°C)	0.817-0.861
* Predicted	

Table 8. Properties are summarized for esters of palmitic acid derived from a variety of short chained alcohols.

Palmitic Acid	Cetane Number	Melting Point [°C]	YSI
Methyl Ester	74.5 <sup>a</sup>	30.0 <sup>c</sup>	104 <sup>d</sup>
Ethyl Ester	85.9 <sup>b</sup>	21.7 <sup>c</sup>	109 <sup>d</sup>
Propyl Ester	93.1 <sup>b</sup>	20.4 <sup>c</sup>	115 <sup>d</sup>
Butyl Ester	82.6 <sup>b</sup>	16.9 <sup>c</sup>	121 <sup>d</sup>
Isobutyl Ester	84.8 <sup>b</sup>	-	127 <sup>d</sup>

<sup>a</sup> Klopfenstein 1985  
<sup>b</sup> Knothe 2009  
<sup>c</sup> Knothe and Dunn 2009  
<sup>d</sup> Calculated using YSI prediction tool (St. John 2018)

The properties of FAFEs are described in more detail by Monroe et. al. (2020), with some data from that work reprinted here as Figure 16. Similar to FAME biodiesel, the fuel properties of a FAFE sample are heavily dependent on the fatty acid profile of the lipid source used. Lipid sources with more saturated fatty acids will have a higher cloud point and DCN, while the reverse trends will be true for increased unsaturation. The potential variability in the fusel alcohol composition used to make the FAFE mixtures adds an additional element of variability in the fuel properties, with longer chained alcohols leading to increases in boiling point, YSI, LHV, CP, and DCN. The ranges shown in Table 8 capture the variability within fusel alcohol compositions while assuming a standard corn oil lipid profile. Figure 24 shows how the fuel properties of FAFEs derived from corn oil compare to FAMES with the same fatty acid profile.

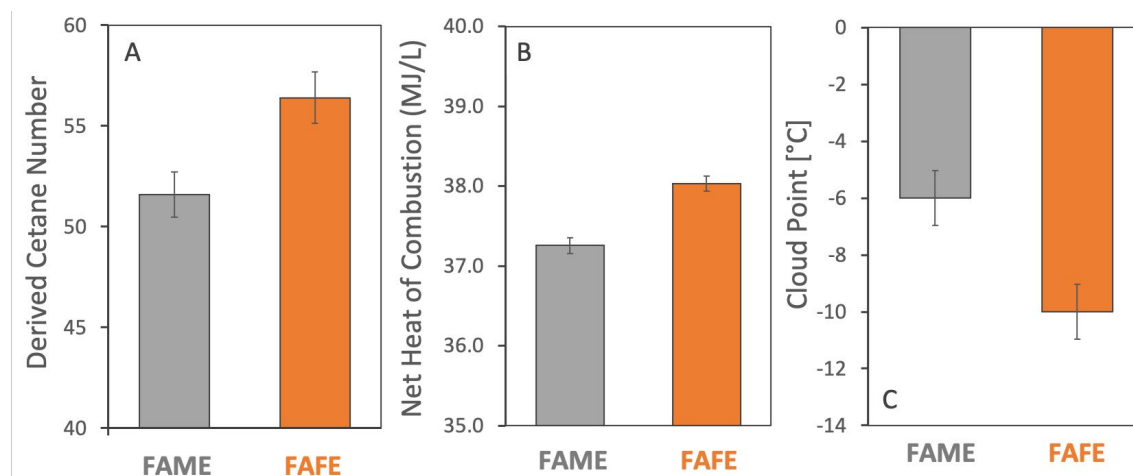


Figure 24. Comparison of FAME vs. FAFE properties for DCN, net volumetric heat of combustion, and CP. FAFE and FAME mixtures were both made from the same corn oil sample with identical fatty acid profiles. FAFE mixture is composed of 50 mol% isobutyl esters and 50 mol% isopentyl esters. Data adopted from Monroe (2020).

### 3.1.8.2 Production from Biomass

In general, the production of FAFEs will be similar to existing production methods for FAME biodiesel (see Figure 23). The alcohol mixture generated via fermentation can be used as a direct replacement for methanol in the base-catalyzed transesterification reaction used by many commercial producers, although reaction process conditions and the corresponding yields, rates and purification steps will be slightly different with fusel alcohols. FAFEs can be produced from traditional vegetable oil feedstocks as well as many waste oils and other next-generation biomass feedstocks with high lipid content such as algal biomass. Additionally, FAFEs could improve enzymatic conversion due to the decreased inhibitory effect of longer alcohols on lipases as compared to methanol. Monroe (2020) demonstrated that fusel alcohols produced from fermentations were able to be utilized by commercial lipases for FAFE production.

### 3.1.8.3 TEA/LCA

The process for producing FAFEs is based on the lignocellulosic corn stover conversion to sugars via the DMR/EH process. Fusel alcohol production starts with lignocellulosic sugars that then are biologically upgraded to fusel alcohols (predominately C4 and C5 branched primary alcohols - isobutanol, 2-methyl-1-butanol and 3-methyl-1-butanol) via anaerobic conversion (Dunn et al. 2018). Other components produced are 1,4-butanediol, benzyl alcohol and ethanol. The latter two components were removed prior to upgrading in the transesterification step. The conversion of fusel alcohols to FAFE was based on reaction with purchased soybean oil (\$0.33/lb), similar to biodiesel pathways using methanol to make FAME. Liquid lipase Eversa enzyme (\$6.8/lb) and deionized water are added to the alcohol mixture in a 5:1 alcohol-to-oil ratio and the enzyme and deionized water loadings are 2% w/w each of soybean oil [3]. The extent of reaction for fusel alcohols was estimated from literature to be 80% for isobutanol and ~13% each for methyl-1-butanol and 3-methyl-1-butanol. This conversion is achieved by setting a maximum FAFE-to-oil yield of 97 wt%. The outlet stream from the reactor containing

unconverted fusel alcohol, oil, FAFE, glycerol, and enzyme is processed through a series of separation units to obtain the final product FAFE with > 99.8 wt% purity. Glycerol co-product is obtained at a purity of 89.7 wt%, which was assumed to be sold as hydrolysis crude glycerol (\$0.27/lb). Obtaining a higher by-product credit would require further purification but the temperature constraint for glycerol (thermal degradation above 150°C [2]) prevents additional purification by distillation. Similarly, the temperature of streams containing soybean oil and FAFE cannot exceed 350°C and 250°C, while performing separation which required vacuum distillation to achieve. This is a significant processing difference between FAME and FAFE processes. Methanol and FAME are easily separated at acceptable temperatures whereas FAFE and fusel alcohols require vacuum distillation to stay below the upper temperature limits. Based on these temperature restrictions some residuals components are combusted for process heat and electricity generation rather than attempting to recycle them within the process. The MFSP for this process was estimated to be about \$3.5/GGE at the target conditions for fusel alcohol production from sugars. Because most of the energy content and fuel yield in FAFE comes from the soybean oil, the contribution from corn stover feedstock is only 12% of the MFSP on a per-GGE basis. Purchased chemicals, including soybean oil and enzyme, make up 77% of the MFSP. Financial factors contribute 16% of the MFSP. The life cycle GHG emissions for FAFEs are 43 gCO<sub>2</sub>e/MJ, putting it in the neutral range with a GHG reduction of 53% compared to petroleum diesel. Fossil energy use is 69% less than that for petroleum diesel. Feedstock production and NaOH used in the pretreatment of corn stover were the primary contributors to GHG emissions. GHG emissions associated with induced land use change also play a role as increased use of the soybean oil feedstock is assumed to have associated market effects. Figure 25 shows the MFSP and GHG emissions for FAFEs made from fusel alcohols and soybean oil.

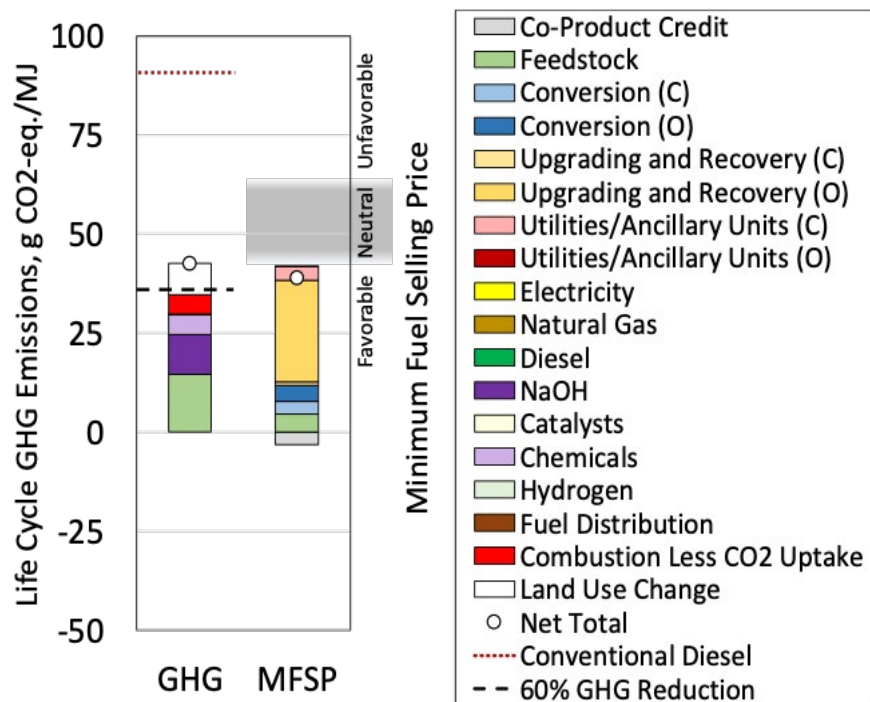


Figure 25. Market-average life cycle GHG emissions and MFSP for FAFEs made from FOG and methanol, showing the variation in market cost.

#### 3.1.8.4 Challenges, Barriers, and R&D Needs

While the production of FAFEs will be similar to existing production methods for FAME biodiesel, the use of longer chained alcohols has important implications for the esterification/transesterification processes utilized in biodiesel production plants. The impact of these changes on yield, separations and other parts of the process will require additional development to understand impacts on production costs and fuel quality. Further research also is needed to scale up fusel alcohol fermentation.

Research is needed to better understand the impacts of changing the methyl group on FAME to the fusel alcohols on the full suite of properties required for use as a diesel fuel. First, the freezing point is high compared to the target value and composition, or processing may need to be tuned to achieve target values of the freezing point. Second, the higher viscosity resulting from substitution of the methyl group with larger alkanes must be better understood and potentially mitigated. Finally, tuning the distillation curve of the product mixture (e.g., through modification of the fermentation or esterification steps) may be required.

### 3.2 Top Five Candidates with Fuel Property, TEA, and/or LCA Barriers

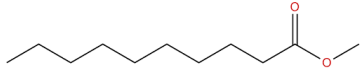
This section describes six blendstocks that have the potential to reduce criteria pollutant and GHG emissions and improve CN or operability but that also face significant barriers to deployment. These blendstocks are all oxygenates (four ethers and two esters) and face barriers including fuel properties, projected cost and GHG emissions reductions, all of which may be mitigated by additional research and development.

#### 3.2.1 Short-Chain Esters from Oilseed Crops

Some oilseed crops such as various cuphea cultivars (*Cuphea sp.*) produce fatty acids with a smaller carbon number profile than is currently used to produce biodiesel (e.g., C10–C14 vs. C16–C18). These oilseed crops could be used to produce a fatty acid methyl ester (biodiesel) with potentially better low-temperature characteristics and reduced engine-out NO<sub>x</sub> emissions, at the expense of a slight decrease in energy density. Currently, cost and scale are the primary barriers to adoption, as no suitable crops are cultivated at a cost that would be commercially viable for this purpose. Furthermore, potential GHG reductions have not been determined and fuel property barriers include viscosity.

### 3.2.1.1 Property Summary

The reaction of short chain fatty acids such decanoic acid with methanol produces fatty acid methyl esters such as methyl decanoate, a C10 FAME. Chemically, other than the smaller carbon numbers, these FAME molecules are identical to those found in biodiesel. The main oilseed crop producing medium-chain triglycerides (C8–C12) is cuphea cultivars, with species such *C. painteri*, *C. koehneana*, and *C. carthagenensis* representing cultivars producing a majority of C8, C10, and C12 fatty acids (Knothe 2014), although an engineered bacterial route has also been proposed (Kim and Gonzalez 2018). Coconut oil, a traditional biodiesel feedstock in Southeast Asia, contains small amounts of decanoic acid but is a primary source of dodecanoic and tetradecanoic acids (Firestone 2013).

Short-Chain Esters from Oilseed Crops	
	
Formula	$\text{CH}_3(\text{CH}_2)_n\text{CO}_2\text{CH}_3$ , n=8-12
ICN	52
T <sub>b</sub> (°C)	224
Flash point (°C)	111
MP (°C)	-18
Water solubility (mg/L)	<0.1
YSI	50*
Energy density (MJ/L)	29.6
Specific energy (MJ/kg)	34
Kinematic viscosity	1.7
mm <sup>2</sup> /s@40°C)	
Density (g/mL@20°C)	0.871
* Predicted	

The shorter chain length of these methyl esters impacts the properties, as they relate to current biodiesel specification. Shorter chain lengths reduce the flash point and the viscosity of the esters. The ASTM D6751 specification for biodiesel allows for a reduced flash point of shorter esters, with a minimum of 93°C. Ester viscosity also varies with chain length and shorter esters have lower kinematic viscosity. Methyl decanoate, for instance, has a kinematic viscosity (1.7 mm<sup>2</sup>/s) slightly below the specification minimum of 1.9 mm<sup>2</sup>/s. However, when blended into conventional diesel, the slightly lower kinematic viscosity of methyl decanoate should not cause long term operability issues. Furthermore, tuning the chain length distribution of the esters could increase the kinematic viscosity to meet the specification. The ignition quality of methyl decanoate readily exceeds the minimum specification of 40 and should increase the CN when blended with a petroleum base fuel; increasing the chain length would be expected to increase CN further (assuming no branching or points of unsaturation).

### 3.2.1.2 TEA/LCA

Production of short-chain esters from oilseed crops is expected to be similar to traditional FAME biodiesel (see Figure 23) and in this analysis is assumed produced from tricaprins-rich PSR23 cuphea seed oil feedstock (hybrid *Cuphea viscosissima* x *Cuphea lanceolata*). Seeds are pressed, heated, degummed, and bleached to produce refined seed oil (Evangelista and Cermak 2007). The oil undergoes transesterification with reactant methanol (CH<sub>3</sub>OH) and sodium methoxide (NaOCH<sub>3</sub>) base catalyst (Haas 2006), in which glycerol is produced as a side product. The ester-rich oil phase is then decanted from the glycerol-rich aqueous phase and glycerol is purified via distillation and produced as a co-product. The decanted oil then undergoes an acid wash, and the oil-rich phase is then decanted from the aqueous phase and flash dried to remove any remaining water, resulting in a C8–C12 ester-rich biodiesel.

### 3.2.1.3 TEA/LCA

Estimating the current and future potential costs for the cuphea-derived oil is challenging. A study by (Gesch 2010) estimated that a farmer would need to be compensated \$1830 per ton of harvested seed (Gesch 2010) or \$4.58/kg oil produced. While other transportation and handling costs are likely to come into play, this number was used as a baseline feedstock cost estimate to generate an MFSP of more than \$16/GGE. While future cuphea cultivation and agronomics are unknown, to achieve a target cost of \$5.5/GGE, cuphea oil would need to be produced and delivered to a biorefinery at a cost of approximately \$1200/ton or less. The Co-Optima target case compares the maturation price of cuphea oil to that of canola oil, which decreased threefold in the first three years of commercial production (1974–1977) and then steadily decreased another threefold over the next 25 years. Accounting for inflation (Futures 2020), this would lead to a cuphea oil price of \$1.50/kg oil in 2023, and an equivalent of \$0.50/kg oil in 2045.

Environmental metrics are also challenging to estimate. For example, life cycle GHG emissions and fossil energy use could vary significantly depending on the feedstock assumption used for the analysis. If cuphea oil can be produced in a similar way as canola oil and equivalent upstream emissions are used, the GHG emissions and fossil fuel consumption of this pathway are 53% and 77% lower, respectively, compared to petroleum diesel (Figure 26). Of course, availability of data on cuphea farming is limited because cuphea is not a commercial crop yet. (Gesch 2010) compared the budgets and production yields for the production of cuphea, corn, and soybean in an attempt at cuphea commercialization. Co-Optima analysts estimated the energy consumption and materials usage of cuphea farming from the average data of corn and soybean farming reported by (Gesch 2010), scaled by the ratios of energy and materials usage of corn/soybean farming to cuphea farming. Using these estimates of cuphea oil upstream emissions, the GHG and fossil reductions are 20% and 44% compared to petroleum diesel (Figure 27).

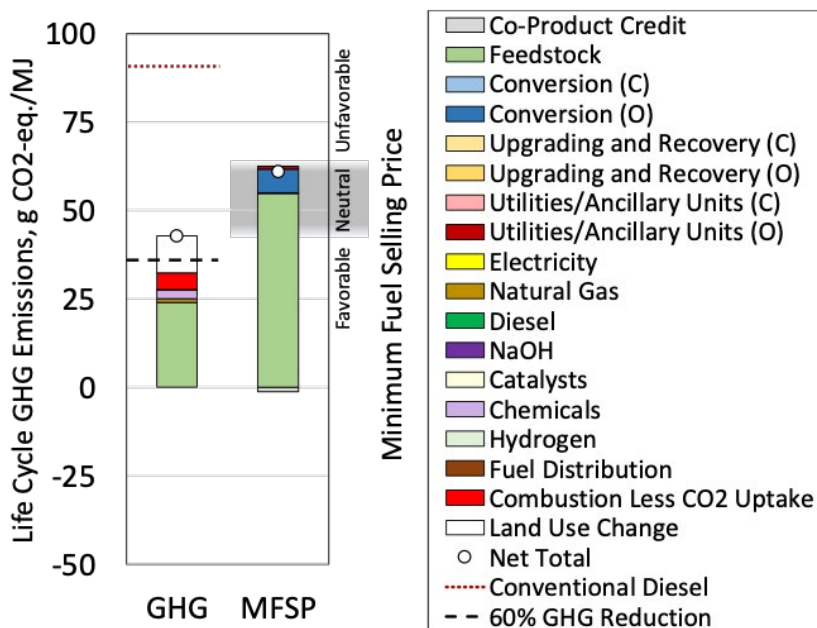


Figure 26. Life cycle GHG emissions and MFSP for short chain esters from cuphea oil, using production values for canola oil as a proxy.

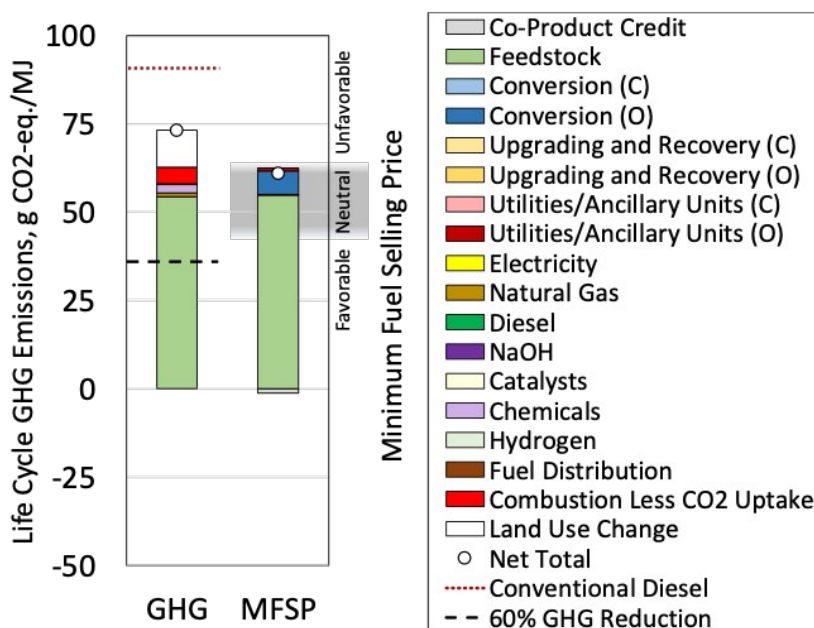


Figure 27. Life cycle GHG emissions and MFSP for short chain esters from cuphea oil, using estimated production values for cuphea oil.

### 3.2.1.4 Challenges, Barriers, and R&D Needs

Production volumes remain a barrier to wide-scale use of short-chain oilseed crops as fuel blendstocks. Research to increase crop yields, oil productivity and tune the chain length, along with increases in cultivation area while avoiding competition with food crops, are needed. Other approaches to economical production of C<sub>10</sub>–C<sub>14</sub> fatty acid chains should also be pursued.

Additionally, traditional biodiesel quality methods may not apply to light FAMES. Alleman (2019) have shown significant issues with glyceride reporting (i.e., glyceride persisting in the upgraded blendstock with negative impacts on performance) from novel feedstocks. The application and modification of current biodiesel analytical methods should be completed to ensure the blendstock is fit-for-purpose. The lower kinematic viscosity may limit the acceptable blending level.

### 3.2.2 Polyoxymethylene Ethers and Derivatives

POMEs are a class of low-soot and high-cetane oxygenate oligomers of structure C<sub>x</sub>H<sub>y</sub>O-(CH<sub>2</sub>O-)<sub>n</sub>-C<sub>x</sub>H<sub>y</sub> with different chain lengths (*n*) and end groups (C<sub>x</sub>H<sub>y</sub>) that determine their diesel-like fuel properties. They can be produced from renewable carbon sources when employing methanol derived from biomass, bio-gas, or municipal solid waste (Feng 2011, Holmgren 2014, Morandan and Harvey 2015). While POMEs have high CNs and low sooting tendencies, barriers to adoption and use include low energy density, high water solubility, potential issues with hydrolytic stability and oxidative stability and infrastructure compatibility.

### 3.2.2.1 Property Summary

POME research efforts can be traced back to the early 1990s with increased interest in the last 7 years (Awad 2020). The first process patents describing POME production were in the late 1990s and early 2000s by BP and BASF, respectively (Hagan and Spangler 1998, Blagov 2005). Dibutoxymethane (DBM), the dibutyl acetal of formaldehyde, is one example of such a structure (POME<sub>1</sub>-MM). It has found use as a solvent in dry-cleaning, paint-removal, and other applications (Feng 2011, Holmgren 2014, Morandan and Harvey 2015) due to its good solvent properties and low toxicity (Feng 2011, Awad 2020, Hagan and Spangler 1998). DBM suppresses the distillation curve of the diesel, likely leading to an increased premixed burn fraction and improved combustion efficiency (Blagov 2005). However, its uses in fuels have been mostly limited to experimental studies. DBM has not received any substantial market adoption as a fuel blendstock, primarily because of the lack of scalable production routes.

Polyoxymethylene Ethers	
Formula	R-O-(CH <sub>2</sub> O) <sub>n</sub> -R
CN	73-75
T <sub>b</sub> (°C)	156-287
Flash point (°C)	62-63
MP (°C)	<0
Water solubility (mg/L)	0.6-258
YSI	2.1-37
Energy density (MJ/L)	–
Specific energy (MJ/kg)	19-30
Kinematic viscosity (mm <sup>2</sup> /s@40°C)	–
Density (g/mL@15°C)	1.0662

Most recent work on POMEs has focused on chain lengths of 3–6 and methyl end groups, giving the structure CH<sub>3</sub>O-(CH<sub>2</sub>O)<sub>3-6</sub>-CH<sub>3</sub>, termed here POME<sub>3-6</sub>-MM. Production is predominantly in China with a volume of approximately 240,000 ton/year (Awad 2020). POME<sub>3-6</sub>-MM are mostly used as solvents and as diesel-fuel additives. Diesel engines have been reported to operate without need of modifications at blend levels of 30–50% POME<sub>3-6</sub>-MM mixed with diesel fuel. These POME-diesel blends enhanced engine efficiency and significantly reduced soot and carbon monoxide emissions (Li 2017, Liu 2017).

Co-Optima researchers generated a series of mixtures with mixed methyl and butyl end-groups. The fuel properties for this mixture are provided in Table 9, along with the fuel properties for a mixture of methyl-terminated POMEs.

Table 9. Fuel properties measured for two POME mixtures.

Fuel Property	POME <sub>3-6</sub> MM	POME <sub>1-6</sub> MB, BB
Boiling Range (°C)	156-259	169 – 287
Flash Point (°C)	63	62
Cloud Point (°C)	-19	-27
Water solubility (g/L)	258	0.6
Corrosion (TAN) (mg KOH/g)	0.18	0.19
CN	73	75
YSI	2.1	37
LHV (MJ/kg)	19	30
Kinematic viscosity (mm <sup>2</sup> /s) @ 40°C	1.9 (20%)	-

Fuel Property	POME <sub>3-6</sub> MM	POME <sub>1-6</sub> MB, BB
Lubricity ( $\mu\text{m}$ )	462 (20%)	-
Conductivity (pS/m)	23	-
Oxidation stability (min)	129	-
Blend Cetane Number	47 (10%), 48 (20%), 49 (30%)	-

### 3.2.2.2 Production from Biomass

POMEs of varying chemical structures can be synthesized using feedstocks that provide the end-group ( $\text{C}_x\text{H}_y\text{O}-$ ) and the repeating chain-group ( $-\text{CH}_2\text{O}-$ ). Chain-group precursors can be formaldehyde, trioxane, or paraformaldehyde. For POME<sub>3-6</sub>-MM, the end-group precursors can be methanol, dimethyl ether, or dimethoxymethane (methylal, the simplest POME-MM with  $n=1$ ). Methanol is the preferred reactant for large-scale production (Figure 28). The end-group reagent reacts with the chain-group precursor to form POME-MM structures in an equilibrium-controlled reaction in the presence of a strongly acidic catalyst. Chain length distribution depends on the concentration of the chain-group reactant, with higher concentrations yielding longer chain lengths (Burger 2012, Held 2019, Ouda 2017). POMEs with longer end-groups (e.g., diethyl [EE], dipropyl [PP], dibutyl [BB]) have been identified to have better fuel properties when compared to their methyl-ended counterparts. For example, POME<sub>1-4</sub>-EE structures possess higher heating values and lower autoignition points than their individual POME<sub>1-4</sub>-MM analogs (Lautenschütz 2016). More importantly, a mixture of POME<sub>1-6</sub> with mixed methyl-butyl (MB) and dibutyl (BB) end-groups has been identified by the Co-Optima team as a promising diesel blendstock, combining the advantaged fuel properties of low-soot and high-cetane with a higher heating value and low water-solubility.

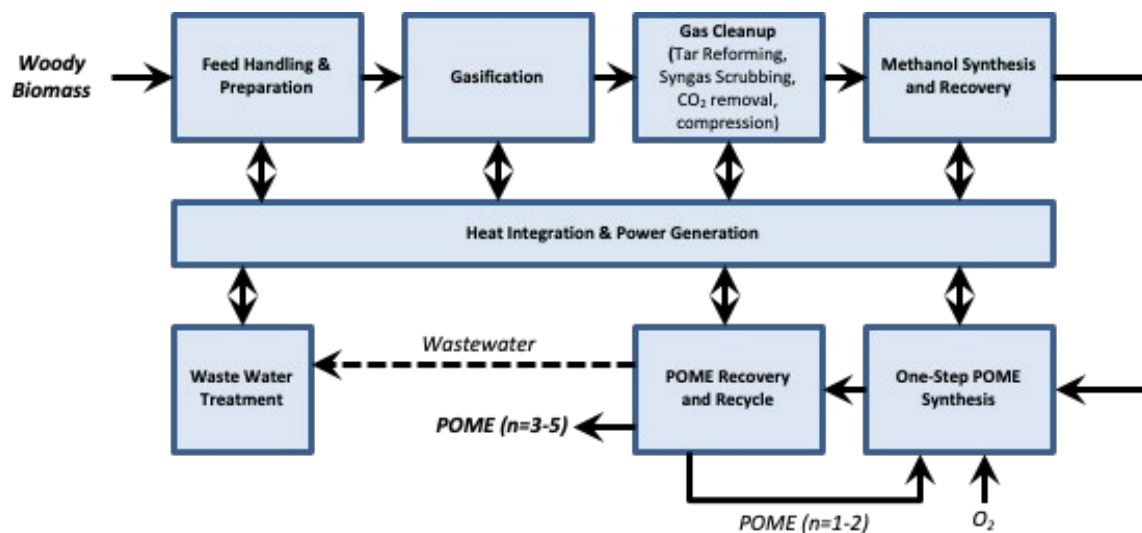


Figure 28. Process flow diagram for production of 4-butoxyheptane from woody biomass.

### 3.2.2.3 TEA/LCA

Polyoxymethylene dimethyl ethers could be sustainably produced from biomass when biomass-derived methanol is used as a starting point for synthesis (Lautenschütz 2016, Liu 2018). An

earlier TEA estimated that the production costs of POME<sub>1-8</sub>-MM from bio-derived methanol and formaldehyde can range between \$1.93/L–\$1.66/L (\$7.31/gal–\$6.28/gal), depending on the biomass feedstock utilized and assuming a production rate of 97–99.80 MT/day over 20 years. As a comparison, the cost of POME<sub>1-8</sub>-MM produced from fossil-fuel derived methanol would be \$0.63/L (\$2.38/gal). However, this work does not consider the cost of separation of the desired POMEs from the product stream, which includes byproducts and excess reactants, arguably one of the biggest challenges of the process (Oyedun 2018).

While there is no baseline case for the oxidative one-step pathway evaluated under Co-Optima, target case results show a MFSP between \$4.00–4.50/GGE for POMEs produced via this route, with the potential for a lower MFSP if residence time could be reduced or a greater approach to thermodynamic equilibrium could be achieved. Life cycle GHG emissions and fossil energy use of the POME pathway are favorable compared to those of petroleum diesel (92 g CO<sub>2</sub>-eq/MJ), where the modeled pathway achieves around 81% GHG emission reduction, demonstrating this pathway can meet advanced biofuel criterion of at least 60% GHG emissions reduction. These LCA results are consistent with another literature report of the potential GHG emissions reductions using POMEs (Mahbub 2017). Figure 29 summarizes these analysis results.

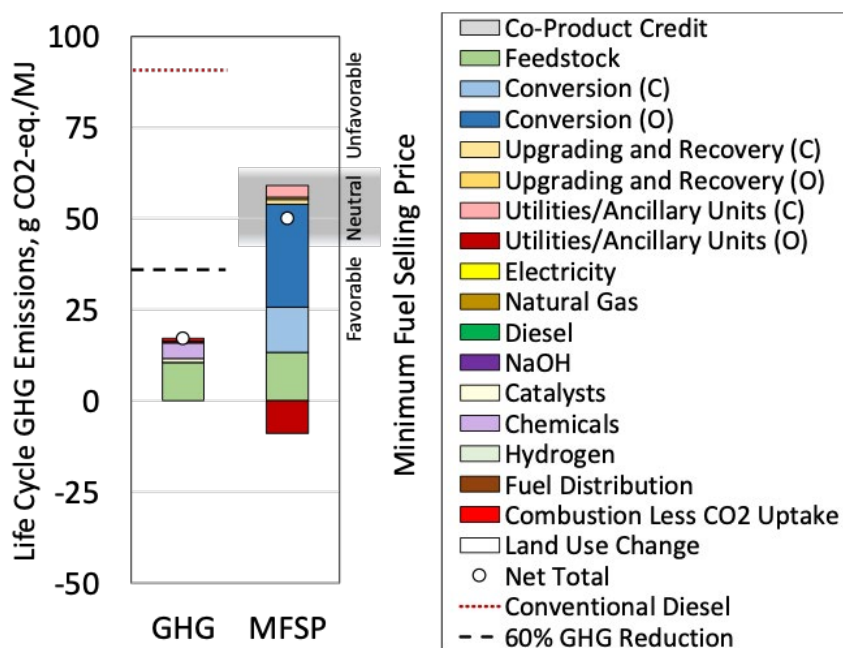


Figure 29. Life cycle GHG emissions and MFSP for POMEs.

### 3.2.2.4 Key Challenges, Barriers, and R&D Needs

Methylal (POME<sub>1</sub>-MM) (also known as dimethoxymethane or DMM) has gained attention as a diesel blendstock that lowers soot emissions. Despite the soot-reducing advantage, POME<sub>1</sub>-MM faces many shortcomings, especially its low CN, low flash point, and low boiling point that limit its widespread application (Ruijun 2009). Instead, a POME<sub>3-6</sub>-MM mixture has been identified to possess improved fuel properties, specifically a higher flash point, CN, and boiling point, while retaining the low-sooting characteristics. However, the POME<sub>3-6</sub>-MM mixture has a low heating value and high water-solubility, which hinders large-scale deployment due to limited fuel economy benefits and environmental risks of groundwater contamination upon leakage from any part of the fueling distribution system. Continued R&D is

needed for the production of the butyl-exchanged POME<sub>1-6</sub> blendstock at sufficient quantities to be assessed against Tier 1 and Tier 2 criteria. POME<sub>1</sub>-MM does not by itself meet the diesel lubricity specification (0.622  $\mu\text{m}$  in the ASTM D6079 wear scar test vs. 520  $\mu\text{m}$  maximum specified in ASTM D975); in blends, lubricity improvers may be required depending on the blend level. The same may hold true for other POMEs. Hydrolytic and oxidative stability need to be demonstrated under relevant conditions. This one-step oxidative process for POME production was the only process evaluated under Co-Optima that was entirely based on theoretical thermodynamic equilibrium, and further research will be required to confirm assumptions used in the process simulation.

<b>4-Butoxyheptane</b>	
Formula	C <sub>11</sub> H <sub>23</sub> O
CN	80
T <sub>b</sub> (°C)	230
Flash point (°C)	64
MP (°C)	<-80
Water solubility (mg/L)	<0.1
YSI	58
Energy density (MJ/L)	30.8
Specific energy (MJ/kg)	39.0
Kinematic viscosity mm <sup>2</sup> /s@40°C)	0.795
Density (g/mL@40°C)	0.791

### 3.2.3 4-Butoxyheptane

4-Butoxyheptane is a C<sub>11</sub> branched ether that can be derived from the catalytic upgrading of butyric acid. Research is needed into production of 4-butoxyheptane from biomass, ensuring cost, GHG reduction and scale targets can be met. Additional fuel property assessments need to be made to ensure lubricity, conductivity, and oxidation stability.

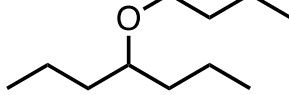
#### 3.2.3.1 Property Summary

The neat bioblendstock meets the Tier 1 MCCI fuel property targets, with the benefits of exceptionally high CN (80) and low sooting tendency intrinsic to ethers (YSI = 58; see Table 10) (Fioroni 2019a, b; Huq 2019). The structural branching resulted in an MP below -80°C, well below the 0°C requirement. Despite the oxygenated functionality, the lower heating value of 39 MJ/kg was comparable to fossil diesel, and water solubility was negligible at 15 mg/L.

Table 10. Fuel property values for 4BH as a neat bioblendstock and as a 20% blend with fossil diesel (Fioroni 2019a, b; Huq 2019). ND = not determined; \*tests with 90% pure 4BH; \*\*measured using a diesel fuel surrogate instead of a petroleum diesel

4-Butoxyheptane properties	Neat blendstock	Base petroleum diesel	20% Blend of 4-butoxyheptane in petroleum diesel
MP (°C)	< -80	--	--
Cloud point (°C)	--	-9.7	-11.4
Boiling point/T90 (°C)	197.5	335	268
Flash point (°C)	64.4	61	62
Density (g/mL)	0.791	0.863	0.833
Viscosity at 40°C (cSt)	0.795	2.66	2.12
LHV (MJ/kg)	39.2	42.9	40
Cetane Number**	80.0	46.8	48.8
YSI/NSC**	58/NA	215**/ND	173**/ND
Water solubility (mg/L)	15	Low	4
Carbon Residue (wt%)	ND	0.09	0*
Lubricity (mm)	ND	0.520	0.578*
Conductivity (pS/m)	ND	1	1*
Oxidation Stability (min)	ND	69.6	23.2*/67 with additive

4-Butoxyheptane was tested as a 20 vol% blend in clay-treated base petroleum diesel. The blend showed a modest improvement in autoignition with a CN of 49, as well as a decrease in the normalized sooting concentration of 11%. The cloud point of the blend was slightly lowered to -11.7°C with the addition of the branched blendstock. The kinematic viscosity of the blend at 40°C was 2.12 cSt, which was within specification limits despite the low viscosity of the neat bioblendstock. While the blend failed the oxidation stability test at 23 min, the addition of a common antioxidant (100 ppm butylated hydroxytoluene) resulted in a suitable stability of 67 min. Initial polymer compatibility swell tests also confirmed no major issues with exposure. Preliminary analysis using EPI Suite's BIOWIN suggests that the 4-butoxyheptane would likely be low risk for toxicity if released to the environment.

<b>4-Butoxyheptane</b>	
	
Formula	C <sub>11</sub> H <sub>23</sub> O
CN	80
T <sub>b</sub> (°C)	230
Flash point (°C)	64
MP (°C)	<-80
Water solubility (mg/L)	<0.1
YSI	58
Energy density (MJ/L)	30.8
Specific energy (MJ/kg)	39.0
Kinematic viscosity mm <sup>2</sup> /s@40°C)	0.795
Density (g/mL@40°C)	0.791

### 3.2.3.2 Production from Biomass

4-Butoxyheptane can be produced from biomass-derived butyric acid in a manner similar to 5-ethyl-4-propylnonane, using an alternative downstream catalytic conversion route that retains oxygen (Huq 2019, Hafenstine 2020), as shown in Figure 30.

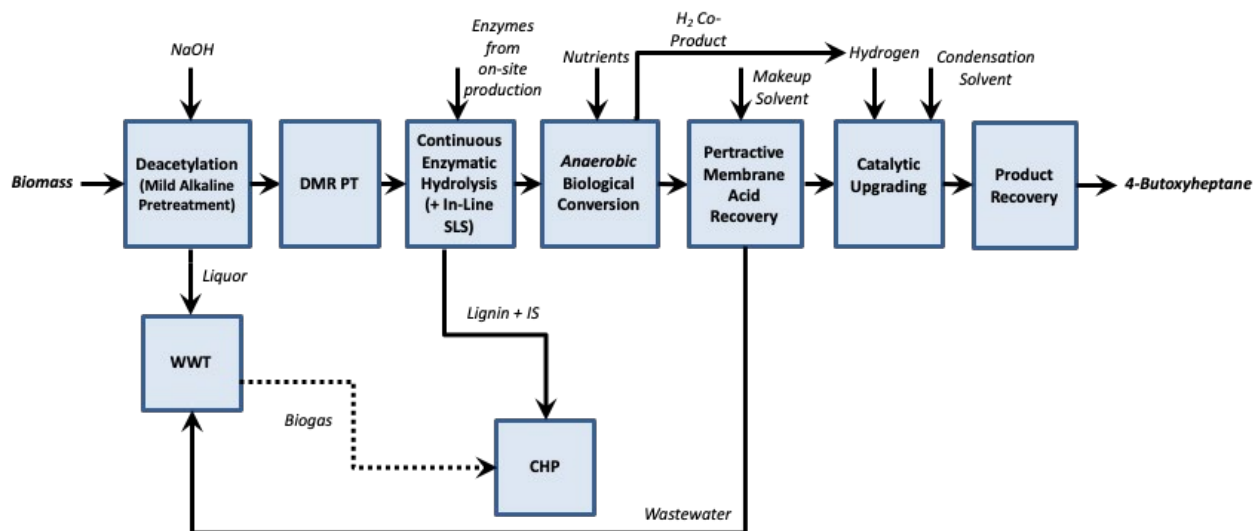


Figure 30. Process flow diagram for production of 4-butoxyheptane from corn stover.

In this process (Davis 2018), corn stover is initially deconstructed to sugars for anaerobic fermentation and recovery of butyric acid. After recovery via pertractive extraction and distillation from the extraction solvent, the intermediate is then split to two reactors operating in parallel. In the first reactor, the butyric acid is catalytically converted to 4-heptanone, following assumptions previously described by Davis (2018). The second reactor uses hydrogen and an acid catalyst to reduce the butyric acid to n-butanol (Lee 2014). The products of each reactor (4-heptanone and n-butanol) are then sent to the etherification reactor where they are catalytically converted to 4-butoxyheptane (Huq 2019, Hafenstine 2020). Side products produced in the etherification reaction are either disposed of, utilized as a gasoline-range co-product, or included in the final diesel blendstock, depending on fuel properties. However, these side-products make up only a small fraction of the reactor effluent and offer only minor impacts on process economics.

### 3.2.3.3 TEA/LCA

Techno-economic analysis found the MFSP of 4-butoxyheptane to be just under \$7/GGE, using current baseline experimental parameters of conversions, yields, and recoveries. When considering target experimental parameters, an MFSP of under \$6/GGE was projected, which is among the upper one-third of selling price for Co-Optima evaluated pathways. Life cycle GHG emissions of 4-butoxyheptane were considered unfavorable at only 27% GHG emission reduction compared to petroleum diesel. Similarly fossil energy use is reduced only 21% compared to petroleum diesel. Energy requirements for this ether pathway, especially electricity used during conversion of corn stover to ether, contribute significantly to GHG emissions, even though lignin was combusted to meet internal energy demand and displacement credits were applied due to co-production of sodium sulfate. These cases assume that the lignin fraction of the biomass is burned to generate energy for the process in the form of steam. In an alternative configuration, the lignin fraction can be deconstructed and upgraded to a high-value co-product such as adipic acid (Davis 2018). Though this technology has not yet been realized at a commercial scale, it is a subject of ongoing research (Schutyser 2018, Beckham 2016, Vardon 2015). When this lignin valorization step is considered in combination with target process

parameters, TEA shows a potential to reach an MFSP close to \$2.50/GGE (Huq 2019). Additionally, through this modification in the process there is potential to reduce GHG emissions by 50%–271% relative to petroleum diesel, depending on the co-product treatment used (Huq 2019). Figure 31 shows the results of these analyses.

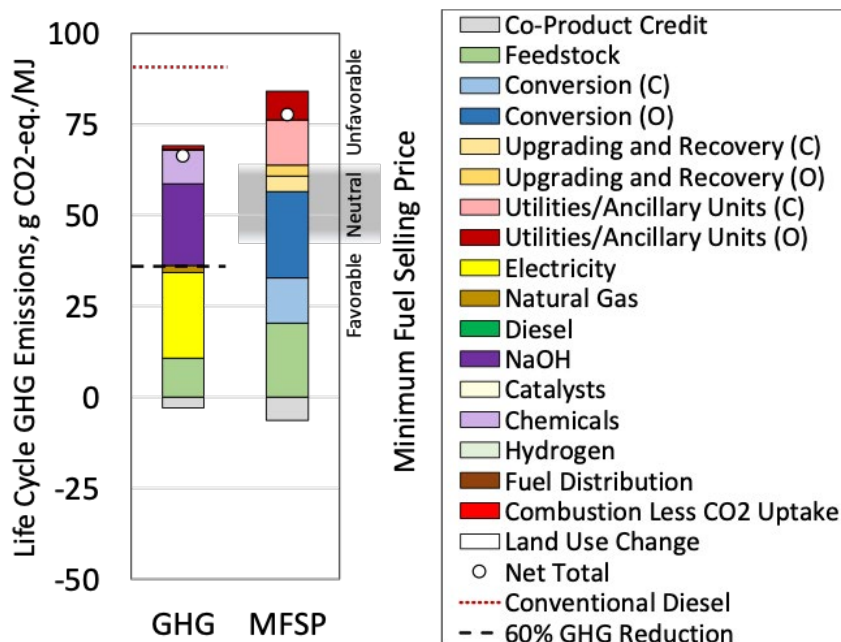


Figure 31. Life cycle GHG emissions and MFSP for 4-butoxyheptane.

### 3.2.3.4 Challenge, Barriers, and R&D Needs

From a fuel property standpoint, the ether functionality of 4-butoxyheptane requires further work to ensure suitable lubricity, conductivity, and oxidation stability with common additives. While preliminary tests show stability with 100 ppm of BHT additive, long-term storage and oxidation stability tests are needed to ensure safe handling, as well as mechanical testing of exposed elastomers. Experimental confirmation also is needed to confirm cetane and sooting improvements extend to an engine environment. In terms of bioblendstock production, research is needed to demonstrate production of 4-butoxyheptane from biomass and assess the impact of non-target products and impurities. As common to the fermentation pathways that rely on lignocellulosic sugars, additional work is needed to evaluate the use of low-cost wet-waste feedstocks to decrease production costs and GHG emissions.

### 3.2.4 Alkoxyalkanoates Derived from Lactate Esters

Alkoxyalkanoate ether-esters are hydroxyalkanoic acids coupled to alcohols to generate a suite of C<sub>6</sub>–C<sub>14</sub> ether-ester conjugates with the stoichiometry of one hydroxyalkanoate to two alcohols. Not surprisingly given the early stage of research into the fuel properties of these molecules, more fuel property measurements must be conducted prior to adoption and use, such as oxidative stability, compatibility, conductivity, etc. Cost and scale also are barriers to adoption.

### 3.2.4.1 Property Summary

Co-Optima researchers investigated chemical coupling of a series of hydroxyalkanoic acids and alcohols to generate a suite of C8–C14 ether-ester conjugates with the stoichiometry of one hydroxyalkanoate to two alcohols. A representative procedure for preparation of hydroxyacid ester-derived alkoalkanoates is shown in Figure 32, and the full suite of AOA structures for which fuel properties were measured is shown in Figure 33 and Table 11. Of the nine compounds shown in Figure 33 and Table 11, one meets (>40), three exceed (>45), and five greatly exceed (>50) the CN target. All of the AOAs measured had low YSIs, ranging from 30 to 82, and low freezing points of <-50. The LHVs were relatively low for some AOAs due to the high oxygen content; however, larger AOAs with higher C:O ratios had specific energy values nearing that of biodiesel. Within this set of AOAs investigated, clear structure property relationships can be seen. Comparison of AOA-1, AOA-2, AOA-3, and AOA-5 shows that increasing the chain length of either R group increases DCN, LHV, and YSI. Comparing AOA-1 to AOA-7 demonstrates that keeping the carbon number constant but increasing branching leads to a reduction in DCN and a slight increase in LHV and YSI. When carbon number and branching are controlled, R group location has only a minor impact on DCN as demonstrated by AOA-4 and AOA-5. AOAs with different hydroxyalkanoate “backbone” structures also were investigated, with longer unbranched structures leading to higher DCNs and increased LHVs and only slightly increased YSIs. Overall, YSI values as low as 30 and DCN and lower heating values as high as 62 and 34.5, respectively, were achieved. In general, LHV and YSI values are both positively correlated with C:O ratios of the AOAs.

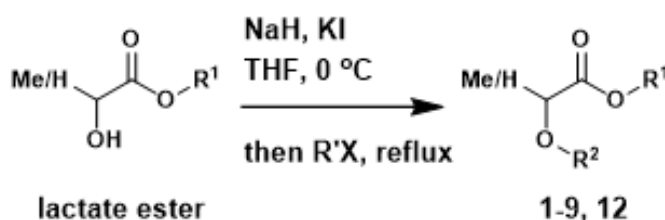
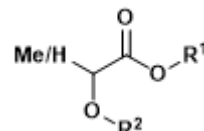


Figure 32. Chemical coupling of lactate esters with fusel alcohols to generate an AOA.

#### Alkoxyalkanoates Derived from Lactate Esters



Formula	$\text{R}^2\text{-O-CH(H or Me)-C(=O)-O-R}^1$
CN	44-62
$T_b$ ( $^\circ\text{C}$ )	190-280
Flash point ( $^\circ\text{C}$ )	65-117
MP ( $^\circ\text{C}$ )	<-50
Water solubility (mg/L)	<0.1*
YSI	30-82
Energy density (MJ/L)	–
Specific energy (MJ/kg)	25.5-35.5
Kinematic viscosity ( $\text{mm}^2/\text{s}@40^\circ\text{C}$ )	1.1-2.3*
Density ( $\text{g/mL}@25^\circ\text{C}$ )	0.90-0.93

\*predicted

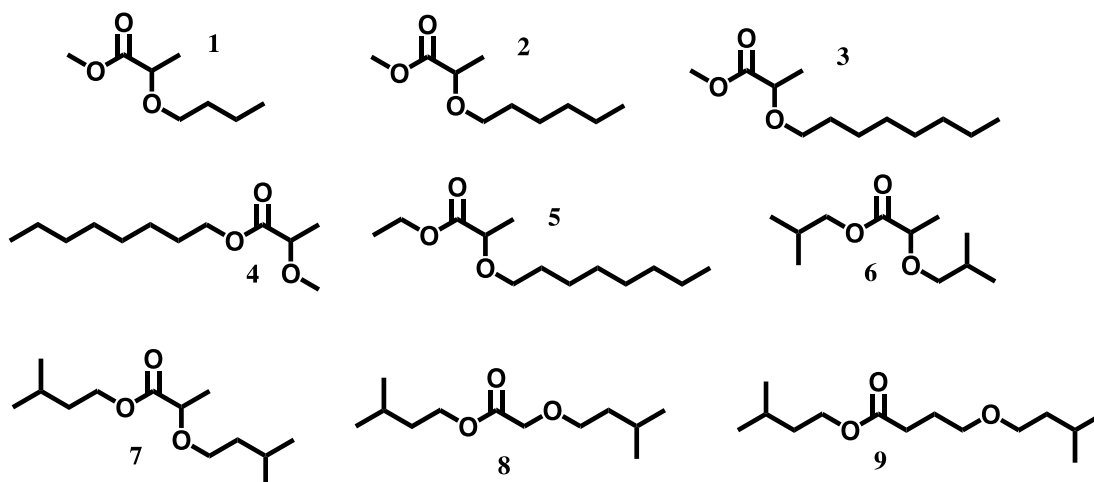


Figure 33. Structures of AOA ether-esters evaluated for use as MCCI blendstocks.

Table 11. MCCI properties.

Compound	Structure	C:O ratio	DCN	LHV (MJ/kg)	YSI	CP (°C)
AOA-1		2.67	46	27.1	30 ±8.9	<-50
AOA-2		3.33	53	29.5	42.8 ±8.9	<-50
AOA-3		4	59	30.79	55.6 ±9.0	<-50
AOA-4		4	58	31.71	55.6 ±9.0	<-50
AOA-5		4.33	62	32.2	60.5 ±9.1	<-50
AOA-6		3.67	48	25.3	58.5 ±9.3	<-50
AOA-7		4.33	44	34.5	71.3 ±9.4	<-50
AOA-8		4	47	31.8	69.1 ±9.3	<-50
AOA-9		4.67	62	32.5	81.9 ±9.4	<-50

### 3.2.4.2 Production from Biomass

Among the biochemical intermediates within 1-2 enzymatic steps from central metabolism are a variety of alpha-hydroxy acids, including lactate, glycolate, alpha-hydroxy butyrate, and alpha-hydroxy valerate; gamma-hydroxy acids, including 3-hydroxy-propionate, and

4-hydroxy-butyrate; and various short-chain (C2–C5) alcohols, including ethanol, (iso)butanol, isoamyl alcohol, hexanol, and octanol, commonly denoted as ‘fusel’ alcohols (Noor 2010, Liu et al. 2019). Although fermentation-derived alcohols have achieved significant market penetration as spark-ignition fuel bioblendstocks, there has been limited success in using these short-chained biochemical intermediates directly in MCCI applications. Central metabolism-derived intermediates provide the opportunity to maximize carbon yield, which has been shown to offset the potential advantages for separations provided by long-chain (i.e., lipid, terpenoid, etc.) intermediates conventionally used for diesel or similar distillate range fuel applications (Paap 2013).

Conversion of biomass hydrolysates using biological catalysts (including *Saccharomyces*, *E. coli*, *Lactobacillus*, *Clostridium*, and a host of other organisms) generates a variety of common high-yielding intermediates from various acidogenic and solventogenic biochemical pathways in homo- or heterofermentative processes (Moat 2002). Recent advances in synthetic biology and metabolic engineering significantly expand the ability to generate many of these biochemical intermediates with substantially improved bioconversion rates, yields, and titers (Choi 2019). The process to produce AOAs aligns with existing and on-going biochemical conversion pathways (Humbird 2011, Davis 2018) whereby lignocellulosic biomass is deconstructed to mono-sugars for biological conversion. The most technically mature route used in the baseline case (Figure 34) is fermentative production of fusel alcohols, and a separate fermentative route to lactate that can be produced at titers up to ~100 g/L and precipitated via lime addition (PEP 2014a).

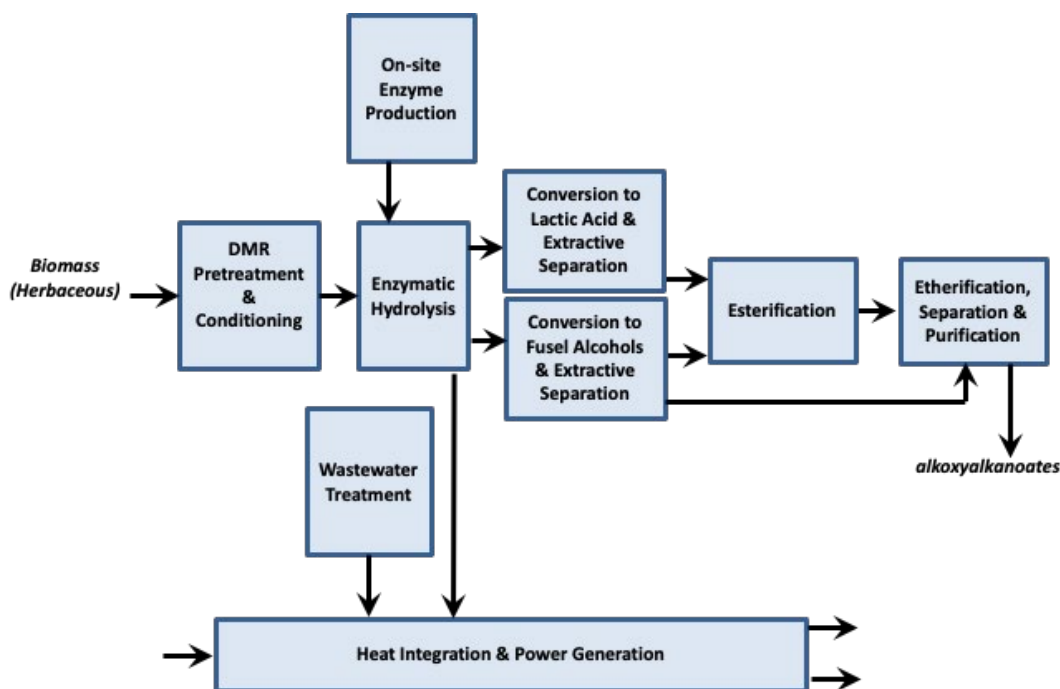


Figure 34. Process flow diagram for production of alkoxyalkanoates derived from lactate esters, based on current lactic acid production process.

This is followed by chemical conjugation of the fusel alcohols with the lactate using the same esterification conditions as that for biodiesel (PEP 2014b), and then further followed by etherification of the lactate fusel ester product to form mixtures that are predominantly (~75%) isobutyl 2-isobutoxypropanoate (C11), isopentyl 2-isopentoxypropanoate (C13), and the C12 mixed alcohol conjugates such as isopentyl isobutoxypropanoate and isobutyl isopentoxypropanoate. As in biodiesel production, the fuel products phase separates from the aqueous phase.

The target case (Figure 35) involves in vivo production to generate the lactate esters referred to above in high yield. This requires optimization to achieve titers competitive with the ex vivo approach. The target concept has been demonstrated with in vivo production of ethyl lactate, which provides a very high theoretical yield (0.675 g product/g glucose) (Moat 2002).

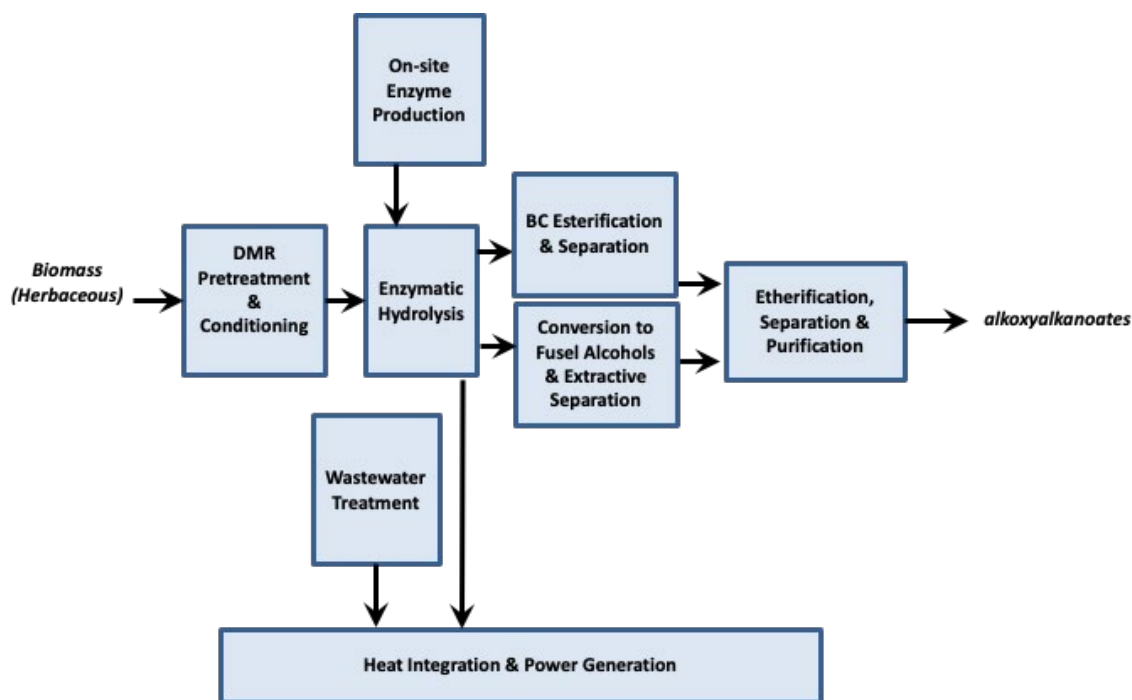


Figure 35. Process flow diagram for production of alkoxyalkanoates derived from lactate esters, based on target production process.

### 3.2.4.3 TEA/LCA

The TEA for this pathway showed a baseline MFSP near \$5/GGE when modeled using current data from the literature and a future target MFSP approaching \$3/GGE. These economic results were achieved with minimal co-product credits and are favorable due in part to the high metabolic yield to intermediates and products associated with this pathway. Additionally, this pathway has the potential to meet the advanced biofuel criterion as life cycle GHG emissions were 65% less GHG intensive and 61% less fossil energy-intensive than petroleum diesel fuel. The major contributor to GHG emissions during the conversion process is the significant amount of NaOH used during pretreatment and conditioning of the feedstock, a very GHG-intensive chemical. Figure 37 shows the results of these analyses.

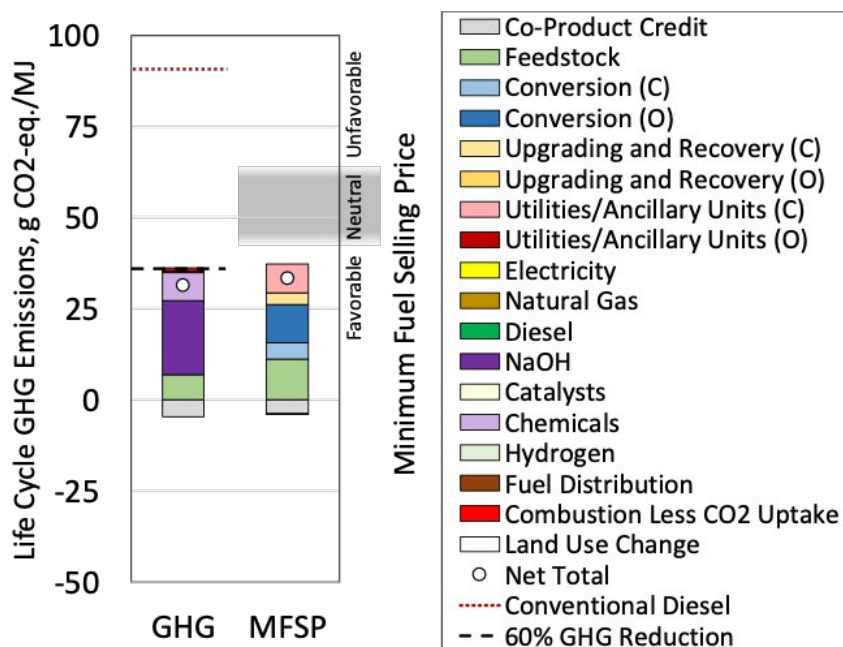


Figure 36. Life cycle GHG emissions and MFSP for alkoxyalkanoates derived from lactate esters.

#### 3.2.4.4 Challenges, Barriers, and R&D Needs

To support scaleup and to meet established MCCI fuel metrics, more fuel properties need to be evaluated, including testing of individual fuel candidates and mixtures of AOAs. These include properties not described here such as lubricity, conductivity, and oxidation stability. The presence of mixed ether and ester chemical moieties in AOAs indicates the potential for peroxide formation under long term storage. Although intermediate-term storage (i.e., exceeding 1 month) and testing have not indicated significant oxidative degradation of AOAs, further evaluation will be required to determine safe-handling practices and compatibility with fuel system elastomers.

An experimental evaluation also is needed to confirm that engine performance improvements are realized in real-world engine operation. To further improve the techno-economic feasibility of production of AOAs for MCCI applications, research is needed to demonstrate scalable chemistries for formation of the ether bond and full process integration. Furthermore, a better understanding will be required for the acceptable ranges of reaction byproducts and impurities in the bioblendstock. Finally, as with most commodity target-focused bioprocesses, additional research is needed to enable incorporation of low-cost or waste feedstocks to further improve carbon efficiency and economic viability.

#### 3.2.5 Fatty Alkyl Ethers

FAEs are ethers derived from fatty acids, similar to traditional FAME biodiesel but with one oxygen in the ether state (Figure 37). The primary barriers to adoption and use are cost, scale and fuel property gaps resulting from the relatively early stage of development of the etherification process.

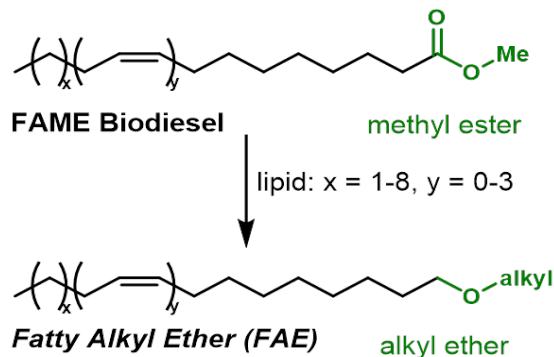


Figure 37. The chemical structure of FAEs is similar to fatty acid methyl esters.

### 3.2.5.1 Property Summary

FAEs generated from fatty acids with same profile as biodiesel showed improvement in derived CN (29% shorter ignition delay), increased specific energy (+4.7 MJ/kg), lower relative sooting tendency (-7 YSI/MJ), and decreased cloud point (15°C lower). The development of FAEs as fuel blendstocks is at the early stages, with other fuel properties still to be measured. The fuel properties of the FAE product vary based on the short-chained alcohol used in the reaction, with longer alcohols generally leading to increased DCN and lower CP, but slightly higher soot formation and boiling points. As with traditional FAME biodiesel, the fatty acid profile of the lipid source used also has important impacts on the fuel properties of the FAE product, with saturated fatty acids having higher DCN and lower CP than unsaturated fatty acids. The FAEs described here were made utilizing a soybean oil lipid source, which is generally high in C18 mono and di-unsaturated fatty acids (Kostik 2013). The structure property relationships of FAEs are described in detail by Carlson (2020), and a figure from that study is reprinted below as Figure 38.

<b>Fatty Alkyl Ethers</b>	
lipid: $x = 1-8, y = 0-3$	
Formula	$\text{CH}_3-(\text{CH}_2)_x-(\text{CH}_2-\text{CH}=\text{CH})_y-(\text{CH}_2)_8-\text{O}-\text{R}$ where R = alkyl, $x = 1-8$ and $y = 0-3$
DCN	74-104
T <sub>b</sub> (°C)	310-370
Flash point (°C)	>150
MP (°C)	-5 to -16
Water solubility (mg/L)	<0.1
YSI	163-198
Energy density (MJ/L)	34-36
Specific energy (MJ/kg)	41-42
Kinematic viscosity (mm <sup>2</sup> /s@40°C)	–
Density (g/mL@40°C)	0.83-0.85

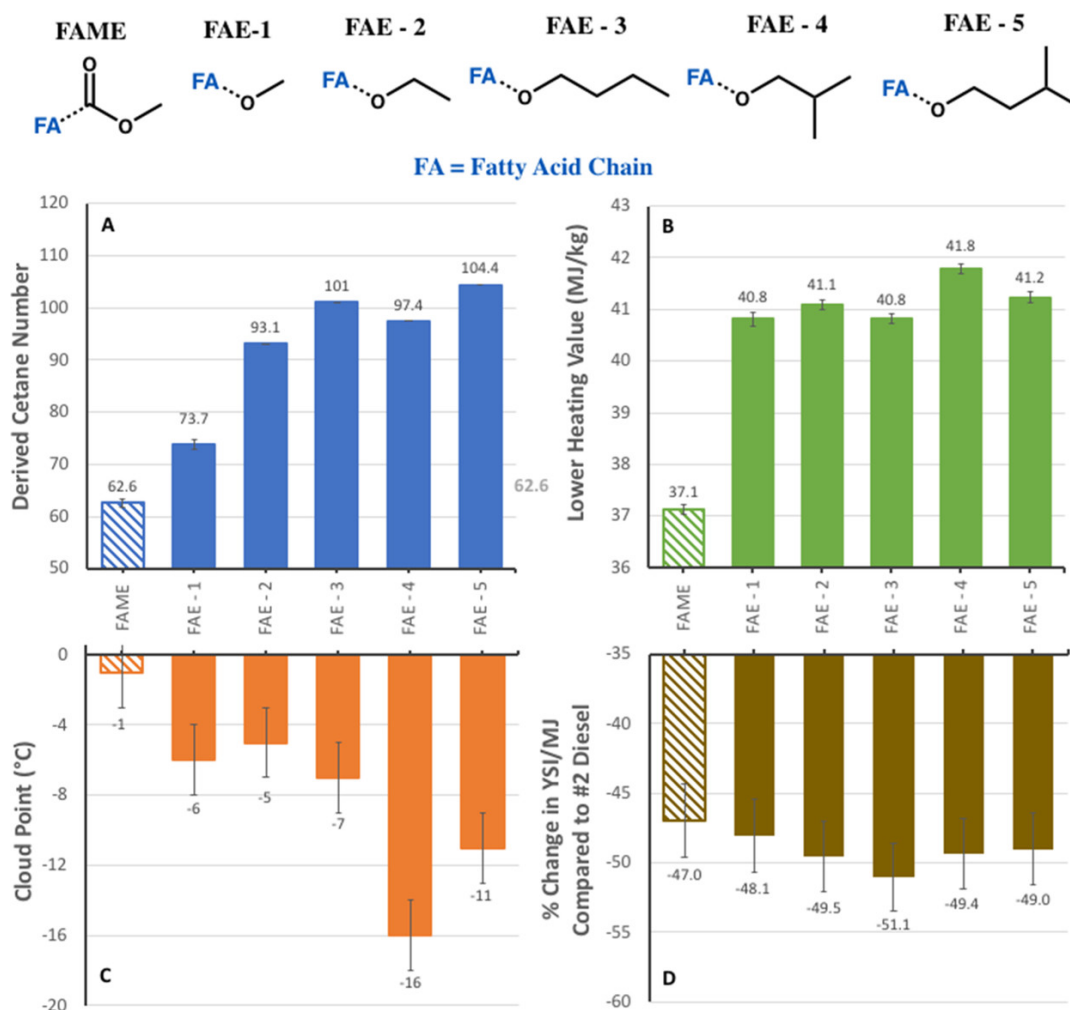


Figure 38. Full property measurements of FAE derivatives and a FAME for comparison. (A) DCN; (B) LHV; (C) CP; and (D) reduction in YSI/MJ compared to diesel fuel. All FAEs show a significant improvement vs. a FAME control in every property except YSI/MJ, where the measured improvement is within the uncertainty of the measurement. Increasing the carbon chain length improved DCN, LHV, and CP, while increased branching lowered DCN but improved LHV and CP. Reprinted with permission from Carlson, J.S, Monroe, E.A., Dhaoui, R., et al. (2020), *Energy & Fuels* 34 (10), 12646-12653. © (2020) American Chemical Society.

### 3.2.5.2 Production from Biomass

Fatty acid ethers are produced from a triglyceride feedstock. Co-Optima analysts evaluated a process for commercial scale production from either soybean oil, waste yellow grease, or a combination of the two. The feedstock is first degummed using phosphoric acid. The oil-acid mixture is stirred and centrifuged, then dried to produce a degummed oil. An additional degumming step including NaOH may be necessary depending on the nature of phospholipids present in the waste feedstock. The degummed oil is then processed through a mild (95°C, 1 atm) hydrolysis step to convert the degummed triglycerides to fatty acids. Sulfuric acid is used as a catalyst in the hydrolysis step and glycerol is produced as co-product. The fatty acid product

of the hydrolysis step is separated from water, glycerol, and sulfuric acid by simple phase separation in a settling tank. The fatty acid product is then reduced (50% oxygen removed) to a fatty alcohol using hydrogen. The water produced in the reduction reaction is separated from the fatty alcohol by phase separation; however, distillation may be needed to ensure more complete separation. The fatty alcohol is then combined with methanol and processed through an ion exchange etherification bed to produce the target FAEs. More water is produced as a byproduct of the etherification step, which must be separated by distillation.

### 3.2.5.3 TEA/LCA

Co-Optima techno-economic analysis indicate an MFSP of near \$4/GGE for all feedstock combinations—100% soybean oil (Figure 39), 100% yellow grease (Figure 40), and 60% soybean oil + 40% yellow grease (Figure 41)—based on optimistic target assumptions such as simple degumming process and adequate phase separation after the hydrolysis and reduction steps.

Alternative processing methods such as combined hydrolysis/reduction and reactive distillation for the etherification step may serve as opportunities to reduce costs. Life cycle GHG emissions and fossil energy use of FAEs pathways are significantly lower than those of petroleum diesel with values ranging from 57–75% less GHG emissions and 76% (for all three cases) less fossil energy use compared to those of petroleum diesel. The major difference between these pathways is the emission burden allocated to upstream feedstock production. Soybean oil production is more energy- and resource-intensive than yellow grease. Yellow grease is a waste from restaurant operation and therefore minimal impacts are assigned to it. However, the emissions and energy consumption of yellow grease collection and transportation are included in the calculation. For pathways using soybean oil, we considered the effects of the indirect land use change associated with the market effects of increased soybean demand. The type of feedstock used for each pathway also significantly affects life cycle water consumption. For instance, the FAE with 100% yellow grease has the lowest water consumption (1.5 gal/GGE) among the three cases, while the soybean oil-based pathway has the highest water consumption values (78 gal/GGE). The major contributor to soybean oil water consumption is the water used during crop production. Despite favorable economic and life cycle metrics, however, when compared to lignocellulosic biomass, the oils and greases used to produce FAEs are relatively expensive at over \$500/ton, have existing markets such as in food products or animal feed, and in the case of yellow grease may be limited in regional availability.

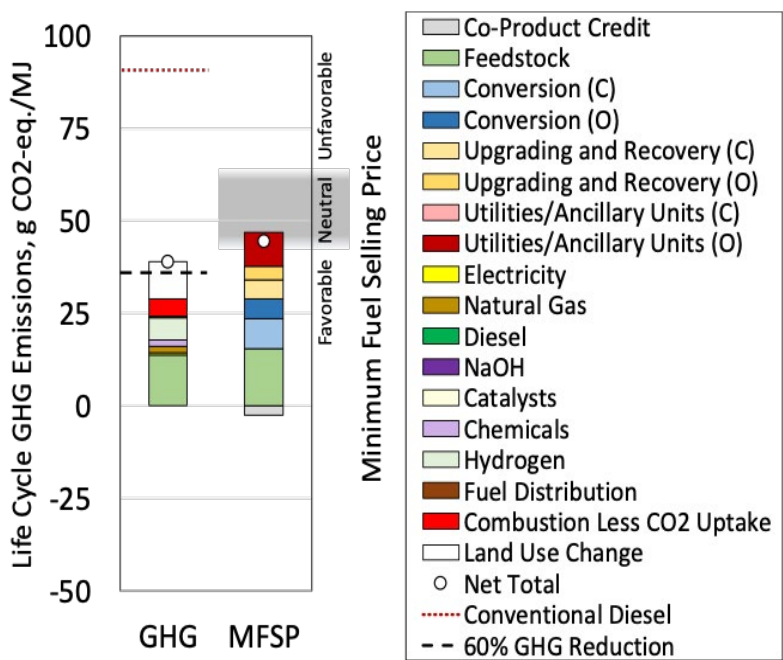


Figure 39. Life cycle GHG emissions and MFSP for FAEs produced from soybean oil.

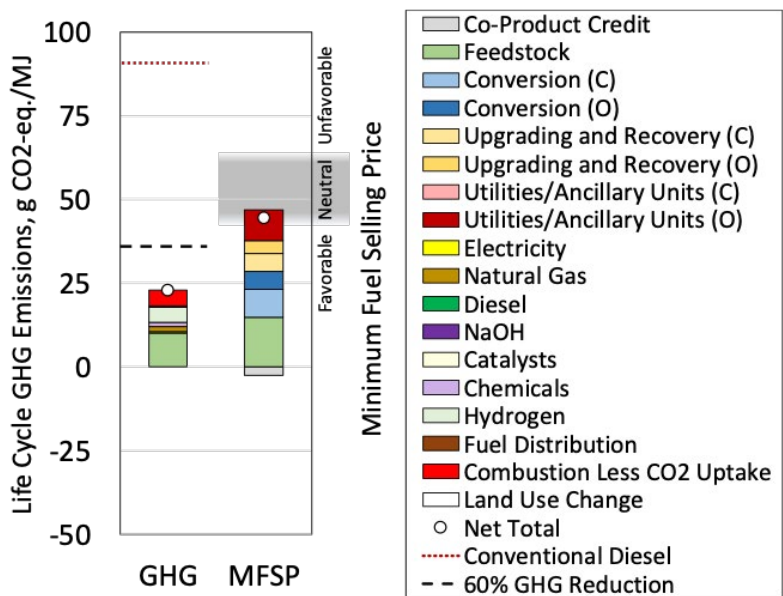


Figure 40. Life cycle GHG emissions and MFSP for FAEs produced from yellow grease.

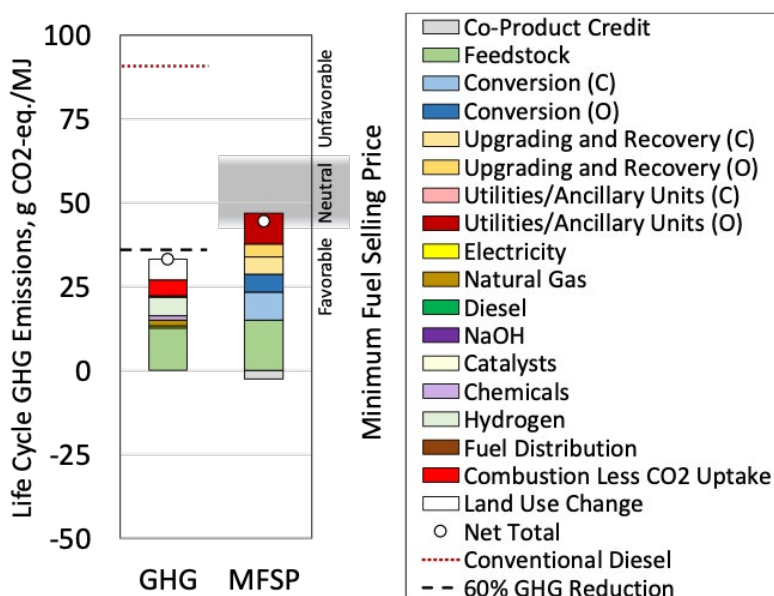


Figure 41. Life cycle GHG emissions and MFSP for FAEs produced from a 60/40 mixture of soybean oil and yellow grease.

### 3.2.5.4 Challenges, Barriers, and R&D Needs

The primary challenges to production and use of FAEs as market blendstocks are cost, scale, and fuel property gaps resulting from the relative early stage of development of the etherification process. There is also a regulatory barrier to the use of ethers in diesel engines at the blend levels proposed. The oils and greases used to produce FAEs are relatively expensive at over \$500/ton, have existing markets such as in food products or animal feed, and in the case of yellow grease may be limited in regional availability. The etherification coupling needs a process engineering effort to meet target process efficiency at scales larger than laboratory scale.

The early stage of research implies that additional barriers are likely to be identified as more properties are measured. Key fuel properties, such as oxidative stability and fuel system compatibility need to be demonstrated.

## 3.3 Candidates with substantial life cycle, techno-economic and/or fuel property barriers to adoption determined to be unsuitable for use

The following nine candidates in this section show promise as MCCI blendstocks but were determined to be unsuitable for use. The blendstocks in this section were either found in the literature or proposed and studied by Co-Optima researchers or both. Each passed some or all the Tier 1 fuel property metrics but was ultimately determined to be unsuitable for use as an MCCI blendstock. The alcohols could be blended at relatively low levels (engine tests at room temperature with 30% 1-decanol were successful), but the high viscosity, modest CN for linear alcohols (and CN below the target value for branched alcohols), and modest reductions in GHG emissions (the direct fermentation pathways have the smallest GHG emissions reduction with emissions comparable to petroleum diesel, while the catalytic conversion of ethanol is close to the 60% target) led Co-Optima researchers to conclude these likely not provide the value sought. Dipentyl ether fails the oxidative stability test, conductivity and a facile route from

biomass was not identified. The mixed dioxolanes are peroxide formers. The other candidates—oligocyclopropanes, bicyclohexane/bicyclopentane, substituted myrcenes, *n*-undecane, hexyl hexanoate, dioxolanes and oxetanes—all failed TEA and/or LCA screening.

### 3.3.1 Oligocyclopropanes

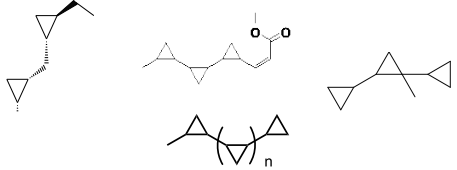
Oligocyclopropanes are hydrocarbons containing multiple cyclopropane moieties. Barriers to adoption and use are primarily related to the early stage of their development as diesel blendstocks. Scalable, low-cost synthesis meeting GHG emissions reduction goals remain to be demonstrated. Many of the fuel properties are predicted and must be measured experimentally to confirm performance.

#### 3.3.1.1 Property Summary

Cyclopropane is the most energy-dense organic ring structure, with an enthalpy of formation of +53.30 kJ/mol (Knowlton and Rossini 1949). The most widely deployed cyclopropane to date is syntin (1'-methyl-1,1':2',1''-tercyclopropane), created for the Soviet Soyuz-U2 rocket to capitalize on the increased volumetric energy compared to the commonly used Rocket Propellant-1. The use of syntin was ultimately discontinued due to high synthesis cost (Edwards 2003).

Polycyclopropanated hydrocarbons and methyl esters are attractive MCCI fuel candidates due to their high volumetric energy density and greater resistance to oxidation than corresponding alkenes. Several different approaches have been taken to produce cyclopropanated fuels. 1,1-oligocyclopropanes (also known as ivyanes) have been produced catalytically from dendralenes. The measured heat of combustion of ivyane is  $50.8 \pm 2.5$  MJ/kg, one of the highest values ever recorded for a hydrocarbon (Bojase 2011, Davis 2013).

Saturated 1,2-oligocyclopropanes with five and six cyclopropane groups have predicted properties compatible with diesel fuel standards with predicted energy densities up to 50 MJ/L due to their high bulk density. Predicted energy density, boiling point, and DCN were found to increase proportionally with chain length. Lower heating value, energy density, and boiling point predictions were obtained using gSAFT molecular thermodynamic methods (Dufal 2014) and EPI Suite group contribution methods adapted from Stein and Brown (EPA 2020). DCN predictions obtained by a group contribution method (Dahmen and Marquardt 2015) and vapor pressure predictions from gSAFT and EPI Suite. Predicted fuel properties are shown in Figure 42.

Oligocyclopropanes		
		
Formula		varies
DCN		28-55*
T <sub>b</sub> (°C)		120-320*
Flash point (°C)		–
MP (°C)		–
Water solubility (mg/L)		<0.1*
YSI		–
Energy density (MJ/L)		–
Specific energy (MJ/kg)		43-47*
Kinematic viscosity mm <sup>2</sup> /s@40°C		–
Density (g/mL@40°C)		0.851**
* Predicted		
** Literature value for syntin		

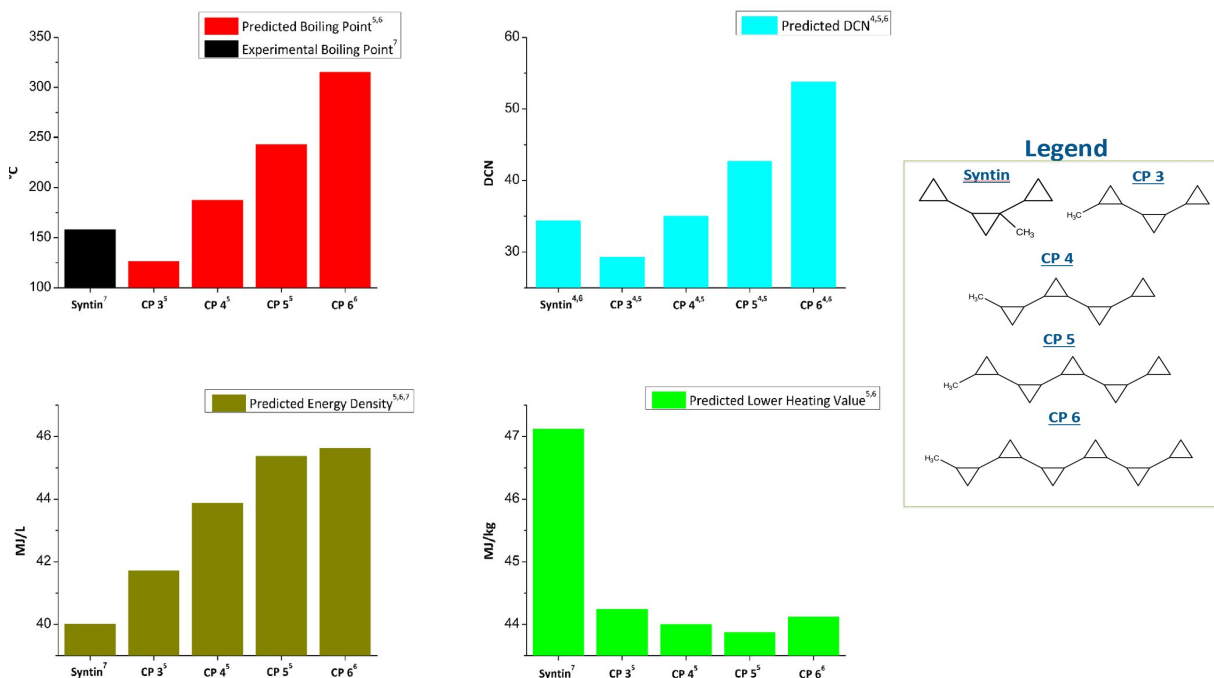


Figure 42. Predicted fuel properties for five oligocyclopropanes.

### 3.3.1.2 Production from Biomass

At present, generation from biomass has only been shown via cyclopropanation of the alkene groups of fatty acid methyl esters. This approach did not significantly increase the specific energy of the cyclopropanated biofuels but did increase the volumetric energy density due to the increased density of the cyclopropanated FAMES (Langlois and Lebel 2010). 1,2-Oligocyclopropanes represent a promising target for direct biochemical production, as they can be synthesized both *in vivo* and *in vitro* via an iterative jawsamycin polyketide synthase (Hiratsuka 2014).

### 3.3.1.3 TEA/LCA

The production of oligocyclopropanes is based on the conversion of sugars from cellulosic feedstocks which are then biologically converted by aerobic fermentation (Humbird 2011, Davis 2018). The sugars are converted to high energy-density hydrocarbons consisting of varying degrees of cyclopropanation as illustrated in Figure 43.

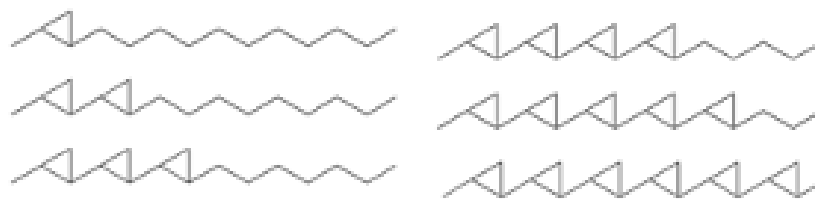


Figure 43. Cyclopropanated oligomers produced by aerobic fermentation of sugars showing varying degrees of cyclopropanation.

This pathway is derived from natural pathways for the polyketide synthase-derived molecule jawsamycin, which features iterative cyclopropane units (Hiratsuka et al. 2014; Hiratsuka et al. 2017). Molecules with 1-6 repeating cyclopropane units are targeted, as either alkanes or terminal alcohols. Based on production of similar, highly-reduced, long-chain molecules, the estimated maximum titer, rate, and yield are approximately 0.25 g cyclopropane molecules/g glucose, 90 g/L final titer, and 1.5 g/L-hr maximum production rate. The modeled cetane is highly dependent on the specific molecules, but candidates with CN exceeding 40 are available, depending on chain length, branching, and degree of cyclopropanation, all of which can be tuned to achieve the desired properties. The substrate is based on DMR of corn stover with 5 g/L ammonium sulfate, 0.5 g/L magnesium sulfate, and 100mM phosphate at 500 g/L of total sugar (18 g/g). The estimated MFSP for cyclopropanes at the target production conditions would be over \$6.50/GGE. The use of aerobic fermentation incurs high power costs to operate air compressors; electricity costs make up 5% of the total MFSP with feedstock and catalyst/chemicals each contributing about 25% to the MFSP. The largest single contributor to MFSP are capital-related expenses for depreciation and return on investment which represent over 40% of the MFSP.

Life cycle GHG emissions of cyclopropane do not meet the 60% target for emissions reduction compared to conventional petroleum diesel. One of the reasons is the significant amount of NaOH used to pretreatment step of corn stover.

#### 3.3.1.4 Challenges, Barriers, and R&D Needs

While biological production of 1,2-oligocyclopropanes has been shown in vivo, this pathway requires significant further development to improve fermentation titer, rate, and yield (unpublished data). These molecules are currently produced as complex mixtures of fatty acids with 3–8 cyclopropane units. Further engineering is required to decarboxylate or functionalize the fatty acids and to control the chain length and number of cyclopropane units. As with other biochemically synthesized MCCI fuels, ultimate production cost is dependent on availability of low-cost cellulosic feedstocks and on aeration requirements during fermentation.

#### 3.3.2 1,1'-Bicyclohexane and 1,1'-Bicyclopentane

Cyclohexanes and related compounds are saturated hydrocarbons that are components in petroleum-derived market fuels; coupled cyclohexanes and cyclopentanes—1,1'-bi(cyclohexane) and 1,1'-bi(cyclopentane)—were identified as potential MCCI blendstocks. These compounds can be produced via simple and scalable aldol condensation of cyclohexanone (CHO) or cyclopentanone (CPO). Barriers to adoption and use include production of a clean starting material from biomass, demonstration of a scalable production method that meets GHG emissions reductions targets (TEA and LCA are in progress). Finally, the full set of MCCI fuel properties has not been determined for each of these compounds; the reported properties were measured on the neat material in the presence of impurities carried through the synthetic process.

### 3.3.2.1 Property Summary

Mixtures of the target compounds were generated from the precursors CHO and CPO. Each contained small amounts of the trimer aldol condensation product and residual oxygenates. Each was evaluated after hydrogenation-hydrodeoxygenation and without further purification to mimic large-scale production with minimum processing. Fuel properties were measured as reported. YSI could not be obtained due to the heterogeneity of the mixture; therefore, NSC was calculated against a fully formulated ultra-low sulfur diesel fuel as a reference. The resulting blendstock met the ASTM D975 diesel fuel specifications (i.e., CN  $\geq$ 40,  $T_{\text{boiling}} \leq 338^\circ\text{C}$ , cloud point and pour point  $< 0^\circ\text{C}$ ) and Co-Optima targets. The fuel properties for the two mixtures are provided in Table 12.

### 3.3.2.2 Production from Biomass

Co-Optima researchers demonstrated the aldol condensation to produce the bicyclic compounds from the respective ketone at 200g scale, followed by hydrogenation-hydrodeoxygenation by a nickel on alumina (Ni-Al<sub>2</sub>O<sub>3</sub>) catalyst at 250°C. CHO can be produced efficiently from lignocellulosic biomass (phenol, phenol ethers), via a concerted catalysis of Pd/C and a Lewis acid.

Much research has been devoted to the efficient transformation of biomass-derived phenolic compounds to CHO because its use in the production of nylon 6,6 and nylon 6. Most CHO is consumed in the production of nylon precursors, adipic acid and caprolactam. CPO is readily available from bioderived furfural and produced at industrial scale (Sheng 2018, Hronec and Fulajtarová 2012, Jia 2019). Hronec and Fulajtarová (2012) first described the aqueous phase conversion of furfural to CPO using precious metal catalysts such as Pt/C, Pd/C, Ru/C, and Pd–Cu/C. CPO yield was 76.5% over Pt/C and 92% over Pd–Cu. Furfural is first hydrogenated to furfuryl alcohol, which is then converted to tetrahydrofurfuryl alcohol or CPO via competitive pathways. Byproduct tetrahydrofurfuryl is produced by the deep hydrogenation of furfuryl alcohol, while CPO is produced by using water to form the 4-hydroxy-2-cycloentenone, which is subsequently hydrogenated to CPO. Other research reports CPO selectivities between 80%–90% with high conversions (Sheng 2018, Jia 2019).

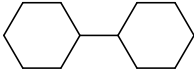
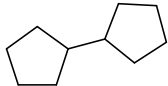
<b>1,1'-Bicyclohexane</b>	
	
Formula	C <sub>12</sub> H <sub>22</sub>
DCN	48
T <sub>b</sub> (°C)	239
Flash point (°C)	92
MP (°C)	<-100
Water solubility (mg/L)	<0.1
YSI	110
Energy density (MJ/L)	30.6
Specific energy (MJ/kg)	34.3
Kinematic viscosity mm <sup>2</sup> /s@40°C	–
Density (g/mL@40°C)	0.891
<b>1,1'-Bicyclopentane Mixture</b>	
	
Formula	C <sub>10</sub> H <sub>18</sub> and impurities including trimer
DCN	42.6
T <sub>90</sub> (°C)	247
Flash point (°C)	53
Cloud point (°C)	-60.1
Water solubility (mg/L)	<0.1
YSI	–
Energy density (MJ/L)	35.7
Specific energy (MJ/kg)	41.5
Kinematic viscosity mm <sup>2</sup> /s@40°C	–
Density (g/mL@40°C)	0.860

Table 12. Select fuel properties.

	Specific Energy (MJ/kg)	Density (g/cm <sup>3</sup> )	DCN	NSC
Cyclohexanone-HDO	40.7	0.872	40.9	0.494
Cyclopentanone-HDO	41.5	0.860	42.6	0.577

HDO = hydrodeoxygenated; DCN = derived cetane number; NSC = normalized soot content relative to No. 2 diesel.

### 3.3.2.3 TEA/LCA

A conceptual process was developed to estimate the MFSP for making bicyclohexane from woody biomass. The process is based on catalytic fast pyrolysis to produce an aromatic-rich bio-oil that is hydrotreated to produce benzene, ethylbenzene, toluene, and xylenes (BETX). BETX is hydrogenated in two reaction stages with a nickel catalyst (PEP 2020). In the first stage, the reactant is mixed with recycled hydrogen (1:4 molar ratio of H<sub>2</sub> to BETX) at 220°C and about 450 psig. The effluent from the first stage is mixed with recycled hydrogen to achieve a H<sub>2</sub>/BETX molar ratio of 70 for the adiabatic second stage reactor. The resulting liquid stream is fractionated to obtain cyclohexanes which are then oxidized to form cyclohexanone products. Finally, the cyclohexanone is reacted to generate bicyclohexanes from cyclohexanones based on two main steps: 1) cyclohexanone-derived Aldol product and 2) hydrodeoxygenation-hydrogenation of the Aldol mixture (Ref 3). The first reaction proceeds at 110-115 C and 1 atm pressure with sulfamic acid (with a 1:10 molar ratio of sulfamic acid to cyclohexanone). The effluent is then water washed to remove salt and distilled to separate the unreacted cyclohexanone from the aldol product. The modeled single-pass conversion was 72%. The aldol product is pumped to 69 atm and heated to 275°C to remove oxygen and saturate the molecule with hydrogen to form bicyclohexane. The MFSP for the bioblendstock produced using this process is \$7.25/GGE. The most expensive steps were the cyclohexane oxidation step and catalytic fast pyrolysis, contributing 27% and 20% of the MFSP, respectively. The feedstock contributes another 24% of the fuel production price. Life cycle GHG emissions of bicyclohexane are significantly higher than those of petroleum diesel. It was estimated that about 44% increase of GHG emission can be expected when producing bicyclohexane from clean pine compared to petroleum diesel. The feedstock (clean pine) contributes significantly to the GHG emissions (about 57%) of this bioblendstock. Moreover, the energy requirements for this pathway, especially natural gas usage during the conversion step, contribute significantly to GHG emissions

### 3.3.2.4 Challenges, Barriers, and R&D Needs

Given the early stage of development, it is expected that additional fuel property measurements will be necessary. Several properties of the product mixtures were not measured, including viscosity. The production process developed by Co-Optima has not been optimized for specificity or yield. A method for production of a clean CHO or CPO starting material from sustainable sources also has not been developed.

### 3.3.3 Substituted Cycloalkanes Derived from Myrcene

Myrcene, a component of a range of plants, can be upgraded via the Diels-Alder reaction to produce substituted cyclohexanes. Barriers to adoption and use include development of specific chemistries that meet fuel property targets, especially kinematic viscosity and sooting tendency, and development of conversion processes that meet techno-economic targets.

#### 3.3.3.1 Property Summary

Terpenes, isomeric hydrocarbons of molecular formula  $(C_5H_8)_n$  constitute a large and diverse family of natural products (de Carvalho and da Fonseca 2006, Gershenzon and Dudareva 2007). These have attracted attention as drop-in replacements and certain terpenes have been shown to be potential drop-in replacements for diesel and jet fuel (Harvey 2015, Peralta-Yahya 2011, Ju 2018). For example, bisabolene, a fully-reduced monocyclic sesquiterpene, has shown to be a potential diesel blendstock (Peralta-Yahya 2011). Myrcene, an acyclic monoterpene, can be converted into a wide range of Diels-Alder products suitable for use as fuels. The synthesis of a series of myrcene derivatives is described below; the fuel properties of these molecules are detailed in Table 13.

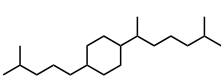
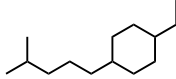
Substituted Cycloalkanes Derived from Myrcene	
	
Formula	varies
DCN	43-58
T <sub>b</sub> (°C)	240-332
Flash point (°C)	88-150
MP (°C)	<-40
Water solubility (mg/L)	–
YSI	131-187
Energy density (MJ/L)	34.8-36.6
Specific energy (MJ/kg)	41.9-43.2
Kinematic viscosity mm <sup>2</sup> /s@40°C)	2.9-9.3
Density (g/mL@40°C)	0.826-0.875

Table 13. Comparative fuel properties of Diels-Alder myrcene products.

Compound	Cetane	LHV (MJ kg <sup>-1</sup> )	YSI	Freezing Point (°C)	Boiling Point (°C)	Viscosity (40°C, mm <sup>2</sup> s <sup>-1</sup> )	Flash Point (°C)	Density (25°C, g/ml)
1	58	43.2	187	< -40	318-332	9.32	155	0.826
2	45	41.9	155	< -40	270-276	4.69	113	0.875
3	43	42.2	131	< -40	245-251	2.92	91	0.836
4	43	42.1	158	< -40	240-246	2.87	88	0.826

The myrcene Diels-Alder products all show high energy density, low freezing point, boiling point appropriate for use in diesel fuel, flash point above the lower safety limit, appropriate density, and good CN. The YSI values are modestly lower than diesel (approximately 250). The kinematic viscosity (Jenkins 2016) of some of the myrcene derivatives tested exceeds the ASTM D975 specification (1.9–4.1 mm<sup>2</sup> s<sup>-1</sup> at 40°C). Both 1 and 2 exceed this as neat fuels but are both below this rating at up to 50% blends with diesel.

### 3.3.3.2 Production from Biomass

Myrcene is a component of a range of plants (Behr and Johnen 2009) and can be produced commercially from the pyrolysis of beta-pinane, which is obtained from turpentine. Additionally, engineered microbial platforms can be used to produce myrcene from sugars in a convenient and cost-effective approach (Kim 2015). Hydrogenated myrcene and other monoterpenes are potential direct diesel replacements, but upgrading this molecule has potential to improve the beneficial properties of the overall fuel by increasing the energy density. Myrcene can undergo thermal Diels-Alder chemistry to produce camphorane, a monocyclic diterpene, in high yield as a mixture of isomers which can be readily reduced to give a mixture of cyclic alkanes (Figure 45, image 1) with the concomitant production of a small fraction of aromatics (11%) (Staples 2019). The Diels-Alder approach can be adapted to give hetero-coupled molecules and reaction of myrcene with 2-cyclopenten-1-one, methylvinyl ketone and crotonaldehyde result in smaller cyclic molecules that can be readily reduced to cyclic alkanes Figure 44, images 2–4).

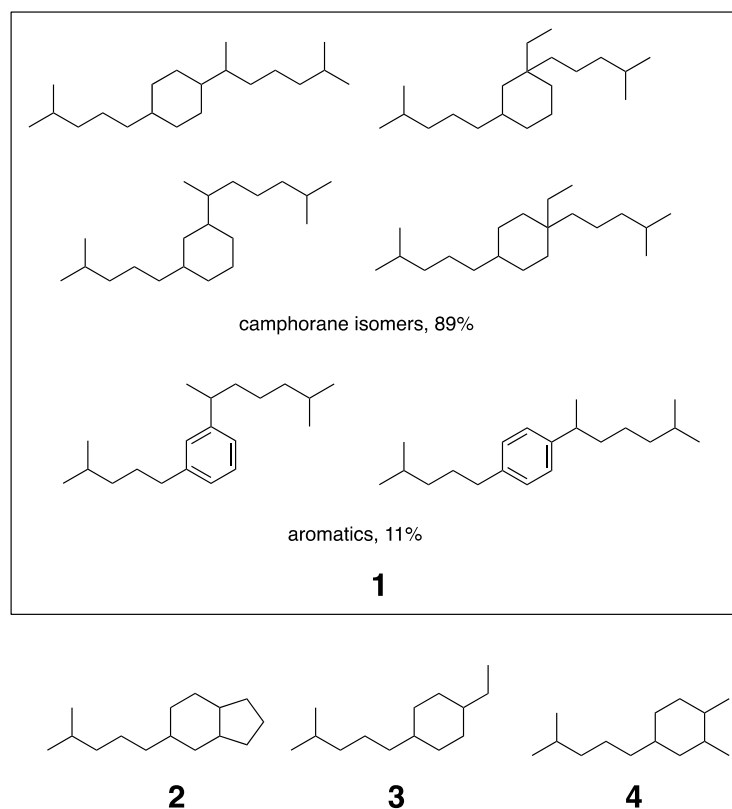


Figure 44. Myrcene homo- and hetero-coupled Diels-Alder products.

### 3.3.3.3 TEA/LCA

The techno-economic and life cycle analyses were not conducted on the myrcene derivatives. Given the multi-step production approach and the relatively small GHG reductions (determined for other aerobic fermentation approaches to hydrocarbon blendstocks [e.g., oligocyclopropanes, etc.]).

### 3.3.3.4 Challenges, Barriers, and R&D Needs

Most of this work has been performed on small scale and comprehensive fuel testing has not been completed. Among the properties tested, the kinematic viscosity of some neat myrcene-derived blendstocks exceeds the ASTM D975 standard. Tuning the structure and composition to meet the standard and blending with a lower viscosity base fuel can both be pursued to ensure the resulting fuel meets the standard. Compatibility, oxidative stability and other properties required to meet the ASTM D975 specification must be confirmed. Given the chemical similarity to components of diesel fuel, most properties are expected to meet the specification values.

Full TEA has not been initiated but is likely strongly tied to myrcene cost, which would need to approach approximately \$500/ton to realize a \$2.50 GGE. Developing and commercializing low-cost terpenes is essential to widespread utilization of this class of compound as fuels.

### 3.3.4 *n*-Undecane

*n*-Undecane is a C11 normal hydrocarbon that can be derived by the catalytic upgrading of hexanoic acid. Barriers to adoption and use include the need to evaluate the technical viability of conversion routes from renewable resources, as well as determine the cost of production and life cycle impacts.

#### 3.3.4.1 Property Summary

The neat *n*-undecane bioblendstock shows suitable Tier 1 MCCI fuel properties, with the benefits of improved cold weather performance, elevated CN, and reduced intrinsic sooting tendency (see Table 14). Despite having a linear carbon backbone, the MP of -26°C was well within the Tier 1 cutoff of 0°C for the neat bioblendstock. Of note, the CN of 71 was significantly higher than base petroleum diesel and the C11 backbone resulted in a high flash point of 74°C. However, the lower heating value of 34 MJ/kg was significantly lower when compared to conventional diesel due to the low density. The fully saturated hydrocarbon structure resulted in a YSI of 65, approximately one-third the value of fossil diesel.

<i>n</i> -Undecane	
Formula	C <sub>11</sub> H <sub>24</sub>
DCN	71
T <sub>b</sub> (°C)	196
Flash point (°C)	65
MP (°C)	<-26
Water solubility (mg/L)	<0.1
YSI	64.7
Energy density (MJ/L)	32.7
Specific energy (MJ/kg)	44.2
Kinematic viscosity mm <sup>2</sup> /s@20°C)	1.6
Density (g/mL@40°C)	0.74

*n*-Undecane can be readily obtained from commercial sources for Tier 2 blend testing. Blending at 20 vol% in a base clay-treated diesel showed the T90 was decreased due to the low volatility of the *n*-undecane. The cloud point of the blend was slightly lowered to -12.7°C and the CN favorably increased to 51. The kinematic viscosity of the blend at 40°C was 2.17 cSt, which was within limits despite the low viscosity of the neat bioblendstock. The lubricity of and conductivity of blend were both out of spec, likely due to the lack of additives, while the oxidation stability of the blend slightly improved.

Table 14. Fuel property values for *n*-undecane as a neat bioblendstock and as a 20% blend with fossil diesel (Fioroni 2019). – = not measured

n-Undecane Properties	Neat Blendstock	Base Diesel	20% Blend
MP (°C)	<-26	–	–
Cloud point (°C)	–	-9.7	-12.7
Boiling point/T90 (°C)	196	335	327
Flash point (°C)	65	61	–
Density (g/mL)	0.74	0.863	–
Viscosity at 40°C (cSt)	–	2.663	2.170
LHV (MJ/kg)	44.2	42.9	–
Cetane number	71	46.8	51
YSI/NSC	64.7/NA	NA/1	–
Water solubility (mg/L)	0.044	Low	–
Carbon Residue (wt%)	–	0.09	0
Lubricity (mm)	–	0.520	0.590
Conductivity (pS/m)	–	1	<1
Oxidation Stability (min)	–	69.6	99.6

### 3.3.4.2 Production from Biomass

*n*-Undecane can be produced from biomass by the catalytic upgrading of hexanoic acid (Gaertner 2009, Huo 2019). Hexanoic acid can be derived from anaerobic fermentation routes actively in development with lignocellulosic sugars and other waste carbon streams (Cavalcante 2017). Similar to production routes that use butyric acid as a biologically derived intermediate, hexanoic acid can be produced with *Clostridium* and related strains and subsequently recovered by extraction from fermentation broth. The use of hexanoic acid enables simplified downstream catalytic process chemistry, relative to butyric acid, as ketonization and hydrodeoxygenation alone can produce undecane as a bioblendstock with suitable flash point for diesel fuel applications.

### 3.3.4.3 TEA and LCA

*n*-Undecane can be produced from biomass by the catalytic upgrading of hexanoic acid, (Gaertner 2009, Huo 2019), which can be derived from anaerobic fermentation of lignocellulosic sugars (Cavalcante 2017, Nelson 2017). Similar to the production of 5-ethyl-4-propyl-nonane described by Davis et al. (2018), lignocellulosic sugars derived from corn stover undergo anaerobic fermentation to carboxylic acids. However, while the Davis pathway targets butyric acid as the primary fermentation product, the *n*-undecane pathway targets hexanoic acid. A “state of technology” (SOT) case considers the TEA of the production of *n*-undecane with experimentally demonstrated fermentation productivities and yields from literature (Nelson 2017). In this case, hexanoic acid accounts for 35% of the acids produced, with the remainder attributed to butyric (60%) and acetic (5%) acids. A target case assumes that advancements in fermentation or metabolic engineering research and development result in 100% selectivity to hexanoic acid; the overall acid productivity and yield for the target case are consistent with targets identified by Davis et al. (Davis 2018). Acids produced in fermentation are recovered in situ by a pertractive membrane. In the SOT case, acetic and butyric acids are separated from the hexanoic acid via distillation and sold as co-products, while the target case produces pure

hexanoic acid. In either case, the hexanoic acid undergoes ketonization and HDO to *n*-undecane. Ketone and HDO are assumed to proceed to 100% conversion. TEA found the MFSP of *n*-undecane to be approximately \$5.5/GGE for the target case. When assuming current baseline experimental parameters for fermentation, an MFSP of just under \$15/GGE was observed. This disparity can be attributed to higher conversion of sugars and selectivity to hexanoic acid in the target case. Life cycle GHG emissions of the *n*-undecane bioblendstock were 59 gCO<sub>2e</sub>/MJ, representing a 35% GHG emission reduction compared to conventional petroleum diesel. Therefore, this bioblendstock does not meet the 60% GHG emission requirement and was classified as unfavorable for the GHG emission metric. Fossil energy use is 0.9 MJ/MJ.

### 3.3.4.4 Challenge, Barriers, and R&D Needs

Additional research is needed to evaluate technical viability of conversion routes from renewable resources, as well as determine the cost of production and life cycle impacts.

### 3.3.5 Long-Chain Linear and Branched Alcohols

Linear and branched long-chain alcohols, also called fatty alcohols, can be produced in a variety of ways. The strong hydrogen bonding increases viscosity and reduces CN; branching may decrease viscosity slightly but also decreases CN. Barriers to adoption and use include these fuel property shortcomings, and the high cost of production and low GHG emissions reductions determined for direct fermentation approaches.

#### 3.3.5.1 Property Summary

Straight-chain fatty alcohols are commonly used as detergents, surfactants, thickeners, co-emulsifiers, and emollients (Noweck and Grafahrend 2000), with current industrial production closely divided between natural (plant oil) and synthetic (petrochemical) sources. Co-Optima researchers looked at two different approaches to making straight and branched fatty alcohols—via direct fermentation and catalytic upgrading of ethanol.

Fuel properties of branched, long-chain alcohols, with production shown *in vitro*, were computationally modeled to determine the likely impact of methylation and chain length on MP and DCN. A number of methylated dodecanol derivatives were predicted to retain cetane values above 40 with MPs below -40°C. In particular, the highly branched molecule 2,4,6-trimethyldodecanol has a predicted DCN of 43.9 with a predicted MP of -70.1°C. These predictions are shown in Table 15.

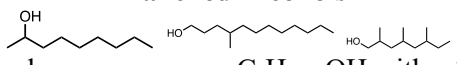
Fatty Alcohols/Long-Chain Linear and Branched Alcohols	
	
Formula	C <sub>n</sub> H <sub>2n+1</sub> OH with n > 8
DCN	22 to >50
T <sub>b</sub> (°C)	196
Flash point (°C)	>96
MP (°C)	-19 to -41*
Water solubility (mg/L)	–
YSI	36-69*
Energy density (MJ/L)	>31
Specific energy (MJ/kg)	>40
Kinematic viscosity	>5.4
mm <sup>2</sup> /s@20°C	
Density (g/mL@40°C)	0.789-827
*predicted	

Table 15. Predicted fuel properties of branched, long-chain alcohols.

Chemical Name	Formula	DCN (pred.)	Boiling Point (°C)	MP (°C)	Energy Density (MJ/L)	Specific Energy (MJ/kg)	YSI	Flash Point (°C)	Solubility in H <sub>2</sub> O (mg/L)
2-methyldodecanol	C <sub>13</sub> H <sub>28</sub> O	43.9	276.6	-18.8	35.8	43.1	83.5	105.5±6.5	3.40
4-methyldodecanol	C <sub>13</sub> H <sub>28</sub> O	43.9	261.9	-26.4	35.8	43.1	83.5	105.5±6.5	3.40
6-methyldodecanol	C <sub>13</sub> H <sub>28</sub> O	43.9	261.9	-34.0	35.8	43.1	83.5	105.5±6.5	3.40
2,4-dimethyldodecanol	C <sub>14</sub> H <sub>30</sub> O	41.6	281.9	-40.6	36.0	43.4	95.2	130.9±8.7	1.10
2,6-dimethyldodecanol	C <sub>14</sub> H <sub>30</sub> O	41.6	281.9	-48.1	36.0	43.4	95.2	130.9±8.7	1.10
4,6-dimethyldodecanol	C <sub>14</sub> H <sub>30</sub> O	41.6	268.7	-55.7	36.0	43.4	95.2	130.9±8.7	1.10
2,6,10-trimethylundecanol	C <sub>14</sub> H <sub>30</sub> O	37.7	272.0	-89.6	36.0	43.4	100.3	114.9±8.6	1.63
2,4,6-trimethyldodecanol	C <sub>15</sub> H <sub>32</sub> O	43.9	284.1	-70.1	36.2	43.5	106.8	122.7±8.6	0.37

One challenge for longer chain alcohols is their high kinematic viscosity, which arises from the hydrogen bonding of the alcohol moiety. Experimentally determined kinematic viscosity measurements for mixed alcohols generated from ethanol condensation are shown Table 16. The ASTM D975 requirement for the kinematic viscosity of a finished diesel fuel is 1.9–4.1 mm<sup>2</sup>/s. For comparison, the measured kinematic viscosities for single alcohols from C5–C10 are shown in Table 17. The kinematic viscosity of branched long chain alcohols with carbon number greater than 7 falls outside the required range; however, if blended with lower viscosity fuel, these alcohols could meet the kinematic viscosity requirement. For a given alcohol carbon number, the alcohol functional group position and the level of branching plays a significant role in determining the kinematic viscosity. For example, the measured kinematic viscosity of 1-nonanol is 6.9 mm<sup>2</sup>/s vs. 5.4 mm<sup>2</sup>/s for the 4-nonanol

Table 16. Mixed alcohol kinematic viscosities measured using the ASTM D445 method and DCN measured using ASTM D6890.

Alcohol Mixture Carbon #s	Viscosity at 40°C (mm <sup>2</sup> /S)	DCN
C5+	3.3	22
C7–C9	4	24.8
>C9+	8.9	37.6

Table 17. Measured densities and kinematic viscosities for a variety of single alcohols measured at 40°C.

	Density (g/cm <sup>3</sup> )	Viscosity (mm <sup>2</sup> /s)
2-Pentanol	0.7918	2.4503
4-Methyl-2-Pentanol	0.7894	2.8122
1-Pentanol	0.7995	2.9058
2-Heptanol	0.8004	3.6274
4-Undecanol	0.8116	7.2917
2-Undecanol	0.8124	8.2012
4-Nonanol	0.8066	5.3935
4-Heptanol	0.801	3.5606
2-Nonanol	0.8079	5.6113
1-Heptanol	0.8074	4.6203
1-Nonanol	0.8134	6.8975
1-Undecanol	0.8178	9.9018

### 3.3.5.2 Production from Biomass

In addition, direct biochemical production of straight-chain fatty alcohols has been demonstrated in engineered *Saccharomyces cerevisiae*, with extracellular titers of 6.0 g/L achieved in fed-batch fermentation (d’Espaux 2017). Fatty alcohols excreted during fermentation are recovered readily via phase separation with demulsification. Canonical, biological production of fatty alcohols via the fatty acid synthase pathway is currently limited to straight-chain fatty alcohols, resulting in relatively high MPs and poor cold flow. An alternative biochemical approach for production of branched, long-chain hydrocarbons was recently demonstrated by Curran (2018),

leveraging an iterative, modular, polyketide synthase to produce molecules with tunable chain length and degree of methylation.

Fatty alcohols also can be generated via catalytic conversion of intermediates from biomass sources via several pathways. For example, myrcene (C<sub>10</sub> unsaturated hydrocarbon that can be extracted from plants or generated via fermentation) can undergo oxidation followed by hydrogenation to form C<sub>10</sub> branched alcohols (Behr and Johnen 2009). Fatty acids can be converted to long-chain alcohols via 1) oxidative cleavage of the fatty acid to aldehyde/acid followed by reduction to the alcohol, or 2) direct hydrogenation of a fatty acid or its ester to the fatty alcohol (Wu 2016). These approaches to generate long chain alcohols for use as fuel blendstocks are rather expensive due to high feedstock cost and/or process complexity. More recently, conversion of renewable ethanol to C<sub>3</sub>+ ketones was demonstrated over a Pd-ZrO<sub>2</sub>-ZnO catalyst (Subramaniam 2020). The ketones dimerized and were hydrogenated to generate a mixture of C<sub>6</sub>+ long chain alcohols. The alcohol mixture contained a mixture of branched and normal secondary alcohols. The catalytic upgrading processes can use one of several routes to cellulosic ethanol production. For example, biochemical ethanol (Humbird 2011) and mixed alcohols (Dutta 2011) are both suitable, as is a biochemical conversion pathway (Davis 2018) in which sugar is converted biologically to a mixture of ethanol and 2,3-butanediol. Regardless of the ethanol source, ethanol is converted to a C<sub>6</sub>+ alcohol mixture via cross aldol condensation-dimerization-hydrogenation chemistry. The carbon yield to mixed alcohols from ethanol is greater than 70% (Subramaniam 2020).

### 3.3.5.3 TEA/LCA

The TEA of the catalytic upgrading strategy consisted of two parts. First, biochemical conversion of corn stover to ethanol was based on the design report published by Humbird (2011). Second, the ethanol from the biochemical area of the process was upgraded to long-chain alcohols. The MFSP based on current catalyst performance and laboratory-scale yields of ethanol to long-chain alcohols was calculated to be \$5/GGE at an industrial-scale facility with a nominal corn stover feed rate of 2000 dry metric tons/day. The annual production of ethanol to long chain alcohols was 32 MM GGE/yr, and the corn stover to long chain alcohols yield was 42.8 GGE/dry U.S. ton.

Estimated GHG emissions for branched, long-chain alcohol production from lignocellulosic feedstock via biochemical pathways are 83 gCO<sub>2e</sub>/MJ, similar to the value for petroleum diesel of 92 gCO<sub>2e</sub>/MJ. Major contributors to the GHG emissions include upstream emission during feedstock production and NaOH used during pretreatment and conditioning of the feedstock.

### 3.3.5.4 Challenges, Barriers, and R&D Needs

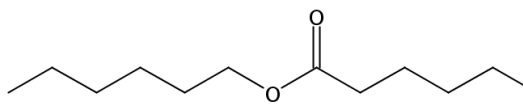
Large-scale biochemical production of fatty alcohols from lignocellulosic feedstocks will require lower-cost biomass deconstruction methods, as well as significant improvements in critical fermentation parameters—titer, rate, and yield. Because of their amphiphathic nature, recovery of fatty alcohols from fermentation broth is challenged by emulsion formation (d’Espaux 2017). In addition, while production of shorter chain branched products has been demonstrated using an engineered, modular type 1 polyketide synthase pathway (Yuzawa 2018), additional pathway development will be required to achieve similar in vivo results for long-chain branched alcohols.

### 3.3.6 Hexyl Hexanoate

Hexyl hexanoate is produced by esterification of hexanoic acid with 1-hexyl alcohol; hexanoic acid, and 1-hexanol can be generated via fermentation or upgrading of smaller alcohols and carboxylic acids. Barriers to adoption include the marginal CN, high water solubility, and limited evidence for scalable, and cost-effective production from biomass that meets the GHG emissions reductions target.

#### 3.3.6.1 Property Summary

Hexyl hexanoate would be considered a biodiesel under the ASTM D6751 specification for fatty acid alkyl esters. As the composition of fatty acid alkyl esters deviates from FAME, there are changes in fuel properties. As ester alkyl chain length decreases, cloud point, viscosity, and flash point also decrease. As alcohol chain length increases, viscosity increases and cloud point will increase up through approximately C4 alcohols, although few data are available. Most available data on ester chain length are limited to esters found in conventional oil seeds and most alcohol data are limited to methyl, ethyl, and sometimes t-butyl alcohols. Hexyl hexanoate meets the flash point specification for diesel fuels. Hexyl hexanoate increased the oxidation stability of a clay-treated diesel when blended at 20 vol%, increasing the oxidation stability induction time (ASTM D7545) from 70–120 min) (Fioroni 2019b). While the kinematic viscosity (1.795 mm<sup>2</sup>/s@40°C) is slightly below the ASTM D975 No.2 diesel fuel specification of 1.9–4.1 mm<sup>2</sup>/s@40°C, after blending with a base fuel it is expected to meet the specification. The CN of hexyl hexanoate is on the low end of the diesel fuel specification. Cetane improver additives or a higher CN blendstock could be used to increase the final fuel CN.

Hexyl Hexanoate	
	
Formula	C <sub>12</sub> H <sub>24</sub> O <sub>2</sub>
ICN	40
T <sub>b</sub> (°C)	246
flash point (°C)	99
MP (°C)	-55
Water sol (mg/L)	3.52*
YSI	61*
Energy density (MJ/L)	30.2
Specific energy (MJ/kg)	34.8
Kinematic viscosity (mm <sup>2</sup> /s@40°C)	1.795
Density (g/mL@20°C)	0.869
* Predicted	

#### 3.3.6.2 Production from Biomass

Hexanoic acid can be produced by fermentation of sugars (Jeon and Kim 2010, San-Velero 2019, Liu 2016) or mixtures of ethanol and small acids (e.g., acetic acid and butyric acid) followed by conversion to hexyl hexanoate through a simple basic transesterification route. Alternatively, hexanoic acid can be esterified with 1-hexanol generated via fermentation (Phillips 2015, Diender 2016) of synthesis gas or carbon monoxide produced by gasifying biomass. Catalytic production of 1-hexanol from ethanol also has been reported (Ramasamy 2016, Ramasamy 2018); however, production from a biomass feedstock through these steps has not been demonstrated.

### 3.3.6.3 TEA/LCA

Hexyl hexanoate can be produced from biomass by the catalytic upgrading of hexanoic acid (Gaertner 2009, Huo 2019), which can be derived from anaerobic fermentation of lignocellulosic sugars (Cavalcante 2017). The current state of technology for production of short-chain VFAs via anaerobic fermentation yields mixtures of acetic (3.7%), butyric (59%), and hexanoic (37%) acids (Nelson 2017). A target case assumes that advancements in fermentation or metabolic engineering research and development result in 100% selectivity to hexanoic acid. Acids produced in fermentation are recovered in situ by a pertractive membrane system. In the SOT case, acetic and butyric acids are separated from the hexanoic acid via distillation and sold as co-products. In both cases, half the hexanoic acid is reduced to n-hexanol via hydrogenation over a bimetallic Rh/Mo catalyst (He 1995). The alcohol and carboxylic acids are fed in stoichiometric amounts to a reactive stripping column containing a heterogeneous zeolite BEA catalyst, where compressed air is used to remove inhibitory water from the esterification reaction (Schildhauer 2009). The hexyl hexanoate product is separated from the remaining reactants which are recycled back to the esterification reactor. Evaluation of the baseline case gives an MFSP of approximately \$10/GGE due to relatively low fermentation yields of the intermediate hexanoic acid, leading to reduced fuel yields. Under target case assumptions, increased selectivity to hexanoic acid may reduce MFSP to between \$5–\$5.5/GGE, slightly lower than other similar biochemical routes with acid intermediates due to lower processing and higher overall carbon efficiency to final fuel (33%).

Life cycle GHG emissions and fossil fuel consumption of hexyl hexanoate were not favorable compared to those of petroleum diesel, representing only 37% reduced GHG emissions and 28% less fossil fuel use compared to petroleum diesel. The major contributor to these metrics is the use of highly GHG- and energy-intensive chemicals such as NaOH used during pretreatment of corn stover.

### 3.3.6.4 Challenges, Barriers, and R&D Needs

Cost and scalable production must be demonstrated from a biomass feedstock, including identifying sufficient feedstock volume. LCA has not been conducted to determine whether the GHG emissions reductions meet the target value of at least 60%.

Additionally, conventional test methods should be validated and updated, as necessary, to fully describe the fuel quality. In particular, the ASTM D6584: *Standard Test Method for Determination of Total Monoglycerides, Total Diglycerides, Total Triglycerides, and Free and Total Glycerin in B-100 Biodiesel Methyl Esters by Gas Chromatography* will need to be modified, as the current method is highly specific for methyl esters from C16/C18 feedstocks. The glyceride content of biodiesel has been well documented to have significant impacts on fuel quality (Chupka 2012, Chupka 2014).

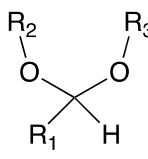
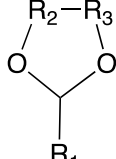
### 3.3.7 Dioxolanes

Acetals are polyethers with the general structure  $R_2C(OR')_2$  where the R groups are organic groups or hydrogen and the R' are organic groups and may or may not be equivalent, leading to

symmetric or mixed acetals, respectively. Dioxolanes are heterocyclic acetals with the general formula  $RO_2(R'_2)$  and are often used as protecting groups for ketones and aldehydes in organic chemistry. The pathways examined for the production of dioxolanes do not meet the GHG emissions reduction target and further research is required to identify alternative approaches requiring less or no NaOH.

### 3.3.7.1 Property Summary

Other than the polyoxymethylene ethers described in Section 3.2.4, no acetals were identified that could be easily made from biomass and possessed the requisite fuel properties for use in MCCI applications. While the production of these molecular classes have been extensively studied for their fuel potential<sup>1</sup>, their fuel properties have been less well investigated. The fuel properties of these molecules are structure dependent. The fuel properties are influenced by the carbon chain length and branching, with high DCN and CN reported for symmetric ethoxyacetals (Figure 46). Additional fuel properties for these structures have not been measured and additional investigation into this class of molecule may be warranted. However, based on work on POMEs, the lability of the ethoxy group and subsequent stability may be an area of concern and variation of the appending alcohol may be sufficient to impart greater stability. The fuel properties of dioxolanes evaluated in this work and several from the literature (Harrison and Harvey 2018) are shown in Figure 45.

Dioxolanes and Acetals	
	
Acetal	Dioxolane
Formula	$R_1-CH-(O-R_2)-O-R_3$
CN	33-91
$T_b$ (°C)	174-188
Flash point (°C)	32-69.5
MP (°C)	<-100
Water solubility (mg/L)	–
YSI	36-69
Energy density (MJ/L)	–
Specific energy (MJ/kg)	28-34.4
Kinematic viscosity $mm^2/s@40^\circ C$	0.94-5.15
Density (g/mL@40°C)	0.883-0.894

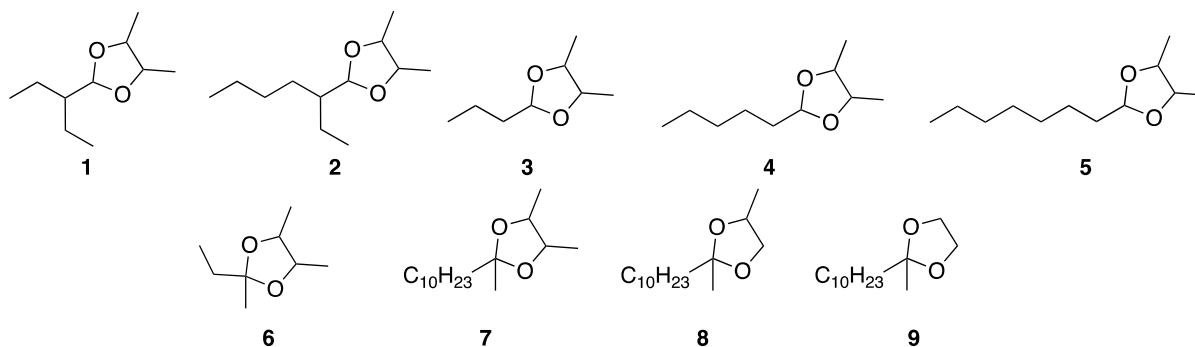


Figure 45. Structures of dioxolanes 1–9 referenced in this section.

### 3.3.7.2 Production from Biomass

Acetals and dioxolanes are formed through condensation reactions between an aldehyde and two alcohols and are generally catalyzed by homogeneous or heterogeneous acids. Co-Optima

researchers have evaluated both acetals and dioxolanes. The aldehydes reported by Staples (2018) were synthesized using aldol condensation of ethanol-derived acetaldehyde resulting in C6 and C8 branched aldehydes. Additional straight-chain aldehydes were used for comparison. The use of methylketones has also been demonstrated; methylketones can also be readily derived from biomass. The alcohols reported by Staples (2018) were ethanol and 2,3-butanediol (2,3-BDO), both of which are available through fermentation of biomass-derived hydrolysates in high titer, giving fully bio-derived fuel molecules.

Dioxolanes have been studied in much more detail. They can be synthesized directly from ethylene glycol and syngas (Fan 2009) to give mixtures with tail carbon numbers ranging from 3–12 with only preliminarily physical properties reported (see Table 18). More recently, 2,3-BDO has been used to synthesize 2-ethyl-2,4,5-trimethyl-1,3 dioxolane (compound 6) and 4,5-dimethyl-2-isopropyl dioxolane (Harvey 2018) leading to a range of 2-methyl ketone derived dioxolanes (Harrison 2018) (compounds 7–8).

Table 18. Fuel properties of select dioxolanes.

Compound	Cetane	LHV (MJ kg <sup>-1</sup> )	YSI	Freezing Point (°C)	Boiling Point (°C)	Viscosity (40°C, mm <sup>2</sup> s <sup>-1</sup> )	Flash Point (°C)	Water Solubility (mg/L)
1	45	33.0	57.8	< -100	174	1.26	54.4	< 40
2	64	34.4	68.5	< -100	184	1.88	58.3	< 40
3	33	31.0	36.5	< -100	161	0.94	42.5	< 40
4	48	32.9	48.7	< -100	177	1.49	69.5	< 40
5	69	34.0	63.2	< -100	188	2.34	79.5	< 40
6	-	28.3	-	-	-	-	32.0	8000
7 <sup>a</sup>	84	28.0	-	-51	-	4.44	-	-
8 <sup>a</sup>	91	27.9	-	-48	-	5.15	-	-
9 <sup>a</sup>	81	28.5	-	-25	-	4.98	-	-

<sup>a</sup> Harrison 2018

Additional testing has been performed on compounds 1–5 as blends with a seven-component surrogate with DCN of 44.5 and cloud point of -7°C. The cloud points measured upon blending of compounds 1–5 with surrogate at levels from 10% to 30% decreased from -10 to -13°C. Compatibility studies with common elastomers and materials used in the fuel system showed borderline incompatibility with hydrogenated nitrile butadiene rubbers, similar to biodiesel, and no other signs of incompatibility.

The biomass-derived dioxolane (2-ethyl-2,4,5-trimethyl-1,3-dioxolane or C<sub>8</sub>H<sub>16</sub>O<sub>2</sub>) is produced via the acetalization of 2,3-butanediol (2,3-BDO) with C<sub>4</sub>+ aldehydes intermediates, a process recently developed by Staples (2018). Both intermediates are derived from biomass feedstock, namely a blended herbaceous biomass (primarily corn stover) (Davis 2018). 2,3-BDO is derived via aerobic fermentation of whole-slurry hydrolysate containing C<sub>5</sub> and C<sub>6</sub> sugars. The hydrolysate stream is split into two streams for separate 2,3-BDO and ethanol production based on the stoichiometric ratio of the two reactants for dioxolanes production.

An engineered strain of *Zymomonas mobilis* converts a portion of the sugars to 2,3-BDO. The rest of the sugars is sent to an anaerobic bioreactor for ethanol production. Ethanol is converted to acetaldehyde via dehydrogenation. Acetaldehyde in turn undergoes poly-aldol condensation

using Amberlyst 15 and Pd/C catalysts in cyclohexane solution to produce C<sub>4</sub>+ aldehydes, namely 2-ethylhexanal (C<sub>8</sub>H<sub>16</sub>O). The condensation step requires hydrogen; however, the process is hydrogen self-sufficient due to the excess hydrogen produced from the ethanol dehydrogenation. Process conditions for production of C<sub>4</sub>+ aldehydes are obtained from Moore (2017). The major upstream processing steps for the biorefinery that include biomass feedstock handling, biomass pretreatment via deacetylation and mechanical refining, and enzymatic hydrolysis and hydrolysate conditioning, are consistent with those from literature (Davis 2018).

### 3.3.7.3 TEA/LCA

The MFSP of dioxolanes using current baseline experimental parameters of conversions, yields, and recoveries was between \$6–7/GGE with over half of the cost associated with the upgrading and product recovery steps. Future research to improve catalyst lifetime and performance, process optimization and intensification, and improved solvent recovery and recycle can improve the biorefinery economics. The MFSP estimate uses the total fuel yield of 43.2 GGE/dry U.S. ton feedstock and 31.3 MM GGE per annum assuming 2000 dry metric tons/day of biomass feed into the process. Life cycle GHG emissions and fossil energy use of dioxolane fell into the unfavorable category compared to other MCCI bioblendstocks. The GHG emissions of this acetal pathway represents only 42% less GHG emissions than those of petroleum diesel, even though some emission credits are assigned to this pathway because of the displacement of conventional fossil-based GHG emission from sodium sulfate, a co-product of this pathway generated during the waste-water treatment process. Moreover, the fossil energy use of dioxolane increases slightly (by 1%) compared to fossil energy use for petroleum diesel. Major contributors to these metrics are the use of highly GHG and energy intensive chemicals such as NaOH used during pretreatment of corn stover and cyclohexane, a solvent used during corn stover conversion. Similar to other biochemically produced bioblendstocks evaluated in this report, these economic and environmental factors could be improved with lignin conversion to co-products.

### 3.3.7.4 Challenges, Barriers, and R&D Needs

The oxidative stability of dioxolane fuels was studied to examine the possibility of peroxide formation during fuel storage. Accelerated aging experiments were undertaken at two laboratories to measure peroxide formation and final oxidation products. Peroxide quantification was performed by means of titration experiments during accelerated aging at 40°C in the open air. After six weeks, up to 6000 ppm peroxide was detected in select dioxolane samples. At temperatures below ambient, dioxolane samples have been shown to exhibit no peroxide formation. Further assessment of the oxidation of these fuels has revealed a terminal oxidation product to be diol monoesters, formed through an initial dioxolane-peroxide intermediate that reacts with additional dioxolane to yield the final product (Kuramshin 1989) (Figure 46).

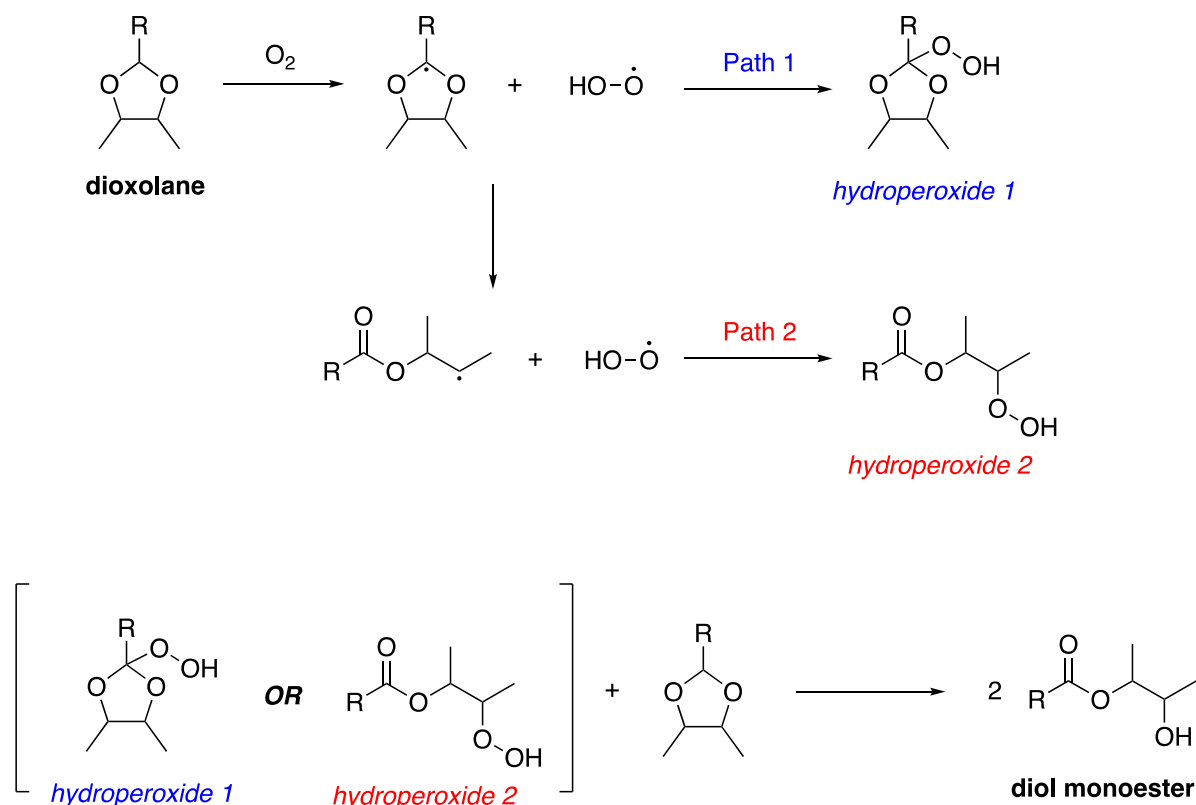


Figure 46. Dioxolane peroxide formation and terminal oxidation product.

The glycol monoesters have been characterized by gas chromatography-mass spectrometry with further spectroscopic studies ongoing to further characterize the reaction mechanism and products. Trace amounts of aldehydes, which are feedstocks for dioxolane production, are oxidized to carboxylic acids during accelerated aging experiments and these carboxylic acids have been identified using gas chromatography-mass spectrometry. Further studies are needed to determine 1) if trace aldehydes are produced during accelerated aging or are present in the starting materials and 2) if dioxolanes blended into base fuels exhibit peroxide formation during accelerated aging experiments and/or storage.

Although synthesis of these molecules for testing purposes is straightforward and multi-gallon quantities of have been prepared (Trifoli 2016, Fan 2009, Harvey et al, 2016, Harrison and Harvey 2018, Staples 2018), no scalable, low-cost approach to making these compounds from biomass, which also met the GHG emissions reduction target, was identified. Alternative approaches which reduce or eliminate the use of GHG-intensive chemicals such as NaOH and cyclohexane could improve the emissions characteristics of dioxolane production. A viable commercial pathway takes advantage of the immiscibility of dioxolanes with water. Dioxolanes phase separate, and these can be synthesized directly from BDO fermentation broth. A simple decantation of the top layer gives pure dioxolanes leaving behind fermentation by-products.

Additional measurements are necessary to ensure all of the requisite fuel properties are provided. This includes engine tests to establish combustion and emissions performance.

### 3.3.8 Oxetanes

Oxetanes are four-membered heterocycles with three carbon atoms and one oxygen atom. Barriers to adoption and use include lack of a clear and scalable route from biomass, along with significant fuel property knowledge gaps, including oxidative stability and compatibility.

#### 3.3.8.1 Property Summary

Alkyl substituted oxetanes would combine all the structural elements to provide a low-soot, high cetane fuel with higher energy content. Oxetanes are an important group of oxygen-containing heterocyclic compounds found in natural products and widely used in synthetic organic chemistry, polymer science, and materials science (Crivello 2007, Das and Damador 2011, Hailes and Behrendt 2008, Schulte 2013, Shibutani and Tsutsum 2012). Oxetane is a four-membered ring containing an oxygen atom with an inherent ring strain of  $106 \text{ kJ mol}^{-1}$ , which may be compared to epoxides ( $112 \text{ kJ mol}^{-1}$ ) and tetrahydrofurans ( $25 \text{ kJ mol}^{-1}$ ) (Eigenmann 1973, Pell and Pilcher 1965). Because of this property, oxetanes are used extensively in high-energy materials, such as propellants and energetic polymers. Oxetanes have also been used to improve combustion of liquid fuels (Baker and Daly 2003), reduce particulate, CO, NO<sub>x</sub>, and hydrocarbon emissions, increase power output, lessen misfiring, and enhance fuel efficiency. However, in these reports, 50–50,000 ppm 3,3-dimethoxyoxetane and 1-methoxy-2-methylpropyleneoxide were blended into liquid fuels, providing only a limited understanding of the fuel properties of oxetanes. To the best of the authors' knowledge, there are no reported direct applications of oxetanes as fuels.

#### 3.3.8.2 Production from Biomass

The synthesis and chemistry of oxetanes have been reviewed many times (Bull 2016). As far as the authors know, no routes to their production from biomass have been demonstrated, although such a route is theoretically possible as the intermediates such as alkenes and carbonyl compounds can be obtained from biomass. The photochemical Paterno-Buchi [2+2] reactions of carbonyl compounds with alkenes (Auria and Racioppi 2013), intramolecular Williamson etherification (Jenkinson and Fleet 2011), and ring expansion of epoxides with sulfoxonium ylides (Butova 2012) are established methods for their synthesis. Paterno-Buchi reactions are generally limited to aromatic aldehydes or ketones with alkenes; and the substituent requirements for photochemical activation have perhaps limited the application of this methodology, therefore, the ring expansion of epoxides, the one-step transformation of ketones to oxetanes with sulfoxonium ylides, and the intramolecular Williamson etherification seem to be the best reactions for our purposes. The ring expansion of epoxides and the one-step Corey-Chaykovsky epoxidation of ketones, followed by a ring expansion were used to obtain 2-alkyl (2) and 2,2-dialkyl oxetanes (4), respectively. The structures and fuel properties measured to date are given in Figure 47 and Table 19.

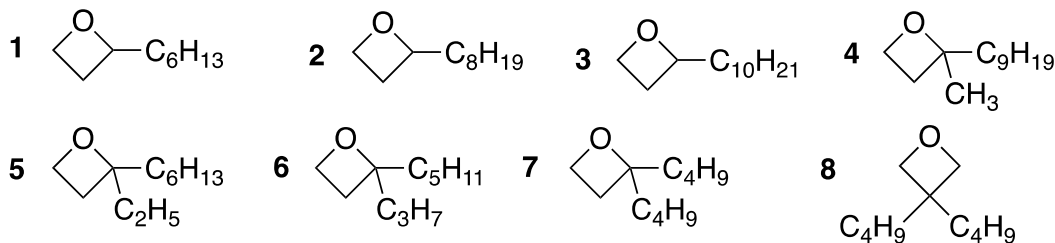


Figure 47. Synthetic variants of oxetanes evaluated in this work.

Table 19. Fuel properties of oxetanes shown in Figure 47. \* Predicted CN (Kubic 2017)

Compound	CN*	LHV (MJ kg <sup>-1</sup> )	YSI	Freezing Point (°C)	Boiling Point (°C)	Viscosity (40°C, mm <sup>2</sup> s <sup>-1</sup> )	Density (25°C, g mL <sup>-1</sup> )
1	55	37.4	52.7	< -40	197	0.94	0.817
2	62	38.5	67.1	< -40	238	1.30	0.814
3	69	39.0	78.9	-20	273	2.81	0.845
4	59	39.1	90.2	< -40	282	1.77	0.828
5	59	38.5	73.2	< -40	223	1.57	0.845
6	59	38.5	87.5	< -40	219	1.50	0.842
7	59	38.4	74.7	< -40	220	1.44	0.836
8	59	37.2	89.3	< -40	227	1.61	0.861

The two general trends investigated are increasing carbon number and maintaining total carbon number and changing functional groups. As carbon number increases (compounds 1–3), all physical properties increase, which is expected as the carbon chain increases. Distributing the carbons between two chains adjacent to the oxygen atom does not change the fuel properties significantly and moving the carbon chains beta to the oxygen slightly lowers the LHV and raises the YSI. These are subtle changes with good fuel properties throughout the series.

### 3.3.8.3 TEA/LCA

These analyses were not conducted. The difficulty generating these molecules from biomass and low reaction yields did not provide a useful proposed pathway for TEA.

### 3.3.8.4 Challenges, Barriers, and R&D Needs

Most of this work has been performed at small scale using direct synthetic rather than catalytic approaches. Scaling to large volumes has not been demonstrated, and especially not from a biomass feedstock.

The fuel properties of these molecules are good and comparable with other potential fuel properties but without a clear performance advantage. These two aspects provide significant challenges and barriers to further scale up and implement these molecules. Should these molecules be pursued further for use as fuels, key properties such as oxidative stability and compatibility should be measured.

### 3.3.9 Dipentyl Ether

Dipentyl-ether (DNPE), also known as pentyl ether or (n-)amyl ether, is a symmetric ether that can be produced by dehydration of 1-pentanol. Barriers to use and adoption include oxidative stability, low conductivity, and tendency to form peroxides, as well as demonstration of a low-cost, scalable route from biomass with the potential GHG emissions reductions.

#### 3.3.9.1 Property Summary

DNPE, also known as pentyl ether or (n-)amyl ether, was selected among more than 400 potential biomass-derived compounds as a promising diesel blendstock candidate by Co-Optima researchers (Fioroni 2019a). Indeed, DNPE meets the basic requirements for diesel blending with a CN of 111, a flashpoint equal to 57°C, and a boiling point of 190°C (Fioroni 2019a, Murphy 2002). In addition, DNPE has been shown to effectively reduce diesel exhaust emissions when blended with commercial diesel fuel (Giavazzi 1991; Van Heerden 1998). Co-optima researchers investigated the fuel properties impact when adding DNPE to a seven components diesel surrogate (i.e., a-methylnaphthalene, t-decalin, 2,2,4,4,6,8,8-heptamethylnonane, n-butylcyclohexane, n-hexadecane, tetralin, n-dodecylbenzene) (Fioroni 2019a).

Dipentyl Ether	
Formula	C <sub>10</sub> H <sub>22</sub> O
ICN	111
T <sub>b</sub> (°C)	190
Flash point (°C)	57
MP (°C)	-69
Water solubility (mg/L)	27
YSI	44
Energy density (MJ/L)	30.6
Specific energy (MJ/kg)	39.0
Kinematic viscosity mm <sup>2</sup> /s@40°C	2.1
Density (g/mL@40°C)	0.785

#### 3.3.9.2 TEA/LCA

These analyses were not performed due to failure of dipentyl ether to meet fuel property targets.

#### 3.3.9.3 Production from Biomass

DNPE can be produced via simple dehydration of 1-pentanol. However, there are only a few early-stage thermochemical pathways leading to the formation of 1-pentanol from biomass feedstocks. 1-pentanol can be obtained via a cascade of reactions from gamma valerolactone (Lange 2010) including ring-opening/hydrogenation of it into valeric acid followed by hydrogenation/ dehydration into 1-pentanol. Similarly, 1-pentanol could also be produced from hydrogenation of biomass-derived furfural (Wojcik 1948). Alternatively, 1-pentanol can be obtained via hydroformylation of 1-butene (Slami 2009), which can be obtained from waste-derived ethanol and biomass-derived ethanol (Dagle 2020).

#### 3.3.9.4 Challenges, Barriers, and R&D Needs

DNPE has several fuel properties that present barriers to adoption and use. From a safety standpoint, DNPE is a known peroxide former. Furthermore, DNPE conductivity (it has a conductivity  $<1$  pS/m, below the requirement for conductivity of  $\geq 25$  pS/m) and oxidative stability (55.9 min, below the ASTM D7545 requirement of 60 min) do not meet specifications, although additives may be able help a blended fuel meet these fuel specifications.

## 4 Conclusions

Co-Optima cast a wide net to identify lower-carbon intensity renewable hydrocarbon and oxygenate blendstock chemistries that could improve compression ignition engine performance and provide environmental benefits through reduced emissions. The thousands of molecules and mixtures were winnowed down through a tiered screening process, during which structure-property relationships were developed through modeling, small-scale experiments, and single-cylinder testing. These molecular correlations provide industry and other researchers a solid scientific basis to expand production to larger scale and engine tests to multicylinder engines. Ultimately, market actors will need to optimize performance with individual blendstocks that offer the greatest performance and economic opportunity.

While it is difficult to generalize overall engine testing conditions, Co-Optima has identified some very promising blendstocks that offer significant opportunities for future engines. Additionally, Co-Optima has shown the benefits of coupling new blendstocks with DFI to further reduce emissions and possibly decouple the soot-NO<sub>x</sub> tradeoff. In several categories of blendstocks, reduced propensity for sooting and NO<sub>x</sub> reduction with increased EGR has been shown, while meeting or exceeding current diesel performance in CN, freezing point, and sometimes energy density. The most promising blendstocks are predominantly compatible with current infrastructure; one of the most promising blendstocks (POMEs and derivatives) may not be compatible with some materials and mitigation may be necessary if they are to be used. All these improvements have been attained while reducing the carbon intensity of the blendstock and reducing the GHG emissions of the blendstock relative to diesel by more 60%.

Taking advantage of the lower sooting tendency of the top-performing blendstocks, DFI, and/or increased EGR show the potential to reduce both simultaneously more than 50%. Furthermore, some blendstocks were identified that can maintain fuel energy density and possibly increase efficiency slightly.

As this report shows, researchers within Co-Optima and elsewhere have identified promising blendstocks to reduce GHG and criteria pollutant emissions. For the potential of this work to be realized, extensive engine and other testing remains to be completed. Finally, there is significant work to be done in the biofuels community to drive efficiency in the production, integration, and scale-up of biofuels for economic MD/HD applications.

## 5 References

- Alleman, T.L., E.D. Christensen, and B.R. Moser. 2019. "Improving biodiesel monoglyceride determination by ASTM method D6584-17." *Fuel* 241:65-70. doi.org/10.1016/j.fuel.2018.12.019
- Alleman, T.L. *Assessment of BQ-9000 Biodiesel Properties for 2019*. NREL/TP-5400-76840. 2020. National Renewable Energy Laboratory, Golden, Colorado
- Alternative Fuels Data Center. 2021. Accessed May 4, 2021 at [https://afdc.energy.gov/files/u/publication/fuel\\_comparison\\_chart.pdf](https://afdc.energy.gov/files/u/publication/fuel_comparison_chart.pdf) (undated webpage).
- American Chemical Society. 2020. *SciFinder – Chemical Abstracts Service*. SciFinder.CAS.org.
- Ashley, S. 2019. "Can Diesel Finally Come Clean?" *Scientific American*. Accessed December 2020 at <https://www.scientificamerican.com/article/can-diesel-finally-come-clean/> (undated webpage).
- ASTM International. 2018. *Standard Test Method for Evaluating Lubricity of Diesel Fuels by the High-Frequency Reciprocating Rig (HFRR)*. ASTM D6079-18. West Conshohocken, Pennsylvania.
- ASTM International. 2019a. *Standard Test Method for Oxidation Stability of Middle Distillate Fuels—Rapid Small Scale Oxidation Test (RSSOT)*. ASTM D7545-14(2019)e1. West Conshohocken, Pennsylvania.
- ASTM International. 2019b. *Standard Test Method for Smoke Point of Kerosene and Aviation Turbine Fuel*. ASTM D1322-19. West Conshohocken, Pennsylvania.
- ASTM International. 2020a. *Standard Specification for Biodiesel Fuel Blend Stock (B100) for Middle Distillate Fuels*. ASTM D6751-20a. West Conshohocken, Pennsylvania.
- ASTM International. 2020b. *Standard Specification for Diesel Fuel Oil, Biodiesel Blend (B6 to B20)*. ASTM D7467-20a. West Conshohocken, Pennsylvania.
- ASTM International. 2020c. *Standard Specification for Diesel Fuel*. ASTM D975-20a. West Conshohocken, Pennsylvania.
- Atasoy, M., I. Owusu-Agyeman, E. Plaza, Z. Cetecioglu. 2018. "Bio-based volatile fatty acid production and recovery from waste streams: Current status and future challenges." *Bioresource Tech.* 268:773–786. <https://doi.org/10.1016/j.biortech.2018.07.042>.
- Auria, M. and R. Racioppi. 2013. "Oxetane Synthesis through the Paternò-Büchi Reaction." *Molecules*. 18(9):11384-11428.
- Awad, O.I., X. Ma, M. Kamil, O.M. Ali, Y. Ma, S. Shuai. 2020. "Overview of Polyoxymethylene Dimethyl Ether Additive as an Eco-Friendly Fuel for an Internal Combustion

Engine: Current Application and Environmental Impacts.” *Sci. Total Environ.* 715:136849. <https://doi.org/10.1016/j.scitotenv.2020.136849>.

Bacha, J., J. Freel, A. Gibbs, L. Gibbs, G. Hemighaus, K. Hoekman, J. Horn, M. Ingham, L. Jossens, D. Kohler, D. Lesnini, J. McGeehan, M. Nikanjam, E. Olsen, R. Organ, B. Scott, M. Sztenderowicz, A. Tiedemann, C. Walker, J. Lind, J. Jones, D. Scott, and J. Mills. 2007. *Diesel Fuels Technical Review*. Chevron, San Ramon, California. <https://www.chevron.com/-/media/chevron/operations/documents/diesel-fuel-tech-review.pdf>.

Baker, M.R. and D.T. Daly. 2003. *Strained ring compounds as combustion improvers for normally liquid fuels*. WO2003020852.

Barrientos, E.J., M. Lapuerta, and A.L. Boehman. 2013. “Group additivity in soot formation for the example of C-5 oxygenated hydrocarbon fuels.” *Combust Flame* 160(8):1484-1498.

Beckham, G.T., C.W. Johnson, E.M. Karp, D. Salvachúa, and D.R. Vardon. 2016. “Opportunities and challenges in biological lignin valorization.” *Curr. Opin. Biotechnol.* 42:40-53. <https://doi.org/10.1016/j.copbio.2016.02.030>.

Behr, A. and L. Johnen. 2009. “Myrcene as a natural base chemical in sustainable chemistry: a critical review.” *ChemSusChem*, 2:1072-1095.

Bertola, A. and K. Boulouchos. 2000. “Oxygenated fuels for particulate emissions reduction in heavy-duty DI-diesel engines with common-rail fuel injection.” *SAE Transactions* 2705-2715.

Bhatt, A.H, Z.J. Ren, and L. Tao. 2020. “Value Proposition of Untapped Wet Wastes: Carboxylic Acid Production through Anaerobic Digestion.” *iScience* 23:101221. doi: 10.1016/j.isci.2020.101221.

Billing, J.M., R.T. Hallen, P.A. Marrone, D.C. Elliott, J.C. Moeller, A.J. Schmidt, T.R. Hart, P. Kadota, and M.A. Randel. 2017. “Bench-Scale Evaluation of the Genifuel Hydrothermal Processing Technology for Wastewater Solids.” In Proceedings of the Water Environment Federation, (WEFTEC 2017), September 30-October 4, 2017, Chicago, Illinois, 3032-3061. Alexandria, Virginia: Water Environment Federation. PNNL-SA-127937. doi:10.2175/193864717822157702.

Blagov, S., H. Hasse, and E. Stroefel. 2005. *Polyoxymethylene Dimethyl Ether Synthesis Reaction Process for Product Separation*. DE102005027701A.

Boborodea, A., F. Collignon, and A. Brookes. 2015. “Characterization of Polyethylene in Dibutoxymethane by High-Temperature Gel Permeation Chromatography with Triple Detection.” *Int. J. Polymer Anal. Char.* 20:316-322.

Böhm, H., H. Jander, and D. Tanke. 1998. “PAH growth and soot formation in the pyrolysis of acetylene and benzene at high temperatures and pressures: Modeling and experiment.” *Symposium (International) on Combustion* 1998, 27(1):1605-1612.

- Bojase, G., T.V. Nguyen, A.D. Payne, A.C. Willis, and M.S. Sherburn. 2011. "Synthesis and properties of the ivyanes: the parent 1,1-oligocyclopropanes." *Chem. Sci* 2:229–232. doi:10.1039/C0SC00500B.
- Bomgardner, M.M. 2020. "California refiners shift production to renewable diesel: New entrants will compete with chemical industry for cheap feedstocks." *Chemical & Engineering News* 98(32). <https://cen.acs.org/energy/biofuels/California-refiners-shift-production-renewable/98/i32>.
- Brooks, K., L. Snowden-Swan, S. Jones, M. Butcher, G.-S. Lee, D. Anderson, J. Frye, J.E. Holladay, J. Owen, L. Harmon, F. Burton, I. Palou-Rivera, J. Plaza, R. Handler, and D. Shonnard. 2016. "Low-carbon aviation fuel through the alcohol to jet pathway." *Biofuels for Aviation* 2016:109-150.
- Brookshear, D.W., M.J. Lance, R.L. McCormick, and T.J. Toops. 2017. "Investigations of the impact of biodiesel metal contaminants on emissions control devices." *Catalysis* 29:317-342.
- Bull, J.A., R.A. Croft, O.A. Davis, R. Doran, and K.F. Morgan. 2016. "Oxetanes: Recent Advances in Synthesis, Reactivity, and Medicinal Chemistry." *Chem. Rev.* 116 (19):12150-12233.
- Burger, J., E. Ströfer, and H. Hasse, 2012. "Chemical Equilibrium and Reaction Kinetics of the Heterogeneously Catalyzed Formation of Poly(Oxymethylene) Dimethyl Ethers from Methylal and Trioxane." *Ind. Eng. Chem. Res.* 51 (39):12751–12761. <https://doi.org/10.1021/ie301490q>.
- Butova, E.D., A.V. Barabash, A.A. Petrova, C.M. Kleiner, P.R. Schreiner, and A.A. Fokin. 2010. "Stereospecific Consecutive Epoxide Ring Expansion with Dimethylsulfoxonium Methylide." *J. of Org. Chem.* 75 (18):6229-6235.
- Cai, H., L. Ou, M. Wang, E. Tan, R. Davis, A. Dutta, L. Tao, D. Hartley, M. Roni, D. Thompson, L. Snowden-Swan, Y. Zhu, and S. Jones. 2020. *Supply Chain Sustainability Analysis of Renewable Hydrocarbon Fuels via Indirect Liquefaction, Ex Situ catalytic fast pyrolysis, Hydrothermal liquefaction, Combined Algal Processing and biochemical conversion: Update of the 2019 State-of-technology Cases*. ANL/ESD 20/2. [https://greet.es.anl.gov/publication-renewable\\_hc\\_2019](https://greet.es.anl.gov/publication-renewable_hc_2019)
- Calcote, H.F. and D.M. Manos. 1983. "Effect of molecular structure on incipient soot formation." *Combust. Flame* 49 (1–3):289-304. [https://doi.org/10.1016/0010-2180\(83\)90172-4](https://doi.org/10.1016/0010-2180(83)90172-4).
- Carroll, F.A., C.-Y. Lin, and F.H. Quina. 2011. "Simple Method to Evaluate and to Predict Flash Points of Organic Compounds." *Ind. Eng. Chem. Res.* 50(2011):4796-4800. <https://doi.org/10.1021/ie1021283>.
- Carlson, J.S., E.A. Monroe, and R. Dhaoui, 2020. "Biodiesel Ethers: Fatty Acid-Derived Alkyl Ether Fuels as Improved Bioblendstocks for Mixing-Controlled Compression Ignition Engines." *Energy & Fuels* 34(10):12646-12653.

Cavalcante, W., R.C. Leitão, T.A. Gehring, L.T. Angenent, and S.T. Santaella. 2017. “Anaerobic fermentation for n-caproic acid production: A review.” *Process Biochemistry* 54 (2017):106–119.

Chamberlain, J. 2015. *Safer consumer products alternatives analysis development*. University of California, Santa Barbara.

Christensen, E. and R.L. McCormick. 2014. “Long-term storage stability of biodiesel and biodiesel blends.” *Fuel Process. Technol.* 128:339–348.

Christensen, E., T.L. Alleman, and R.L. McCormick. 2018. “Re-additization of commercial biodiesel blends during long-term storage,” *Fuel Process. Technol.* 177:56-65.

Coordinating Research Council (CRC). 2016. *Diesel Fuel Low Temperature Operability Guide*: <http://crbsite.wpengine.com/wp-content/uploads/2019/05/CRC-671.pdf>

Chen, W.-T., Y. Zhang, J. Zhang, L. Schidema, G. Yu, P. Zhang, and M. Minarick. 2014. *Applied Energy* 128 (2014):209-216. <http://dx.doi.org/10.1016/j.apenergy.2014.04.068>

Chen, C.-T. and J.C. Liao. 2016. “Frontiers in microbial 1-butanol and isobutanol production.” *FEMS Microbiology Letters*, 363(5) fnw020.

Choi, K., B. Jeon, B.C. Kim, M.K. Oh, Y. Um, and B.-I. Sang. 2013. “In Situ Biphasic Extractive Fermentation for Hexanoic Acid Production from Sucrose by *Megasphaera Elsdenii* NCIMB702410,” *Appl. Biochem. Biotechnol.* 171:1094-1107.

Choi, R.K., W.D. Jang, D. Yang, J.S. Cho, D. Park, and S.Y. Lee. 2019. “Systems metabolic engineering strategies: Integrating systems and synthetic biology with metabolic engineering” *Trends in Biotechnology*. <https://doi.org/10.1016/j.tibtech.2019.01.003>.

Chupka, G.M., L. Fouts, and R.L. McCormick. 2012. *Energy Environ. Sci.* 5(2012):8734-8742. <https://doi.org/10.1039/C2EE22565D>

Chupka, G.M., L. Fouts, J.A. Lennon, T.L. Alleman, D.A. Daniels, and R.L. McCormick. 2014. *Fuel Process. Technol.* 118(2014):302-309. <https://doi.org/10.1016/j.fuproc.2013.10.002>

Clark, R.H., G.T. Kalghatgi, and E.M. Liney. 2005. *Method to increase the cetane number of gas oil by blending*. WO2003087273A1.

Coleman, T., A. Blankenship, and E. Eckart. 2010. *Preparation of Dibutoxymethane*. U.S. Patent 2010.0076226A1.

Crivello, J.V. 2007. “Hybrid free radical/cationic frontal photopolymerizations.” *J. Polymer Sci. A: Polymer Chem.* 45(18):4331-4340.

Curran, S.C., A. Hagen, S. Poust, L.J.G. Chan, B.M. Garabedian, T. de Rond, M.J. Baluyot, J.T. Vu, A.K. Lau, S. Yuzawa, C.J. Petzold, L. Katz, and J.D. Keasling. 2018. "Probing the Flexibility of an Iterative Modular Polyketide Synthase with Non-Native Substrates in Vitro." *ACS Chem Biol.* 13(8):2261–2268.

d'Espaux, L., A. Ghosh, W. Runguphan, M. Wehrs, F. Xu, O. Konzock, I. Dev, M. Nhan, J. Gin, A. Reider Apel, C.J. Petzold, S. Singh, B.A. Simmons, A. Mukhopadhyay, H.G. Martín, and J.D. Keasling. 2017. "Engineering high-level production of fatty alcohols by *Saccharomyces cerevisiae* from lignocellulosic feedstocks." *Metab Eng.* 42:115–25.

Dagle, V., A. Winkelman, N. Jaegers, J. Saavedra-Lopez, J.Z. Hu, M. Engelhard, S. Habas, S. Akhade, L. Kovarik, V-A Glezakou, R. Rousseau, Y. Wang, and R. Dagle. 2020. "Single-step conversion of ethanol to n-butene over Ag-ZrO<sub>2</sub>/SiO<sub>2</sub> catalysts." *ACS Catalysis*, Accepted.

Dahmen, M. and W. Marquardt. 2015. "A novel group contribution method for the prediction of the derived cetane number of oxygenated hydrocarbons." *Energy Fuels* 29: 5781–5801. doi:10.1021/acs.energyfuels.5b01032.

Das, B.D. and K. Damodar. 2011. "Epoxides and Oxetanes." *Heterocycles in Natural Product Synthesis*, K.C. Majumdar and S.K. Chattopadhyay, Eds. Wiley-VCH: Weinheim, pp 63-90.

Das, D.D., C.S. McEnally, T.A. Kwan, J.B. Zimmerman, W.J. Cannella, C.J. Mueller, and L.D. Pfefferle. 2017. "Sooting tendencies of diesel fuels, jet fuels, and their surrogates in diffusion flames." *Fuel* 197:445-458.

Das, D.D., P.C. St. John, C.S. McEnally, S. Kim, and L.D. Pfefferle. 2018. "Measuring and predicting sooting tendencies of oxygenates, alkanes, alkenes, cycloalkanes, and aromatics on a unified scale." *Combust. Flame*, 190:349-364.

Davis, R., A. Bartling, and L. Tao. 2020. *Biochemical Conversion of Lignocellulosic Biomass to Hydrocarbon Fuels and Products: FY19 State of Technology and Future Research*. NREL/TP-5100-76567. National Renewable Energy Laboratory, Golden, Colorado.

Davis R, L Tao, E.C.D. Tan, M.J. Bidy, GT Beckham, C Scarlata, J Jacoson, K Cafferty, J Ross, J. Lukas, D Knorr, and P Schoen. 2013. *Process Design and Economics for the Conversion of Lignocellulosic Biomass to Hydrocarbons: Dilute-Acid and Enzymatic Deconstruction of Biomass to Sugars and Biological Conversion of Sugars to Hydrocarbons*. National Renewable Energy Laboratory, Golden, Colorado. doi:10.2172/1107470.

Davis, R.E., N.J. Grundl, L. Tao, M.J. Bidy, E.C. Tan, G.T. Beckham, D. Humbird, D. Thompson, and M.S. Roni. 2018. *Process Design and Economics for the Conversion of Lignocellulosic Biomass to Hydrocarbon Fuels and Coproducts: 2018 Biochemical Design Case Update; Biochemical Deconstruction and Conversion of Biomass to Fuels and Products via Integrated Biorefinery Pathways*. NREL/TP-5100-71949, National Renewable Energy Laboratory, Golden, Colorado.

de Carvalho, C.C.C.R. and M.M.R. da Fonseca. 2006. "Biotransformation of terpenes." *Biotechnol. Advances*, 24 (2):134-142.

- Dangol, N., D.S. Shrestha, and J.A. Duffield. 2020. "Life cycle energy, GHG, and cost comparison of camelina-based biodiesel and biojet fuel." *Biofuels*. 11(4):399-407. <https://doi.org/10.1080/17597269.2017.1369632>
- Delfort, B., I. Durand, A. Jaecker-Voirol, T. Lacôme, F. Paillé, and X. Montagne. 2002. "Oxygenated compounds and diesel engine pollutant emissions performances of new generation of products." *SAE Transactions* 1871-1880.
- Deur, J.M. 2018. "Biofuel Opportunities and Challenges for Heavy Duty Diesels: Cummins' Perspective," presented at ABLC Next, San Francisco, California, November 9, 2018.
- Diender, M., A.J.M. Stams, and D.Z. Sousa. 2016. "Production of medium-chain fatty acids and higher alcohols by a synthetic co-culture grown on carbon monoxide or syngas." *Biotechnol. Biofuels* 9 (2016) 82. <https://doi.org/10.1186/s13068-016-0495-0>.
- Dufal, S., V. Papaioannou, M. Sadeqzadeh, T. Pogiatzis, A. Chremos, C.S. Adjiman, G. Jackson, and A. Galindo. 2014. "Prediction of Thermodynamic Properties and Phase Behavior of Fluids and Mixtures with the SAFT- $\gamma$  Mie Group-Contribution Equation of State." *J Chem Eng Data* 59: 3272–3288. doi:10.1021/je500248h.
- Dutta, A., M. Talmadge, J. Hensley, M. Worley, D. Dudgeon, D. Barton, P. Groenendijk, D. Ferrari, B. Stears, E.M. Searcy, C.T. Wright, and J.R. Hess. 2011. *Process Design and Economics for Conversion of Lignocellulosic Biomass to Ethanol*. NREL/TP-5100-51400. National Renewable Energy Laboratory, Golden, Colorado.
- Eckerle, W., V. Sujan, and G. Salemme. 2017. "Future challenges for engine manufacturers in view of future emissions legislation." SAE Technical Paper.
- Edwards, T. 2003. "Liquid Fuels and Propellants for Aerospace Propulsion: 1903-2003." *Journal of Propulsion and Power* 19:1089–1107. doi:10.2514/2.6946.
- Eigenmann, H.K., D.M. Golden, and S.W. Benson. 1973. "Revised group additivity parameters for the enthalpies of formation of oxygen-containing organic compounds." *J. Phys. Chem.*, 77 (13):1687-1691.
- Elliott, D.C., T.R. Hart, A.J. Schmidt, G.G. Neuenschwander, L.J. Rotness, M.V. Olarte, A.H. Zacher, K.O. Albrecht, R.T. Hallen, and J.E. Holladay, *Algal Research* 2(4):445-454. <https://doi.org/10.1016/j.algal.2013.08.005>
- Ely, J.F. and H.J.M. Hanley. 1981. *A Computer Program for the Prediction of Viscosity and Thermal Conductivity in Hydrocarbon Mixtures*. National Bureau of Standards Technical Note 1039.
- Emam, E.A. 2018. "Clay Adsorption Perspective on Petroleum Refining Industry." *Ind. Eng.* 2(1):19-25. doi: 10.11648/j.ie.20180201.13
- Evangelista, R.L., and S.C. Cermak. 2007. "Full-Press Oil Extraction of Cuphea (PSR23) Seeds." *J. Am. Oil Chem. Soc.*, 84:1169-1175.

Fan, X.-B., N. Yan, Z.-Y. Tao, D. Evans, C.-X. Xiao, and Y. Kou. 2009. "One-Step Synthesis of 2-Alkyl-dioxolanes from Ethylene Glycol and Syngas." *ChemSusChem*, 2 (10):941-943.

Fasahati, P. and J. Liu. 2014. "Techno-economic analysis of production and recovery of volatile fatty acids from brown algae using membrane distillation." *Computer Aided Chemical Engineering*, M.R. Eden, J.D. Siirola, and G.P. Towler, eds. (Elsevier), 34:303-308.

Feng, W., P. Ji, B. Chen, and D. Zheng. 2011. "Analysis of Methanol Production from Biomass Gasification." *Chem. Eng. Technol.* 34 (2):307–317. <https://doi.org/10.1002/ceat.201000346>.

Fiorini, G., L. Fouts, J. Luecke, D. Vardon, N. Huq, E. Christensen, X. Hua, T. Alleman, R. McCormick, M. Kass, E. Polikarpov, G. Kukkadapu, and R. Whitesides. 2019a. *Screening of potential biomass-derived streams as fuel blendstocks for mixing controlled compression ignition combustion.* SAE Technical Paper 2019-01-0570.

Fiorini, G., L. Fouts, J. Luecke, D. Vardon, N. Huq, E. Christensen, X. Huo, T. Alleman, R. McCormick, and M. Kass, 2019b. "Screening of potential biomass-derived streams as fuel blendstocks for mixing controlled compression ignition combustion." *SAE International Journal of Advances and Current Practices in Mobility* 1:1117-1138. doi:10.4271/2019-01-0570.

Firestone, D. 2013. *Physical and Chemical Characteristics of Oils, Fats, and Waxes, 3rd ed.* AOCS Press, Urbana, Illinois.

Fitzgerald, R.P., K. Svensson, G. Martin, Y. Qi, and C. Koci. 2018. "Early Investigation of Ducted Fuel Injection for Reducing Soot in Mixing-Controlled Diesel Flames," *SAE Int. J. Engines* 11(6):817-833. doi:10.4271/2018-01-0238.

Freedman, B. and M.O. Bagby. 1989. "Heats of Combustion of Fatty Esters and Triglycerides." *J Am Oil Chem Soc.* 66(11):1601-5. doi.org//10.1007/Bf02636185.

Frenklach, M., D.W. Clary, W.C. Gardiner, Jr, S.E. Stein. 1985. "Detailed kinetic modeling of soot formation in shock-tube pyrolysis of acetylene." *Symposium (International) on Combustion* 20(1):887-901.

Frenklach, M. 2002. "Reaction mechanism of soot formation in flames." *Phys. Chem. Chem. Phys.* 4 (11):2028-2037.

Fuels Institute. 2020. "Biomass-Based Diesel – A Market and Performance Analysis." [https://www.fuelsinstitute.org/getattachment/ed72f475-8038-415c-b1fd-591b213d4815/Biomass-Based-Diesel\\_Report.pdf](https://www.fuelsinstitute.org/getattachment/ed72f475-8038-415c-b1fd-591b213d4815/Biomass-Based-Diesel_Report.pdf)

Futures. 2020. "Canola Historical Prices / Charts. (n.d.)." Retrieved December 14, 2020, from <https://futures.tradingcharts.com/historical/CA/1974/0/continuous.html>.

Gaertner, C.A., J. Serrano, D.J. Braden, and J.A. Dumesic. 2009. "Catalytic coupling of carboxylic acids by ketonization as a processing step in biomass conversion." *J. Catal.* 266:71–78.

Gai, C., Y. Li, N. Peng, A. Fan, and Z. Liu. 2015. *Bioresource Technology* 185(2015):240-245. <http://dx.doi.org/10.1016/j.biortech.2015.03.015>.

Gálvez-Martos, J.-L., S. Greses, J.-A. Magdalena, D. Iribarren, E. Tomás-Pejó, C. González-Fernández. 2021. “Life cycle assessment of volatile fatty acids production from protein- and carbohydrate-rich organic wastes.” *Bioresource Technology* 321:124528. <https://doi.org/10.1016/j.biortech.2020.124528>.

Gaspar, D.J. 2019. Top Ten Blendstocks For Turbocharged Gasoline Engines: Bioblendstocks With Potential to Deliver the for Highest Engine Efficiency. PNNL-28713, Pacific Northwest National Laboratory. Doi: 10.2172/1567705.

Gehmlich, R.K., C.J. Mueller, D.J. Ruth, C.W. Nilsen, SA Skeen, and J Manin. 2018. “Using Ducted Fuel Injection to Attenuate or Prevent Soot Formation in Mixing-Controlled Combustion Strategies for Engine Applications.” *Applied Energy* 226:1169-1186. doi:10.1016/j.apenergy.2018.05.078.

George, K.W., J. Alonso-Gutierrez, J.D. Keasling, and T.S. Lee. 2015. “Isoprenoid drugs, biofuels, and chemicals--artemisinin, farnesene, and beyond.” *Adv Biochem Eng Biotechnol.* 148:355–389. doi:10.1007/10 2014 288.

Gershenzon, J., and N. Dudareva. 2007. “The function of terpene natural products in the natural world.” *Nature Chemical Biology*, 3(7):408-414.

Gesch, R.W., D.W. Archer, and F. Forcella. 2010. “Rotational Effects of Cuphea on Corn, Spring Wheat, and Soybean.” *Agron. J.* 102(1):145-153. <https://doi.org/10.2134/agronj2009.0215>

Ghysels, M. 1924. “The Formals of the Primary Alcohols.” *Bull. Soc. Chim. Belg*, 33:57-78.

Giavazzi, F., D. Terna, D. Patrini, F. Ancillotti, G.C. Pecci, R. Trere, and M. Benelli. 1991. *IX International Symposium on Alcohol Fuels* 1:327.

Granda, C.B., M.T. Holtzapfle, G. Luce, K. Searcy, D.L. Mamrosh. 2009. “Carboxylate Platform: The MixAlco Process Part 2: Process Economics.” *Appl Biochem. Biotechnol.* 156 107–124. <https://doi.org/10.1007/s12010-008-8481-z>.

Gray, D., S. Sato, F. Garcia, R. Eppler, and J. Cherry. 2014. Amyris, Inc. Integrated Biorefinery Project Summary Final Report - Public Version. U.S. Department of Energy, Golden Field Office, Golden, Colorado. doi:10.2172/1122942.

Guo, Y., T. Yeh, W. Song, D. Xu, and S. Wang. 2015. *Renew. and Sust. Energy Rev.* 48 (2015):776-790. <https://doi.org/10.1016/j.rser.2015.04.049>

Haas, M.J., A.J. McAloon, W.C. Yee, and T.A. Foglia. 2006. “A Process Model to Estimate Biodiesel Production Costs.” *Bioresour. Technol.*, 97:671-678. <https://doi.org/10.1016/j.biortech.2005.03.039>

Hafenstine, G.R., N.A. Huq, D.R. Conklin, M.R. Wiatrowski, X. Huo, Q. Guo, K.A. Unocic, and D.R. Vardon. 2020. "Single-phase catalysis for reductive etherification of diesel bioblendstocks." *Green Chemistry* 22.14:4463-4472. doi:10.1039/D0GC00939C.

Hagen, G.P. and M.J. Spangler. 1998. *Preparation of Polyoxymethylene Dimethyl Ethers by Catalytic Conversion of Dimethyl Ether with Formaldehyde Formed by Oxy-Dehydrogenation of Dimethyl Ether*. US5959156A.

Hailes, H.C. and J.M. Behrendt. 2008. Oxetanes and Oxetenes: Monocyclic. *Comprehensive Heterocyclic Chemistry III*, AR Katritzky, Ed. Pergamon: Oxford, Vol. 2, p 321.

Harmon, L., R. Hallen, M. Lilga, B. Heijstra, I. Palou-Rivera, and R. Handler. 2017. *A Hybrid Catalytic Route to Fuels from Biomass Syngas*. doi:10.2172/1423741.

Han, J., M. Mintz, and M. Wang. 2011. Waste-to-wheel analysis of anaerobic-digestion-based renewable natural gas pathways with the GREET model. Argonne National Laboratory.

Han, J., L. Tao, and M. Wang. 2017. Well-to-wake analysis of ethanol-to-jet and sugar-to-jet pathways. *Biotechnology for Biofuels* 10 (21). <https://doi.org/10.1186/s13068-017-0698-z>

Hansen, C.M. 2007. *Hansen Solubility Parameters: A User's Handbook, 2<sup>nd</sup> Edition*. CRC Press, Taylor and Francis Group: Boca Rotan, Florida.

Harrison, K.W. and B.G. Harvey. 2018. "High cetane renewable diesel fuels prepared from bio-based methyl ketones and diols." *Sustainable Energy & Fuels*, 2 (2):367-371.

Harvey, B.G., W.W. Merriman, and R.L. Quintana. 2016. "Renewable Gasoline, Solvents, and Fuel Additives from 2,3-Butanediol." *ChemSusChem*, 9(14):1814-1819.

Harvey, B.G., W.W. Merriman, and T.A. Koontz. 2015. "High-Density Renewable Diesel and Jet Fuels Prepared from Multicyclic Sesquiterpanes and a 1-Hexene-Derived Synthetic Paraffinic Kerosene." *Energy Fuels*, 29(4):2431-2436.

He, D.H., N. Wakasa, and T. Fuchikami. 1995. "Hydrogenation of Carboxylic Acids Using Bimetallic Catalysts Consisting of Group 8 to 10, and Group 6 or 7 Metals." *Tetrahedron Letters* 36:1059-1062. doi: 10.1016/0040-4039(94)02453-I.

Hegart, C., PACCAR. 2019. "Future Fleets: A Heavy-duty Truck OEM Perspective", Presented at the Smoky Mountains Mobility Conference, Chattanooga, Tennessee.

Held, M., Y. Tönges, D. Pélerin, M. Härtl, G. Wachtmeister, and J. Burger. 2019. "On the Energetic Efficiency of Producing Polyoxymethylene Dimethyl Ethers from CO<sub>2</sub> Using Electrical Energy." *Energy Environ. Sci.* 12(3):1019–1034. <https://doi.org/10.1039/c8ee02849d>.

Heredia-Langner, A., J.R. Cort, K. Grubel, M.J. O'Hagan, K. Jarman, J.C. Linehan, K.O. Albrecht, E. Polikarpov, D.L. King, T.D. Smurthwaite, and J.T. Bays, *Energy Fuels* 34:12556–12572. <https://dx.doi.org/10.1021/acs.energyfuels.0c00883>

Hiratsuka, T., H. Suzuki, R. Kariya, T. Seo, A. Minami, and H. Oikawa. 2014. "Biosynthesis of the structurally unique polycyclopropanated polyketide-nucleoside hybrid jawsamycin (FR-900848)." *Angew. Chem. Int. Ed. Engl.* 53:5423–5426. doi:10.1002/anie.201402623.

Holik, M.J. and J.F. Kraemer. 1997. *Foundry core composition of aggregate and a binder therefor*. U.S. Patent 4,172,068.

Holmgren, K.M., E. Andersson, T. Berntsson, and T. Rydberg. 2014. "Gasification-Based Methanol Production from Biomass in Industrial Clusters: Characterisation of Energy Balances and Greenhouse Gas Emissions." *Energy*, 69:622–637. <https://doi.org/10.1016/j.energy.2014.03.058>.

Hronec, M. and K. Fulajtarová. 2012. "Selective transformation of furfural to cyclopentanone." *Catalysis Communications* 5(4):100-104.

Huber, M.L. and H.J.M. Hanley. 1996. *The Corresponding-States Principle: Dense Fluids. In Transport Properties of Fluids: Their Correlation, Prediction and Estimation*. J Millat, JH Dymond, and DA Nieto de Castro, Eds. Cambridge University Press, New York, pp. 283–295.

Humbird, D., R. Davis, L. Tao, C. Kinchin, D. Hsu, A. Aden, P. Schoen, J. Lukas, B. Olthof, M. Worley, D. Sexton, and D. Dudgeon. 2011. *Process Design and Economics for Biochemical Conversion of Lignocellulosic Biomass to Ethanol: Dilute-Acid Pretreatment and Enzymatic Hydrolysis of Corn Stover*. NREL/TP-5100-47764. National Renewable Energy Laboratory, Golden, Colorado.

Huo, X., N.A. Huq, J. Stunkel, N.S. Cleveland, A.K. Starace, A.E. Settle, A.M. York, R.S. Nelson, D.G. Brandner, L. Fouts, P.C. St. John, E.D. Christensen, J. Luecke, J.H. Mack, C.S. McEnally, P.A. Cherry, L.D. Pfefferle, T.J. Strathmann, D. Salvachúa, S. Kim, R.L. McCormick, G.T. Beckham, and D.R. Vardon. 2019. "Tailoring diesel bioblendstock from integrated catalytic upgrading of carboxylic acids: a "fuel property first" approach." *Green Chemistry* 21.21:5813–5827.

Huq, N.A., X. Huo, G.R. Hafenstine, S.M. Tiffit, J. Stunkel, E.D. Christensen, G.M. Fioroni, L. Fouts, R.L. McCormick, P.A. Cherry, C.S. McEnally, L.D. Pfefferle, M.R. Wiatrowski, P. T. Benavides, M.J. Bidy, R.M. Conatser, M.D. Kass, T.L. Alleman, P.C. St. John, S. Kim, and D.R. Vardon. 2019. "Performance-advantaged ether diesel bioblendstock production by a priori design." *Proceedings of the National Academy of Sciences* 116.52:26421-26430.

Jarvis, J.M., K.O. Albrecht, J.M. Billing, A.J. Schmidt, R.T. Hallen, T.M. Schaub. 2018. *Energy Fuels* 32:8483-8493. <http://dx.doi.org/10.1021/acs.energyfuels.8b01445>

Jeon, B.S., B.-C. Kim, Y. Um, and B.-I. Sang. 2010. *Appl. Microbiol. Biotechnol.* 88:1161-1167. <https://doi.org/10.1007/s00253-010-2827-5>

Jenkins, R.W., C.M. Moore, T.A. Semelsberger, C.J. Chuck, J.C. Gordon, and A.D. Sutton. 2016. "The Effect of Functional Groups in Bio-Derived Fuel Candidates." *ChemSusChem*, 9:922.

- Jenkinson, S.F. and G.W.J. Fleet. 2011. Oxetanes from the ring contraction of alpha-triflates of gamma-lactones: oxetane nucleosides and oxetane amino acids. *Chimia (Aarau)*, 65(1-2):71-75.
- Jia, P., X. Lan, X. Li, and T. Wang. 2019. "Highly selective hydrogenation of furfural to cyclopentanone over a NiFe bimetallic catalyst in a methanol/water solution with a solvent effect." *ACS Sustain. Chem. Eng.* 7(18):15221-9.
- Jindal, M.K. and M.K. Jha. 2016. "Hydrothermal liquefaction of wood: A critical review." *Reviews in Chemical Engineering* 32(4):459-488. <https://doi.org/10.1515/revce-2015-0055>
- Joback, K.G. and R.C. Reid. 1987. "Estimation of pure-component properties from group-contributions." *Chem. Eng. Comm.* 57:233-243.
- Jones, S., Y. Zhu, F. Anderson, R. Hallen, D. Elliott, A. Schmidt, K. Albrecht, T. Hart, M. Butcher, C. Drennan, L. Snowden-Swan, R. Davis, and C. Kinchin. 2014. *Process Design and Economics for the Conversion of Algal Biomass to Hydrogens: Whole Algae Hydrothermal Liquefaction and Upgrading*. PNNL-23227, Pacific Northwest National Laboratory, Richland, Washington. [https://www.pnnl.gov/main/publications/external/technical\\_reports/PNNL-23227.pdf](https://www.pnnl.gov/main/publications/external/technical_reports/PNNL-23227.pdf)
- Ju, C., M. Wang, Y. Huang, Y. Fang, and T. Tan. 2018. "High-Quality Jet Fuel Blend Production by Oxygen-Containing Terpenoids Hydroprocessing." *ACS Sustain. Chem. Eng.* 6 (4):4871-4879.
- Kass, M.D., T.J. Theiss, C.J. Janke, S.J. Pawel, and S.A. Lewis. 2011. *Intermediate Ethanol Blends Infrastructure Materials Compatibility Study: Elastomers, Metals, and Sealants*. ORNL/TM-2010/88, Oak Ridge National Laboratory, Oak Ridge, Tennessee.
- Kass, M. 2018. "Corrosion Potential for Selected Bioblendstock Fuel Candidates for Boosted Spark-Ignition Engines." ORNL/TM-2018/1023, Oak Ridge National Laboratory, Oak Ridge, Tennessee.
- Kass, M., C. Janke, R.M. Connatser, S. Lewis, J. Baustian, L. Wolf, and W. Koch. 2020. "Performance of Vehicle Fuel System Elastomers and Plastics with Test Fuels Representing Gasoline Blended with 10% Ethanol (E10) and 16% Isobutanol (iBu16)." *SAE Int. J. Fuels Lubr.* 13(2):137-150.
- Kim, D., J. Martz, and A. Violi. 2016. "Effects of fuel physical properties on direct injection spray and ignition behavior." *Fuel* 180:481-496.
- Kim, E.-M., J.-H. Eom, Y. Um, Y. Kim, and H.M. Woo. 2015. "Microbial Synthesis of Myrcene by Metabolically Engineered *Escherichia coli*." *Journal of Agricultural and Food Chemistry* 63 (18):4606-4612.
- Kim, S. and R. Gonzalez. 2018. "Selective production of decanoic acid from iterative reversal of b-oxidation pathway." *Biotechnol. and Bioeng.* 115(5):1311-1320. <https://doi.org/10.1002/bit.26540>

- Klopfenstein, W.E. 1985. "Effect of Molecular-Weights of Fatty-Acid Esters on Cetane Numbers as Diesel Fuels." *J. Am. Oil Chem.Soc.* 62(6):1029-31.
- Knothe, G., A.C. Matheaus, and T.W. Ryan. 2003. "Cetane numbers of branched and straight-chain fatty esters determined in an ignition quality tester." *Fuel* 82(8):971-975. doi 10.1016/S0016-2361(02)00382-4
- Knothe, G. and R.O. Dunn, 2009. "A Comprehensive Evaluation of the Melting Points of Fatty Acids and Esters Determined by Differential Scanning Calorimetry." *J. Am. Oil Chem. Soc.* 86(9):843-56.10.1007/s11746-009-1423-2.
- Knothe, G. 2014. "Cuphea Oil as a Potential Biodiesel Feedstock to Improve Fuel Properties." *J. Energy Eng.* 140(3). [https://doi.org/10.1061/\(ASCE\)EY.1943-7897.0000194](https://doi.org/10.1061/(ASCE)EY.1943-7897.0000194)
- Knowlton, J.W. and F.D. Rossini. 1949. "Heats of combustion and formation of cyclopropane." *J. Res. Nat. Bur. Stand.* 43:113–115. doi:10.6028/jres.043.013.
- Kostik, V., S. Memeti, and B. Bauer. 2013. *Fatty acid composition of edible oils and fats. J. Hyg. Eng.* 4:112-116.
- Kruger, J.S., E.D. Christensen, T. Dong, S. Van Wychen, G.M. Fioroni, P.T. Pienkos, and R.L. McCormick. 2017. "Bleaching and Hydroprocessing of Algal Biomass-Derived Lipids to Produce Renewable Diesel Fuel." *Energy Fuels* 31(10):10946-19953. <http://dx.doi.org/10.1021/acs.energyfuels.7b01867>
- Kubic, W.L., R.W. Jenkins, C.M. Moore, T.A. Semelsberger, and A.D. Sutton. 2017. "Artificial Neural Network Based Group Contribution Method for Estimating Cetane and Octane Numbers of Hydrocarbons and Oxygenated Organic Compounds." *Ind. Eng. Chem. Res.* 56(42):12236-12245.
- Kuramshin, E.M., L.G. Kulak, M.N. Nazarov, S.S. Zlotsky, and D.L. Rakhmankulov. 1989. "Oxidation of Cyclic Acetals as a Preparative Method of Diol Monoester Production." *J. prakt. Chem.* 331:591-599.
- Kursanov, D.N., V.N. Setkina, and V.M. Rodionov. 1950. "n-Butyl n-octyl formal, *Akad. Nauk SSSR, Inst. Org. Khim. Sintezy Org. Soedinenii Sbornik* 15-16.
- Kurtz, E. and C.J. Polonowski. 2017. *SAE Int. J. Fuels Lubr.* 10(3):664-671. <https://doi.org/10.4271/2017-01-9378>.
- Lappas, A. and E. Heracleous. 2011. "Production of biofuels via Fischer-Tropsch synthesis: biomass-to-liquids." in *Handbook of Biofuels Production*, ed. R. Luque, J. Campelo, and J. Clark. Woodhead Publishing Ltd, Cambridge.
- Liaw, H., Y. Lee, C. Tang, H. Hsu, and Y. Liu. 2002. "A mathematical model for predicting the flash point of binary solutions." *J. Loss Prev. Process Ind.* 15:429–438.

Lance, M., T. Toops, R. Ancimer, H. An, J. Li, A. Williams, P. Sindler, A. Ragatz, and R.L. McCormick. 2016. "Evaluation of Fuel-Borne Sodium Effects on DOC-DPF-SCR Heavy-Duty Engine Emission Control System: Simulation of Full-Useful Life." *SAE Int. J. Fuels Lubr.* 9(3). doi:10.4271/2016-01-2322.

Lange, P., R. Price, P.M. Ayoub, J. Louis, L. Petrus, L. Clarke, and H. Gosselink. 2010. "Valeric Biofuels: A platform of Cellulosic Transportation Fuels." *Angew. Chem. Int. Ed.* 49(2010):4479-4483.

Langlois, A. and O. Lebel. 2010. "To cyclopropanate or not to cyclopropanate? A look at the effect of cyclopropanation on the performance of biofuels." *Energy Fuels* 24:5257–5263. doi:10.1021/ef100884b.

Lanjekar, R.D. and D. Deshmukh. 2016. "A review of the effect of the composition of biodiesel on NOx emission, oxidative stability and cold flow properties." *Renew. Sust. Energ. Rev.* 54:1401-1411. <https://doi.org/10.1016/j.rser.2015.10.034>.

Lautenschütz, L., D. Oestreich, P. Seidenspinner, U. Arnold, E. Dinjus, and J. Sauer. 2016. "Physico-Chemical Properties and Fuel Characteristics of Oxymethylene Dialkyl Ethers." *Fuel* 173:129–137. <https://doi.org/10.1016/j.fuel.2016.01.060>.

Lee, J.-M., P.P. Upare, J.-S. Chang, Y.K. Hwange, J.H. Lee, D.W. Hwang, D.-Y. Hong, S.H. Lee, M.-G. Jeong, Y.D. Kim, and Y.-U. Kwon. 2014. "Direct Hydrogenation of Biomass-Derived Butyric Acid to n-Butanol over a Ruthenium–Tin Bimetallic Catalyst." *ChemSusChem* 7.11:2998-3001.

Lee, U., J. Han, M. Wang. 2017. "Evaluation of landfill gas emissions from municipal solid waste landfills for the life-cycle analysis of waste-to-energy pathways." *J. Cleaner Production* 166:335–342. <https://doi.org/10.1016/j.jclepro.2017.08.016>.

Li, B., Y. Li, H. Liu, F. Liu, Z. Wang, and J. Wang. 2017. "Combustion and Emission Characteristics of Diesel Engine Fueled with Biodiesel/PODE Blends." *Appl. Energy* 206:425–431. <https://doi.org/10.1016/j.apenergy.2017.08.206>.

Liaw, H., Y. Lee, C. Tang, H. Hsu, and Y. Liu. 2002. "A mathematical model for predicting the flash point of binary solutions." *J. Loss Prev. Process Ind.* 15:429–438.

Lilga, M.A., R.T. Hallen, K.O. Albrecht, A.R. Cooper, J.G. Frye, and K.K. Ramasamy. 2017a. *Systems and processes for conversion of ethylene feedstocks to hydrocarbon fuels*. U.S. Patent 9,663,416.

Lilga, M.A., R.T. Hallen, K.O. Albrecht, A.R. Cooper, J.G. Frye, and K.K. Ramasamy. 2017b. *Systems and processes for conversion of ethylene feedstocks to hydrocarbon fuels*. U.S. Patent 9,771,533.

Lilga, M.A., R.T. Hallen, K.O. Albrecht, A.R. Cooper, J.G. Frye, and K.K. Ramasamy. 2018a. *Systems and processes for conversion of ethylene feedstocks to hydrocarbon fuels*. U.S. Patent 10,005,974.

- Lilga, M.A., R.T. Hallen, K.O. Albrecht, A.R. Cooper, J.G. Frye, and K.K. Ramasamy. 2018b. *Systems and processes for conversion of ethylene feedstocks to hydrocarbon fuels*. U.S. Patent 9932531.
- Liu, H., T. Jiang, B. Han, S. Liang, and Y. Zhou. 2009. "Selective phenol hydrogenation to cyclohexanone over a dual supported Pd-Lewis acid catalyst." *Science* 306:1250–1252.
- Liu, Y., F. Lu, L. Shao, and P. He. 2016. "Alcohol-to-acid ratio and substrate concentration affect product structure in chain elongation reactions initiated by unacclimatized inoculum." *Bioresour. Technol.* 218:1140-1150. <https://doi.org/10.1016/J.BIORTECH.2016.07.067>
- Liu, H., Z. Wang, J. Zhang, J. Wang, and S. Shuai. 2017. "Study on Combustion and Emission Characteristics of Polyoxymethylene Dimethyl Ethers/Diesel Blends in Light-Duty and Heavy-Duty Diesel Engines." *Appl. Energy* 185:1393–1402. <https://doi.org/10.1016/j.apenergy.2015.10.183>.
- Liu, F., R. Wei and T. Wang. 2018. "Identification of the Rate-Determining Step for the Synthesis of Polyoxymethylene Dimethyl Ethers from Paraformaldehyde and Dimethoxymethane." *Fuel Process. Technol.* 180:114-121. <https://doi.org/10.1016/j.fuproc.2018.08.005>.
- Liu, F., P. Lane, J.C. Hewson, V. Stavila, M.B. Tran-Gyamfi, M. Hamel, T.W. Lane, and R.W. Davis, 2019. "Development of a closed-loop process for fusel alcohols production and nutrient recycling from microalgae biomass." *Bioresour. Technol.* 283:350-357.
- Magnotti, G. and S. Som. 2019. "Assessing Fuel Property Effects on Cavitation and Erosion Propensity Using a Computational Fuel Screening Tool." *Proceedings of the ASME 2019 Internal Combustion Engine Division Fall Technical Conference. ASME 2019 Internal Combustion Engine Division Fall Technical Conference*. Chicago, Illinois, USA. October 20–23, 2019. V001T06A011.
- Mahbub, N., A.O. Oyedun, A. Kumar, D. Oestreich, U. Arnold, and J. Sauer. 2017. "A Life Cycle Assessment of Oxymethylene Ether Synthesis from Biomass-Derived Syngas as a Diesel Additive." *J. Clean. Prod.* 165:1249–1262. <https://doi.org/10.1016/j.jclepro.2017.07.178>.
- Marrero, J. and R. Gani. 2001. "Group-contribution based estimation of pure component properties." *J. Fluid Phase Equilib.* 183:183-208.
- Marrone, P.A., D.C. Elliott, J.M. Billing, R.T. Hallen, T.R. Hart, P. Kadota, and J.C. Moeller, In *Proceedings of the Water Environment Federation*, (WEFTEC 2017), September 30-October 4, 2017, Chicago, Illinois.
- Marrone, P.A., D.C. Elliott, J.M. Billing, R.T. Hallen, T.R. Hart, P. Kadota, J.C. Moeller, M.A. Randel, and A.J. Schmidt. 2018. "Bench-Scale Evaluation of Hydrothermal Processing Technology for Conversion of Wastewater Solids to Fuels." *Water Environment Research* 90(4):329-342. doi:10.2175/106143017X15131012152861.

McCormick, R.L. and T.L. Alleman. 2016. *Renewable Diesel Fuel*. National Renewable Energy Laboratory, Golden, Colorado.

[https://cleancities.energy.gov/files/u/news\\_events/document/document\\_url/182/McCormick\\_Alleman\\_RD\\_Overview\\_2016\\_07\\_18.pdf](https://cleancities.energy.gov/files/u/news_events/document/document_url/182/McCormick_Alleman_RD_Overview_2016_07_18.pdf).

McCormick, R.L., G. Fioroni, L. Fouts, E. Christensen, J. Yanowitz, E. Polikarpov, K. Albrecht, D.J. Gaspar, J. Gladden, A. George. 2017. "Selection Criteria and Screening of Potential Biomass-Derived Streams as Fuel Blendstocks for Advanced Spark-Ignition Engines." *SAE Int. J. Fuels Lubr.* 10(2):442-460. <https://doi.org/10.4271/2017-01-0868>.

McEnally, C.S. and L.D. Pfefferle. 2007. "Improved sooting tendency measurements for aromatic hydrocarbons and their implications for naphthalene formation pathways." *Combust. Flame* 148 (4):210-222.

McEnally, C.S. and L.D. Pfefferle. 2011. "Sooting Tendencies of Oxygenated Hydrocarbons in Laboratory-Scale Flames." *Environ. Sci. Technol.* 45(6):2498–2503. <https://doi.org/10.1021/es103733q>.

McEnally, C.S., D.D. Das, and L.D. Pfefferle. 2017. *Yield Sooting Index Database Volume 2: Sooting Tendencies of a Wide Range of Fuel Compounds on a Unified Scale*. Harvard Dataverse, Cambridge, Massachusetts.

Meadows, A.L., K.M. Hawkins, Y. Tsegaye, E. Antipov, Y. Kim, L. Raetz, R.H. Dahl, A. Tai, T. Mahatdejkul-Meadows, L. Xu, L. Zhao, M.S. Dasika, A. Murarka, J. Lenihan, D. Eng, J.S. Leng, C.-L. Liu, J.W. Wenger, H. Jiang, L. Chao, P. Westfall, J. Lai, S. Ganesan, P. Jackson, R. Mans, D. Platt, C.D. Reeves, P.R. Saija, G. Wichmann, V.F. Holmes, K.R. Benjamin, P. Hill, T.S. Gardner, and A.E. Tsong. 2016. "Rewriting yeast central carbon metabolism for industrial isoprenoid production." *Nature* 537:694–697. doi:10.1038/nature19769.

Moat, A.G., F.W. Foster, and M.P. Spector. 2002. "Chapter 11: Fermentation Pathways." *Microbial Physiology*. Wiley-Liss, Inc. ISBN: 0-471-39483-1.

Moore, C.M., O. Staples, R.W. Jenkins, T.J. Brooks, T.A. Semelsberger, and A.D. Sutton. 2017. "Acetaldehyde as an ethanol derived bio-building block: an alternative to Guerbet chemistry." *Green Chemistry* 19:169-174.

Monroe, E., S. Shinde, J.S. Carlson, T.P. Eckles, F. Liu, A.M. Varman, A. George, and R.W. Davis. 2020. "Superior performance biodiesel from biomass-derived fusel alcohols and low grade oils: Fatty acid fusel esters (FAFE)." *Fuel* 268:117408. <https://doi.org/10.1016/j.fuel.2020.117408>.

Morandin, M. and S. Harvey. 2015. *Methanol via Biomass Gasification Thermodynamic Performances and Process Integration Aspects in Swedish Chemical Cluster and Pulp and Paper Sites*. Göteborg, Sweden, 2015. <https://doi.org/10.13140/RG.2.1.4272.1443>.

Mueller, C.J., W.J. Cannella, T.J. Bruno, B. Bunting, H.D. Dettman, J.A. Franz, M.L. Huber, M. Natarajan, W.J. Pitz, M.A. Ratcliff, and K. Wright. 2012. "Methodology for Formulating Diesel

Surrogate Fuels with Accurate Compositional, Ignition-Quality, and Volatility Characteristics.” *Energy Fuels* 26:3284.

Mueller, C.J., C.W. Nilsen, D.J. Ruth, R.K. Gehmlich, L.M. Pickett, and S.A. Skeen. 2017. "Ducted Fuel Injection: A New Approach for Lowering Soot Emissions from Direct-Injection Engines." *Applied Energy* 204:206-220. doi:10.1016/j.apenergy.2017.07.001.

Mueller, C.J., C.W. Nilsen, and D.E. Biles. 2020. "Effects of Fuel Oxygenation and Ducted Fuel Injection on the Performance of a Mixing-Controlled Compression-Ignition Optical Engine Equipped with a Two-Orifice Fuel Injector," Society of Automotive Engineers World Congress Experience 2020, Combustion in Compression-Ignition Engines (PFL220), April 21, 2020.

Müller-Langer, F., S. Majer, and S. O’Keeffe. 2014. “Benchmarking biofuels—A comparison of technical, economic, and environmental indicators.” *Energy, Sustainability, and Society* 4(20). <https://doi.org/10.1186/s13705-014-0020-x>

Murphy, M.J. 1999. *Safety and industrial hygiene issues related to the use of oxygenates in diesel fuel*. SAE Technical Paper 1999-01-1473.

Murphy, M. 2002. "Oxygenate Compatibility with Diesel Fuels," SAE Technical Paper 2002-01-2848. <https://doi.org/10.4271/2002-01-2848>.

Natarajan, K., S. Leduc, P. Pelkonen, E. Tomppo, and E. Dotzauer. 2014. "Optimal locations for second generation Fischer Tropsch biodiesel production in Finland.” *Renewable Energy*. 62:319-330. doi:10.1016/j.renene.2013.07.013.

Nelson, R.S., D.J. Peterson, E.M. Karp, and G.T. Beckham. 2017. "Mixed carboxylic acid production by *Megasphaera elsdenii* from glucose and lignocellulosic hydrolysate." *Fermentation* 3:10. doi: 10.3390/fermentation3010010.

Neste. 2020. *Neste Renewable Diesel Handbook*. [https://www.neste.com/sites/default/files/attachments/neste\\_renewable\\_diesel\\_handbook.pdf](https://www.neste.com/sites/default/files/attachments/neste_renewable_diesel_handbook.pdf). Accessed 11/23/2020.

Nilsen, C.W., D.E. Biles, and C.J. Mueller. 2019. "Using Ducted Fuel Injection to Attenuate Soot Formation in a Mixing-Controlled Compression Ignition Engine," *SAE Int. J. Engines* 12(3):309-322. doi:10.4271/03-12-03-0021.

Nilsen, C.W., D.E. Biles, B.F. Yraguen, and C.J. Mueller. 2020. "Ducted Fuel Injection Versus Conventional Diesel Combustion: An Operating-Parameter Sensitivity Study Conducted in an Optical Engine with a Four-Orifice Fuel Injector," *SAE Int. J. Engines* 13(3):345-62. doi:10.4271/03-13-03-0023.

Noor, E., E. Eden, R. Milo, and U. Alon. 2010. “Central carbon metabolism as a minimal biochemical walk between precursors for biomass and energy.” *Molecular Cell* 39(5):809-820.

Noweck, K. and W. Grafahrend. 2000. “Fatty Alcohols.” Wiley-VCH Verlag GmbH & Co. KGaA, editor. *Ullmann’s Encyclopedia of Industrial Chemistry*. Weinheim, Germany.

National Renewable Energy Laboratory (NREL). 2017. *NREL YSI Prediction Tool* website. National Renewable Energy Laboratory, Golden, Colorado. <https://ysi.ml.nrel.gov/> (undated website).

National Renewable Energy Laboratory (NREL). 2020. *Co-Optimization of Fuels & Engines: Fuel Property Database*. National Renewable Energy Laboratory, Golden, Colorado. Accessed October 2020 at <https://fuelsdb.nrel.gov/fmi/webd/FuelEngineCoOptimization>.

Ou, L., H. Cai, H.J. Seong, D.E. Longman, J.B. Dunn, J.M.E. Storey, T.J. Toops, J.A. Pihl, M.J. Biddu, and M. Thornton. 2019. "Co-Optimization of Heavy-Duty Fuels and Engines: Cost Benefit Analysis and Implications." *Environ. Sci. Technol.* 53(21):12904-12913. doi:10.1021/acs.est.9b03690.

Ouda, M., G. Yarce, R.J. White, M. Hadrich, D. Himmel, A. Schaadt, H. Klein, E. Jacob, and I. Krossing. 2017. "Poly(Oxymethylene) Dimethyl Ether Synthesis-A Combined Chemical Equilibrium Investigation towards an Increasingly Efficient and Potentially Sustainable Synthetic Route." *React. Chem. Eng.* 2 (1):50–59. <https://doi.org/10.1039/c6re00145a>.

Oyedun, A.O., A. Kumar, D. Oestreich, U. Arnold, and J. Sauer. 2018. "The Development of the Production Cost of Oxymethylene Ethers as Diesel Additives from Biomass." *Biofuels, Bioprod. Biorefining* 12 (4):694–710. <https://doi.org/10.1002/bbb.1887>.

Paap, S.M., T.H. West, D.K. Manley, E.J. Steen, H.R. Beller, J.D. Keasling, D.C. Dibble, S. Change, and B.A. Simmons. 2013. "Biochemical production of ethanol and fatty acid ethyl esters from switchgrass: A comparative analysis of environmental and economic performance." *Biomass and Bioenergy* 49:49-62.

Page, E.H., D. Ceballos, A. Oza, W. Gong, and C.A. Mueller. 2015. *Evaluation of occupational exposures at drycleaning shops using SolvonK4 and DF-2000*. National Institute for Occupational Safety and Health HETA 2012-0084-3227.

Palczewska-Tulińska, M. and A.M. Szafranski. 2000. "Selected physicochemical properties of dibutoxymethane." *Journal of Chemical & Engineering Data* 45:988-990.

Pei, Y., R. Torelli, T. Tzanetakis, Y. Zhang, M. Traver, D.J. Cleary, and S. Som. 2017. "Modeling the Fuel Spray of a High Reactivity Gasoline Under Heavy-Duty Diesel Engine Conditions." *Proceedings of the ASME 2017 Internal Combustion Engine Division Fall Technical Conference. Volume 2: Emissions Control Systems; Instrumentation, Controls, and Hybrids; Numerical Simulation; Engine Design and Mechanical Development*. Seattle, Washington, USA. October 15–18, 2017. V002T06A002.

Pell, A.S. and G. Pilcher. 1965. "Measurements of heats of combustion by flame calorimetry. Part 3. Ethylene oxide, trimethylene oxide, tetrahydrofuran and tetrahydropy." *Trans. Faraday Soc.* 61(0):71-77.

PEP Yearbook: Biodiesel. 2014b.

PEP Yearbook: Lactic Acid. 2014a.

PEP Yearbook: Cyclohexane. 2020.

Peralta-Yahya, P.P., M. Ouellet, R. Chan, A. Mukhopadhyay, J.D. Keasling, and T.S. Lee. 2011. "Identification and microbial production of a terpene-based advanced biofuel." *Nature Comm.* 2(1):483.

Phillips, J.R., H.K. Atiyeh, R.S. Tanner, J.R. Torres, J. Saxena, M.R. Wilkins, and R.L. Huhnke. 2015. "Butanol and hexanol production in *Clostridium carboxidivorans* syngas fermentation: Medium development and culture techniques." *Bioresour. Technol.* 190:114-121. <https://doi.org/10.1016/j.biortech.2015.04.043>

Poling, E., J.M. Prausnitz, and J.P. O'Connell. 2001. *The Properties of Gases and Liquids*, 5th ed. McGraw-Hill, New York.

Raj, A., M.J. Al Rashidi, S.H. Chung, and S.M. Sarathy. 2014. "PAH Growth Initiated by Propargyl Addition: Mechanism Development and Computational Kinetics." *J. Phys. Chem. A* 118 (16):2865-2885.

Ramasamy, K.K., M. Gray, and H. Job. 2016. "Tunable catalytic properties of bi-functional mixed oxides in ethanol conversion to high value compounds." *Catal. Today* 269:82-87. <https://doi.org/10.1016/j.cattod.2015.11.045>

Ramasamy, K.K., M.F. Guo, M.J. Gray, and S. Subramanian. 2018. "Method of Converting Ethanol to Higher Alcohols." U.S. Patent Application 20190031585 16/046395.

Richter, H. and J.B. Howard. 2000. "Formation of polycyclic aromatic hydrocarbons and their growth to soot—a review of chemical reaction pathways." *Progress in Energy and Combustion Science* 26 (4–6):565-608.

Ruijun, Z., W. Xibin, M. Haiyan, H. Zuohua, G. Jing, and J. Deming. 2009. "Performance and Emission Characteristics of Diesel Engines Fueled with Diesel-Dimethoxymethane (DMM) Blends." *Energy Fuels* 23 (1):286–293. <https://doi.org/10.1021/ef8005228>.

Saboe, P.O., L.P. Manker, W.E. Michener, D.J. Peterson, D.G. Brandner, S.P. Deutch, M. Kumar, R.M. Cywar, G.T. Beckham, E.M. Karp. 2018. "In situ recovery of bio-based carboxylic acids." *Green Chem* 20:1791–1804. <https://doi.org/10.1039/C7GC03747C>.

San-Valero, P., A. Fernandez-Naveira, M.C. Veiga, and C. Kennes. 2019. *J. Environ. Manage.* 242 (2019):515-521. <https://doi.org/10.1016/j.jenvman.2019.04.093>

Sappok, A., M. Santiago, T. Vianna, and V.W. Wong. 2009. *Characteristics and Effects of Ash Accumulation on Diesel Particulate Filter Performance: Rapidly Aged and Field Aged Results*. SAE Technical Paper. doi:10.4271/2009-01-1086.

Sappok, A. and V.W. Wong. 2010. "Ash Effects on Diesel Particulate Filter Pressure Drop Sensitivity to Soot and Implications for Regeneration Frequency and DPF Control." *SAE Int. J. Fuels Lubr.* 3(1):380-396. doi:10.4271/2010-01-0811.

- Schildhauer, T.J., I. Hoek, F. Kapteijn, and J.A. Moulijn. 2009. "Zeolite BEA catalyzed esterification of hexanoic acid with 1-octanol: Kinetics, side reactions and the role of water." 358:141-145. doi: 10.1016/j.apcata.2009.02.004.
- Schulte, B., C.A. Dannenberg, H. Keul, and M. Möller. 2013. "Formation of linear and cyclic polyoxetanes in the cationic ring-opening polymerization of 3-allyloxymethyl-3-ethyloxetane and subsequent postpolymerization modification of poly(3-allyloxymethyl-3-ethyloxetane)." *J. Polymer Sci. A: Polymer Chem.* 51 (5):1243-1254.
- Schutyser, W., T. Renders, S. Van den Bosch, S.-F. Koelewijn, G.T. Beckham, and B.F. Sels. 2018. "Chemicals from lignin: an interplay of lignocellulose fractionation, depolymerisation, and upgrading." *Chem. Soc. Rev.* 47(3):852-908.
- Seiple, T.E., A.M. Coleman, and R.L. Skaggs. 2017. "Municipal wastewater sludge as a sustainable bioresource in the United States." *J. Environ. Manage.* 197:673-680.
- Serdari, A., E. Lois, and S. Stournas. 1999. "Impact of Esters of Mono- and Dicarboxylic Acids on Diesel Fuel Quality." *Ind. Eng. Chem. Res.* 38:3543.
- Shahabuddin, M., M.T. Alam, B.B. Krishna, T. Bhaskar, and G. Perkins. 2020. "A review on the production of renewable aviation fuels from the gasification of biomass and residual wastes." *Bioresour. Technol.* 312:123596. [10.1016/j.biortech.2020.123596](https://doi.org/10.1016/j.biortech.2020.123596).
- Sharma, Y.C. Sharma, M. Yadav, and S.N. Upadhyay. 2019. "Latest advances in degumming feedstock oils for large-scale biodiesel production." *Biofuels, Bioprod. Bioref.* 13:174-191.
- Shen, T., R. Hu, C. Zhu, M. Li, W. Zhuang, C. Tang, and H. Ying. 2018. "Production of cyclopentanone from furfural over Ru/C with Al 11.6 PO 23.7 and application in the synthesis of diesel range alkanes." *RSC Advances* 8(66):37993-8001.
- Shibutani, R. and H. Tsutsumi. 2012. "Fire-retardant solid polymer electrolyte films prepared from oxetane derivative with dimethyl phosphate ester group." *J. Power Sources* 202:369-373.
- Singh, N., C.J. Rutland, D.E. Foster, K. Narayanaswamy, and Y. He. 2009. *Investigation into Different DPF Regeneration Strategies Based on Fuel Economy Using Integrated System Simulation*. SAE Technical Paper. doi:10.4271/2009-01-1275.
- Slami, T., J. Ahlqvist, A. Bernas, J. Wärna, P. Mäki-Arvela, C. Still, J. Lehtonen, and D.Y. Murzin. 2009. "Hydroformylation of 1-butene on Rh Catalyst." *Ind. Eng. Chem. Res.* Vol 48:1325-1331.
- Smagala, T.G., E.D. Christensen, K.M. Christison, R.E. Mohler, E. Gjersing, and R.L. McCormick. 2013. "Hydrocarbon Renewable and Synthetic Diesel Fuel Blendstocks: Composition and Properties." *Energy Fuels* 27:237-246. doi.org/10.1021/efef3012849.

Snowden-Swan, L.J., R.T. Hallen, Y. Zhu, T.R. Hart, M.D. Bearden, J. Liu, T.E. Seiple, K.O. Albrecht, S.B. Jones, S.P. Fox, A.J. Schmidt, G.D. Maupin, J.M. Billing and D.C. Elliott. 2017. *Conceptual Biorefinery Design and Research Targeted for 2022: Hydrothermal Liquefaction Processing of Wet Waste to Fuels*. PNNL-27186. Pacific Northwest National Laboratory, Richland, Washington. <http://dx.doi.org/10.2172/1415710>

Snowden-Swan, L.J., J.M. Billing, M.R. Thorson, A.J. Schmidt, D.M. Santosa, S.B. Jones, and R.T. Hallen. 2020. *Wet Waste Hydrothermal Liquefaction and Biocrude Upgrading to Hydrocarbon Fuels: 2019 State of Technology*. PNNL-29882. Richland, WA: Pacific Northwest National Laboratory.

Som, S., D.E. Longman, A.I. Ramírez, and S.K. Aggarwal. 2010. "A comparison of injector flow and spray characteristics of biodiesel with petrodiesel." *Fuel* 89/12:4014-4024.

Soriano, J.A., R. García-Contreras, D. Leiva-Candia, and F. Soto. 2018. "Influence on Performance and Emissions of an Automotive Diesel Engine Fueled with Biodiesel and Paraffinic Fuels: GTL and Biojet Fuel Farnesane." *Energy Fuels*. 32:5125–5133. doi:10.1021/acs.energyfuels.7b03779.

Spalding, M.A. and A. Chatterjee. 2017. *Handbook of Industrial Polyethylene and Technology: Definitive Guide to Manufacturing, Properties, Processing, Applications and Markets Set*. John Wiley & Sons, Hoboken, New Jersey.

Starck, L., L. Pidol, N. Jeuland, T. Chapus, P. Bogers, and J. Bauldreay. 2016. "Production of Hydroprocessed Esters and Fatty Acids (HEFA) – Optimization of Process Yield." *Oil Gas Sci. Technol. – Rev. IFP Energies nouvelles* 71(1). <https://doi.org/10.2516/ogst/2014007>

St. John, P.C., P. Kairys, D.D. Das, C.S. McEnally, L.D. Pfefferle, D.J. Robichaud, M.R. Nimlos, B.T. Zigler, R.L. McCormick, T.D. Foust, Y.J. Bomble, and S. Kim. 2017. "A quantitative model for the prediction of sooting tendency from molecular structure." *Energy Fuels* 31:9983-9990.

Staples, O., C.M. Moore, J.H. Leal, T.A. Semelsberger, C.S. McEnally, L.D. Pfefferle, and A.D. Sutton. 2018. "A simple, solvent free method for transforming bio-derived aldehydes into cyclic acetals for renewable diesel fuels." *Sustain. Energy Fuels* 2 (12):2742-2746.

Staples, O., J.H. Leal, P.A. Cherry, C.S. McEnally, L.D. Pfefferle, T.A. Semelsberger, A.D. Sutton, and C.M. Moore. 2019. "Camphorane as a Renewable Diesel Blendstock Produced by Cyclodimerization of Myrcene." *Energy Fuels* 33 (10):9949-9955.

Subramaniam, S., M.F. Guo, T. Bathena, M. Gray, X. Zhang, A. Martinez, L. Kovarik, K.A. Goulas, and K.K. Ramasamy. 2020. "Direct Catalytic Conversion of Ethanol to C5+ Ketones: Role of Pd-Zn Alloy on Catalytic Activity and Stability." *Angew. Chem. Int. Ed. Engl.* 59(34). <https://doi.org/10.1002/anie.202005256>.

Svensson, K.I. and G.C. Martin. 2019. *Ducted Fuel Injection: Effects of Stand-Off Distance and Duct Length on Soot Reduction*. SAE Technical Paper. doi:10.4271/2019-01-0545.

Tan, E.C.D., D. Ruddy, C. Nash, D. Dupuis, A. Dutta, D. Hartley, and H. Cai. 2018. *High-Octane Gasoline from Lignocellulosic Biomass via Syngas and Methanol / Dimethyl Ether Intermediates: 2018 State of Technology and Future Research*. NREL/TP-5100-71957. National Renewable Energy Laboratory, Golden, Colorado.

Tan, E.C.D. and L. Tao. 2019. *Economic Analysis of Renewable Fuels for Marine Propulsion*. Golden, CO: National Renewable Energy Laboratory. NREL/TP-5100-74678. National Renewable Energy Laboratory, Golden, Colorado.  
<https://www.nrel.gov/docs/fy19osti/74678.pdf>.

Tanno, S., J. Kawakami, K. Kitano, and T. Hashizume. 2019. *Investigation of a Novel Leaner Fuel Spray Formation for Reducing Soot in Diffusive Diesel Combustion - Homogenizing Equivalence Ratio Distribution in the Lift-Off Region*. SAE Technical Paper. doi:10.4271/2019-01-2273.

Tao, L., A. Milbrandt, Y. Zhang, and W.-H. Wang. 2017. “Techno-economic and resource analysis of hydroprocessed renewable jet fuel.” *Biotechnology for Biofuels* 10:261.  
<https://biotechnologyforbiofuels.biomedcentral.com/articles/10.1186/s13068-017-0945-3>

To, A.T., T.J. Wilke, E. Nelson, C.P. Nash, A. Bartling, E.C. Wegener, K.A. Unocic, S.E. Habas, T.D. Foust, and D.A. Ruddy. 2020. “Dehydrogenative Coupling of Methanol for the Gas-Phase, One-Step Synthesis of Dimethoxymethane over Supported Copper Catalysts.” *ACS Sustain. Chem. Eng.* 8 (32):12151–12160. <https://doi.org/10.1021/acssuschemeng.0c03606>.

Torelli, R., S. Som, Y. Pei, Y. Zhang, and M. Traver. 2017. “Influence of fuel properties and internal nozzle flow development in a multi-hole diesel injector.” *Fuel* 204:171-184.

Trifoi, A.R., P.S. Agachi, and T. Pap. 2016. “Glycerol acetals and ketals as possible diesel additives. A review of their synthesis protocols.” *Renewable and Sustainable Energy Reviews* 62:804-814.

U.S. Department of Energy (DOE). 2017. *Biofuels and Bioproducts from Wet and Gaseous Waste Streams: Challenges and Opportunities*. Bioenergy Technologies Office, Energy Efficiency and Renewable Energy, Washington, D.C.

U.S. Department of Energy (DOE). 2020. *Bioenergy Technologies Office – 2019 State of Technology*. Office of Energy Efficiency and Renewable Energy.  
<https://www.energy.gov/sites/prod/files/2020/07/f76/beto-2019-state-of-technology-july-2020-r1.pdf>

U.S. Environmental Protection Agency. 2019. *Estimation Program Interface Suite™*. Accessed August 2020 at <https://www.epa.gov/tsca-screening-tools/epi-suitetm-estimation-program-interface>.

Unterreiner, B.V., M. Sierka, and R. Ahlrichs. 2004. “Reaction pathways for growth of polycyclic aromatic hydrocarbons under combustion conditions, a DFT study.” *Phys. Chem. Chem. Phys.* 6 (18):4377-4384.

van der Drift, A and H. Boerrigter. 2006. "Synthesis gas from biomass for fuels and chemicals." Technical Report. Energy Research Centre of the Netherlands.

<http://www.ieatask33.org/app/webroot/files/file/publications/syngasFromBiomassvanderDrift.pdf>.

Van Heerden, J., J.J. Botha, and P.N.J. Roets. 1998. *XII International Symposium on Alcohols Fuels*, Vol. A:3188.

Vardon, D.R., M.A. Franden, C.W. Johnson, E.M. Karp, M.T. Guarnieri, J.G. Linger, M.J. Salm, T.J. Strathmann, and G.T. Beckham. 2015. "Adipic acid production from lignin." *Energy Environ. Sci.* 8:617-628.

Venkateswar R., G. Kumar, G. Mohanakrishna, S. Shobana, R.I. Al-Raoush. 2020. "Review on the production of medium and small chain fatty acids through waste valorization and CO<sub>2</sub> fixation." *Bioresour. Technol.* 309:123400. <https://doi.org/10.1016/j.biortech.2020.123400>.

Wang, M., A. Elgowainy, U. Lee, A. Bafana, P. T. Benavides, A. Burnham, H. Cai, Q. Dai, U. Gracida, T. R. Hawkins, P. V. Jaquez, J. C. Kelly, H. Kwon, X. Liu, Z. Lu, L. Ou, P. Sun, O. Winjobi, H. Xu, E. Yoo, G. G. Zaires, and G. Zang. 2020. Greenhouse gases, Regulated Emissions, and Energy use in Technologies Model ®. Computer Software. USDOE Office of Energy Efficiency and Renewable Energy (EERE). Web. <http://doi.org/10.11578/GREET-Excel-2020/dc.20200912.1>.

Weast, R. 1989. *CRC Handbook of Chemistry and Physics*. CRC Press Inc, Boca Raton, Florida.

Whitmore, L.S., R.W. Davis, and R.L. McCormick. 2016. *Energy and Fuels* 30(10). doi: 10.1021/acs.energyfuels.6b01952.

Williams, A., R.L. McCormick, M.J. Lance, C. Xie, T. Toops, and R. Brezny. "Effect of the Acceleration Factor on the Capture and Impact of Fuel-Borne Metal Impurities on Emissions Control Devices." *SAE Int. J. Fuels Lubr.* 7(2):2014. doi:10.4271/2014-01-1500.

Wojcik, B.H. 1948. "Catalytic hydrogenation of furan compounds." *Ind. Eng. Chem.* 40:210-216.

Wright, M.M., R.C. Brown and A.A. Boateng. 2008. "Distributed processing of biomass to bio-oil for subsequent production of Fischer-Tropsch liquids." *Biofuel Bioprod Biorefin.* 2:229-238. doi: 10.1002/bbb.73

Wu, L., T. Moteki, A.A. Gokhale, D.W. Flaherty, and F.D. Toste. 2016. "Production of Fuels and Chemicals from Biomass: Condensation Reactions and Beyond." *Chem* 1:32-58.

Xu, G., J. Guo, Y. Zhang, Y. Fu, J. Chen, L. Ma, and Q. Guo. 2015. "Selective hydrogenation of phenol to cyclohexanone over pd-hap catalyst in aqueous media." *ChemCatChem.* 7(16):2485-92.

Yalkowsky, S.H. and D. Alantary. 2018. "Estimation of melting points of organics." *J. Pharm. Sci.*, 107:1211-1227.

- Yanowitz, J., M.A. Ratcliff, R.L. McCormick, J.D. Taylor, and M.J. Murphy. 2017. *Compendium of experimental cetane numbers*. NREL/TP-5400-61693. National Renewable Energy Laboratory, Golden, Colorado.
- Yin, S., R. Dolan, M. Harris, and Z. Tan. "Subcritical hydrothermal liquefaction of cattle manure to bio-oil: Effects of conversion parameters on bio-oil yield and characterization of bio-oil." *Bioresource Technol.* 101(10):3657-3664. <https://doi.org/10.1016/j.biortech.2009.12.058>
- Yuzawa, S., M. Mirsiaghi, R. Jovic, T. Fujii, F. Masson, V.T. Benites, E.E.K. Baidoo, E. Sundstrom, D. Tanjore, T.R. Pray, A. George, R.W. Davis, J.M. Gladden, B.A. Simmons, L. Katz, and J.D. Keasling. 2018. "Short-chain ketone production by engineered polyketide synthases in *Streptomyces albus*." *Nat. Commun.* 9(1):4569.
- Zhang, Y., P. Kumar, M. Traver, and D. Cleary. 2016. "Conventional and Low Temperature Combustion Using Naphtha Fuels in a Multi-Cylinder Heavy-Duty Diesel Engine," *SAE Int. J. Engines* 9(2):1021-1035.
- Zhang, Y., S. Sommers, Y. Pei, P. Kumar, A. Voice, M. Traver, and D. Cleary. 2017. Mixing-Controlled Combustion of Conventional and Higher Reactivity Gasolines in a Multi-Cylinder Heavy-Duty Compression Ignition Engine." WCX<sup>TM</sup> 17: SAE World Congress Experience. *SAE International*, Warrendale, Pennsylvania.
- Zhu, J.-F., G.-H. Tao, H.-Y. Liu, L. He, Q.-H. Sun, and H.-C. Liu. 2014. "Aqueous-phase selective hydrogenation of phenol to cyclohexanone over soluble Pd nanoparticles." *Green Chem.* 16:2664–2669.
- Xu, D., G. Lin, L. Liu, Y. Wang, Z. Jing, and S. Wang. 2018. "Comprehensive evaluation on product characteristics of fast hydrothermal liquefaction of sewage sludge at different temperatures." *Energy* 159(2018):686-695. <https://doi.org/10.1016/j.energy.2018.06.191>
- Zuleta, E.C., L. Baena, L.A. Rios, and J.A. Calderon. 2012. "The oxidative stability of biodiesel and its impact on the deterioration of metallic and polymeric materials: A review." *J. Braz. Chem. Soc.* 23:2159–2175.

## Appendix A – Analysis Metrics

Table A.1. Technology readiness metrics.

Metric	Favorable (+)	Neutral (0)	Unfavorable (–)
Process modeling data source	Demonstration-scale (or larger) data available, this includes detailed process analysis from literature	Bench-scale data available	Notional, yields and conversion conditions estimated partly from literature
Production process sensitivity to feedstock type	Feedstock changes result in <i>minor variations</i> in fuel yield/quality	Feedstock changes result in <i>some variations</i> in fuel yield/quality	Feedstock changes can cause <i>significant variations</i> in fuel yield/quality
Robustness of process to feedstocks of different specs	Changes in feedstock specifications <i>minimally</i> influences yield/quality	Changes in feedstock specifications <i>moderately</i> influences yield/quality	Changes in feedstock specifications <i>greatly</i> influences yield/quality
Blending behavior of bioblendstock with current fuels for use in vehicles	Current quality good enough for replacement (i.e., drop-in)	Current quality good enough for blend	Current quality in blend not good or unknown
Bioblendstock underwent testing towards certification	Yes	Limited	None
Bioblendstock will be blendable only in limited levels because of current legal limits	No limit	Blendable at high levels	Significant limit (i.e., on aromatics)

Table A.2. Economic viability metrics.

Metric	Favorable (+)	Neutral (0)	Unfavorable (-)
Co-Optima bioblendstock production baseline cost	Falls in cluster of lowest cost pathways ( $\leq \$5/\text{GGE}$ )	Falls in cluster of moderate cost pathways ( $\$5/\text{GGE} - \$7/\text{GGE}$ )	Falls in cluster of high cost pathways ( $\geq \$7/\text{GGE}$ )
Fuel production target cost	Falls in cluster of lowest cost pathways ( $\leq \$4/\text{GGE}$ )	Falls in cluster of moderate cost pathways ( $\$4/\text{GGE} - \$5.5/\text{GGE}$ )	Falls in cluster of high cost pathways ( $> \$5.5/\text{GGE}$ )
Ratio of baseline-to-target cost	$<2$	2–4	$>4$
Percentage of product price dependent on co-products (i.e., chemicals, electricity, other bioblendstocks/fuels produced as co-product to Co-Optima fuel)	$<30\%$	30–50%	$>50\%$
Competition for the biomass-derived bioblendstock or its predecessor	Bioblendstock is not produced from, nor is itself, a valuable chemical intermediate	Bioblendstock is produced from, or is itself, a raw chemical intermediate	Bioblendstock is produced from, or is itself, a valuable chemical intermediate
Cost of feedstock (in US\$2016)	Cost likely to be at or below target of $\$84/\text{dry ton}$ delivered at reactor throat	Cost likely to be between $\$84/\text{dry ton}$ to $\$120/\text{dry ton}$ delivered at reactor throat	Cost likely to exceed $\$120/\text{dry ton}$ delivered at reactor throat

Table A.3. Environmental impact metrics.\* SOT and target bioblendstock yields were included for reference, but were not ranked on favorability due to different comparative bases on pathways and feedstocks.

Metric	Favorable (+)	Neutral (0)	Unfavorable (-)
Baseline: Efficiency of input carbon (fossil and biomass-derived) to Co-Optima bioblendstock	>30%	10–30%	<10%
Target: Efficiency of input carbon (fossil and biomass -derived) to Co-Optima bioblendstock	>40%	30–40%	<30%
Baseline: Co-Optima bioblendstock yield (GGE/dry ton)*			
Target: Co-Optima bioblendstock yield (GGE/dry ton)*			
Target: Life cycle GHG emission reduction compared to conventional diesel fuel	≥60%	50%–60%	<50%
Target: Life cycle fossil energy use reduction compared to conventional diesel fuel	Likely to use less fossil energy on a life cycle basis than conventional gasoline	Could use less fossil energy on a life cycle basis than conventional gasoline	Unlikely to use less fossil energy on a life cycle basis than conventional gasoline
Target: Life cycle water consumption	≤3gal/GDE	3 gal/GDE - 80 gal/GDE	>80 gal/GDE

